UNIVERSITÀ DEGLI STUDI DI PADOVA

MASTER'S DEGREE IN MECHANICAL ENGINEERING

INDUSTRIAL ENGINEER DEPARTMENT

Damage Evolution in Multifunctional Glass Reinforced Composites

Supervisor:	**Co-supervisor:**	**Student:**
Prof. Marino Quaresimin	Dennis Gibhardt	Leonardo Romio
Prof. Bodo Fiedler	Melissa Walter	2085509

Academic year 2023/2024

This thesis was developed at the **Technische Universität Hamburg Harburg (TUHH)**

2024

Department of Mechanical Engineering

Technische Universität

Hamburg (TU Hamburg)

Am Schwarzenberg-Campus 1

21073 Hamburg

Acknowledgements

First and foremost, special thanks to Professor Bodo Fiedler and the entire research team at TUHH, especially Melissa and Dennis, who welcomed me and supported me throughout this six-month period.

Un sentito ringraziamento anche ai miei compagni Margherita ed Alex che mi hanno sempre supportato e consigliato nel lavoro e fatto divertire al di fuori del laboratorio. Un grazie anche per Elena, Gigi, Pedro e tutto il gruppo Erasmus per le serate ed i bei momenti passati insieme, come le serate al Gustav o anche semplicemente per una passeggiata al lago in compagnia.

Un grande grazie ai miei compagni di università Gabriele, Niccolò e Nicola per avermi sostenuto ed accompagnato in questo percorso fin dal primo anno, dalle prime lezioni in Paolotti agli utili esami. I panini fantasia al bar dei Sumiti, i Mercolegin, le riunioni su zoom durante la pandemia, la mensa Piovego e persino le interminabili e noiosissime lezioni sono tra i ricordi più belli di tutti questi anni passati insieme.

Per ultimo, ma non per importanza, un ringraziamento anche ai miei genitori e alla mia famiglia, che mi hanno permesso di studiare e vivere tutto questo senza mai farmi mancare nulla.

Index

List of figures

List of tables

Abstract

The use of composite materials, particularly glass fiber reinforced polymer (GFRP) composites, is increasingly widespread due to their excellent mechanical performance relative to weight. Additionally, they offer a significantly lower cost compared to other composite materials, such as carbon fiber. However, a critical issue is the damage and consequent loss of stiffness that occurs throughout the component's lifecycle. Therefore, it is essential to understand how damage impacts stiffness degradation and to develop non-invasive methods for damage monitoring.

This thesis investigates the damage evolution in GFRP composites with a modified, conductive matrix achieved by dispersing carbon nanotubes, and observes the associated loss of stiffness using an existing analytical model. The goal is to verify the analytical model considered and to calculate the fundamental for each laminate configuration tested, enabling, in the future, the characterization of each component and the rapid, non-destructive assessment of stiffness degradation during service. Moreover, for configurations where an analytical model for predicting stiffness loss is not yet available, data has been collected to support future studies.

Chapter 1 reviews the literature, introducing composite materials, particularly GFRP, and highlighting the influence of nanoparticles within the matrix and the damage mechanisms. Additionally, the analytical model employed is illustrated, along with its intended application. Chapter 2 describes the material fabrication methodology. Chapter 3 details the tests performed and the equipment used. Chapter 4 presents the results, data analysis, and final considerations.

The thesis demonstrates that an increase in internal cracks leads to a reduction in laminate stiffness and shows how the analytical model accurately describes this loss as a function of internal damage, along with the calculation of the fundamental parameter for various laminate configurations.

Sommario

L'uso di materiali compositi, in particolare i compositi a matrice polimerica rinforzati con fibra di vetro (GFRP), si sta diffondendo sempre di più grazie alle ottime prestazioni meccaniche rispetto al peso. Inoltre, hanno un prezzo molto più contenuto rispetto ad altri materiali compositi, come il carbonio. Tuttavia, un problema rilevante è il danneggiamento e la conseguente perdita di rigidezza durante la vita del componente. Pertanto, è fondamentale capire come il danno influisca sulla perdita di rigidezza e sviluppare metodi non invasivi per monitorare il danneggiamento. Nella tesi si studia l'evoluzione del danno nei GFRP, con matrice modificata e resa conduttiva tramite la dispersione di nanotubi di carbonio, e si osserva la perdita di rigidezza associata, utilizzando un modello analitico esistente. L'obiettivo finale è verificare che il modello analitico funzioni e ricavare il parametro fondamentale di tale modello per ogni tipologia di laminato testato, per permettere, in futuro, di caratterizzare ogni componente e valutare rapidamente e non distruttivamente la perdita di rigidezza durante l'esercizio. Inoltre, per le configurazioni in cui non è ancora disponibile un modello analitico di previsione della perdita di rigidezza, sono stati raccolti dati che potranno supportare studi futuri.

Nel Capitolo 1 viene analizzata la letteratura. Si introducono i materiali compositi, in particolare i GFRP, evidenziando anche l'influenza delle nanoparticelle nella matrice e i meccanismi di danneggiamento. Infine, si illustra il modello analitico utilizzato e come si intende applicarlo. Il Capitolo 2 descrive la metodologia di realizzazione del materiale. Il Capitolo 3 spiega i test eseguiti e gli strumenti impiegati. Nel Capitolo 4 si presentano i risultati, l'analisi dei dati e le considerazioni finali.

La tesi dimostra che l'aumento del numero di cricche interne porta a una perdita di rigidezza del laminato e come il modello analitico descriva correttamente tale perdita in funzione del danno interno, oltre al calcolo del parametro fondamentale per le configurazioni di laminato.

Introduction

Thanks to their mechanical properties, light weight, and relatively low cost, glass fiber-reinforced polymer matrix composites are becoming increasingly popular and widely used. They are prevalent in various sectors such as aerospace, marine, automotive, and wind energy. Despite their advantageous characteristics, certain limitations reduce their appeal: these materials are not environmentally friendly, as they require intensive industrial processing and are non-recyclable. Additionally, they tend to degrade quickly under operational conditions, leading to a significant reduction in their initial stiffness. Efforts are underway to address these challenges. In recent years, research has intensified on more eco-friendly composite materials, and various methodologies are being developed to monitor damage and assess durability.

To improve the sustainability of existing synthetic composites, a natural-origin hardener can be used. This thesis examines glass fiber composites with epoxy resin, employing the plant-based protein L-Arginine as a hardener, finely milled and dispersed in the resin. Currently, several methods exist for monitoring internal damage, such as electron microscopy, ultrasound, X-ray, tomography, and others. However, these techniques do not enable real-time damage analysis during the operation of the component and often require bulky, costly equipment. A simpler solution to these issues involves observing variations in electrical resistance across the component, which can be measured in situ without cumbersome equipment. Electrical resistance typically increases as damage accumulates, due to crack formation and delamination within the matrix that impede current flow. This approach is more straightforward with carbon composites, as carbon fibers are inherently electrically conductive. For glass fiber composites, the matrix must be rendered conductive by dispersing carbon nanotubes within it.

To assess stiffness loss, an analytical model developed by Carraro et al. [1] has been applied to cross-ply laminates. This model correlates the increase in internal cracks and resistance with the stiffness degradation of a laminate. Utilizing this model requires knowledge of the parameter φ, which varies across laminates and indicates

their sensitivity to damage. Therefore, by knowing the necessary parameters and attaching leads to measure the composite component's electrical resistance, even during operation, it becomes possible to estimate its stiffness loss and schedule replacement before reaching failure.

In this thesis, various laminate configurations were fabricated and investigated, using both unmodified resin and resin made electrically conductive by dispersing single-wall carbon nanotubes (SWCNTs). The mechanical properties of each configuration were evaluated, along with the behavior of electrical properties and crack density in conductive laminates. The analytical model [1] was validated by deriving the value of φ and analyzing its variations in cross-ply laminates. Additionally, data useful for future studies on quasi-isotropic laminates were collected, focusing on damage evolution, electrical resistance, and mechanical properties.

1. Composite Materials

Composites are an important class of materials that is increasingly used in recent years. Thanks to their high stiffness and strength, and for a good lightness, they are used in a wide range of applications, including aerospace, automotive, construction, defense and energy. These are highly engineered materials as they are designed and manufactured in such a way as to ensure the best response in terms of performance according to the specific end-use. For this to be possible, a transversal knowledge of several branches of science is required.
This chapter offers an overview of the types of composites; in particular, it will focus on matrix and reinforcement, damage propagation and damage monitoring.

1.1 Matrix and Reinforcement

Composite materials are constituted by two or more constituents, termed phases, designed to achieve a final material with unique and superior characteristics compared to the individual starting materials. Typically, one phase acts as the matrix, while the others provide reinforcement. There are various types of fibers and matrices; the most common composites feature polymeric matrices and reinforcements made of fibers or nanoparticles.

1.1.1 Matrix

The most widespread matrices are polymeric (PMC: polymeric matrix composites), due to their ease of use and production, as well as the ability to achieve materials with high stiffness and specific strength. A disadvantage is that polymeric matrices do not withstand very high operating temperatures; typically, they must be below 150 degrees Celsius.

Other less common types of matrices include metallic matrices (MMC: metal matrix composites) and ceramic matrices (CMC: ceramic matrix composites).

1.1.2 Fibrous reinforcement

Fibrous composites feature reinforcement in the form of thin filaments and represent the most widespread type of reinforcement. There are various types of fibrous reinforcements:

- Long fibers, which can have a random or preferential orientation;
- Short fibers, which can also have a random or preferential orientation;
- Mixed fibers, involving both long and short fibers simultaneously;
- Woven reinforcement, where fibers are interwoven to form a fabric, with fabrics having different weaves that correspond to different characteristics.

The most common fibers include:

- Glass fibers, which are the most economical and widely used in low-cost industries, offering decent mechanical properties but inferior to other types;
- Carbon fibers, which exhibit high mechanical properties but are more expensive. Various types are available, from high-strength fibers to high-modulus fibers;
- Aramid fibers, an example of which is Kevlar. This type of fiber offers high impact resistance and long fatigue life.

Composites are usually formed from various layers of unidirectional fibers oriented at different angles. The final characteristics of a composite laminate, such as stiffness, fatigue and impact resistance, degree of anisotropy, etc., are dictated by the composition and arrangement of these layers, referred to as the layup sequence.

1.1.3 Nano-reinforcement

The term 'nano-reinforcement' indicates that one phase of the material consists of nanoparticles dispersed within the matrix. From studies such as those conducted by Knoll, Riecken et al. [2], these nanoparticles, dispersed in the correct quantity within the matrix, help enhance the matrix's performance, for instance, by increasing its stiffness, strength, and fracture toughness. Furthermore, some

particles, like carbon nanotubes, beyond a critical concentration, render the matrix electrically conductive, which opens the door to numerous other applications, often related to non-destructive damage monitoring.

These particles can be made from various materials and have different shapes, for example, the most commonly used are: Carbon Nanotubes (tubular particles), Carbon Black (spherical particles), Layered Graphene (layered particles), etc. These micro-particles possess distinct properties and characteristics that affect the material in different ways. A general overview of the most commonly used nano-reinforcements and their various attributes is provided in the paper: "Nanocomposite-Based Structural Health Monitoring Approaches for Fibre Reinforced Polymers" [3]. In this paper, it is stated that Carbon Black (CB) and Carbon Nanotubes (CNTs) can be utilized as potential strain and damage sensors for composite materials. CB and CNTs tend to form percolated networks within a viscous matrix. Once the critical percolation threshold (filler concentration) is exceeded, electrically conductive paths are established. With carbon nanotubes can be obtained good electrical conductivity and high deformation sensitivity with a very low filler content: 0,1wt%, while for carbon black it's needed a higher amount, around 6-12wt%. For this reason, carbon nanotubes are the most widely used nanoparticles. There are three different types of carbon nanotubes, each with distinct characteristics and effects on the final properties of the composite material, as explained in the research conducted by Gojny, Wichmann et al.: "Influence of Different Carbon Nanotubes on the Mechanical Properties of Epoxy Matrix Composites – A Comparative Study" [4]. The different types of nanotubes are as follows:

- Single Wall Carbon Nanotubes (SWCNT): These have the largest specific surface area, but achieving a good dispersion in the epoxy matrix is very difficult.
- Multi Wall Carbon Nanotubes (MWCNT): These have the smallest surface area but allow for much easier dispersion.
- Double Wall Carbon Nanotubes (DWCNT): These represent a compromise between the other two.

In this thesis work, single-wall carbon nanotubes were used to achieve the best possible mechanical properties in the matrix, while also striving to attain a good dispersion.

This type of reinforcement is currently not widely used in mass industry due to issues related to production, cycle time, and cost; however, it remains a highly researched field due to the significant potential it offers, particularly concerning damage monitoring.

1.2 Damage

One of the most critical aspects of composite materials is undoubtedly their damage behavior, which does not exhibit predictable and evident characteristics like, for example, metals. Composite materials, being composed of multiple phases, exhibit various modes of damage, such as matrix cracks, debonding between fibers and matrix, delamination of different layers, fiber breakage, and so on. The material failure under load occurs suddenly with very limited deformation (in the order of 1-2%). These materials are also highly sensitive to impact damage; internal delaminations that are not visible from the outside can occur even after relatively minor impacts. Regarding fatigue life, they exhibit a very particular damage evolution, which is highly dependent on the component layup and the type of fiber and matrix used.

1.2.1 Damage evolution

Composite materials subjected to cyclic loads exhibit damage evolution that begins immediately from the very first cycles. Almost instantaneous formation of matrix cracks occurs in the laminate layers that are poorly oriented relative to the load direction (first phase). Once these cracks saturate, delamination and fiber debonding (if the fiber-matrix interface is of poor quality) start to occur (second phase). This is followed by the final phase, where damage rapidly increases due to

the propagation of delaminations, fiber breakage, and eventually catastrophic material failure.

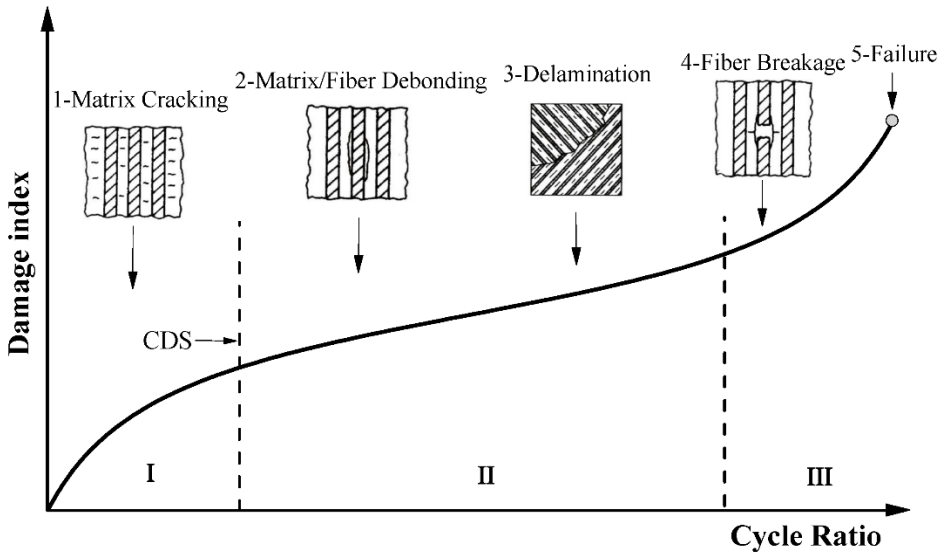

Figure 1.1 - Damage evolution in a composite material under cyclic loads.

The various types of fibers and matrices have a significant influence on the fatigue life and behavior of the material. Carbon fiber allows for a higher number of cycles to failure compared to glass fiber, given the same load and specimen lay-up. The lay-up itself also has a substantial impact; the more layers oriented perpendicularly to the load, the faster the damage evolves, leading to a significantly shorter fatigue life.

The damage in composite materials leads to stiffness degradation over their service life, which can begin as early as the initial cycles and may result in a reduction of up to 10-20%. By monitoring internal damage within the laminate through electrical resistance measurements, it is possible to estimate the extent of damage. However, accurately predicting how stiffness evolves and when failure will occur remains challenging. To address this issue, analytical models have been developed that precisely correlate the increase in electrical resistance of the laminate with the stiffness degradation it undergoes during its service life.

The presence of nanoparticles also affects fatigue life. As demonstrated by the studies reported in the paper: "Influence of carbon nanoparticle modification on the mechanical and electrical properties of epoxy in small volumes" [5], nanoparticles

such as carbon nanotubes and carbon black, when added to the matrix and dispersed in small quantities, can increase the fatigue life. These particles introduce new failure and damage propagation mechanisms that contribute to increasing the energy required to break the material. Such mechanisms can include crack blocking/deviation caused by nanoparticle agglomerates, local plastic deformation of the matrix, particle pullout, particle bridging, and nanotube rupture. However, if there are particles or agglomerates that are too large, they can act as initiation points for cracks, thus serving as local defects and significantly worsening the fatigue resistance.

As previously mentioned, the type of failure in composite materials is always sudden, with no signs of impending failure. This is very dangerous and should be avoided. There are two ways to achieve this: significantly over-dimensioning the material to eliminate any risk of failure, which, however, negates all the advantages of the material's lightness and specific stiffness; or trying to predict how and when the material will fail by introducing sensors that can indicate when the component is approaching imminent failure. This second method is currently under extensive study, and new methodologies are being sought to allow for non-destructive health monitoring of the part during use.

1.2.2 Damage Monitoring

As previously mentioned, damage monitoring is essential for optimizing the use of composite materials. There are numerous damage monitoring methods, such as electron microscopy, ultrasound, radiography, and tomography; however, these methods are either destructive or require heavy and expensive equipment, making it impossible to monitor damage while the component is in service. Alternatively, non-destructive methods exist, such as monitoring the electrical resistance of the composite component for announcing and predicting the failure of a component in service. During service, the matrix cracks, deforms, fibers break, and delamination occurs, causing the resistance to increase if the material is damaged. Monitoring is easier with carbon fiber composites, as the fibers are already electrically

conductive; however, with glass fiber components, conductivity is achieved by dispersing small amounts of nanoparticles such as carbon nanotubes or carbon black. As also reported by [5] and in the paper: "Load and health monitoring in glass fiber reinforced composites with an electrical conductive nanocomposite epoxy matrix" [6], when the nanoparticle concentration is close to the percolation threshold, the resistance becomes very sensitive to the presence of defects and the strain of the material, thus becoming an excellent non-destructive sensor for understanding the extent of internal damage in the material.

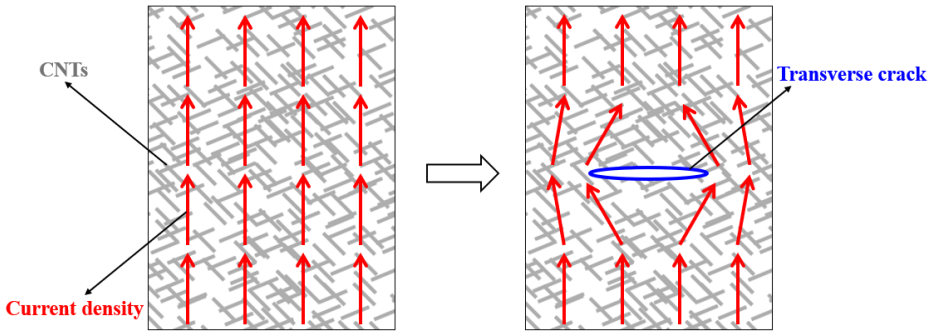

Figure 1.2 - Matrix crack that diverts the current flow, increasing electrical resistance.

Another method for damage monitoring studied in: "Health monitoring of CFRP using printed circuits" [7] involves printing circuits with conductive silver ink on the surface of the material. In this way, by measuring the variation in electrical resistance, it is possible to detect the deformation to which the material subjected to bending is exposed. Additionally, by observing discontinuities in the resistance graph, it is possible to identify the formation of large surface defects, such as cracks or fiber breaks.

In: "Strain sensing in GFRP via fully integrated carbon nanotube epoxy film sensor" [8], an alternative method for damage monitoring is presented, in which a thin layer of matrix containing a small weight percentage of carbon nanotubes is inserted within the composite layers. This method results in an increase in resistance if the material is subjected to tension and a decrease if compression stresses are present. Furthermore, it is also possible to detect residual cracks and delaminations identifiable by irreversible changes in resistance.

In this study, the first method described will be used, i.e., a small amount of single-wall carbon nanotubes will be dispersed within the epoxy matrix. Resistance will be monitored throughout the length and thickness of the laminate, observing the variation in resistance both after various static loading cycles and during fatigue tests.

1.2.3 Analytical Model

The general analytical model was developed by M. Zappalorto, P.A. Carraro, R. Pietrogrande, and M. Quaresimin, and is titled "Modelling the electrical resistance of multidirectional laminates with off-axis cracks." [9]. This model is developed for multidirectional laminates and enables the prediction of stiffness degradation by knowing the variation in electrical resistance and the crack density in each layer of the laminate. A simpler analytical model for cross-ply laminates, also developed by Paolo Andrea Carraro, Michele Zappalorto, and Marino Quaresimin, is explained in the paper: "Health monitoring of cross-ply laminates: Modelling the correlation between damage evolution and electrical resistance change." [1]. The latter model has been employed in this thesis work to predict the stiffness degradation of the laminates produced.

The model consists of the following equations:

$$\frac{R_x}{R_{x0}} = 1 + (1-\varphi)\cdot\frac{2\rho}{\alpha}\cdot\frac{\eta_x^0}{\eta_x^{90}}\cdot\frac{h_{90}}{h_0}\cdot\tanh\frac{\alpha}{2\rho} \tag{1.1}$$

$$\frac{E_x}{E_{x0}} = \left\{1 + k\cdot\frac{E_2}{E_1}\cdot\frac{h_{90}}{h_0}\cdot\frac{\alpha}{\xi}\cdot\frac{\left(\frac{R_x}{R_{x0}}-1\right)}{\left[\omega^{5/2}-\left(\frac{R_x}{R_{x0}}-1\right)^{5/2}\right]^{2/5}}\cdot\tanh\left(\frac{\xi}{\alpha}\cdot\frac{\left[\omega^{5/2}-\left(\frac{R_x}{R_{x0}}-1\right)^{5/2}\right]^{2/5}}{\left(\frac{R_x}{R_{x0}}-1\right)}\right)\right\}^{-1} \tag{1.2}$$

Equation (1.1) represents the electrical aspect of the model, correlating the increase in electrical resistance with the specimen's damage, denoted by ρ, which represents the crack density. The formula includes the following parameters:

- $\frac{R_x}{R_{x0}}$ which indicates the increase in electrical resistance in the form of a ratio between R_x which is the resistance in Ohms of the component at a given point in its service life, and R_{x0}, which is the initial resistance of the virgin

component, prior to undergoing load cycles. The measured electrical resistance is obtained by passing direct current through the plane of the laminate, in a direction perpendicular to the cracks that form in the layers oriented at 90 degrees (x direction in the following figure).

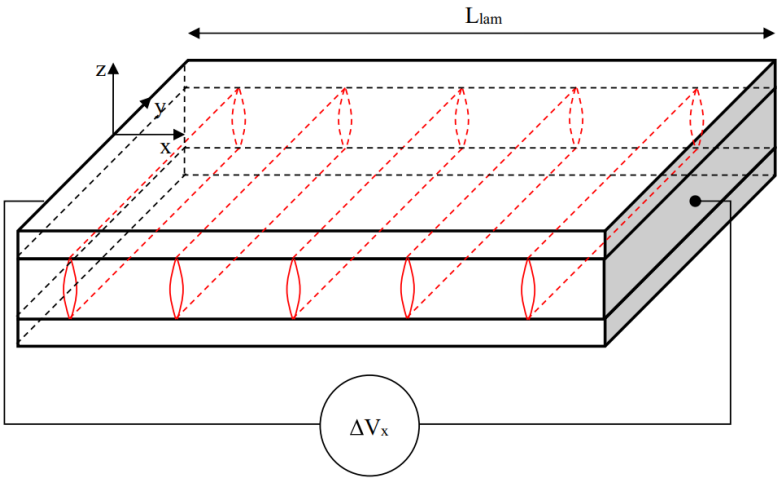

Figure 1.3 - Simplified schematic of the specimen. The electrical resistance is measured along the x-axis, which is perpendicular to the cracks that have formed within the 90-degree plies of the laminate.

- φ is the fundamental parameter of the model. This parameter indicates the sensitivity of the component's resistance to damage: φ = 1 means that the resistance is completely insensitive to damage, meaning that transverse cracks do not cause any increase in electrical resistance. Conversely, φ = 0 indicates full sensitivity. The parameter φ varies from laminate to laminate depending on the configuration and the loading conditions to which it is subjected. The aim of this discussion is to derive φ for different specimen configurations and calculate its range.
- $\rho\ [mm^{-1}]$ is the parameter that indicates the internal damage of the laminate. This damage is expressed as crack density per millimeter. Cracks form in the layers that are transverse to the direction of the load. The crack density can be determined experimentally by counting the cracks under an optical microscope.
- α is given by the following equations:

$$\alpha = \sqrt{H \cdot \frac{h_{90} \cdot \eta_x^0 + h_0 \cdot \eta_x^{90}}{h_{90} \cdot h_0}} \tag{1.3}$$

$$H = \left(\frac{h_0 \cdot \eta_x^0}{3} + \frac{h_{90} \cdot \eta_x^{90}}{6} \right)^{-1} \tag{1.4}$$

- h_{90} and h_0 $[mm]$ are, respectively, the thickness of the individual layers at 90 degrees and 0 degrees of the laminate. These parameters can also be determined experimentally by observing the specimen under a microscope.
- η_x^0 e η_x^{90} $[\Omega \cdot mm]$ indicate the resistivity of a single layer of the material, respectively in the x direction for the layer at 0 degrees and at 90 degrees. These values can be determined experimentally using the resistivity formula:

$$\eta = R \cdot \frac{A}{L} \tag{1.5}$$

  where R [Ohm] is the electrical resistance measured between two points on the layer being tested, L [mm] is the distance between the two considered points, and A [mm²] is the cross-sectional area of the flow tube through which the current passes, in this case represented by the area of the silver paint used to create the wiring of the composite component.

Equation (1.2) represents the electromechanical aspect of the model, specifically the part that correlates an increase in electrical resistance with the stiffness degradation of the laminate. The formula includes the following parameters:

- $\frac{E_x}{E_{x0}}$ indicates the stiffness degradation of the laminate during operation, expressed as the ratio between E_x which is the stiffness in MPa of the component at a given point in its service life, and $E_{x0,}$ which is the initial stiffness of the virgin component prior to undergoing load cycles.
- k is a parameter derived from the following equation:

$$k = -E_1 \cdot \frac{[E_1 \cdot h_{90} + E_2 \cdot (h_0 - (h_0 + h_{90}) \cdot \nu_{12}^2)]^2}{(E_2 \cdot h_0 + E_1 \cdot h_{90})^2 \cdot (E_2 \cdot \nu_{12}^2 - E_1)} \quad (1.6)$$

Where E_1 and E_2 are the elastic moduli in directions 1 and 2 of a single layer of the laminate, respectively, while ν_{12} is the Poisson's ratio of the laminate.

- ξ is a value that is derived from the following formula:

$$\xi^2 = H_m \cdot \frac{(E_2 \cdot h_0 + E_1 \cdot h_{90}) \cdot (E_1 \cdot h_0 + E_2 \cdot h_{90}) - \left(E_2 \cdot (h_{90} + h_0) \cdot \nu_{12}\right)^2}{E_1 \cdot E_2 \cdot h_0 \cdot h_{90} \cdot (E_2 \cdot h_0 + E_1 \cdot h_{90})} \quad (1.7)$$

$$H_m = \frac{3 \cdot G_{23} \cdot G_{13}}{h_{90} \cdot G_{13} + h_0 \cdot G_{23}} \quad (1.8)$$

With G_{13} and G_{23} being the shear moduli in the 1-3 and 2-3 directions, respectively.

- ω deriva da:

$$\omega = (1 - \varphi) \cdot \frac{\eta_x^0}{\eta_x^{90}} \cdot \frac{h_{90}}{h_0} \quad (1.9)$$

The formula includes the parameter φ, which was previously calculated in the electrical portion of the model.

To utilize this model, one begins with the electrical part (Equation (1.1)), where the input parameters are: $\frac{R_x}{R_{x0}}$, ρ, α, η_x^0, η_x^{90}, h_{90}, h_0, all determined experimentally; E_1 and E_2 were analytically calculated using CLT (Classic Lamination Theory), while ν_{12}, G_{13} and G_{23} were assumed. The output derived from this is the parameter φ, which, as previously explained, represents the material's sensitivity to damage and is the fundamental parameter to be obtained. For the calculation of φ, an Excel sheet was used to compute the experimental ratios and the corresponding results provided by the model. Subsequently, the Matlab app "Curve Fitter" was used, where *Formula (1.1)* was entered as a custom function, with the experimental values as input data. The output from Curve Fitter provided the value of φ that best fits the equation. Once the value of φ is determined, it is used in Equation (1.9) to find ω,

which will then be utilized within the electromechanical portion, Equation (1.2). From this equation, it is thus possible to derive the stiffness degradation of the specimen at that specific point in its service life monitoring the increase of electrical resistance.

The model can be applied under various conditions: both when evaluating the specimen under load and when it is unloaded, and it is independent of how the damage was incurred, whether through repeated fatigue cycles or generated by static loading. The only aspect that changes is the value of φ. The model considers only permanent changes in electrical resistance, specifically those caused by internal damage, and does not take into account the piezoresistive effect, which results in a reversible change in electrical resistance. Thus, the model allows for the prediction of stiffness degradation for components produced from the same composite laminate and evaluated under the same conditions, whether under load or unloaded

2 Manufacturing Process

In this chapter, the methodologies and materials adopted for the fabrication of composite material specimens will be illustrated.

Two main types of laminates were produced:

- Cross-Ply Laminates: with a $[0,90]_s$ layup, in two configurations: with standard resin and resin modified by the addition of single-wall carbon nanotubes (FlyCarbon);
- Quasi-isotropic Laminates: with a $[\pm 45, 90, 0]_s$ layup, also in two configurations: with standard resin and resin modified by single-wall carbon nanotubes (Ocsial).

A total of sixteen laminates were produced in four distinct phases:

1. Two cross-ply hand-laminated composites and two Roll Mill-laminated composites were created. For each type, one laminate used standard unmodified resin, while the other used resin modified with the addition of nanotubes. The following plates were thus obtained: HL_1(u), RM_1(u), HL_1, RM_1;
2. The same types of laminates as in the first phase were produced, with adjustments made to the amount of nanotubes in the resin, going from 0,05% to 0,2% by weight; resulting in the following laminates: HL_2(u), RM_2(u), HL_2, RM_2;
3. Two hand-laminated cross-ply composites were created, both with modified resin: HL_3, HL_4. In addition, two other plates were produced solely for the purpose of deriving various material properties and data. These hand-laminated plates consist of one laminate made of 4 unidirectional layers and another made of a single layer: HL_UD, HL_single_layer;
4. Four quasi-isotropic laminates were created, two using standard resin and two using modified resin: QI_1(u), QI_2(u), QI_3, QI_4.

The materials used were:

- Glass fiber (HP-U600E 608 [g/m^2], GF-Fabric X-E-610 [g/m^2]);

- EPIKOTE 827 resin from Westlake (DGEBA-Bisphenol-A-diglycidyl ether);
- L-Arginine vegetable protein (L-Arginine Base Pulver buXtrade) as a hardener mixed with the resin;
- Single Wall Carbon Nanotubes (CarbonFly and Ocsial), also dispersed within the resin.

2.1 Cutting of fibers

The laminate fabrication process is the same for all, with minor differences that will be explained later.

In the first and second phases, cross-ply panels were produced, featuring a [0, 90]s lay-up. Fully unidirectional (UD) layers were used for the hand-laminated panels, while for those manufactured using the roll mill, 90% UD layers were employed, incorporating backing fibers orthogonal to the main fiber direction. The fiber layers without backing fibers were obtained by manually removing the horizontal fiber bundles relative to the main fiber direction using tweezers.

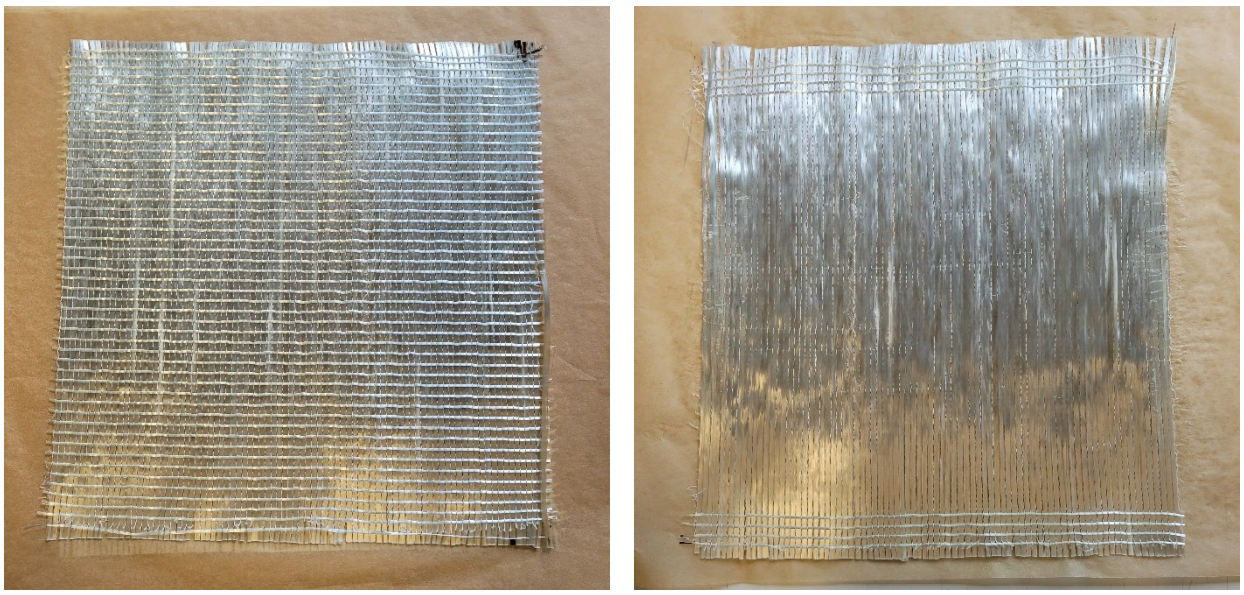

Figure 2.1 - Layer with backing fibers used in the roll mill plates on the left and layer without backing fibers used in the hand laminated plates on the right side.

The type of fiber used is: Glass fiber HP-U600E, consisting of 608 [g/m^2] fibers at 0°, 40 [g/m^2] fibers at 90°, and 15 [g/m^2] stitching.

For the quasi-isotropic laminates, the type of fiber used is GF-Fabric X-E-610 [g/m²]. In this case, the fiber layers were arranged to achieve the following layup: $[\pm 45, 90, 0]_s$.

After the fiber cutting phase, where 30x30 cm layers were obtained, the fiber layers were placed on baking paper sheets, and their edges were impregnated with hair gel. This process made the layers more rigid and stable during lamination, thereby improving the overall quality of the process.

2.2 Resin preparation process

The resin used was EPIKOTE 827 from Westlake (DGEBA-Bisphenol-A-diglycidyl ether), into which 13,74 grams of L-Arginine vegetable protein were mixed for every 100 grams of resin. This protein acts as a natural hardener. To ensure uniform mixing with the resin, the protein was first ground into a finer powder using a mortar and pestle, and then the mixture was processed through a three-roll mill machine. This machine consists of three rollers rotating in opposite directions, with adjustable gaps between the rollers for precise control.

The resin and hardener mixture was passed through the machine multiple times, with the gap being adjusted to achieve uniform dispersion. Similarly, after thoroughly mixing the L-Arginine, carbon nanotubes were dispersed into the resin.

In this initial phase, for the cross-ply laminates, a quantity of 0.05% by weight of CarbonFly single-wall carbon nanotubes was used. This amount was below the threshold for making the material conductive; therefore, in subsequent phases, the quantity was increased to 0.2%.

For the quasi-isotropic laminates, a quantity of 0.25% by weight of Ocsial single-wall carbon nanotubes was used. A lower quantity was used compared to the CarbonFly nanotubes because previous experiments indicated that, at equal

percentages relative to the weight of the resin, the nanotubes supplied by Ocsial make the material slightly less conductive.

The nanotubes were initially manually inserted into the resin using a glovebox and mixed to ensure that the particles were no longer volatile and, therefore, not harmful to humans. Subsequently, the resin-nanotube mixture was made homogeneous and uniform using the three-roll mill.

The working principle of this machine is as follows: high shear forces are generated within the fluid as it flows between the rollers due to the narrow gap and the difference in rotational speeds. These shear forces mix and break apart the agglomerates of micro-particles present in the resin, ensuring a uniform dispersion of both L-Arginine and carbon nanotubes. Multiple passes are required to achieve the desired final configuration, which must be as homogeneous as possible.

This is particularly important because one of the characteristics of single-wall carbon nanotubes is their tendency to form agglomerates and entanglements, leading to clumps within the matrix. These clumps must be avoided as they can degrade the overall mechanical properties of the material and hinder optimal electrical conductivity within the specimen.

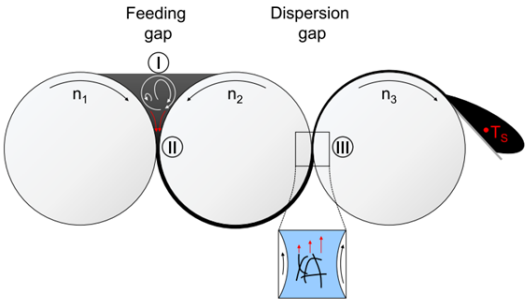

Figure 2.2 - Schematic of the working principle of the three-roll mill machine.

The mixing process has been set up from Meeuwa et al. [10], to avoid cluster, due to high shear force generated between the roller gaps that brakes nanoparticle agglomeration. Thanks to their reserch mixing process is made up the following procedure:

- First gap: 120 μm, second gap: 40 μm (repeated 5 times);
- First gap: 40 μm, second gap: 13 μm (repeated 1 time);

- First gap: 13 µm, second gap: 5 µm (repeated 5 times).

The following steps were performed for the dispersion of the nanotubes:

- First gap: 120 µm, second gap 40 µm (repeated 1 times);
- First gap: 40 µm, second gap: 13 µm (repeated 1 time);
- First gap: 13 µm, second gap: 5 µm (repeated 5 times).

All steps were performed at the same rotational speed:

- First roll: 33 rpm;
- Second roll: 1 [10]00 rpm;
- Third roll: 300 rpm.

Figure 2.3 - Three Roll Mill Machine.

2.3 Lamination Process

As previously mentioned, a pair of modified and unmodified laminates were hand-laminated. The process was carried out using a roller to apply the resin onto the fiber layers and a rigid roller tool to compact and align the layers. Efforts were made to spread a uniform layer of resin across the fibers, with the goal of achieving a final fiber volume fraction of approximately 50%.

Figure 2.4 - Plate hand laminated with modified resin during the lamination process.

The lamination of the remaining pair of laminates was conducted using a Roll Mill, a prototype machine developed by TUHH University, which features two counter-rotating rollers with resin positioned between them. To impregnate the fiber layers, the material is passed through the rollers, with the gap adjusted to control the fiber

volume fraction. Similarly, during the lay-up phase of the laminate, the various layers were compacted using a rigid roller.

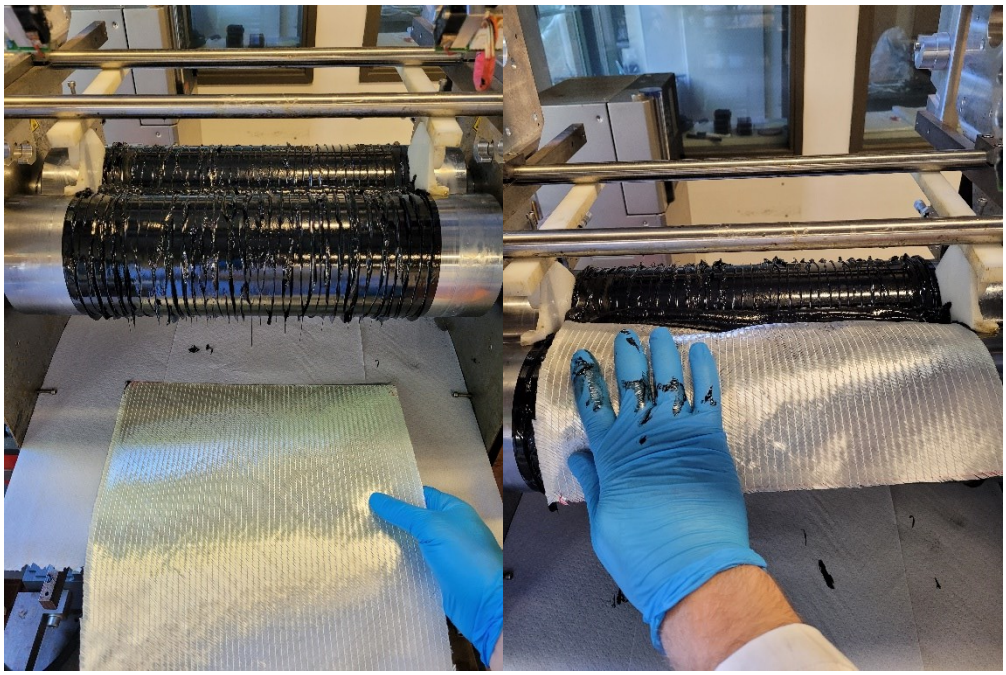

Figure 2.5 - Roll Mill during the impregnation process of a Roll Mill laminate with modified resin.

All quasi-isotropic laminates were exclusively laminated using the roll mill.

2.4 Curing Process

The curing process takes place in the autoclave. The autoclave is essentially a pressurized vessel where the resin polymerization process takes place inside. In this method, the composite part is laid up and enclosed in a vacuum bag. Full or partial vacuum is drawn under the bag, and gas pressure (nitrogen) greater than atmospheric pressure is applied on the exterior of the bag.

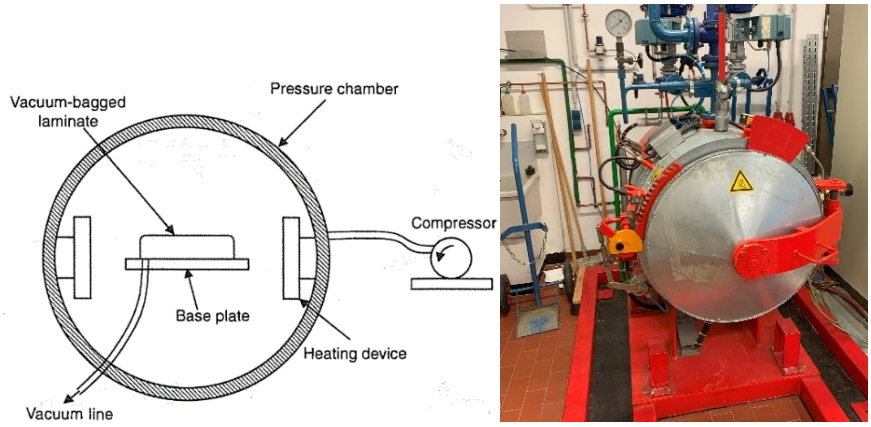

Figure 2.6 - TUHH autoclave.

Initially, the laminates were placed on aluminum molds, followed by the creation of a vacuum bag using the following procedure:

- Covering the aluminum mold with a plastic film, to prevent the laminate from sticking to the mold;
- Placing the laminate wrapped with a silicone gasket, all packed inside another Teflon membrane;
- Adding an absorbent layer, to prevent excess resin from entering the pump lines;
- Completing the vacuum bag, by covering everything with vacuum foil.

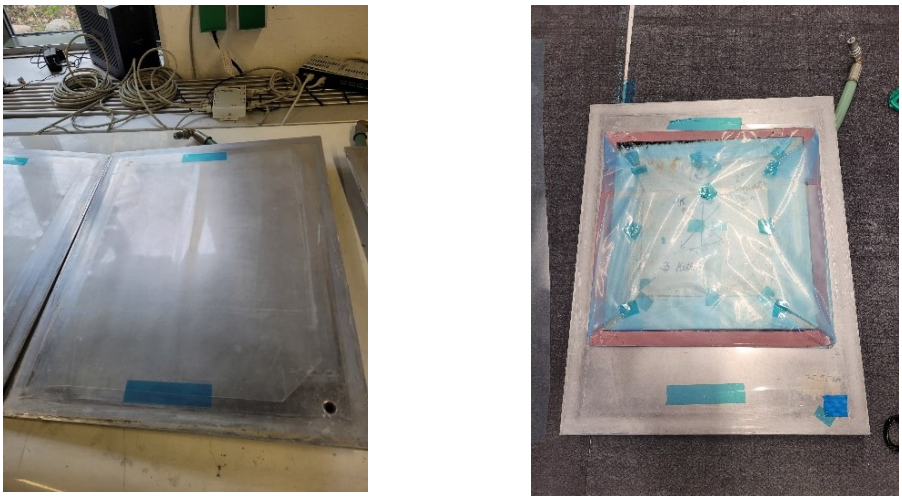

(a) (b)

Figure 2.7 - (a) Aluminum mold covered with a layer of plastic material. (b) Laminate covered with a layer of cellophane and a silicone glasket placed on the mold.

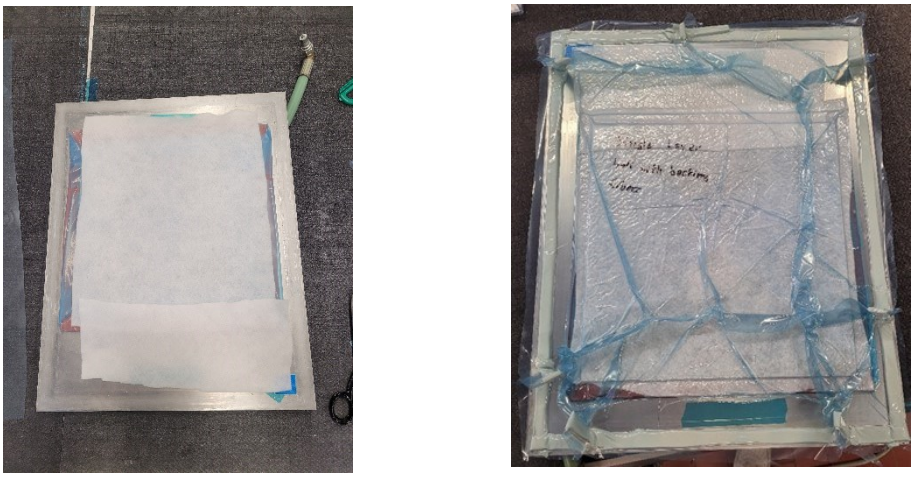

(a) (b)

Figure 2.8 - (a) Addition of an absorbent layer. (b) Completion of the vacuum bag.

Once the vacuum bag was created, the final part of the curing process in the autoclave can begin. The program used for the autoclave is specific for curing the 827 epoxy resin: starting at 20°C, the temperature is increased by 4°C per minute until reaching 167°C. This temperature is maintained for 60 minutes, after which it is increased by 0.05°C per minute until reaching 180°C. The temperature is held at 180°C for 70 minutes, then decreased by 0.5°C per minute until ambient temperature is reached. The pressure also follows a precise pattern: it increases from atmospheric pressure to 7 atm during the first heating ramp and slowly decreases during the cooling phase. The autoclave curing process was the same for all types of laminates produced.

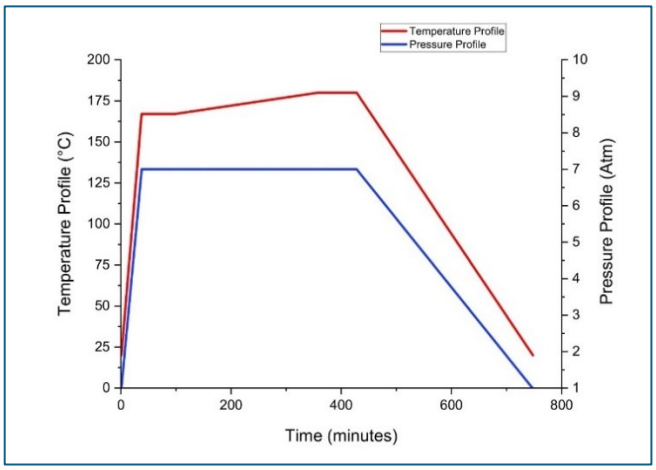

Figure 2.9 - Graph indicating the temperature and pressure profile trend inside the autoclave.

2.5 Plates cutting and samples manufacturing

Once the curing phase was completed and the plates were removed from the autoclave, the laminates were cut, and the specimens were fabricated. This process was carried out in the same manner for all types of specimens produced. It is important to trim the outermost edges of the laminates because those areas typically have an irregular shape and tend to accumulate excess resin.

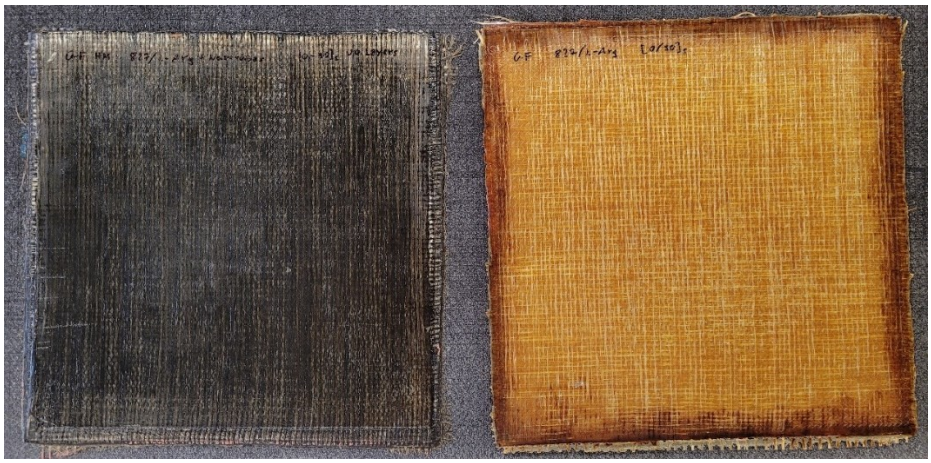

Figure 2.10 - Laminates just removed from the autoclave, where resin accumulation at the edges can be observed. This image depicts cross-ply laminates.

The edge-cutting process was carried out using a circular saw, which was also used to cut the material that will later form the grips. Once the edges were trimmed, the resulting plates are shown in the following figure:

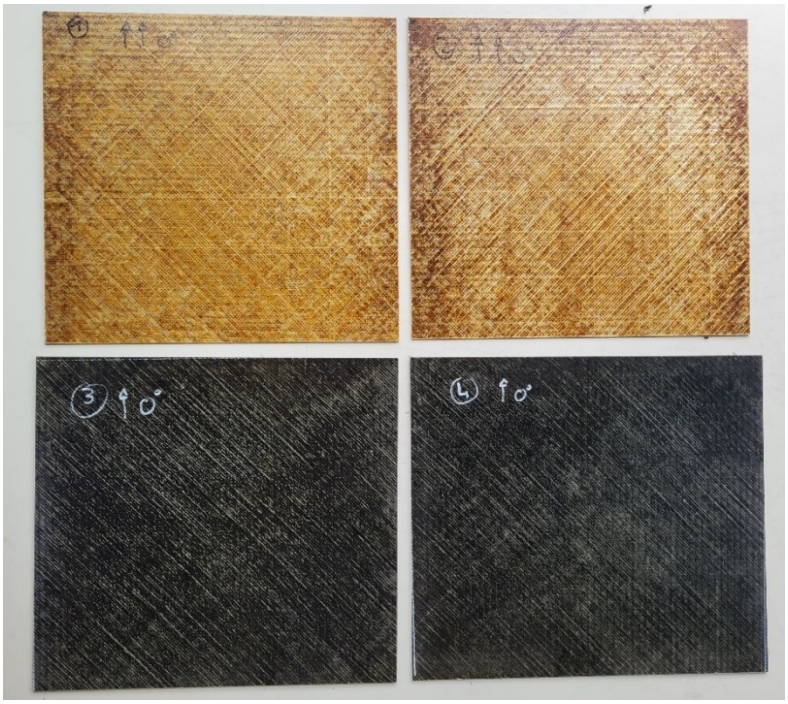

Figure 2.11 - Laminates with trimmed edges using a circular saw. This image shows the quasi-isotropic laminates.

The manufacturing process continued with the creation of the grips. These were made by bonding thin strips of another composite material, 5 cm wide, to the upper and lower ends of the plates. The composite material used consists of a thin layer of fiberglass arranged at ±45°. This arrangement ensures that the forces and stresses generated in the grips are evenly distributed, preventing the specimens from experiencing tab failure. Additionally, the anchors allow for electrical isolation of the specimen from the testing machine. These layers of composite material were bonded to both sides of the laminates. Afterward, the plate was placed in a heated press at 60°C and subjected to a compression of 20 kN to ensure the grips adhered perfectly to the plate and that the adhesive fully cured. The assembly was kept in the press for approximately one hour. Once this process was completed, the plates were cut to form individual specimens. Saw diamond-coated cutting wheel with a Brilliant 265 (ATM, Germany), which ensures dimensional tolerances of the

samples required by the ASTM D-5528-01 and ASTM D7905/D7905M-14 standards was used.

Figure 2.12 - Grinding saw.

From each plate, approximately nine specimens were obtained. According to standards, they have specific dimensions: 25 cm in length (including grips, 15 cm

without grips), 2.5 cm in width, and a thickness between 1.8 and 2.3 mm, depending on the specimen configuration.

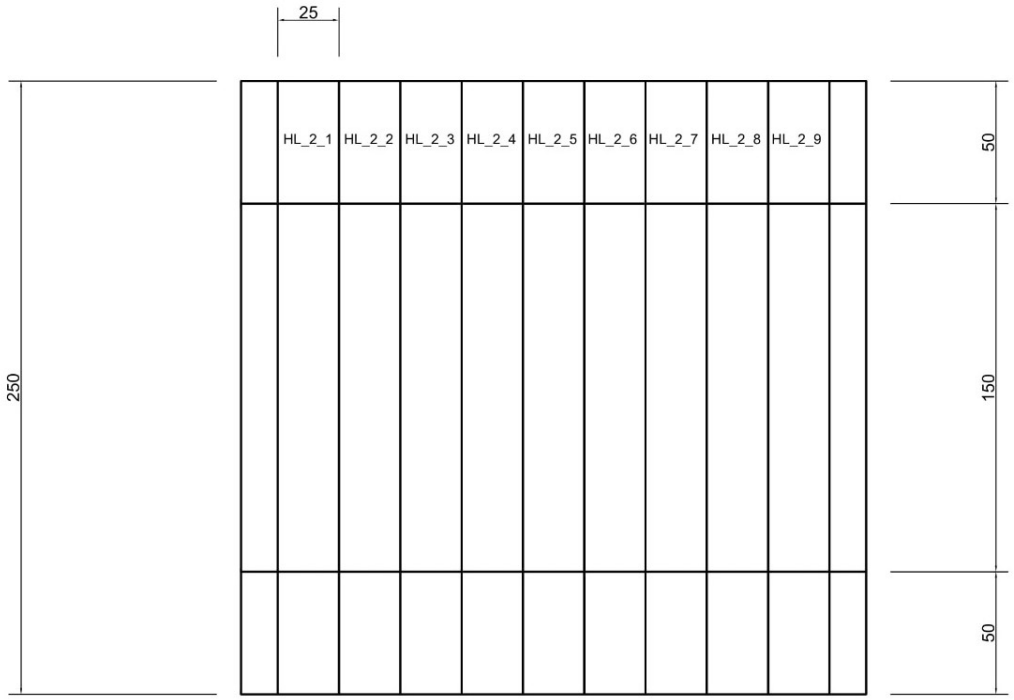

Figure 2.13 - Example of a plate segmented into individual specimens with the corresponding nomenclature. The material on the far right and left edges is considered waste.

For the specimens with modified resin, the wiring process is then carried out: to measure their electrical resistance, copper wires were attached to the ends of the section not covered by the grips. The wires are placed one on each face of the

specimen, ensuring that the current passes through the entire thickness of the specimen.

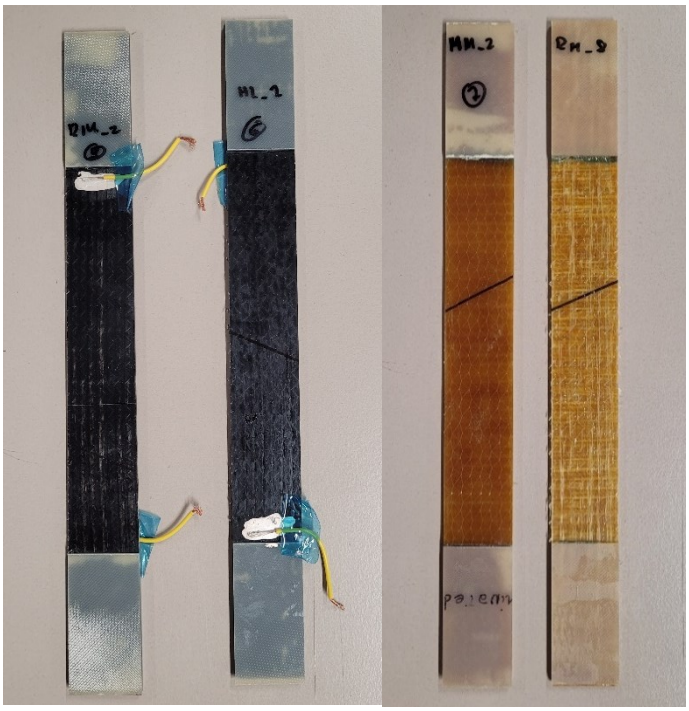

Figure 2.14 - Cross-ply specimens with modified resin on the left and unmodified resin on the right. The difference between specimens made by hand and those produced using a roll mill is evident.

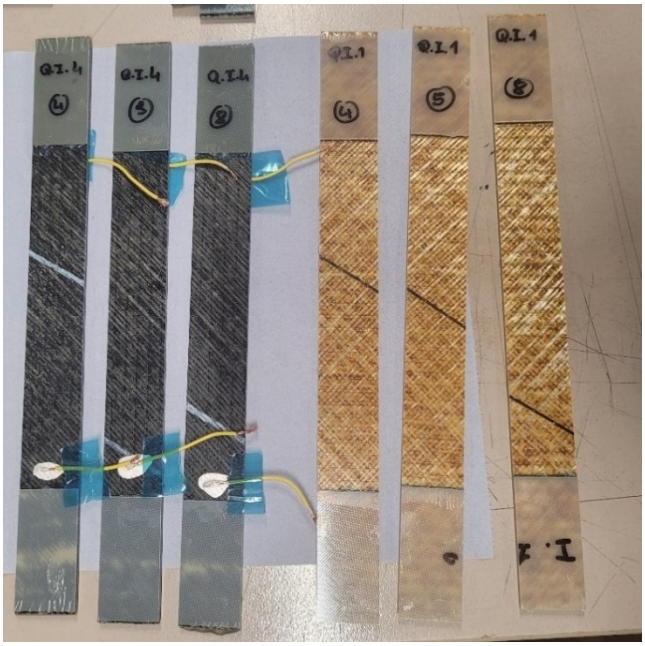

Figure 2.15 - Quasi-isotropic specimens.

2.6 Electrical Characterization

Concurrently with the production of these specimens, two panels were created using the same type of modified resin employed for the cross-ply panels., solely for the purpose of obtaining data and values of the material for the validation of the analytical model. The data collected includes the resistivity in the x and z directions of the 90-degree and 0-degree layers of the cross-ply specimens, as well as the elastic modulus in directions 1 and 2.

Figure 2.16 - Wired panels for experimental data acquisition necessary for model validation.

These panels were made by hand; one panel consists of four layers of material all oriented in direction 1, while the other is composed of a single layer. The panels contain one half with fibers featuring backing fibers to better simulate a panel created using the roll mill process, while the other half is without backing fibers to replicate a hand-laminated panel. From *Figure 2.16*, looking at the panel on the right, it is clearly noticeable that the right side of that panel differs from the left side. The right side has fibers that include the backing fibers, whereas they have been removed on the left side. These panels were wired to experimentally obtain the data needed for the model. Panels of different thicknesses were created to average the results of the desired values, considering the thickness of the panels to achieve more accurate results.

The resistivity of the panels has been calculated using the following formula:

$$\eta = R \cdot \frac{A}{L} \tag{2.1}$$

where R is the electrical resistance measured using the Keithley 2636B instrument, A is the area of the silver paint used for the wiring, and L is the distance between the two points where the measurement was taken.

The wiring was placed in specific positions on both sides of the panels to allow for resistivity measurements in the x and z directions for fibers oriented at both 0 and 90 degrees. During the measurements, wiring connected to the opposite faces of the panel was used, ensuring that the current passed through the entire thickness of the material. The measurements were conducted considering wiring at various distances to achieve more accurate results.

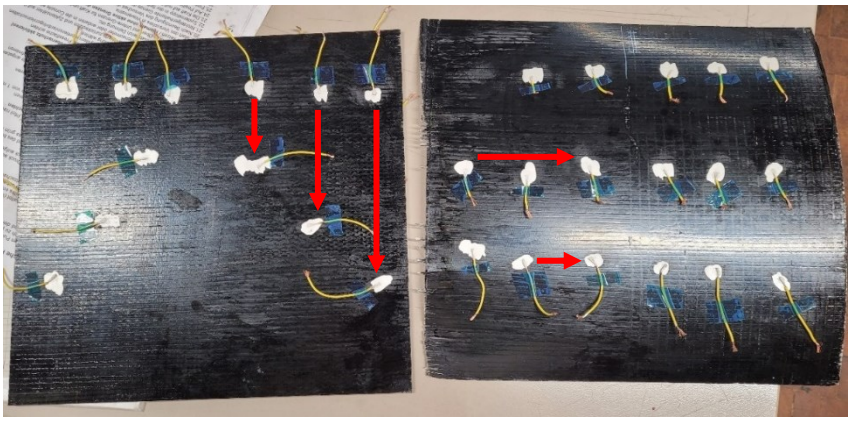

Figure 2.17 - Resistivity measurements taken at different distances and positions along the x-direction for 0° and 90° layers, depending on the measurement orientation.

The resistivity values were obtained by averaging all the calculated measurements. The results are summarized in the table below:

Resistivity (Ohm*mm)	With backing fibers	Without backing fibers
ηx0	1.93E+05	1.93E+05
ηx90	2.62E+05	2.62E+05
ηz	2.08E+06	2.08E+06

Table 2.1 - Table summarizing the obtained resistivity values.

The production of the laminates occurred in four distinct phases, aiming to improve the process each time by adjusting the amount of carbon nanotubes or the quantity of resin deposited during the manual lamination.

Overall, the following laminates were produced:

Production Phase	Laminate Name	Lamination	Lay-up	Resin
1	HL_1(u)	Hand	$[0,90]_s$	Unmodified
1	HL_1	Hand	$[0,90]_s$	SWCNTs 0,05% CarbonFly
1	RM_1(u)	Roll Mill	$[0,90]_s$	Unmodified
1	RM_1	Roll Mill	$[0,90]_s$	SWCNTs 0,05% CarbonFly
2	HL_2(u)	Hand	$[0,90]_s$	Unmodified
2	HL_2	Hand	$[0,90]_s$	SWCNTs 0,2% CarbonFly
2	RM_2(u)	Roll Mill	$[0,90]_s$	Unmodified
2	RM_2	Roll Mill	$[0,90]_s$	SWCNTs 0,2% CarbonFly
3	HL_3	Hand	$[0,90]_s$	SWCNTs 0,2% CarbonFly
3	HL_4	Hand	$[0,90]_s$	SWCNTs 0,2% CarbonFly
3	HL_UD	Hand	$[0]_4$	SWCNTs 0,2% CarbonFly
3	HL_single_layer	Hand	[0]	SWCNTs 0,2% CarbonFly

4	QI_1(u)	Roll Mill	$[\pm 45,90,0]_s$	Unmodified
4	QI_2(u)	Roll Mill	$[\pm 45,90,0]_s$	Unmodified
4	QI_3	Roll Mill	$[\pm 45,90,0]_s$	SWCNTs 0,25% Ocsial
4	QI_4	Roll Mill	$[\pm 45,90,0]_s$	SWCNTs 0,25% Ocsial

Table 2.2 - Table summarizing all produced plates.

2.7 Mechanical Characterization

The use of the model also requires certain mechanical properties of the laminate, such as the elastic moduli E_1 and E_2 of the individual layers, the laminate elastic modulus E_{x0}, and the modulus E_x after various loading cycles to observe stiffness degradation. Additionally, the values of ν_{12}, G_{13}, and G_{23} are required.

Due to material constraints, the elastic moduli E_1 and E_2 were calculated using Classical Lamination Theory (CLT), based on the fiber volume fraction and the mechanical properties of the individual fiber and matrix constituents. The values of ν_{12}, G_{13}, and G_{23} were assumed. The values used are summarized in the following table:

Plates	Hand Laminated	Roll Mill
E_1	31500.00 Mpa	35200.00 Mpa
E_2	5773.00 Mpa	5773.00 Mpa
ν_{12}	0.30	
G_{13}	2300.00 Mpa	
G_{23}	2092.00 Mpa	

Table 2.3 - Mechanical values utilized for the verification of the analytical model.

The values of E_{x0} and E_x were calculated separately for each specimen using the testing equipment. In the initial loading cycles of fatigue tests, highly variable and

inaccurate elastic modulus values were frequently observed, resulting from measurement errors. An example of this can be seen in the following figure.

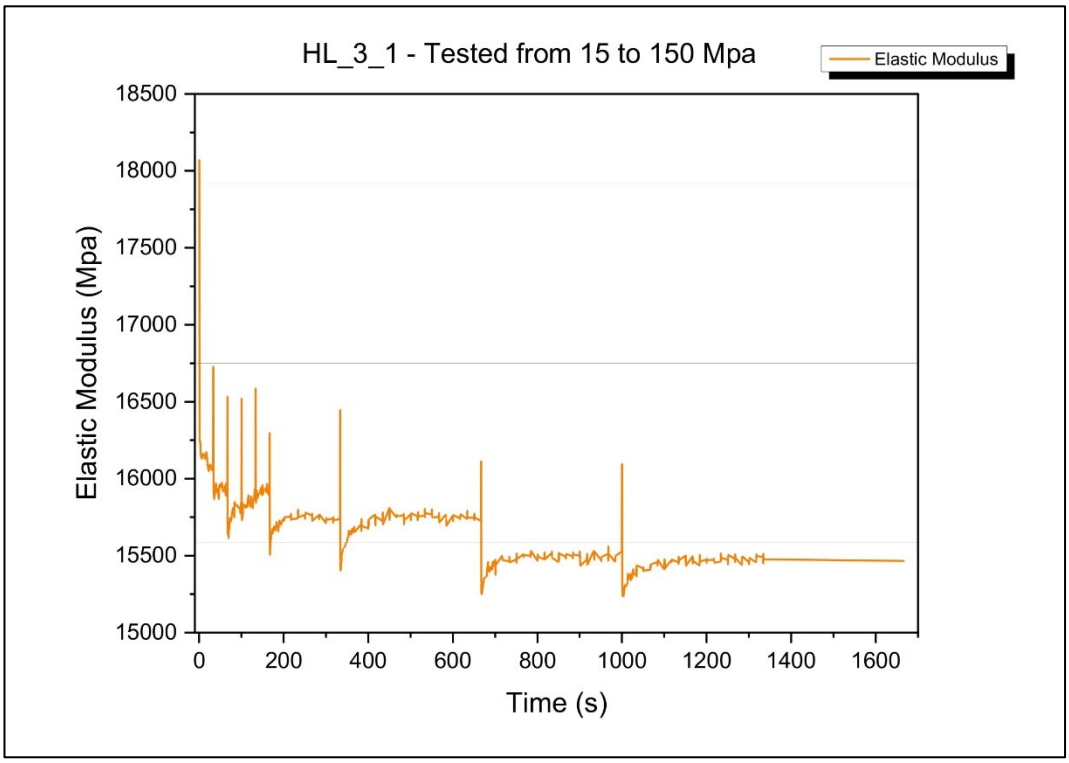

Figure 2.18 - Elastic modulus graph of the specimen HL_3_1.

This specimen was tested by monitoring crack density, so the fatigue test was paused multiple times and then resumed. It is observed that in the first cycle of each resumed test, an unrealistically high elastic modulus is measured. Subsequently, the measured E_x value decreases, then rises and stabilizes at a value slightly lower than that calculated in the previous section of the test.

Therefore, in validating the model, the E_{x0} value was taken as the average between the maximum and minimum peaks recorded by the equipment. For the various E_x values, the last measurement from the previous cycle, before pausing the test, was used.

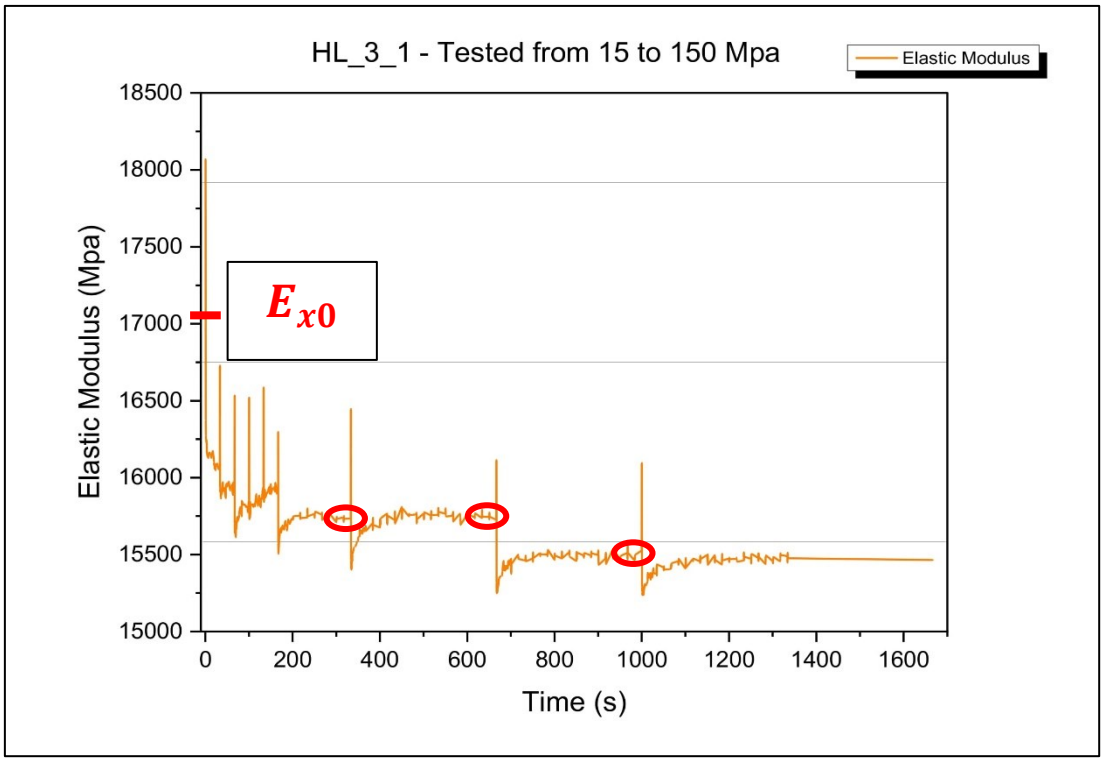

Figure 2.19 - Example of the values considered for Ex0 and Ex.

In the image, the selected E_{x0} value is indicated with a dashed line, while examples of the considered E_x values are marked with circles. This methodology was applied to all specimens that exhibited similar issues with elastic modulus calculation.

3 Testing Methods.

The two main types of tests performed are: static tensile tests and fatigue tests on the specimens. For each type of plate, the following sequence of tests was carried out:

- Static tensile test to failure, to gain a general understanding of the material's mechanical properties. In this phase, a couple of specimens were used for each type, both with modified resin and with unmodified resin, focusing on identifying the material's ultimate tensile strength;
- Static tensile test using various increasing load ramps, conducted only on specimens with modified resin. These tests were used to measure the variations in mechanical and electrical properties as damage increased. This type of test was useful for obtaining the necessary data for validating the analytical model;
- Fatigue tests at various load levels. Two types of fatigue tests were conducted: one to determine the fatigue life of the various types of specimens created with both modified and unmodified resin; the other to obtain the data necessary for validating the analytical model, in this case, only the specimens with nanotubes were tested.

3.1 Static Test

The static tests were conducted using the Z100 machine (Zwick-Roell, Germany) to assess the mechanical properties of the specimens and to obtain the necessary data for validating the analytical model. The first type of tensile test was performed to failure in order to determine the ultimate tensile strength of the specimens. Both

modified resin specimens and standard resin specimens were used. Three specimens for each material configuration were tested to ensure statistically reliable results.

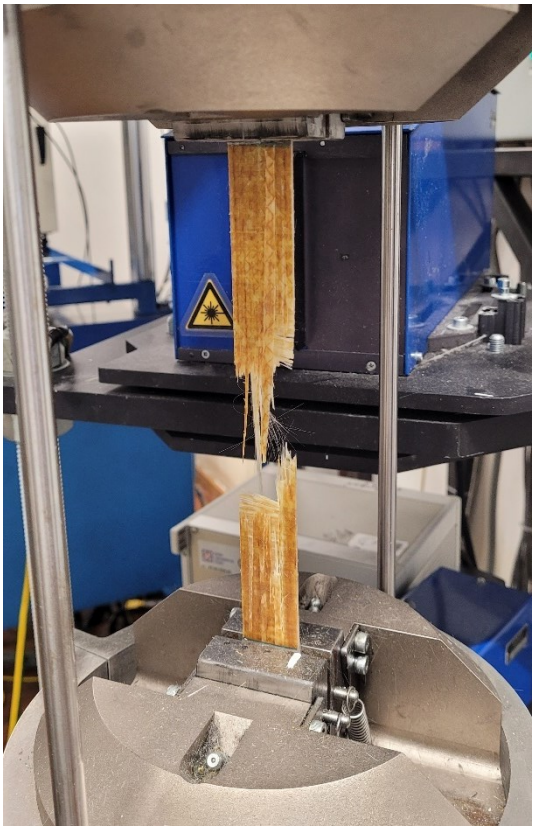

Figure 3.1 - Static tensile failure of an unmodified specimen.

The second type of tensile test was conducted only with specimens containing modified resin to monitor the trends in mechanical properties, electrical resistance, and crack density as the load on the specimen increased. The purpose of this type of test is to obtain numerical values for the decrease in the elastic modulus E, the increase in resistance R, and the value of crack density ρ.

To calculate these parameters, the specimen was tested with progressively increasing load ramps but without reaching failure. The test involved slowly applying the desired load to the specimen, and once it was reached, the specimen was returned to a zero-load condition. A grip separation speed of 2 mm/min was used.

The chosen load values are summarized in the following table:

Static Test Cross-Ply	Static Test Quasi-Isotropic
50 Mpa	50 Mpa
75 Mpa	75 Mpa
100 Mpa	100 Mpa
125 Mpa	125 Mpa
150 Mpa	150 Mpa
200 Mpa	200 Mpa
300 Mpa	-

Table 3.1 - Summary table of the load ramp values from static tensile tests.

For the quasi-isotropic laminates, the tests were stopped at 200 MPa to avoid material failure, as their ultimate tensile strength is significantly lower than that of the cross-ply laminates and close to the value of 300 MPa.

The measurement of crack density was performed between the various load ramps by observing the side of the specimen (which had been properly ground and polished before the test) using an optical microscope. The value of crack density was calculated using the following formula:

$$\rho = \frac{n_c}{d} \tag{3.1}$$

Where ρ is the value of crack density, n_c is the number of cracks identified in the considered interval d which is equal to 6 cm. To be included in the count, the cracks must affect both 90-degree layers and be through-thickness.

(a) (b)

Figure 3.2 - (a) Optical microscope used to measure crack density. (b) Specimen with cracks.

The output of this test consists of numerical results summarized in graphs, which were then analyzed and used to validate the analytical model. Below are examples of graphs obtained from this type of static test conducted on a hand-laminated specimen. The tests and results are presented similarly for all other types of materials.

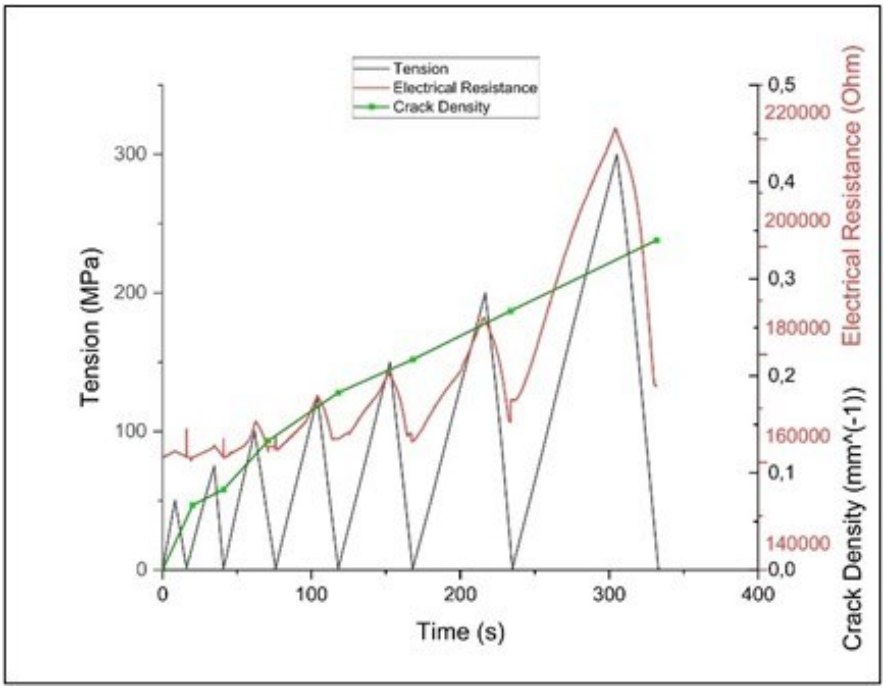

Figure 3.3 - Graph representing the load ramps compared to the evolution of electrical resistance and crack density.

3.2 Fatigue Test

The fatigue tests were conducted using the Instron-Schenk machine equipped with a 100 kN load cell (Instron 8800H2470). Both modified and unmodified specimens were used. The purpose was to monitor the fatigue life of the various types of specimens created and to obtain the necessary data for validating the analytical model.

Fatigue tests to failure were performed at predetermined load levels, maintaining a constant load ratio R equal to 0.1.

$$R = \frac{\sigma_{min}}{\sigma_{max}} = 0{,}1 \tag{3.2}$$

The load levels at which the tests were conducted were chosen considering the ultimate tensile strength of the specimens, which was calculated from the static tests and has the following values:

- 500 Mpa for Cross-Ply specimens.
- 350 Mpa for Quasi-Isotropic specimens.

Test	**Cross-ply σmin – σmax (MPa)**	**Quasi-isotropic σmin – σmax (MPa)**
40% di σf	20 – 200	14 - 140
30% di σf	15 - 150	11 - 110
20% di σf	10 - 100	7 - 70

Table 3.2 - Summary table of the load values at which the fatigue tests were performed.

During the tests of the specimens modified with nanotubes, electrical resistance was also measured, again using the Keithley 2636B device. The resistance was measured continuously for the shorter tests and at regular intervals for the longer tests. Measuring resistance during the fatigue test is useful for understanding the evolution of damage throughout the test.

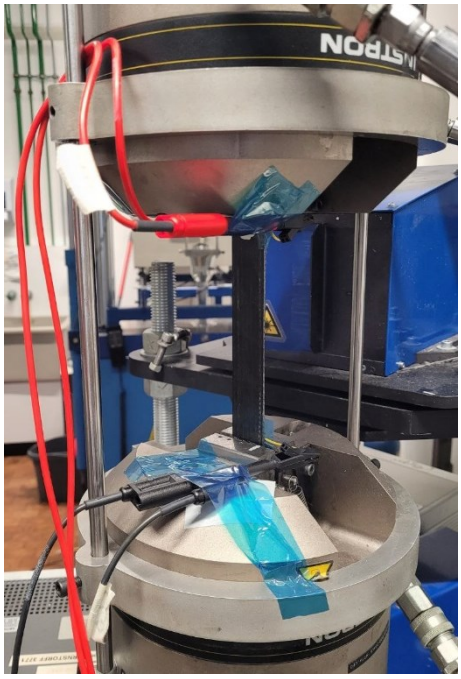

Figure 3.4 - Fatigue machine setup with all electrical connections to the specimen.

As an output from this type of test, graphs are obtained that compare the trend of the elastic modulus with the trend of resistance during the test. The following figure shows the graph of a hand-laminated cross-ply laminate with a number of cycles to failure equal to $N_f = 158091$. The trend of the elastic modulus is represented in yellow; the average measured electrical resistance is shown in red, and the actual resistance measurements during the cycles are depicted in blue. The resistance measurements were taken at regular cycle intervals, with closer intervals at the beginning of the test and more spaced intervals towards the end.

As expected, the resistance, and thus the damage in the specimen, increases rapidly at the beginning, reaching a plateau when the crack saturation within the specimen is achieved. Towards the end of the test, the resistance increases significantly, indicating that the damage is increasing in the form of propagating delaminations until failure occurs.

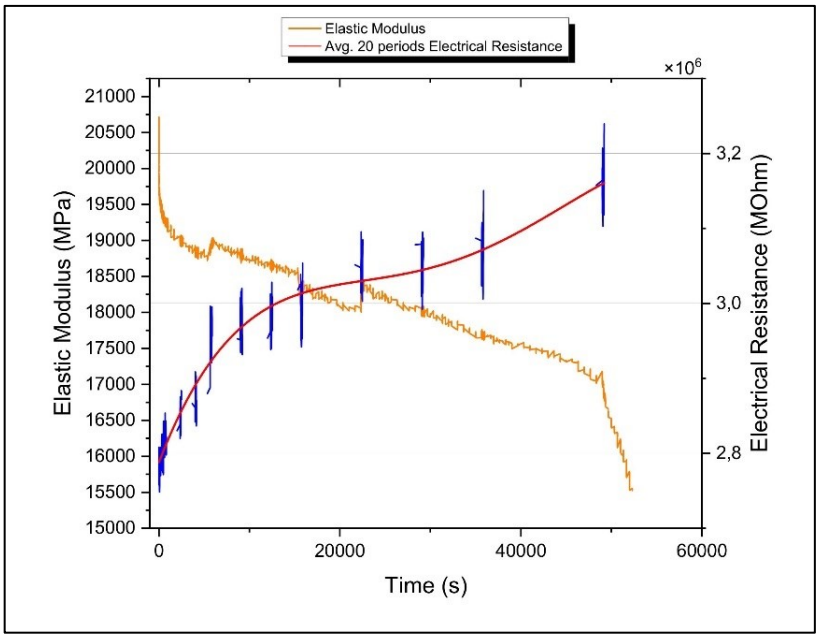

Figure 3.5 - Graph obtained from the fatigue test of a hand-made cross-ply laminate, with a fracture cycle count of 158000 cycles.

The second type of fatigue tests was conducted using the same equipment but with different methods and objectives. The aim of these new tests is to obtain all the necessary data for validating the analytical model, specifically the trend of the elastic modulus E, the values of the increase in resistance R, and the value of crack density ρ. The tests were performed at the same load levels as the previous ones, specifically at 20%, 30%, and 40% of the ultimate tensile strength, while maintaining a load ratio R = 0.1. The difference in this case is that crack density was measured at precise intervals until crack saturation was achieved. From various tests conducted, it was observed that saturation was reached before 5,000 cycles, and optimal intervals for observing crack density were identified as follows:

Fatigue Test - cycles
50
100
200
500
1000
5000

Table 3.3 - Number of cycles at which the test was interrupted to measure the crack density.

The methods for measuring resistance and crack density used are similar to those previously described. As output from this type of test, graphs are obtained showing all the values of elastic modulus E, resistance R, and crack density ρ that are useful for validating the analytical model. Below is an example of a graph where the trend of the elastic modulus is shown in orange, the trend of resistance is shown in red, and that of crack density is shown in green. It is clear from this graph that an increase in crack density corresponds to an increase in the electrical resistance of the specimen.

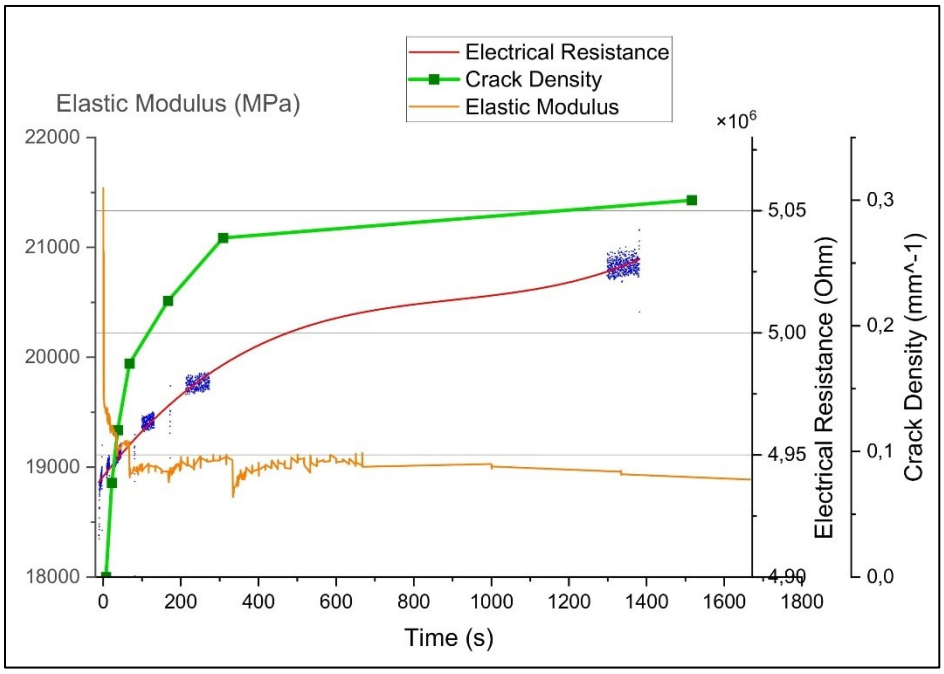

Figure 3.6 - Graph resulting from the fatigue tests used to obtain data for validating the analytical model.

3.3 Electrical resistance measurement

During the tests, the electrical resistance of the conductive specimens was measured, having been properly wired and prepared in advance. The measurements were conducted using the Keithley 2636B device. With this instrument, the electrical resistance was measured by applying a voltage of 1 Volt and a current of

0,5 Amperes across the terminals of the specimen. These parameters were kept constant for all the tests performed.

Figure 3.7 - Keithley 2636b for the electrical resistance measurement.

During the tests, the electrical resistance was measured under two different conditions: in the loaded case, with the specimen under load, and in the unloaded case, with the specimen unloaded. Furthermore, before the commencement of any testing, the the electrical resistance R_0 of the virgin specimen was measured by applying a load of 0.25 kN, corresponding to a stress of 5 MPa and a strain of 0.025%. This choice was made because it yielded data that was less affected by noise and overall more accurate. What has been done is not entirely precise, as, under load conditions, the specimen strain ranges between 0.7% and 1.0%. For a more accurate measurement, in the unloaded condition, the electrical resistance should have been measured at 0% strain. However, since the piezoresistive effect is minimal (as demonstrated in Section 3.3.2, *Electrical Resistance Measurement in Static Test*), the error observed in this type of measurement remains limited.

Significant variability in R_0 values was observed among the various panels, as well as among specimens belonging to the same laminate. An example is presented in the table below, where the variability in R_0 resistance values for a hand-laminated panel and a quasi-isotropic panel can be observed:

HL_3		QI_3	
Provino	**R0 (Ohm)**	**Provino**	**R0 (Ohm)**
HL_3_1	78804.6	QI_3_1	1551.6
HL_3_2	66307.6	QI_3_2	1373.2
HL_3_3	162017.7	QI_3_3	1200.9
HL_3_4	87127	QI_3_4	1142
HL_3_5	282264.5	QI_3_5	1208.8
HL_3_6	50013.3	QI_3_6	1112.7
HL_3_7	184366.6	QI_3_7	1110.6
HL_3_8	142095.9	QI_3_8	1267.9
HL_3_9	134030.3	QI_3_9	1386.2

Table 3.4 - Example of R0 values for a hand laminated plate and a quasi-isotropic plate.

It is observed that the resistance values for the hand-laminated panel are significantly higher and more variable compared to those of the quasi-isotropic laminate. Such a marked difference and variability in R_0 values can be attributed to three factors:

1. Different material configurations: The hand-laminated specimens inevitably exhibit a greater and less uniform quantity of resin compared to the plates laminated using a roll mill, resulting in a more variable resistance value. Furthermore, the various plates were manufactured at different times with different batches of resin.
2. Different types and quantities of nanotubes used: In the cross-ply laminates, carbon nanotubes produced by FlyCarbon were utilized at a quantity of 0.2% by weight of the resin. For the quasi-isotropic laminates, nanotubes from Ocsial were used at 0.25% by weight, as previous tests indicated that these nanotubes were less conductive than the former at equal quantities. These differences resulted in the quasi-isotropic laminates being much more conductive, with resistances on the order of thousands of Ohms, in contrast to the cross-ply laminates, which often exhibited resistances on the order of hundreds of thousands of Ohms.
3. Distribution of nanotubes within the resin: Significant variation in resistance was observed even in specimens taken from the same panel. This is likely

caused by an imperfect distribution of nanotubes within the resin; indeed, despite the extensive dispersion process conducted using the three-roll mill, single-wall nanotubes tend to easily form microscopic agglomerates, which affect the electrical performance of the final material.

Resistance measurements were conducted using different methodologies during static and fatigue tests. The various types of methodologies are described in detail in the following sections.

3.3.1 Electrical resistance measurement in fatigue test

After measuring the electrical resistance R_0 of the virgin specimen, additional measurements were taken during the fatigue test cycles to obtain the measurements for the loaded case. The measurements were performed at a sampling frequency of 10 Hz, allowing for the collection of R values at all stages of the loading cycle. Measurements were initiated approximately one minute before reaching the target number of cycles in order to pause the test and measure the crack density. Once the established number of cycles was reached, the machine reduced the load on the specimen, applying a force of 0,25 kN, which corresponds to an approximate stress of 5 MPa on the specimen and a strain equal to 0,025%. Under these conditions, resistance measurements for the unloaded case were conducted. The measurements were taken at this low load rather than with the specimen completely unloaded because this condition yielded more precise results with less noise.

As a result of these measurements, Resistance vs. Time graphs were obtained, illustrating the variation in resistance throughout the loading cycle, from which useful data were extracted for the verification of the model.

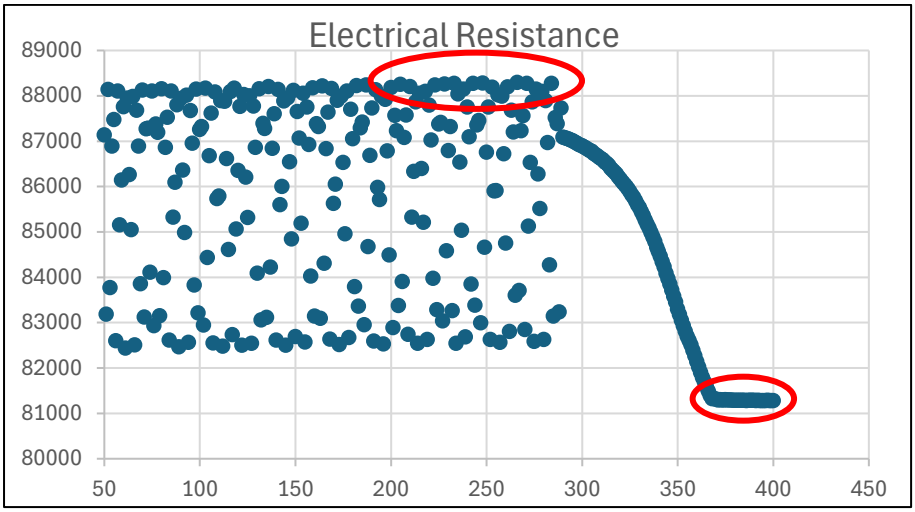

Figure 3.8 - Graph of Resistance/Time during the fatigue test. The highlighted data points represent those considered for the Loaded and Unloaded cases, respectively.

For the loaded case, to obtain an accurate measurement of the electrical resistance, it is essential to consider all measured values at the same level of strain. For this reason, only the maximum values recorded in close proximity to the end of the test were considered, and an average was taken. This approach allowed for the calculation of the loaded resistance at the established number of cycles.

3.3.2 Electrical resistance measurement in static test

The electrical resistance was continuously measured during all loading ramps. For the unloaded case, the resistance was measured while the specimen was subjected to a stress of 5 MPa for the reasons previously explained. For the loaded case, the maximum peak resistance measured during the tests for each loading ramp was used.

To obtain the most accurate measurements possible, efforts were made to quantify the contribution of the piezoresistive effect of the material. This phenomenon leads to an increase in electrical resistance throughout the material due to strain, rather than the opening of cracks. To exclude the contribution of the piezoresistive effect, the increase in current was measured with the specimen subjected to the same level of strain. The maximum strain obtained from the first ramp was used as the reference value, approximately equal to $\varepsilon = 0{,}4\%$. By measuring the resistance at

the same level of strain, any increase in resistance can be attributed solely to the increase in the number of cracks.

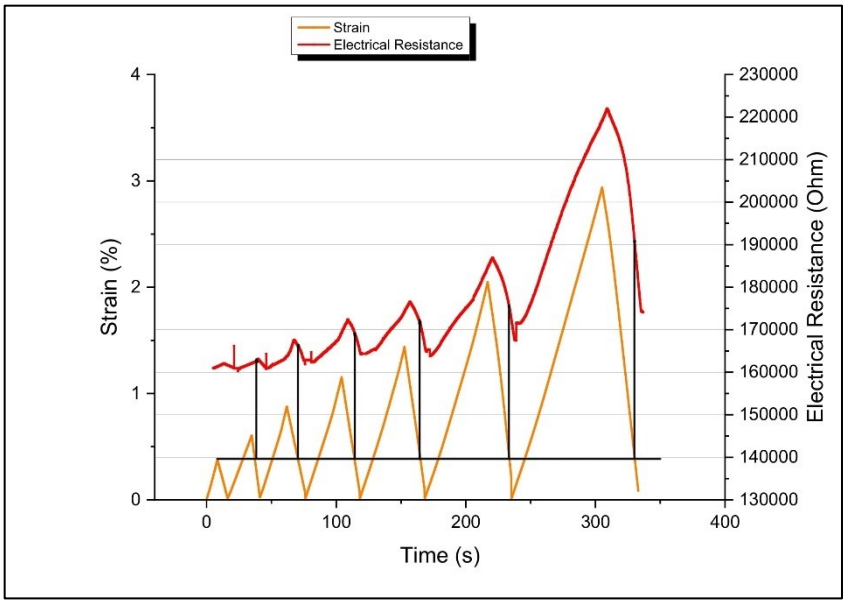

Figure 3.9 - Graph showing how the electrical resistance values were obtained at the same strain level.

Subsequently, the resistance values obtained were compared, taking into account or excluding the piezoresistive effect.

Including the contribution of the piezoresistive effect			**Excluding the contribution of the piezoresistive effect**		
Electrical Resistance (Ohm)					
Specimen	**HL_3_3**	**HL_3_6**	**Specimen**	**HL_3_3**	**HL_3_6**
R0	142095	50013	R0	142095	50013
R1	144459	50324	R1	144557	50024
R2	145390	50711	R2	144989	50422
R3	150540	52053.3	R3	147509	51488.1
R4	155984	53357.8	R4	151509	52158
R5	161447	54759.6	R5	154880	53345
R6	171347	57648	R6	157457	55102

Table 3.5 - Values of the resistance of two specimens calculated first by including the contribution of the piezoresistive effect and then by excluding its contribution.

The table presents two example specimens to compare the resistance data calculated at each loading ramp, initially including the contribution of the piezoresistive effect and subsequently excluding it.

Load ramps (Mpa)	Average difference with or without consideration of the piezoresistive effect
R0	0.00%
R1	0.26%
R2	0.42%
R3	1.55%
R4	2.56%
R5	3.33%
R6	6.26%

Table 3.6 - Percentage difference including the piezoresistive effect.

The calculations indicate that including the piezoresistive effect in the results leads to a maximum increase in resistance of approximately 6% in the worst-case scenario, which occurs during the last loading ramp when the highest stress is reached. In the other ramps, the difference is less than or equal to 3%.

Given that the difference is relatively small, it was decided for the sake of simplicity to include the contribution of the piezoresistive effect in the results. This approach facilitates a more straightforward and quicker data processing, avoiding additional steps that could introduce potential sources of error.

4 Results and Discussion

The objective of this thesis is to validate the analytical model for health monitoring of cross-ply laminates [1] and to tabulate the typical values of the parameter φ for each configuration of cross-ply laminates. For quasi-isotropic laminates, the aim is to gather as much data as possible to enhance the understanding of additional existing models [9]. These data are also valuable due to the limited number of studies on this topic in the literature. Additionally, it is of interest to observe the mechanical behavior of the resin produced by adding the natural hardener L-Arginine, as there is a scarcity of related studies in the current literature.

4.1 Preliminary considerations

Certain considerations must be addressed before proceeding with the analysis of the results.

Firstly, the initial set of laminates created with modified resin contained a nanotube concentration below the minimum threshold required for conductivity. In this first set, 0,05 wt% of single-wall CarbonFly nanotubes were used, which was subsequently increased to 0,2 wt% in the following sets. As a result, the first set of modified plates, designated HL_1 and RM_1, was discarded, as it was not possible to measure electrical resistance. Furthermore, these plates were not subjected to mechanical testing, since the differing nanotube content would alter their mechanical properties relative to the other plates.

Secondly, an effort was made to achieve a constant volumetric fraction for all laminates, set at: $V_f = 53\%$. Achieving an optimal volumetric fraction was relatively straightforward for the laminates produced using the roll mill process, as once the machine was calibrated, the amount of resin per layer remained consistent. For the hand-made laminates, however, the volumetric fraction values were more variable. This variability was due to fluctuations in the amount of resin applied to each layer, arising from the inherent imprecision of manual work. The first set of

hand-made laminates exhibits an average volumetric fraction across the laminates of: $V_f \cong 62\%$. In the second set, an attempt was made to increase the resin content, reaching an average of: $V_f \cong 40\%$. All these factors were taken into account in the subsequent analyses and discussions.

For the quasi-isotropic laminates, Ocsial single-wall carbon nanotubes were used, differing from those employed for the cross-ply laminates. This choice was not optimal but became necessary due to the depletion of the CarbonFly nanotube supply. It is known from experience that Ocsial nanotubes tend to make the resin less conductive compared to the previously used nanotubes. To compensate for this, a higher concentration was used, increasing from 0,2 wt% to 0,25 wt% by resin weight. This increase in nanotube content resulted in the quasi-isotropic laminates' resin being significantly more conductive than that of the cross-ply laminates. On the other hand, in this case, the variations in resistance across different laminates were much lower than those observed in the previous plates.

Finally, the data collected for the quasi-isotropic laminates are insufficient to validate the existing damage prediction models [9]. Indeed, this model does not account for the formation of delaminations within the laminate, whereas significant delaminations between the layers were observed during testing, starting from the first loading cycles.

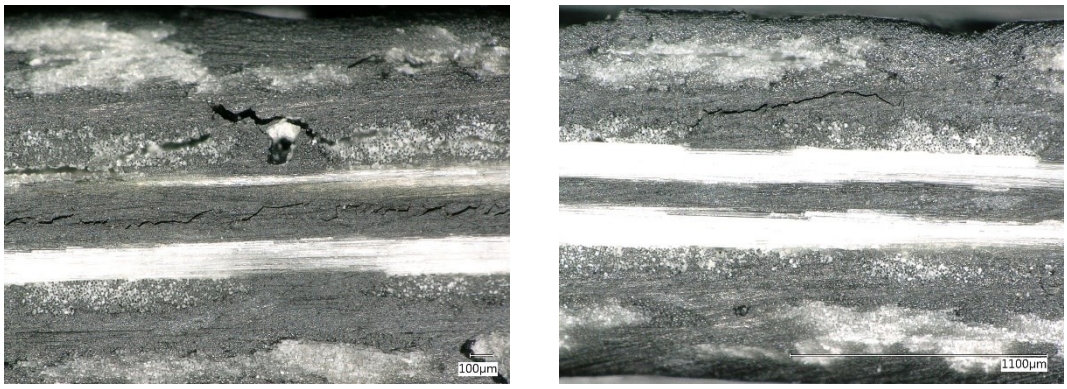

Figure 4.1 - Microscope image of quasi-isotropic laminates. Numerous delaminations are present from the initial loading cycles.

4.2 Fatigue test results

To better understand the fatigue behavior of the material, given the use of the natural hardener L-Arginine in its fabrication, some specimens were tested under fatigue loading until failure, constructing the Wohler curve for each material configuration.

There are various methods for studying the fatigue life of composite materials; one simplified approach is to use the Wohler curve, as is done for metallic materials. The difference lies in the fact that, in composites, phenomena related to oligocyclic fatigue (i.e., failure under low-cycle high-load conditions) are not observed. Furthermore, there is no fatigue limit, meaning there is no stress level beyond which the component has an infinite life. The Wohler curve is described by the following equation:

$$\sigma = A \cdot N_f^{-\frac{1}{k}} \tag{4.1}$$

Where σ is the maximum stress of the cycle to which the component was subjected. A is a constant that can be determined experimentally, indicating the degree to which the Wohler curve is shifted to the right or left on the graph; a higher value of A means the curve is shifted more to the right, indicating that the component has a better fatigue life. k represents the inverse slope of the curve, with a higher k value indicating that the number of cycles to failure increases rapidly with a decrease in the maximum cycle stress. All these values were determined experimentally. It should be noted that the tests were conducted with a load ratio R = 0.1, and the specimens were tested at three different stress levels, namely 40%, 30%, and 20% of the ultimate tensile strength.

4.2.1 Fatigue result Cross-Ply laminates

The Cross-Ply laminates have a tensile strength of $\sigma_f \cong 500\ Mpa$, thus, the tests were conducted with maximum stresses of 200, 150, and 100 MPa. Four laminate configurations were tested:

- Roll Mill Unmodified: specimens manufactured using the roll mill machine, which consist of fiber layers with backing fibers and resin unmodified by nanotubes, were tested to failure. The following specimens were tested:

Roll Mill (u)	σmax	Nf
RM_2_8u	200	9095
RM_2_7u	200	9748
RM_2_2u	150	31149
RM_2_4u	150	29354
RM_2_1u	150	44300
RM_2_5u	100	924318
RM_2_6u	100	609443

Table 4.1 - Table illustrating the unmodified roll mill specimens tested under fatigue.

- Hand Laminated Unmodified: specimens manually fabricated with resin unmodified by nanotubes, consisting of unidirectional fiber layers without backing fibers, were tested to failure. The following specimens were tested:

Hand Laminated (u)	σmax	Nf
HL_1_7u	200	50550
HL_1_9u	200	25827
HL_1_4u	150	238243
HL_1_8u	150	395223
HL_1_3u	100	2000000

Table 4.2 - Table illustrating the unmodified hand laminated specimens tested under fatigue.

- Roll Mill Modified: specimens manufactured using the roll mill machine, consisting of fiber layers with backing fibers and resin modified with the addition of 0,2 wt% of single-wall CarbonFly carbon nanotubes, were tested to failure. The following specimens were tested:

Roll mill	σmax	Nf
RM_2_5	200	2428
RM_2_6	200	3465
RM_2_7	150	10211
RM_2_7	150	12011
RM_2_3	150	25307
RM_2_8	100	443513

Table 4.3 - Table illustrating the modified roll mill specimens tested under fatigue.

- Hand Laminated Modified: specimens manually fabricated with resin modified by the addition of 0,2 wt% of single-wall CarbonFly carbon nanotubes, consisting of unidirectional fiber layers without backing fibers, were tested to failure. The following specimens were tested:

Hand Laminated	σmax	Nf
HL_2_3	200	18116
HL_2_7	200	9672
HL_2_1	150	158091
HL_2_4	100	2000000

Table 4.4 - Table illustrating the modified han laminated specimens tested under fatigue.

All the tests performed are summarized in the following graph, in which clear trends are evident.

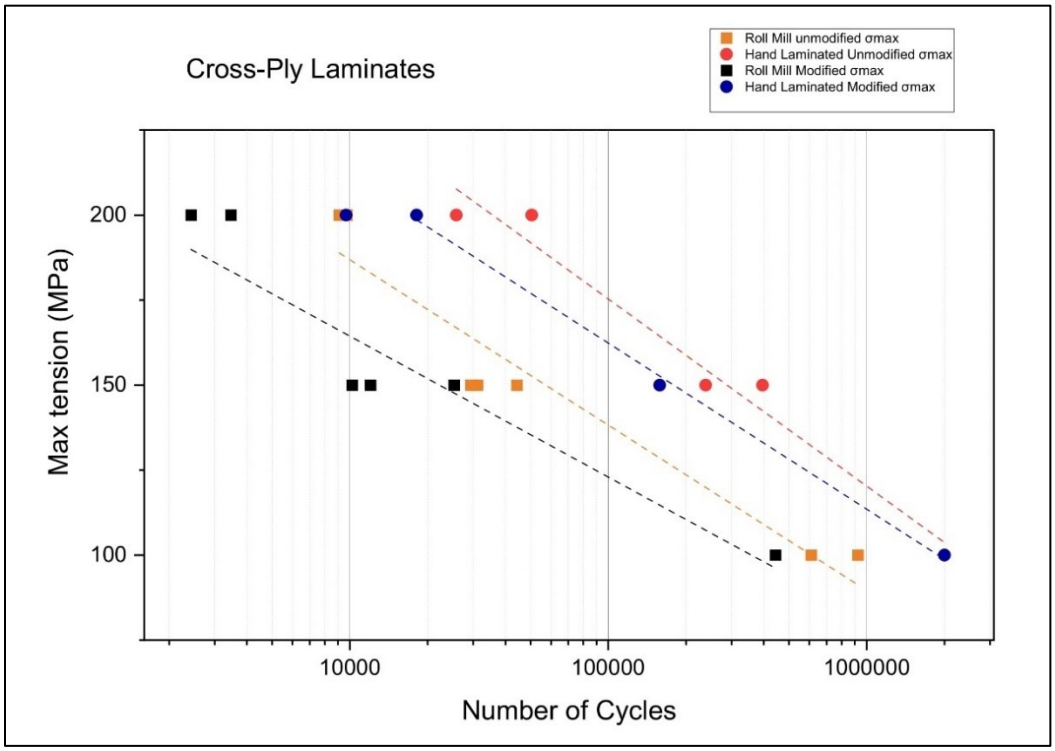

Figure 4.2 – Fatigue test result Cross-Ply laminates.

From the collected data, it is possible to derive the parameters of the Wohler equation for each type of specimen. To calculate the slope k, at least two tests for the same type of specimen are required to determine the number of cycles to failure, after which the following formula can be applied:

$$k = \frac{\log(N_2) - \log(N_1)}{\log(\sigma_1) - \log(\sigma_2)} \tag{4.2}$$

Where "log" represents the logarithm to base 10, while $N_1, N_2, \sigma_1, \sigma_2$ are obtained experimentally from the tests. Once k is calculated, it is then possible to derive the constant A from *Equation (4.1)*. To obtain more accurate results, the value of the slope k was calculated for each possible pair of tests, and the average of the obtained results was taken. The following values were obtained:

Type	k	A
Roll Mill (u)	6.62	756.3
Hand Laminated (u)	6.21	1097
Roll mill	7.52	555.9
Hand laminated	7.41	723.2

Table 4.5 - Table summarizing the slope k values and constant A of the Wohler curve for Cross-Ply laminates.

The graph shows that the hand-made laminates performed significantly better than those produced using the roll mill, as they exhibit a higher value of the constant A compared to the corresponding roll mill versions. This is likely due to the fact that the fiber layers in the hand-made laminates are unidirectional, in contrast to the layers in the roll mill laminates, which include backing fibers. However, it is also observed that the laminates produced via the roll mill have higher inverse slope k values than their hand-made counterparts. This indicates that, for a decrease in the maximum cycle stress, the roll mill laminates show a greater increase in fatigue life compared to the hand-made ones, although still lower overall.

Moreover, it is noted that, in general, the laminates with resin modified by nanotubes performed worse than their unmodified counterparts, showing lower A values but a higher inverse slope k. This result, not entirely expected and inconsistent with what is observed in the literature, may be due to suboptimal dispersion of the nanotubes within the resin. The formation of large agglomerates could lead to stress concentration and act as initiation sites for cracks. This hypothesis aligns with the fact that the electrical resistance measured varies significantly, even among specimens within the same laminate, as explained in *Chapter 3.3: "Electrical Resistance Measurement"*. Nevertheless, these tests provide valuable data for the study of the behavior of more sustainable resins, particularly the natural hardener L-Arginine, as there are few other studies on this topic in the literature.

4.2.2 Fatigue result Quasi-Isotropic laminates

For the quasi-isotropic laminates, the same calculations and steps applied to the previous type of specimens were performed.

The quasi-isotropic laminates exhibit a tensile strength of $\sigma_f \cong 350\ Mpa$, thus, the tests were conducted with maximum stresses of 140, 110, and 70 MPa. Two laminate configurations were tested:

- Roll Mill Unmodified: specimens manufactured using the roll mill machine with unmodified resin. The following specimens were tested to failure:

Quasi Isotropic (u)	σmax	Nf
QI_1_7 (u)	140	38535
QI_2_7 (u)	110	414854
QI_1_9 (u)	110	150569
QI_2_2 (u)	70	2000000

Table 4.6 - Table illustrating the unmodified roll mill specimens tested under fatigue.

- Roll Mill Modified: specimens manufactured using the roll mill machine with resin modified by the addition of 0,25 wt% of single-wall Ocsial carbon nanotubes. The following specimens were tested to failure:

Quasi Isotropic	σmax	Nf
QI_4_7	140	20150
QI_3_4	140	8845
QI_4_4	140	16892
QI_3_3	140	4095
QI_3_5	140	8305
Q_I_4_1	110	275004
QI_3_1	70	1800000

Table 4.7 - Table illustrating the modified roll mill specimens tested under fatigue.

It is noted that many more specimens were tested with a maximum cycle stress at 40% of the tensile strength compared to the other load levels. This is because tests at this stress level were useful for understanding the material's behavior in order to conduct the subsequent model validation tests.

All the tests performed are summarized in the following graph:

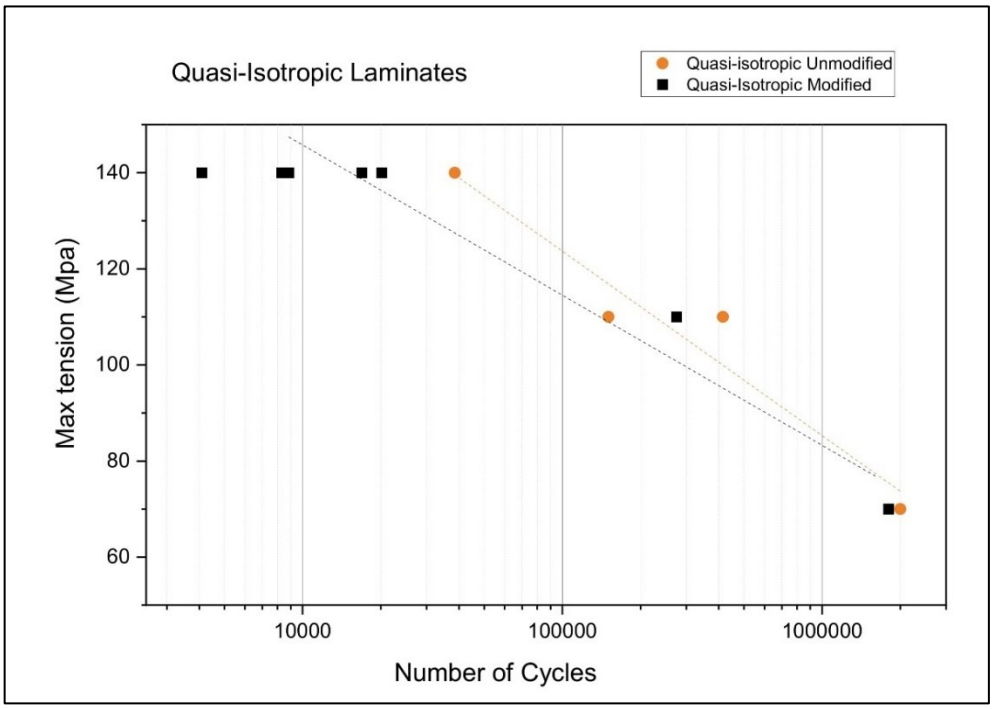

Figure 4.3 - Fatigue test result Quasi-Isotropic laminates.

From the collected data, it is possible to derive the parameters of the Wohler equation for each type of specimen, similar to the procedure already performed for the Cross-Ply specimens. The inverse slope k was calculated from the *Equation (4.2)* and the constant A from the *Equation (4.1)*, obtaining the following results:

Type	k	A
Roll Mill (u)	6.024096386	826.3
Roll mill	8.928571429	388.8

Table 4.8 - Table summarizing the slope k values and constant A of the Wohler curve for Quasi-Isotropic laminates.

The results show that, similarly to what was observed for the Cross-Ply specimens, the laminates with unmodified resin performed better, especially in the tests conducted at high maximum load. Similarly, the modified laminates exhibit a higher inverse slope k, achieving comparable fatigue lives in the tests performed at medium and low loads. Unfortunately, the number of specimens tested is limited and insufficient for more in-depth considerations.

4.3 Analytical Model Validation - Fatigue tests

The main objective of this thesis is to validate the analytical model for the health monitoring of cross-ply laminates [1] for the correlation between internal damage and stiffness degradation of a laminate. As previously introduced, there are other more general models [9] also for the validation of quasi-isotropic laminates, but the data collected and the internal delaminations that occurred during the tests make it impossible to apply such a model to this type of laminate. For this reason, the focus will be primarily on the cross-ply laminates.

In the initial fatigue tests performed, it was observed that the electrical resistance measured at the ends of the specimen increases with the number of cycles. This was observed in every test conducted and for each specimen configuration. From the initial tests, various types of graphs were derived, with continuous resistance measurements taken for the faster tests and intermittent measurements for the longer ones.

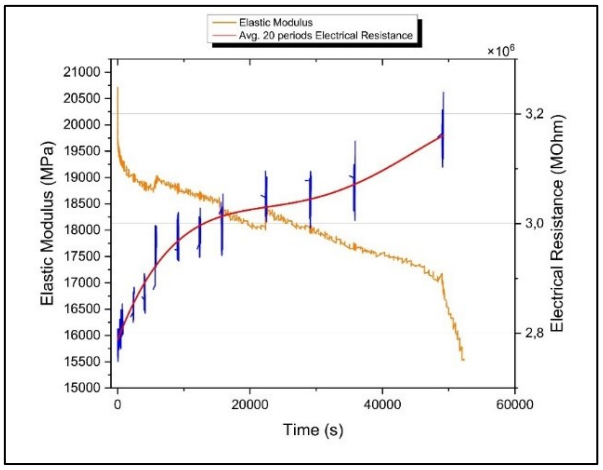

Figure 4.4 - Fatigue graph of specimen: HL_2_1, tested at 15-150 Mpa, intermittent resistance measurement, Nf = 158091 cycles.

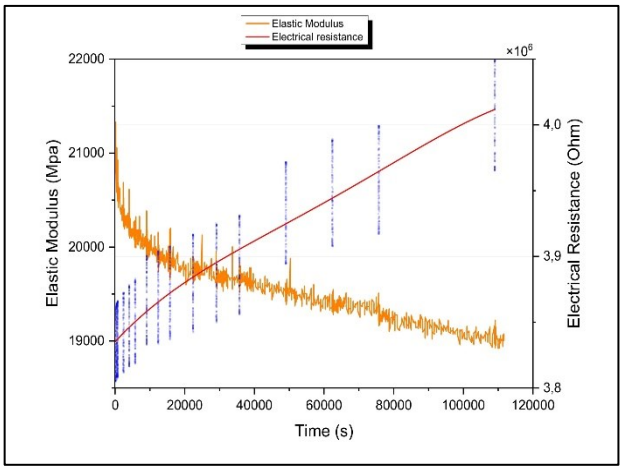

Figure 4.5 - Fatigue graph of specimen: RM_2_8, tested at 10-100 Mpa, intermittent resistance measurement, Nf = 443513 cycles.

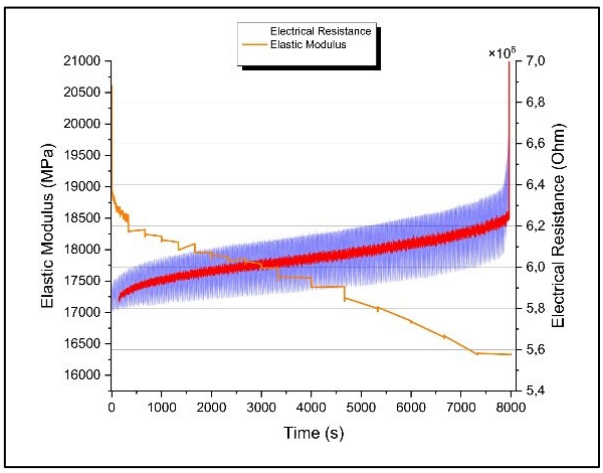

Figure 4.6 - Fatigue graph of specimen: RM_2_3, tested at 15-150 Mpa, continuous resistance measurement, Nf = 25307 cycles.

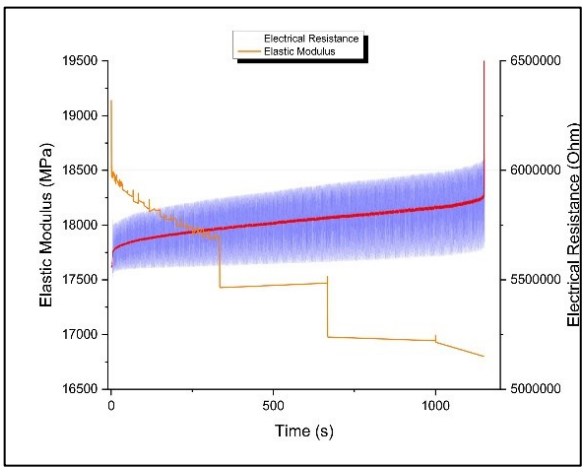

Figure 4.7 - Fatigue graph of specimen: RM_2_6, tested at 20-200 Mpa, continuous resistance measurement, Nf = 3465 cycles.

In the graphs above, the blue bands indicate the fluctuation of the electrical resistance during a single loading cycle of the fatigue test. The red line represents the moving average in graphs where the measurement is continuous and its trend in tests where the measurement is intermittent. In the reported graphs, a clear evolution of the electrical resistance during the tests is visible, which reflects the typical damage progression seen in composite materials. Specifically, a rapid increase in electrical resistance is observed during the first load cycles, followed by

an intermediate phase where the resistance reaches a sort of plateau, and finally, a sharp rise in resistance occurs just before the laminate reaches failure.

The hypothesis of a correlation between damage progression and the increase in electrical resistance is further confirmed in subsequent tests, where material damage was assessed by observing the crack density during the fatigue test. The following graphs present the results of tests on a hand-laminated specimen and one fabricated using the roll mill.

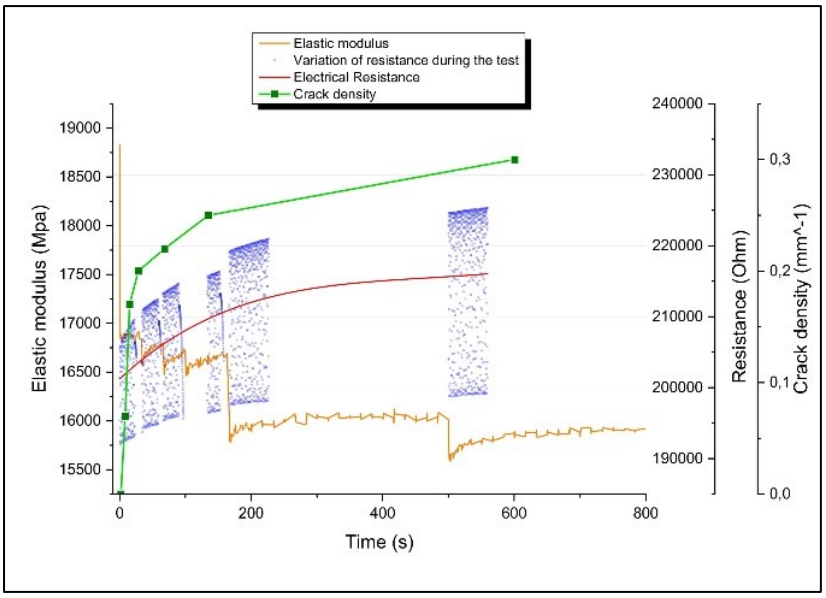

Figure 4.8 - Specimen HL_3_7, tested from 15 to 150 MPa with crack density monitoring during the test.

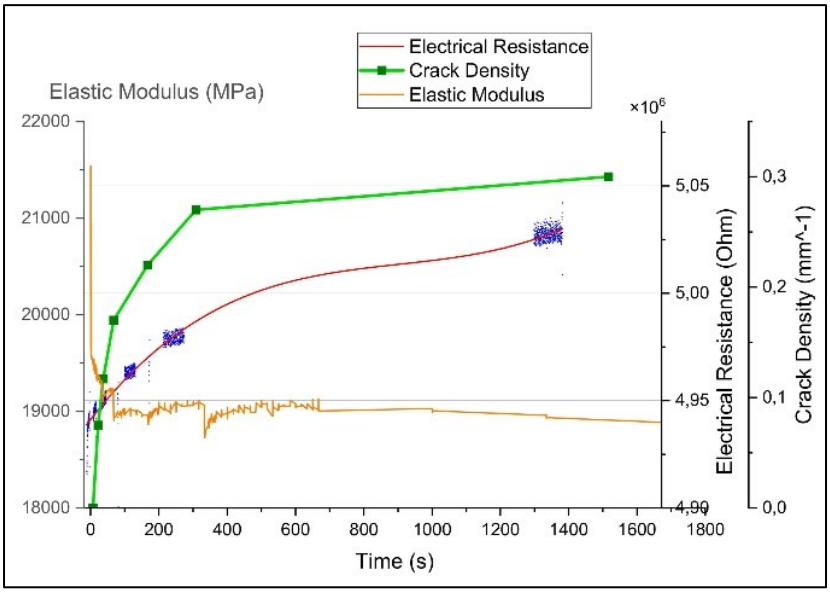

Figure 4.9 - Specimen RM_2_1, tested from 15 to 150 MPa with crack density monitoring during the test.

Compared to the previous graphs, the latter include the crack density data, represented in green. As can be seen, the crack density increases rapidly during the very first load cycles, stabilizing around a value of 0.3 mm^{-1}. This is perfectly consistent with the typical damage progression in composite materials, where the number of cracks in the laminate grows rapidly during the initial load cycles, eventually reaching saturation in a short time. In this case, crack saturation occurs around 5000 cycles. The electrical resistance follows a very similar trend, also stabilizing at a relatively constant value around 5000 cycles, corresponding to the point of crack saturation. An increase in electrical resistance was also recorded in the unloaded case, i.e., measured on the unloaded specimen, with a trend similar to that observed for the loaded specimen, as shown in the graphs.

In the loaded case, a higher average increase in electrical resistance was recorded compared to the unloaded case between the start and end of the test. Additionally, differences were observed between hand-laminated specimens and those made with the roll mill.

Plates	ΔR_{LOADED}	$\Delta R_{UNLOADED}$
Hand Laminate	18,49%	10,11%
Roll Mill	6,95%	1,75%

Table 4.9 - Table that shows the increment of electrical resistance in loaded and unloaded case.

The hand-laminated specimens show an increase in resistance nearly three times higher compared to the other type, likely due to the higher resin content within the hand-laminated layers. However, the most interesting aspect lies in the difference between the delta loaded and delta unloaded: in the loaded case, it is significantly higher. This observation was found in all tested specimens and indicates the sensitivity of electrical resistance to the load applied to the specimen. This means that, when the specimen is loaded, the cracks appear "open"; as a result, the so-called "bridging" phenomenon by the nanotubes occurs less frequently. Nanotube bridging refers to the tendency of the nanotubes to create conductive pathways through the cracks, thus limiting the increase in electrical resistance of the laminate despite the same level of damage.

Therefore, estimating the sensitivity of a laminate to damage is crucial for better understanding the increase in electrical resistance and the consequent loss of stiffness. In the analytical model [1] this task is fulfilled by the parameter φ, which takes a value between 0 and 1 for each laminate. A φ value of 1 indicates that the laminate is completely insensitive to damage; in this case, cracks within the laminate do not cause any increase in electrical resistance. Conversely, when φ is equal to 0, the laminate is fully sensitive, meaning that even a few cracks will result in a marked increase in electrical resistance. To validate the model, the goal is to calculate the value of φ for various laminate configurations.

For the verification of the analytical model [1], Through fatigue testing, a total of nine specimens were tested, belonging to three different laminates. Specifically, two specimens of the laminate made using the roll mill (RM_2), four specimens of the hand-laminated laminate (HL_3), and three specimens of another hand-laminated laminate (HL_4) were tested. The process began by calculating all the necessary data for each individual specimen, as explained in the previous chapters, and then these were used within the model formula. The model is divided into two parts:

$$\frac{R_x}{R_{x0}} = 1 + (1-\varphi)\cdot\frac{2\rho}{\alpha}\cdot\frac{\eta_x^0}{\eta_x^{90}}\cdot\frac{h_{90}}{h_0}\cdot\tanh\frac{\alpha}{2\rho} \tag{4.3}$$

$$\frac{E_x}{E_{x0}} = \left\{1 + k\cdot\frac{E_2}{E_1}\cdot\frac{h_{90}}{h_0}\cdot\frac{\alpha}{\xi}\cdot\frac{\left(\frac{R_x}{R_{x0}}-1\right)}{\left[\omega^{5/2}-\left(\frac{R_x}{R_{x0}}-1\right)^{5/2}\right]^{2/5}}\cdot\tanh\left(\frac{\xi}{\alpha}\cdot\frac{\left[\omega^{5/2}-\left(\frac{R_x}{R_{x0}}-1\right)^{5/2}\right]^{2/5}}{\left(\frac{R_x}{R_{x0}}-1\right)}\right)\right\}^{-1} \tag{4.4}$$

Equation (4.3) represents the electrical part of the model. Using this formula, the sensitivity of the material to damage is determined, specifically the parameter φ for the specimen. *Equation (4.4)* represents the electromechanical part of the model, where this formula correlates the increase in electrical resistance with the loss of

stiffness of the laminate. The parameter φ, previously obtained, indirectly influences *Equation (4.4)*, since it is necessary for the calculation of ω.

For each of the tested specimens, the value of φ, the value of r^2 to indicate how accurate the predictions of the analytical model are, and the standard deviation, to give an indication of how much the calculated φ value can vary, were calculated. It was computed using the following formula:

$$Std\ Dev = \left(\frac{1}{n-1}\right) * ri^2 \tag{4.5}$$

Where *ri* is the sum of the residuals, i.e., the sum of the differences between experimental and analytical data. The term *n* represents the number of data pairs used, which in this thesis typically ranges between six and eight, depending on the acquired data.

4.3.1 Hand Laminated: HL_3

These considerations were made for both the Loaded and Unloaded cases. Starting with the HL_3 laminate, four specimens were tested: HL_3_1, HL_3_4, HL_3_5, HL_3_7. The table below summarizes the values of φ, standard deviation, and r^2 calculated for the Loaded case:

HL_3 - Fatigue Loaded				
Specimen	**φ**	**Std Dev Electrical Model**	**Std Dev Electromechanical Model**	**r^2**
HL_3_1	0.6268	±0.0214	±0.0069	0.8088
HL_3_4	0.5834	±0.0179	±0.0144	0.8754
HL_3_5	0.5155	±0.0145	±0.0099	0.955
HL_3_7	0.5361	±0.0187	±0.0030	0.8742
HL_3	0.5993	±0.0088	±0.0026	0.8827

Table 4.10 - Values of φ, standard deviation, and r2 for HL_3 laminate, fatigue tested. Loaded case.

It can be observed that all the samples have similar values of φ, with a high r^2, indicating that the model predictions accurately replicate the experimental results. The standard deviation indicates the range within which the φ parameter varies. Furthermore, the calculations show that, when moving from the electrical model to the electromechanical model, the error, understood as the standard deviation, decreases in all tested samples.

Individual graphs of the electrical and mechanical models were also obtained for each sample, where experimental data are compared with the calculated values. Here is an example of the electrical and electromechanical model graph for a single sample. For all other samples, please refer to the appendix at the end of the thesis.

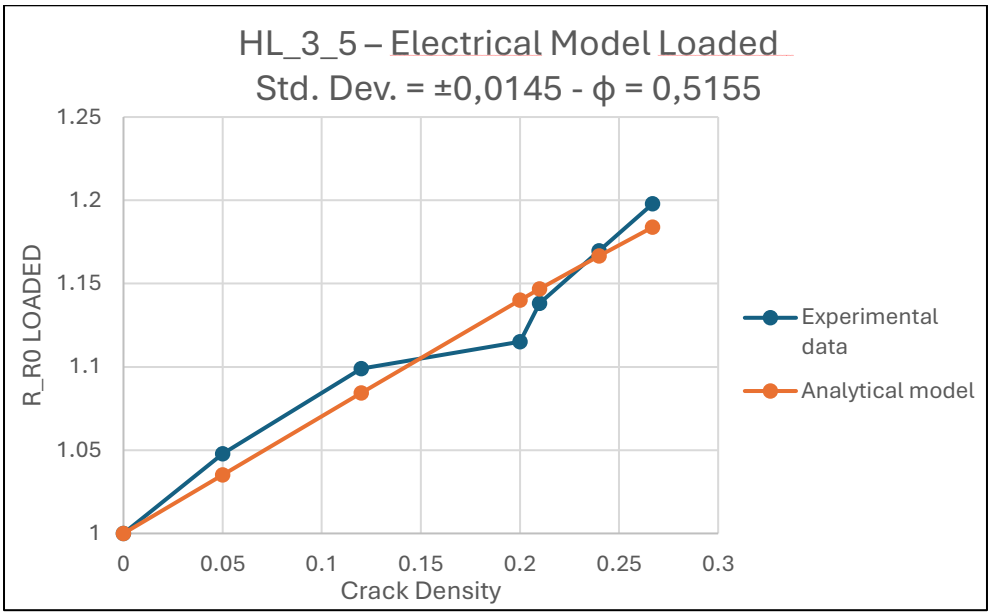

Figure 4.10 - Example of the electrical model graph calculated for each specimen. HL_3_5, fatigue test, loaded case.

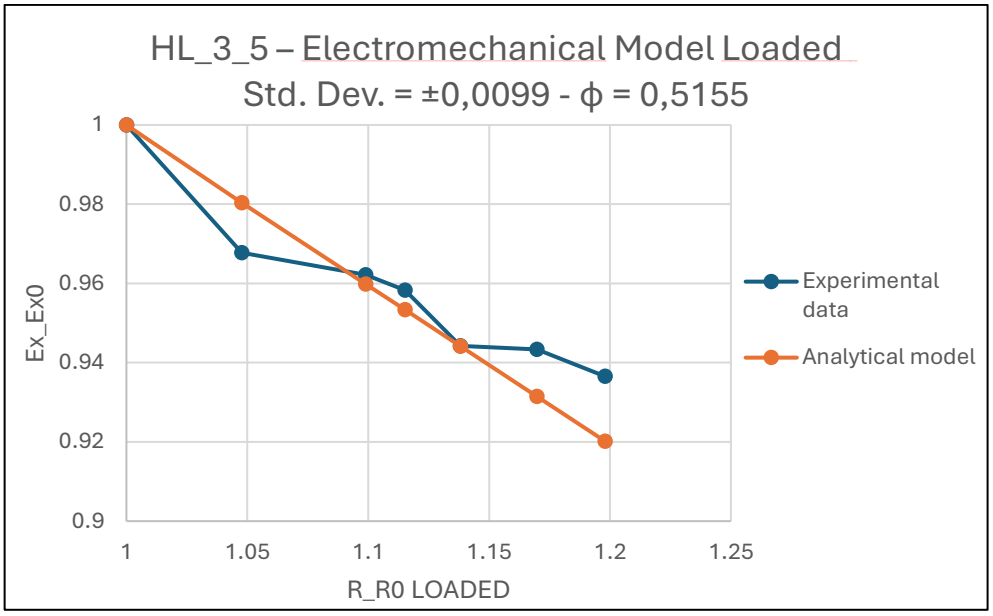

Figure 4.11 - Example of the electromechanical model graph calculated for each specimen. HL_3_5, fatigue test, loaded case.

In the last row of *Table 4.10* the values of φ, r^2, and the overall standard deviation are calculated for the HL_3 plate. By combining the values obtained for each sample, the result is a φ value of 0,5718, with a variation of ±0,0088 for the Electrical model and a variation of ±0,0026 for the Electromechanical model. The r^2 value of 0,8827 indicates that the model's predictions replicate the obtained data with high accuracy.

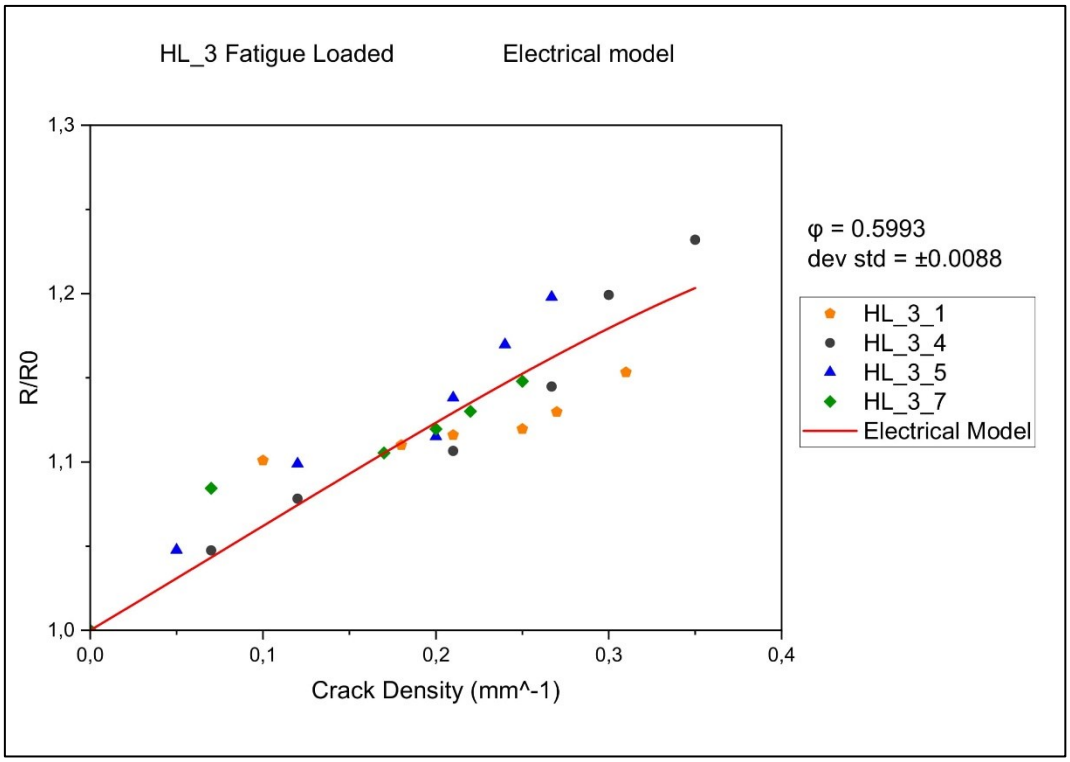

Figure 4.12 - Validation of the electrical model for laminate HL_3, fatigue tested, loaded case.

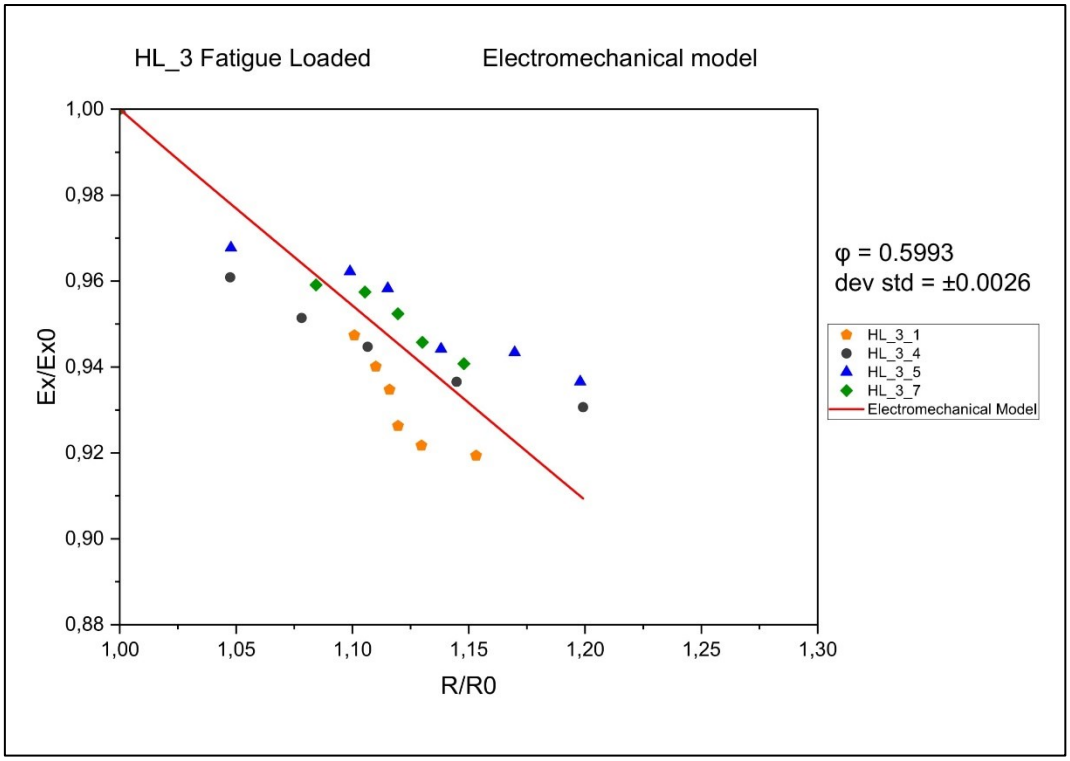

Figure 4.13 - Validation of the electromechanical model for laminate HL_3, fatigue tested, loaded case.

Therefore, it has been verified that the model works for the HL_3 plate in the loaded case.

For the unloaded case, the following results were obtained:

HL_3 - Fatigue Unloaded				
Specimen	**φ**	**Std Dev Electrical Model**	**Std Dev Electromechanical Model**	**r^2**
HL_3_1	0.7863	±0.0126	±0.0066	0.7932
HL_3_4	0.7889	±0.0066	±0.0124	0.9650
HL_3_5	0.5876	±0.0142	±0.0128	0.9503
HL_3_7	0.7286	±0.0135	±0.0026	0.7990
HL_3	0.7277	±0.0050	±0.0023	0.6464

Table 4.11 - Values of φ, standard deviation, and r2 for HL_3 laminate, fatigue tested. Unloaded case.

In this case as well, there is generally a decrease in the standard deviation when moving from the electrical model to the electromechanical model. The values of φ are all very similar, except for the HL_3_5 specimen. This results in a greater dispersion of the results, leading to a decrease in the r2 value when calculating the results for the overall laminate. Again, the graphs for the individual HL_3_5 specimen in the unloaded case are provided.

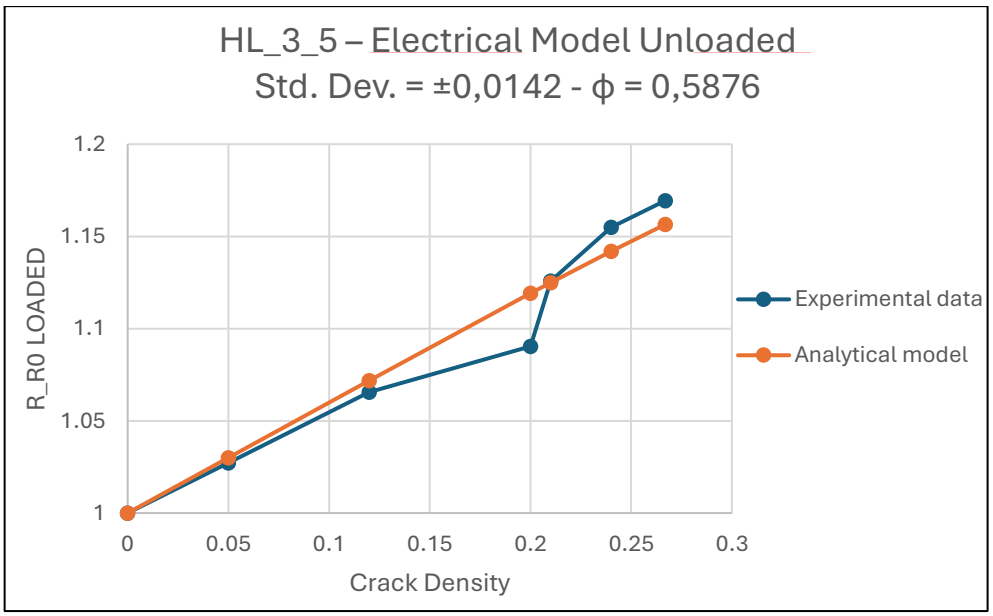

Figure 4.14 - Example of the electrical model graph calculated for each specimen. HL_3_5 Unloaded.

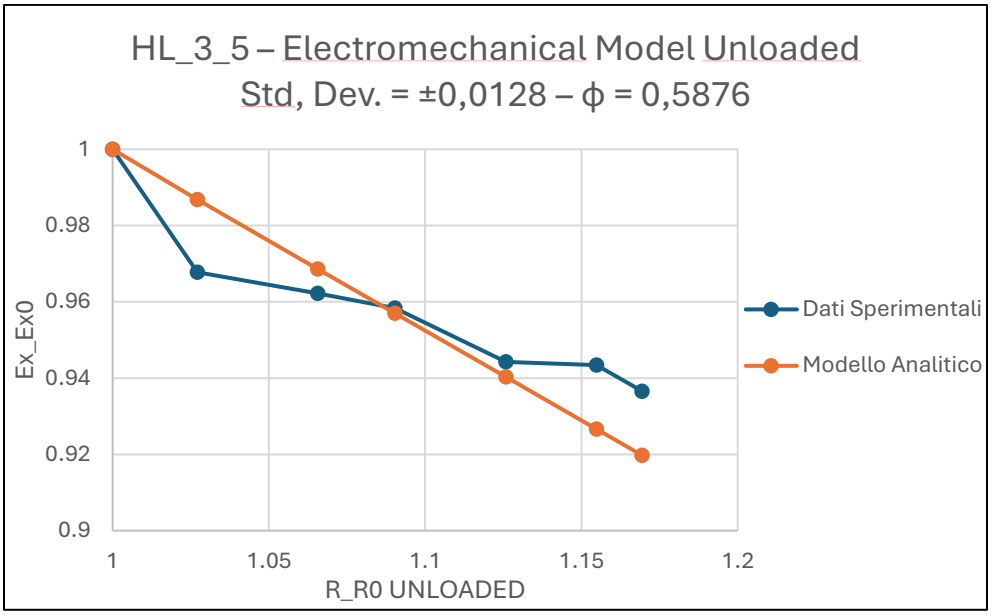

Figure 4.15 - Example of the electromechanical model graph calculated for each specimen. HL_3_5 Unloaded.

For the overall laminate HL_3 in the unloaded case, a φ value of 0,7227 was obtained, which is higher than the value obtained for the loaded case. This indicates that in the unloaded case, the material is less sensitive to damage, as the cracks are more closed. The standard deviations were calculated as a variation of ±0,0050 for the electrical model and ±0,0023 for the electromechanical model, with an r2 value of 0,6464. This suggests that the model's predictions do not closely match the experimental data with high accuracy.

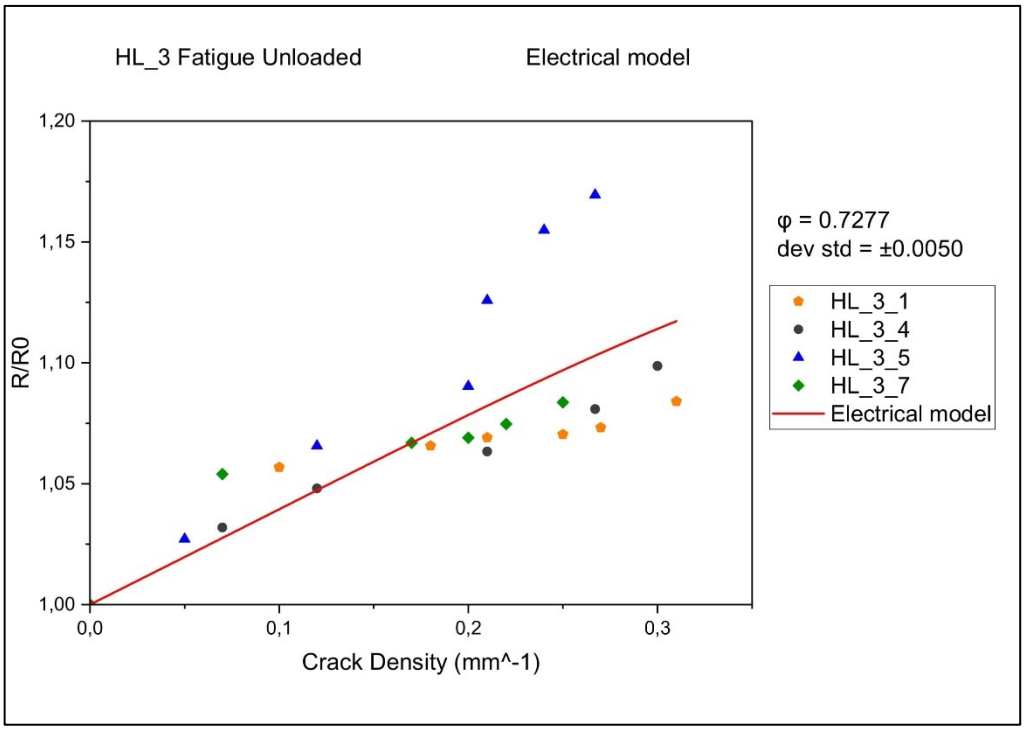

Figure 4.16 - Validation of the electrical model for laminate HL_3, fatigue tested, unloaded case.

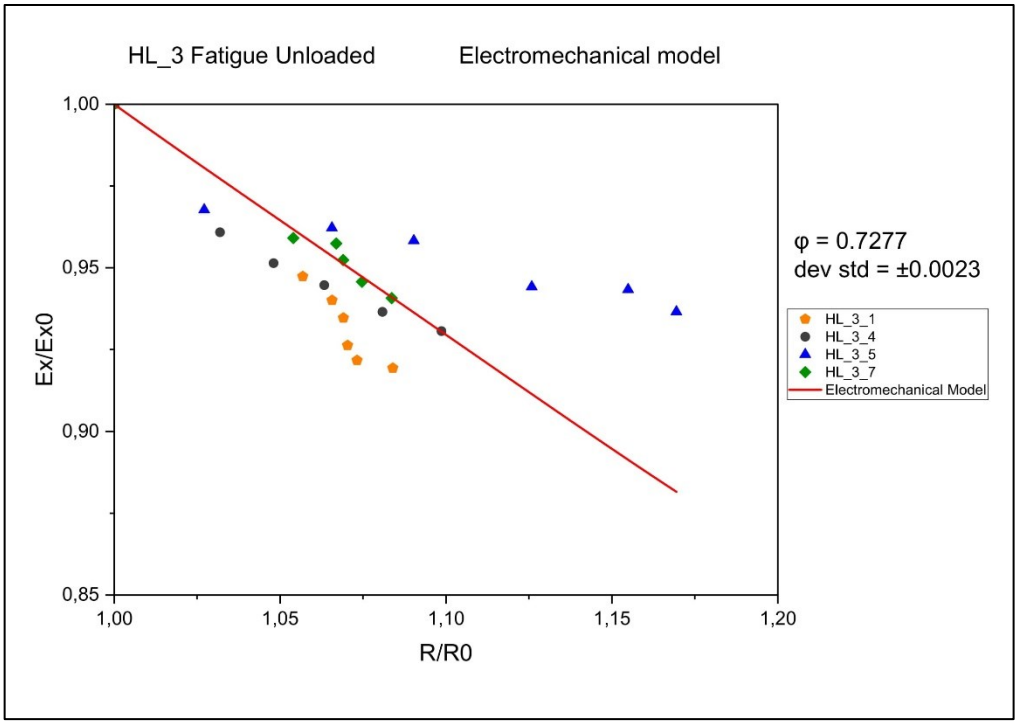

Figure 4.17 - Validation of the electromechanical model for laminate HL_3, fatigue tested, unloaded case.

4.3.2 Hand Laminated: HL_4

For the laminate HL_4, three specimens were tested: HL_4_4, HL_4_5, and HL_4_7. The tests and calculations performed were identical to those conducted for the previous laminate.

HL_4 - Fatigue Loaded				
Specimen	**φ**	**Std Dev Electrical Model**	**Std Dev Electromechanical Model**	**r^2**
HL_4_4	0.4896	±0.0219	±0.0191	0.9336
HL_4_5	0.6432	±0.0155	±0.0075	0.8903
HL_4_7	0.5834	±0.0247	±0.0073	0.7573
HL_4	0.5431	±0.0112	±0.0050	0.7088

Table 4.12 - Values of φ, standard deviation, and r2 for HL_4 laminate. Loaded case.

All the specimens exhibit high values of r2, indicating that the model accurately predicts the experimental data. Furthermore, once again, it is observed that the standard deviation tends to decrease when moving from the electrical model to the electromechanical model. Below are the graphs of the electrical and electromechanical models for the specimen HL_4_4.

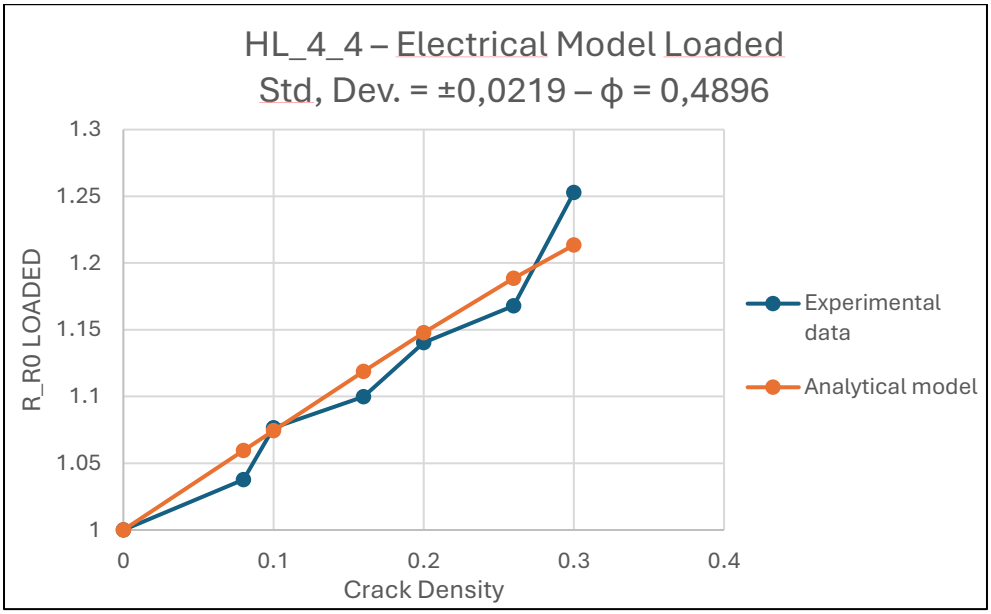

Figure 4.18 - Example of the electrical model graph calculated for each specimen. HL_4_4 Loaded.

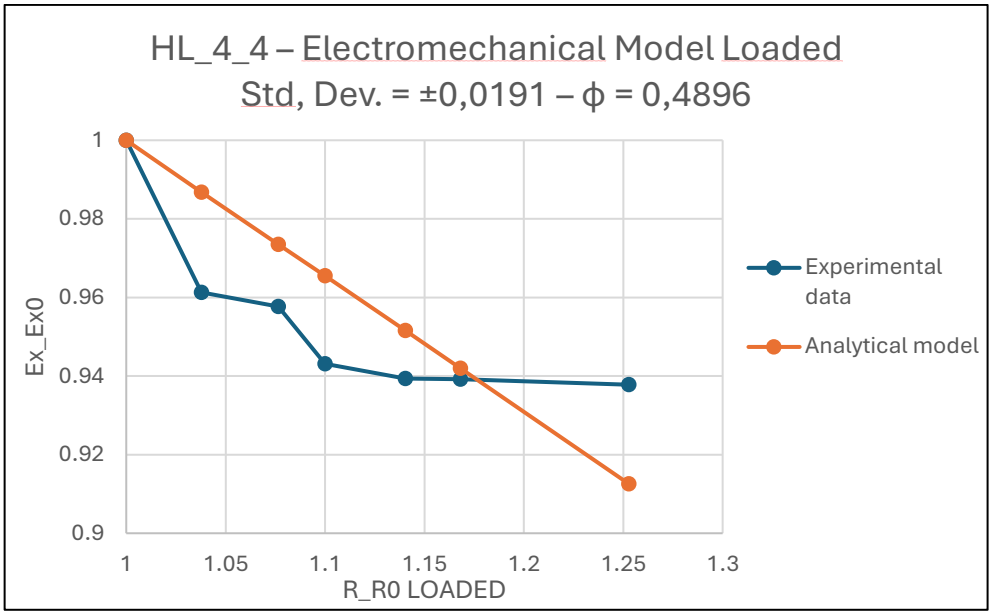

Figure 4.19 - Example of the electromechanical model graph calculated for each specimen. HL_4_4 Loaded.

The value of φ = 0,5431 for the overall laminate HL_4 is similar to that of the previous laminate HL_3, also in the Loaded case. Both laminates have the same structure. However, there is still a slight difference in the value, as it depends on many factors that can vary from plate to plate even with the same configuration, such as resin quantity, dispersion of nanotubes, internal defects, etc. Below are the graphs for laminate HL_4.

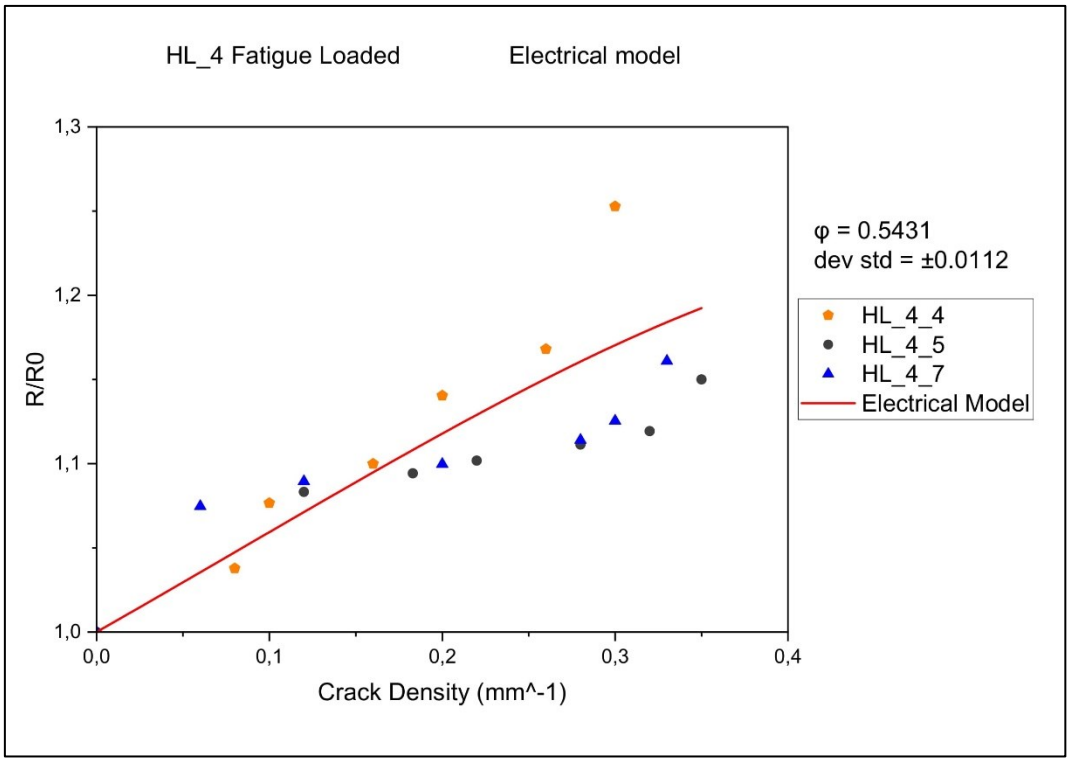

Figure 4.20 - Validation of the electrical model for laminate HL_4, fatigue tested, loaded case.

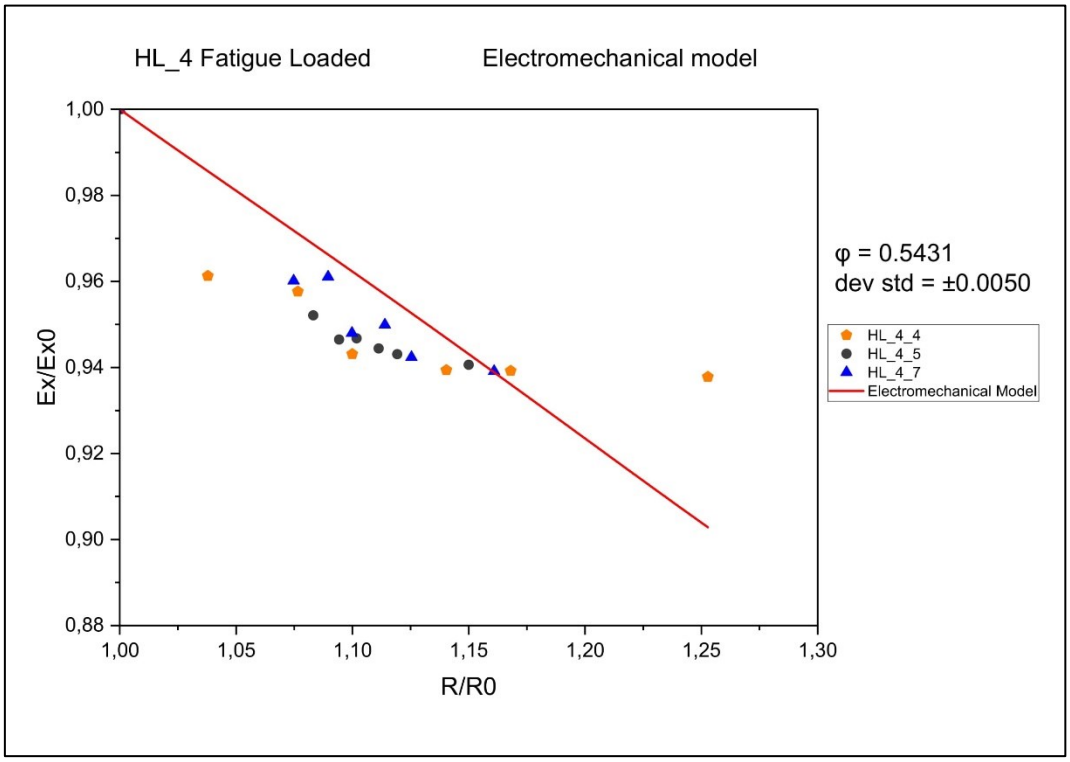

Figure 4.21 - Validation of the electromechanical model for laminate HL_4, fatigue tested, loaded case.

For the unloaded case, the following results were obtained:

HL_4 – Fatigue Unloaded				
Specimen	**φ**	**Std Dev Electrical Model**	**Std Dev Electromechanical Model**	**r^2**
HL_4_4	0.6394	±0.0129	±0.0083	0.9269
HL_4_5	0.7575	±0.0167	±0.0026	0.6868
HL_4_7	0.8890	±0.0064	±0.0068	0.7681
HL_4	0.7442	±0.0054	±0.0023	0.2904

Table 4.13 - Values of φ, standard deviation, and r2 for HL_4 laminate. Unloaded case.

Similarly to the previous case, here too we observe a φ value higher than in the loaded case, indicating that the material is less sensitive to damage when not loaded. It is worth noting that the r^2 value is generally lower for the specimens. Below are the graphs of the electrical and electromechanical models for the specimen HL_4_4 in the unloaded case.

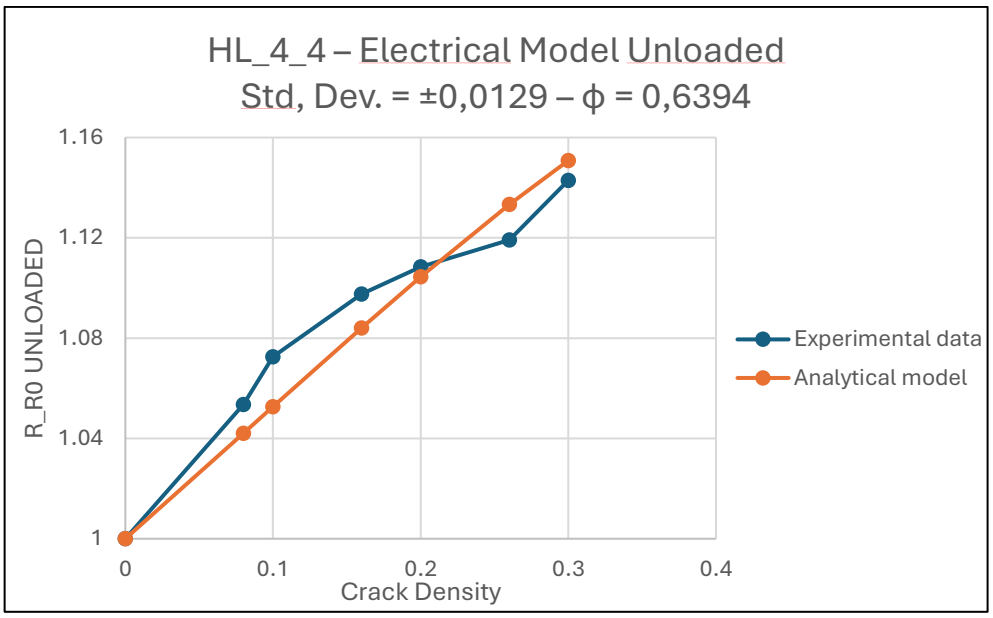

Figure 4.22 - Example of the electrical model graph calculated for each specimen. HL_4_4 Unloaded.

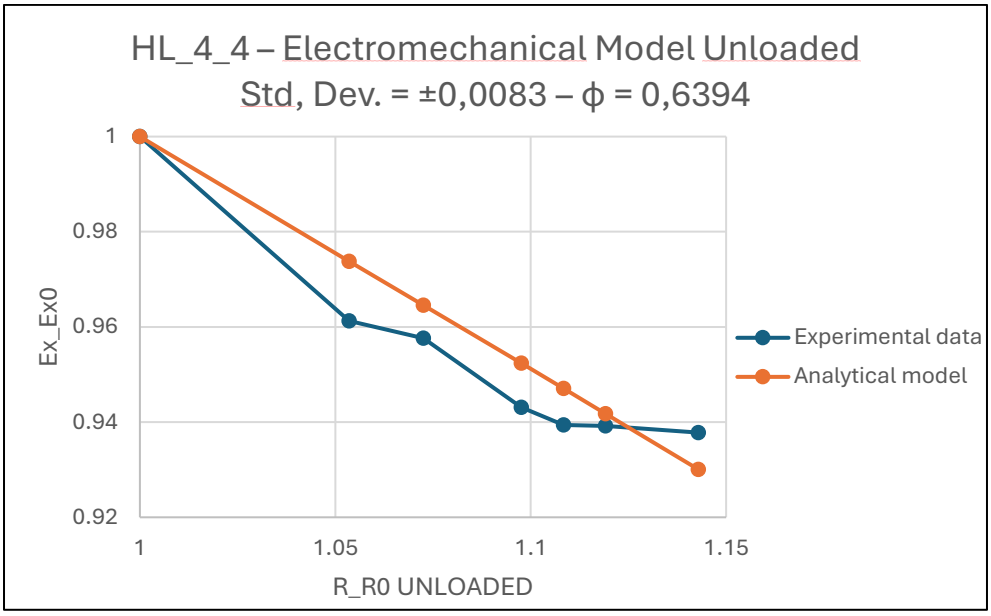

Figure 4.23 - Example of the electromechanical model graph calculated for each specimen. HL_4_4 Unloaded.

From *Table 4.13* is observed that the r^2 value for the entire HL_4 laminate is very low. This indicates that the model does not predict the behavior of the experimental data well. This is due to the much higher dispersion of the experimental data compared to the loaded case, where the r^2 value indicated a much more accurate prediction. The dispersion of the data is clearly visible in the following graphs. The only specimen that closely follows the model is HL_4_5, while the others deviate, particularly the specimen HL_4_7.

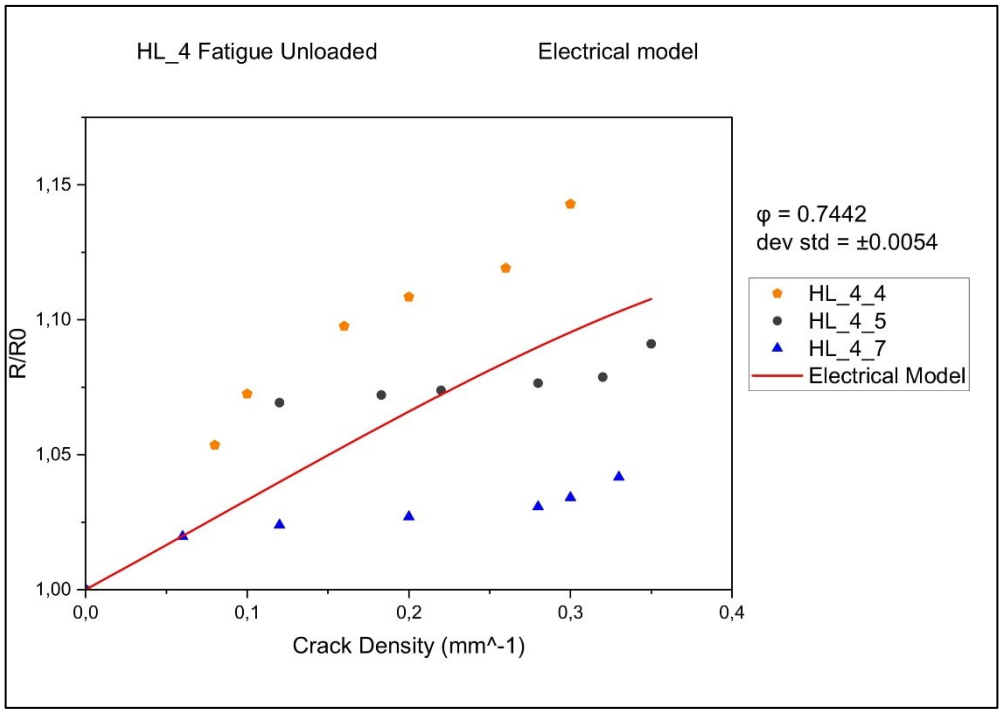

Figure 4.24 - Validation of the electrical model for laminate HL_4, fatigue tested, unloaded case.

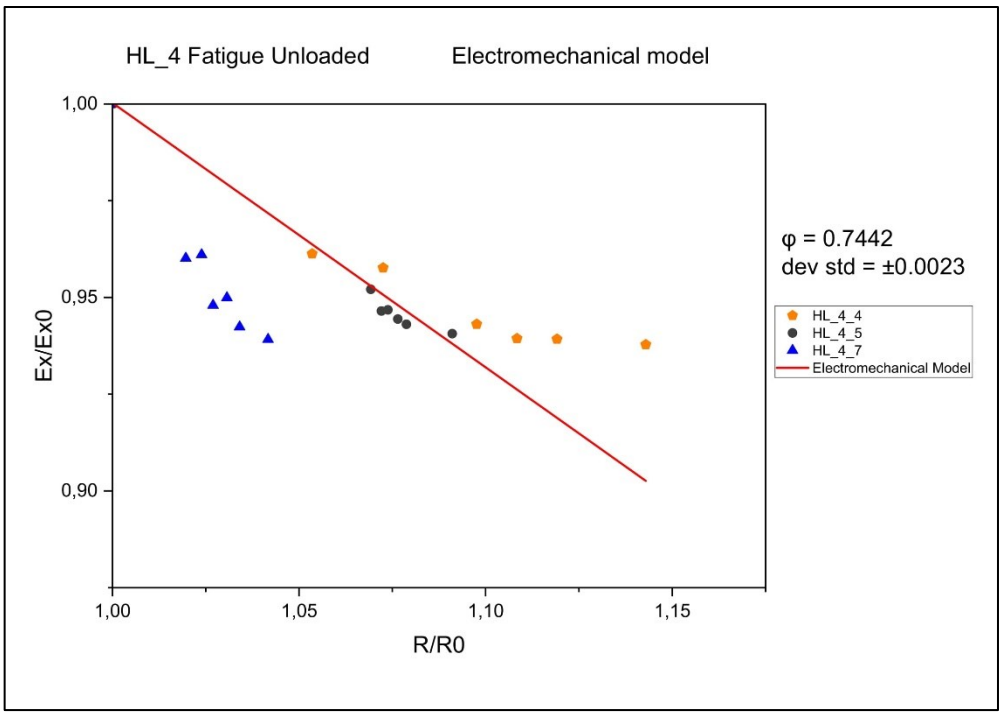

Figure 4.25 - Validation of the electromechanical model for laminate HL_4, fatigue tested, unloaded case.

4.3.3 Roll Mill: RM_2

Due to material limitations, fewer specimens were tested for the roll mill version of the laminates. Only two specimens, RM_2_1 and RM_2_9, were tested under fatigue. The following results were obtained:

RM_2 – Fatigue Loaded				
Specimen	**φ**	**Std Dev Electrical Model**	**Std Dev Electromechanical Model**	**r^2**
RM_2_1	0.6797	±0.0089	±0.0080	0.7030
RM_2_9	0.5999	±0.0109	±0.0053	0.8287
RM_2	0.6380	±0.0069	±0.0044	0.7803

Table 4.14 - Values of φ, standard deviation, and r2 for RM_2 laminate. Loaded case.

Even with this laminate configuration, a decrease in the standard deviation is observed when transitioning from the electrical model to the electromechanical model. The r^2 values are reasonably good, as is the overall value for the RM_2 laminate. Below are the graphs for the individual specimen RM_2_9.

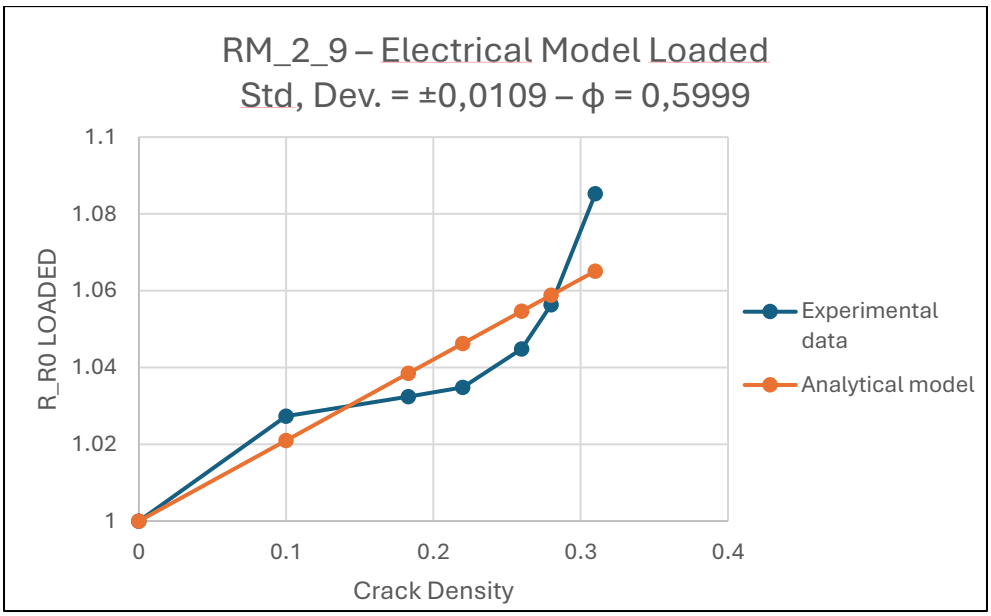

Figure 4.26 - Example of the electrical model graph calculated for each specimen. RM_2_9 Loaded.

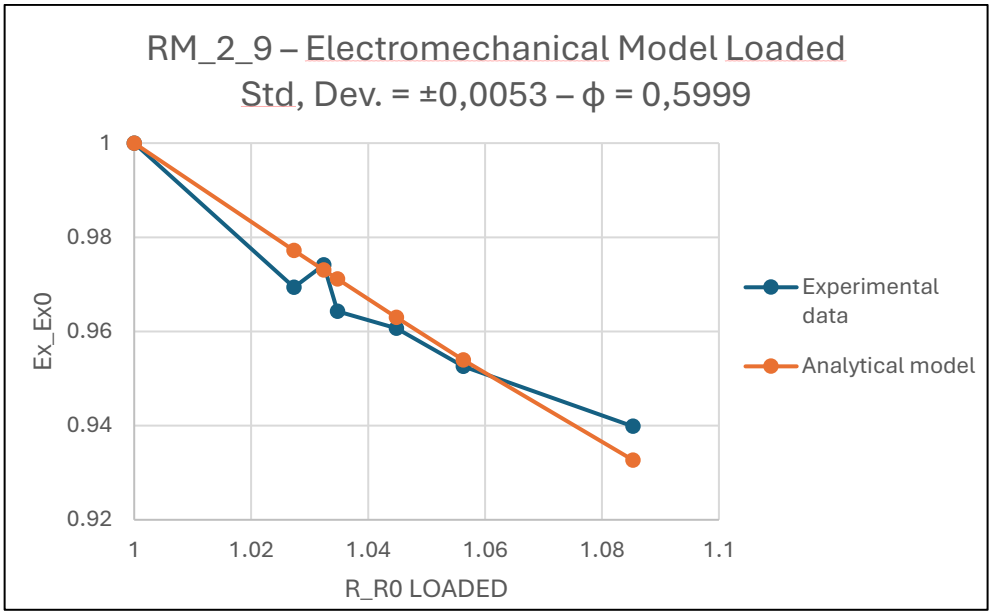

Figure 4.27 - Example of the electromechanical model graph calculated for each specimen. RM_2_9 Loaded.

The following graphs show that the model predicts the experimental results with fairly high accuracy.

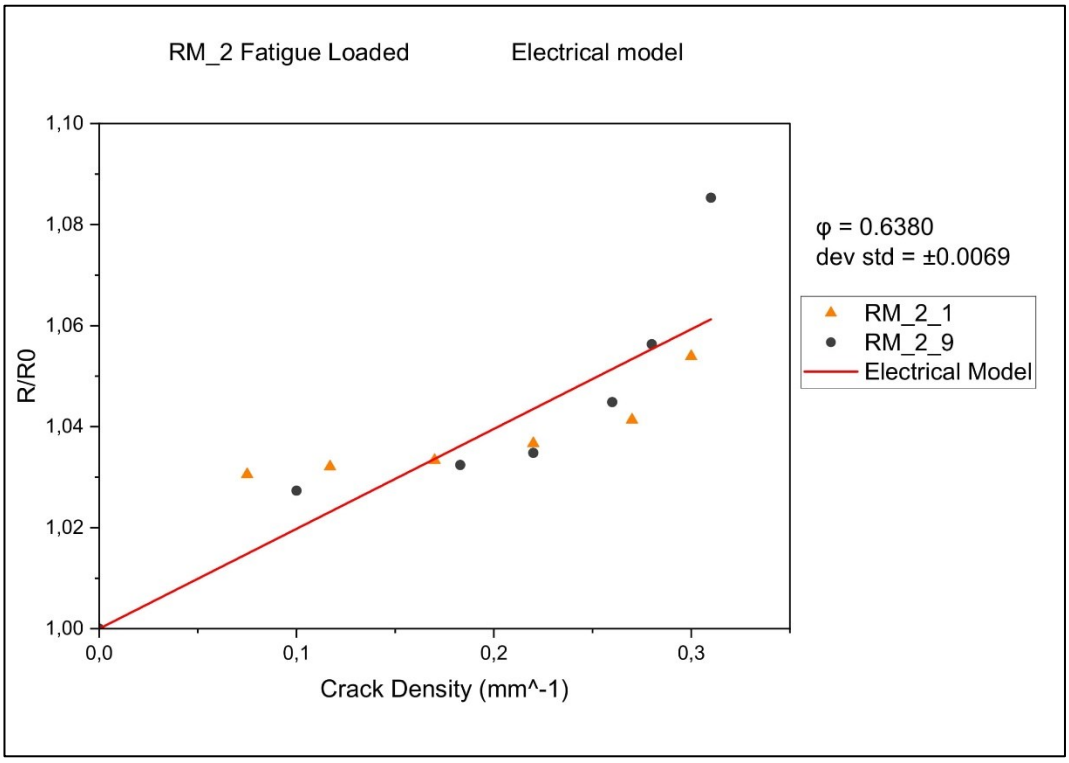

Figure 4.28 - Validation of the electrical model for laminate RM_2, fatigue tested, loaded case.

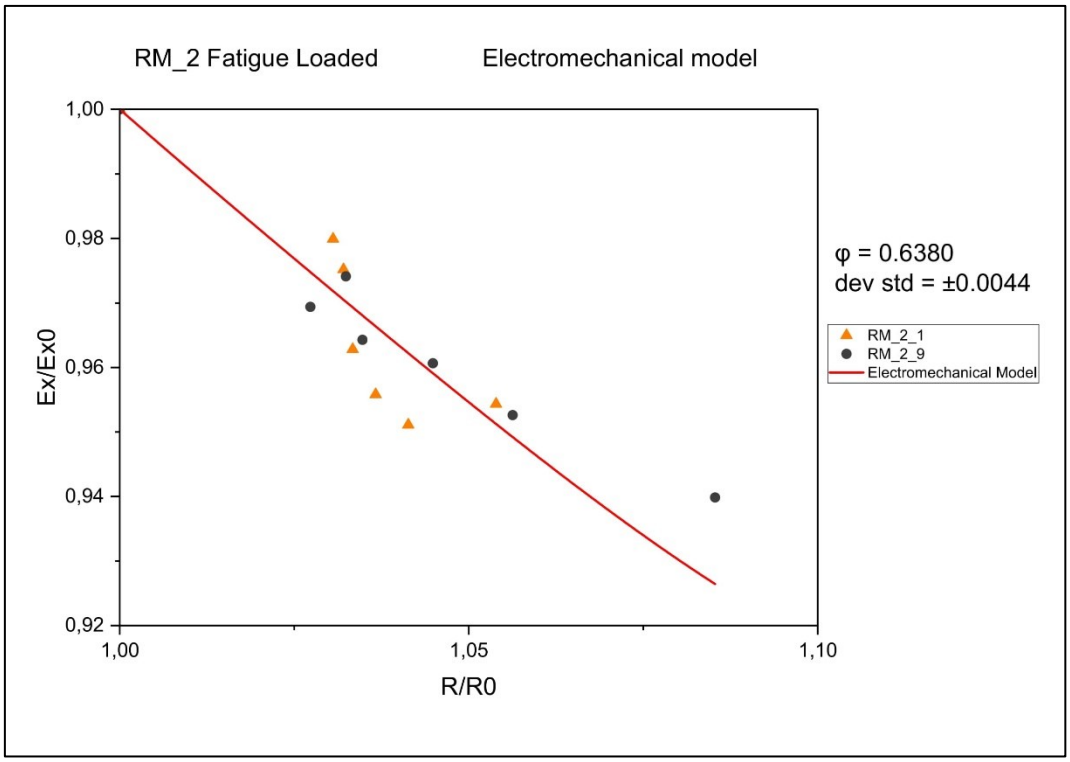

Figure 4.29 - Validation of the electromechanical model for laminate RM_2, fatigue tested, loaded case.

The damage sensitivity of the RM_2 laminate for the loaded case is similar to that obtained for the other two laminates, although slightly lower, highlighting that different laminates exhibit different φ values.

For the unloaded case, the following results were obtained:

RM_2 - Fatigue Unloaded				
Specimen	**φ**	**Std Dev Electrical Model**	**Std Dev Electromechanical Model**	**r^2**
RM_2_1	0.9508	±0.0011	±0.0073	0.8312
RM_2_9	0.8859	±0.0044	±0.0077	0.7146
RM_2	0.9161	±0.0011	±0.0053	0.5405

Table 4.15 - Values of φ, standard deviation, and r2 for RM_2 laminate. Unloaded case.

Contrary to what was obtained so far, in this case the standard deviation slightly increases when transitioning from the electrical model to the electromechanical model. Furthermore, similarly to the previous results for the unloaded case, the sensitivity of the specimens to damage is noticeably lower than when the specimen

is loaded. Below are the graphs showing the model verification for the RM_2_9 specimen.

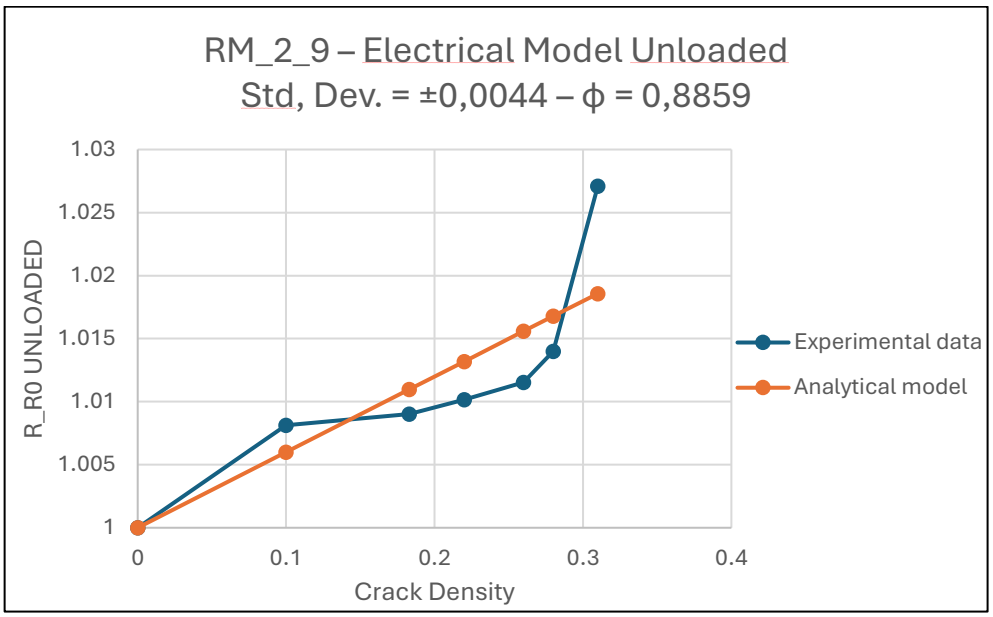

Figure 4.30 ' Example of the electrical model graph calculated for each specimen. RM_2_9 Unloaded.

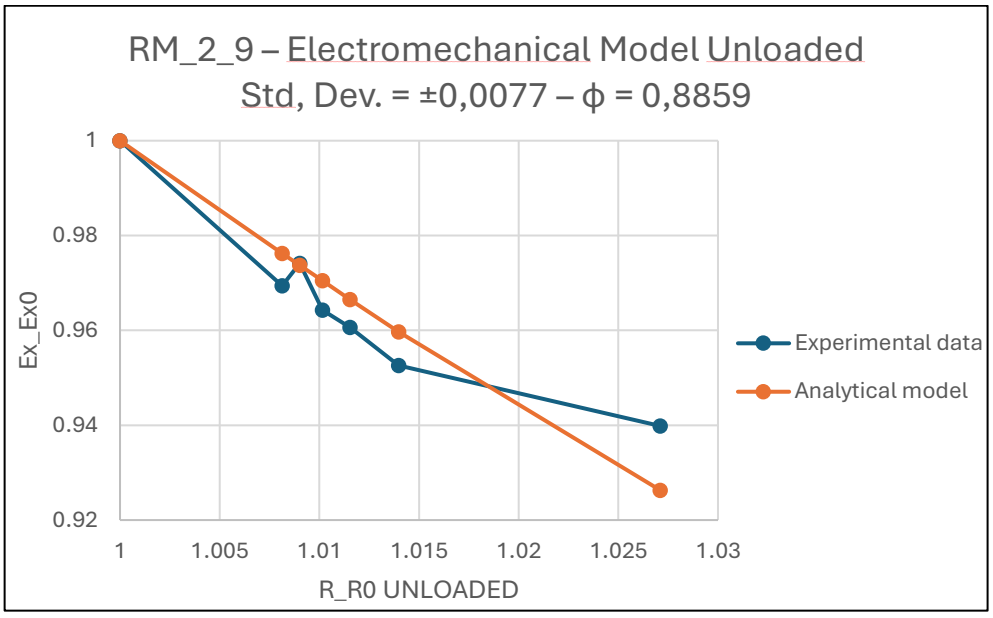

Figure 4.31 - Example of the electromechanical model graph calculated for each specimen. RM_2_9 Unloaded.

The φ value for the overall laminate is 0,9161, and although the obtained standard deviation is not very high, the value of r^2 suggests that the model's predictions are

not highly accurate. This trend has always been more pronounced in the unloaded case. Finally, the graphs for the validation of the electrical and electromechanical models for the overall laminate are shown below.

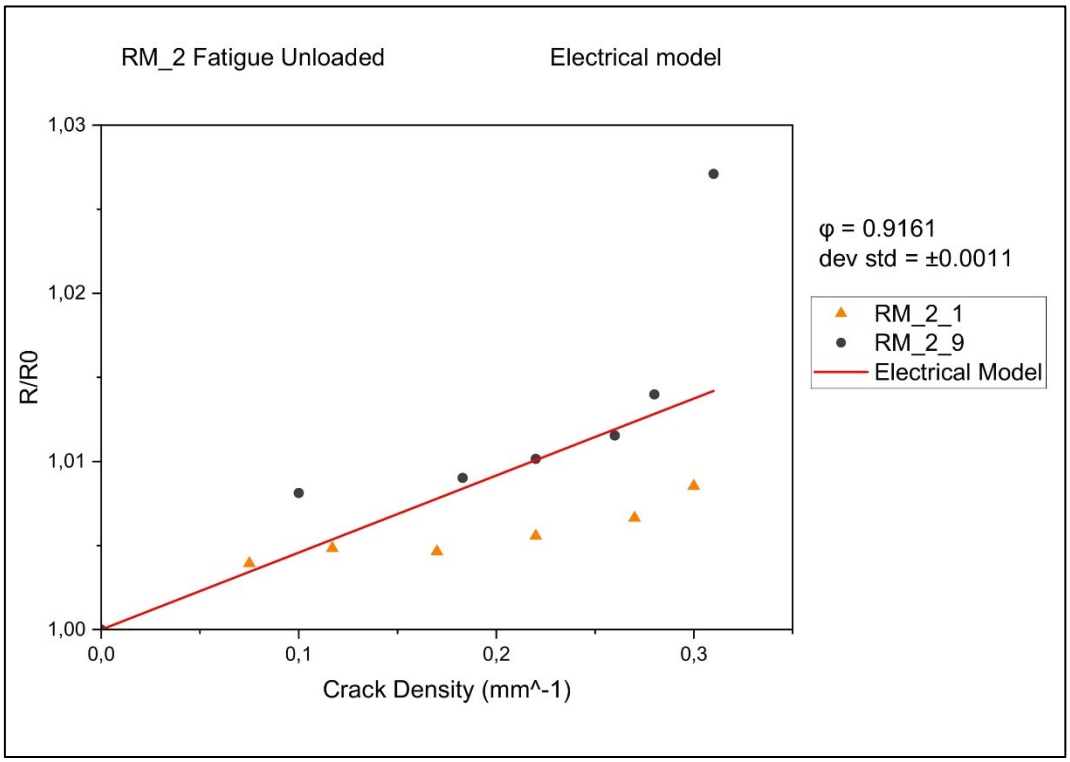

Figure 4.32 - Validation of the electrical model for laminate RM_2, fatigue tested, unloaded case.

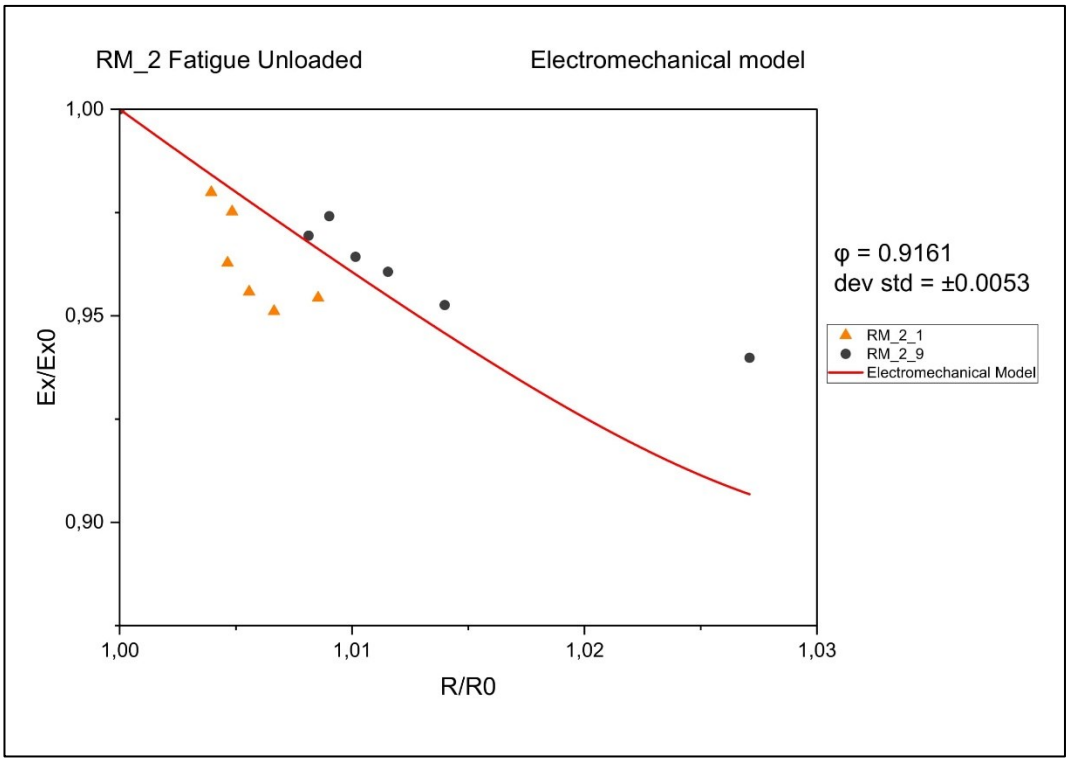

Figure 4.33 - Validation of the electromechanical model for laminate RM_2, fatigue tested, unloaded case.

4.4 Analytical Model Validation - Static tests

Similarly to what was observed in the fatigue tests, an increase in electrical resistance of the specimen was also observed during static tests as the applied tension increased. It was noted that part of this increase in electrical resistance during the loading ramps was irreversible, meaning that even when the specimen was unloaded, the resistance remained higher compared to the virgin specimen. The increase in resistance during the loading phase of the ramps was found to be linear with respect to the increase in strain, indicating that as strain increases, the formation and opening of cracks occurs. The formation of new cracks, and especially their opening, significantly reduces the nanotube bridging phenomenon, which has been extensively described previously, thereby increasing the electrical resistance of the specimen. The following graphs show this behavior:

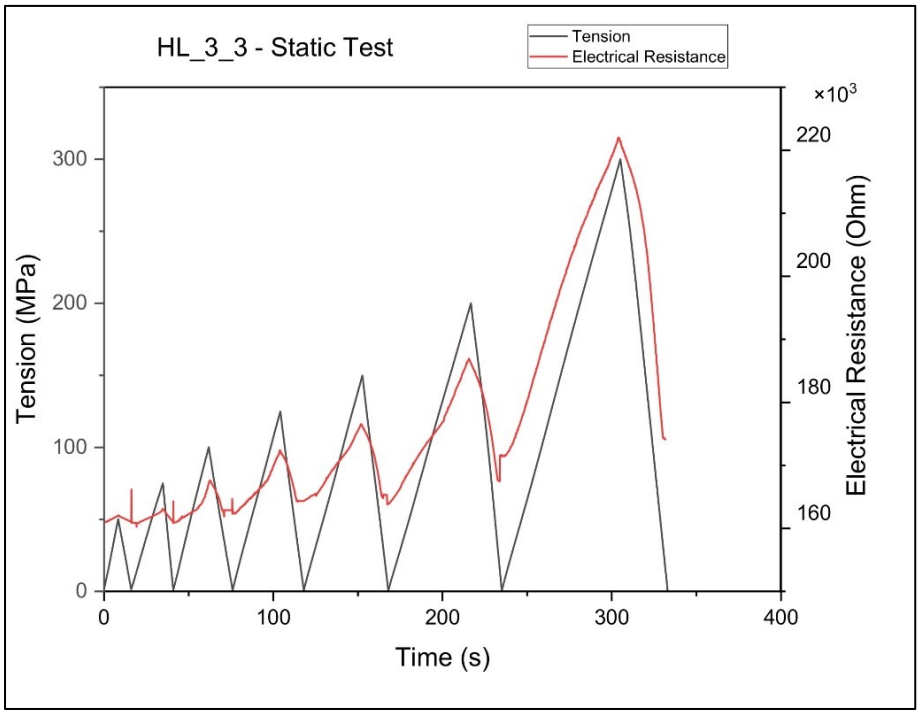

Figure 4.34 - Static test of HL_3_3. The electrical resistance increases with the load ramps.

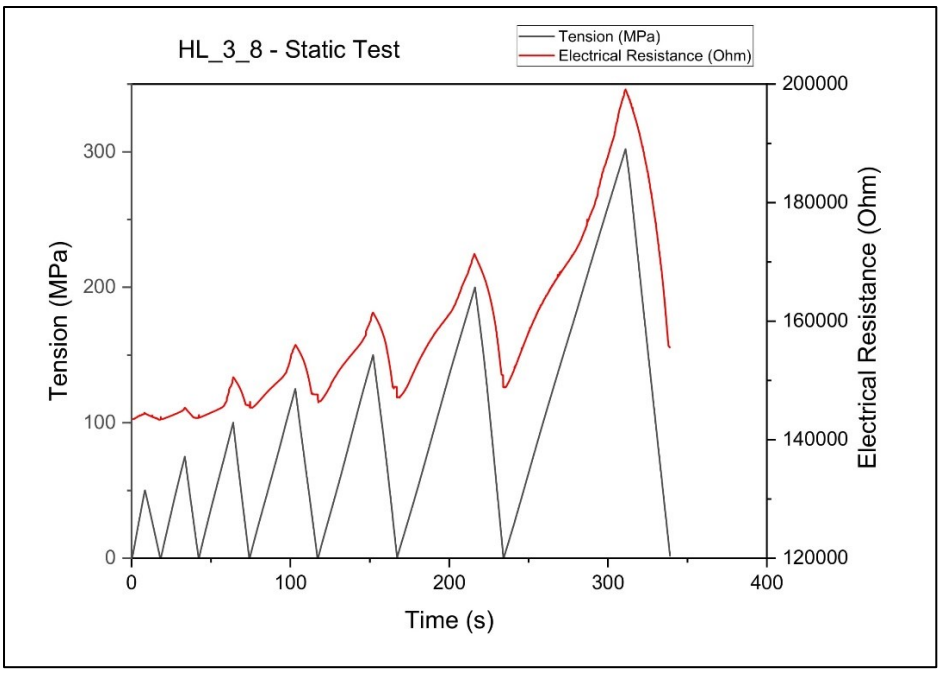

Figure 4.35 - Static test of HL_3_8. The electrical resistance increases with the load ramps.

It is observed that both the trend of resistance under load and that of the unloaded specimen tend to increase. This suggests a correlation between the damage that forms in the specimen and the increase in electrical resistance. By observing the crack density trend at the end of each loading ramp, it was noted that the number of

cracks increases rapidly during the initial loading ramps. The crack density value then tends to stabilize as the specimen reaches the final ramps with higher loads.

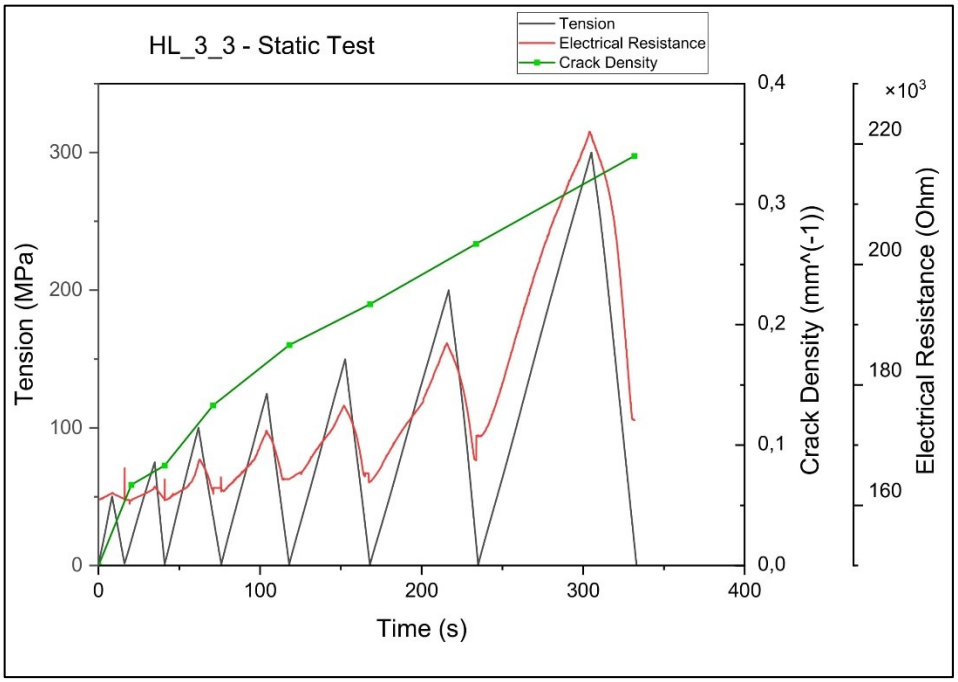

Figure 4.36 - HL_3_3 static tested. The value of crack density rapidly increases during the first load ramps.

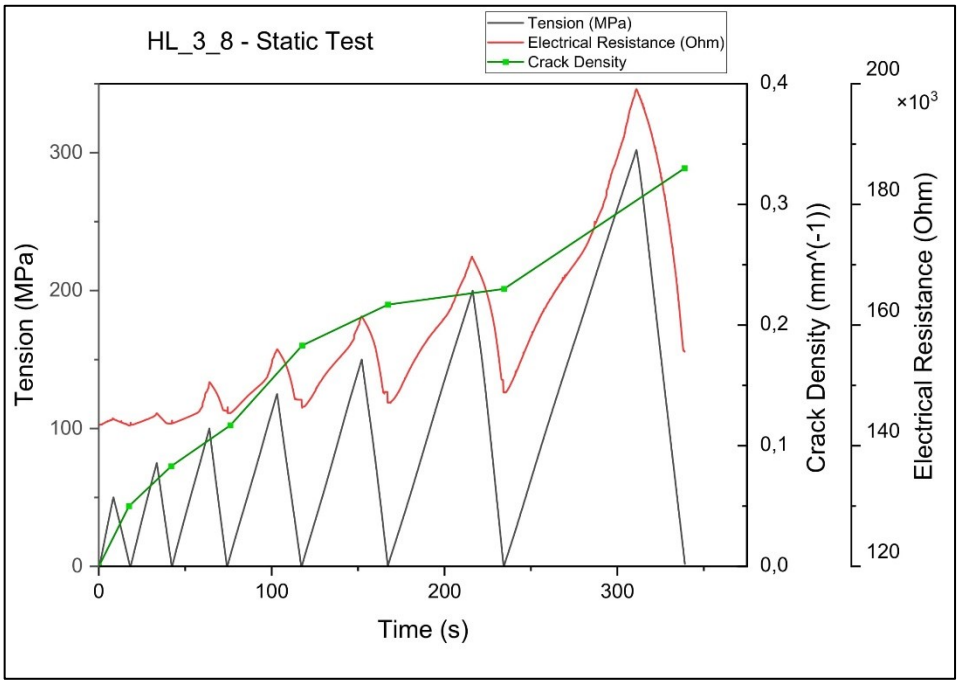

Figure 4.37 - HL_3_8 static tested. The value of crack density rapidly increases during the first load ramps.

The crack density value tends to reach saturation around 0,33 mm^{-1}, which is very similar to the value obtained from the fatigue tests. It is also interesting to observe the trend of the electrical resistance and crack density compared to the strain the material is subjected to.

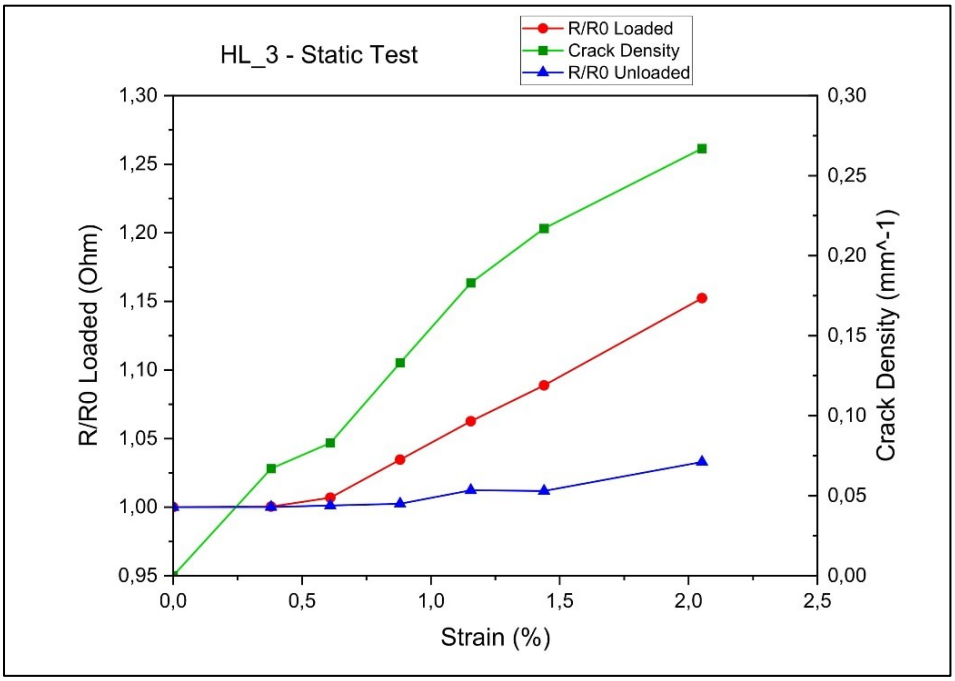

Figure 4.38 - HL_3, comparative analysis of Loaded R/R0, Unloaded R/R0, and Crack Density in relation to % strain.

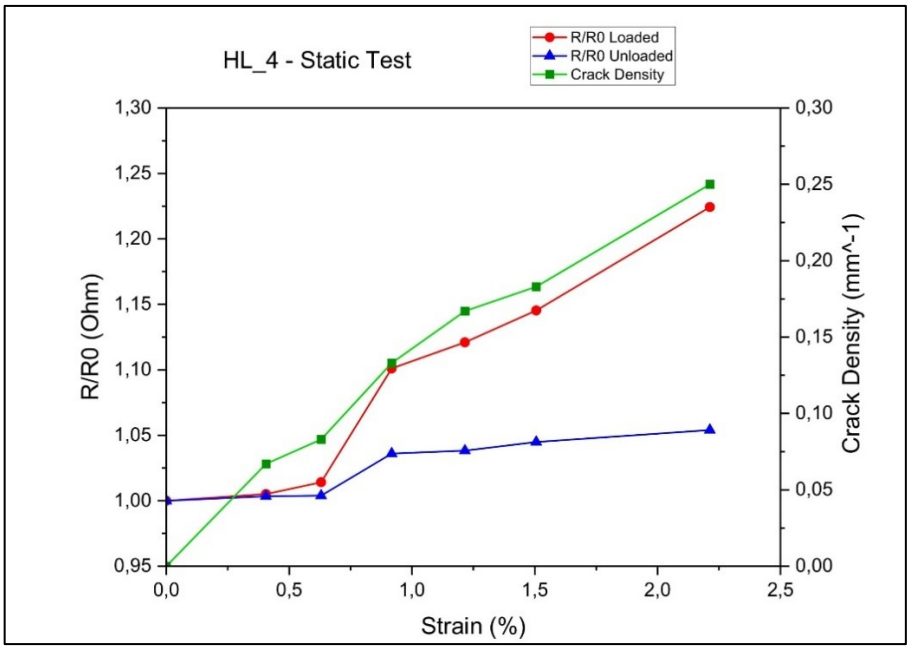

Figure 4.39 - HL_4, comparative analysis of Loaded R/R0, Unloaded R/R0, and Crack Density in relation to % strain.

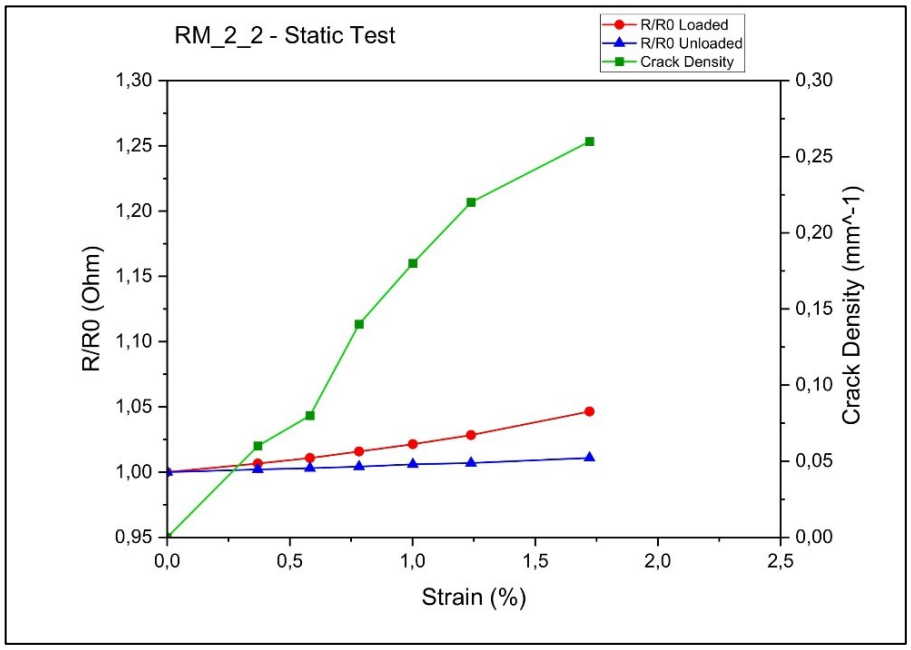

Figure 4.40 - RM_2, comparative analysis of Loaded R/R0, Unloaded R/R0, and Crack Density in relation to % strain.

In all laminates, an increase in crack density is associated with a significant increase in electrical resistance. Furthermore, the trends of crack density and resistance are very similar, especially for the HL_4 laminate, where a sudden increase in crack density is followed by an increase in resistance, both under load and in the unloaded

condition. This again suggests that as the damage in the material increases, the electrical resistance also increases.

Similarly to what was observed in the fatigue tests, a more pronounced increase in electrical resistance was observed in the Loaded case compared to the Unloaded case. This is again linked to the fact that the laminate's sensitivity to damage depends on how open the cracks are. When the material is subjected to a load, the higher the load, the more the cracks will open and the more the electrical resistance will increase, as the effect of nanotube bridging diminishes. The following table shows the maximum percentage increase observed in the different loaded and unloaded test cases.

Plates	ΔR_{LOADED}	$\Delta R_{UNLOADED}$
Hand Laminate	37,6%	8,1%
Roll Mill	4,6%	1,1%

Table 4.16 - Maximum increase of electrical resistance through the test.

The maximum increase in electrical resistance recorded is much higher compared to what was observed in the fatigue tests. In this case, higher stress levels were reached, up to 300 MPa, which means higher strains were also achieved, exceeding 2%, leading to a greater increase in electrical resistance. Similarly to what was reported earlier, in this case, a higher ΔR is observed for the hand-laminated specimens, in both the loaded and unloaded conditions. This further confirms that the specimen exhibits different sensitivity to damage depending on the loading condition.

Once again, it is crucial to understand the laminate's sensitivity to damage, and thus to derive the parameter φ of the model. [1], to better understand the material's behavior. The verification methodologies for the model are entirely similar to those applied previously. For the validation of the analytical model, a total of seven specimens were tested, belonging to three different plates: two hand-laminated plates, HL_3 and HL_4, and one plate fabricated using the roll mill process, RM_2.

4.4.1 Hand Laminated: HL_3

The same considerations were made for both the Loaded and Unloaded cases. It is important to note that the contribution of the piezoresistive effect was not excluded from the results for simplicity, as the associated error is small.

For the HL_3 plate, four specimens were tested: HL_3_3, HL_3_6, HL_3_8, and HL_3_9. The results, including the values of φ, standard deviation, and r^2, are presented in the following table:

HL_3 - Static Loaded				
Specimen	**φ**	**Std Dev Electrical Model**	**Std Dev Electromechanical Model**	**r^2**
HL_3_3	0.4697	±0.0693	±0.0242	0.6869
HL_3_6	0.3578	±0.0793	±0.0435	0.6759
HL_3_8	0.322	±0.0612	±0.0419	0.7852
HL_3_9	0.2936	±0.0750	±0.0754	0.7684
HL_3	0.3645	±0.0351	±0.0183	0.7080

Table 4.17 - Values of φ, standard deviation, and r2 for HL_3 laminate, static tested. Loaded case.

As expected, the values of φ recorded are lower compared to the same laminate tested under fatigue, indicating a higher sensitivity to damage. This result is consistent with expectations, as the variation in electrical resistance during the static test is greater than that typically recorded during fatigue tests, even with the same crack density. This suggests that, in these cases, the specimen is more sensitive to damage. Similarly to what was observed in the fatigue tests, there is generally a decrease in the standard deviation when moving from the verification of the electrical model to the verification of the electromechanical model.

Below are the graphs for the verification of the electrical and electromechanical models for specimen HL_3_6; the graphs for all other specimens are presented in the appendix at the end of the thesis.

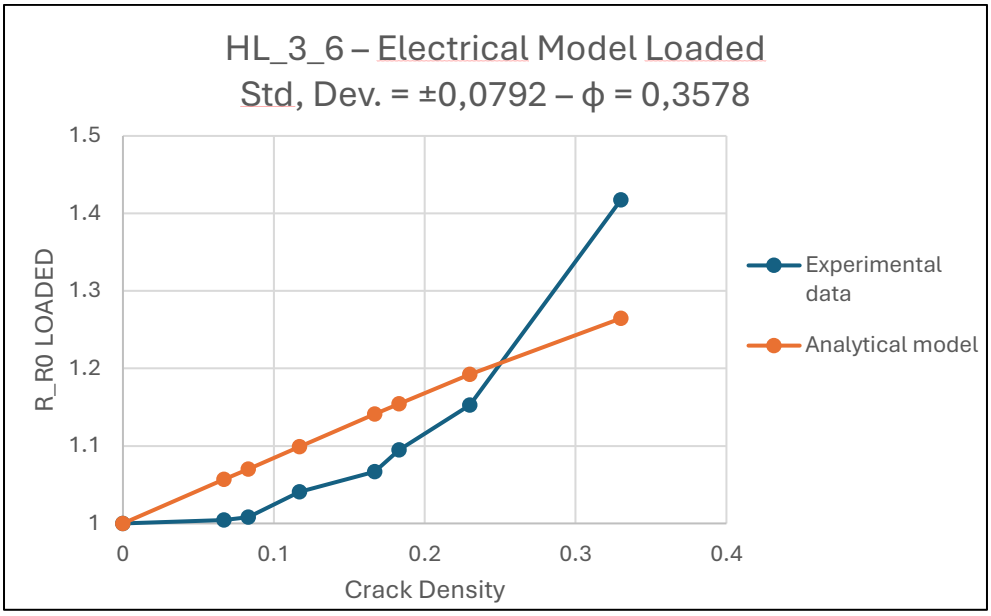

Figure 4.41 - Example of the electrical model graph calculated for each specimen. HL_3_6, static test, loaded case.

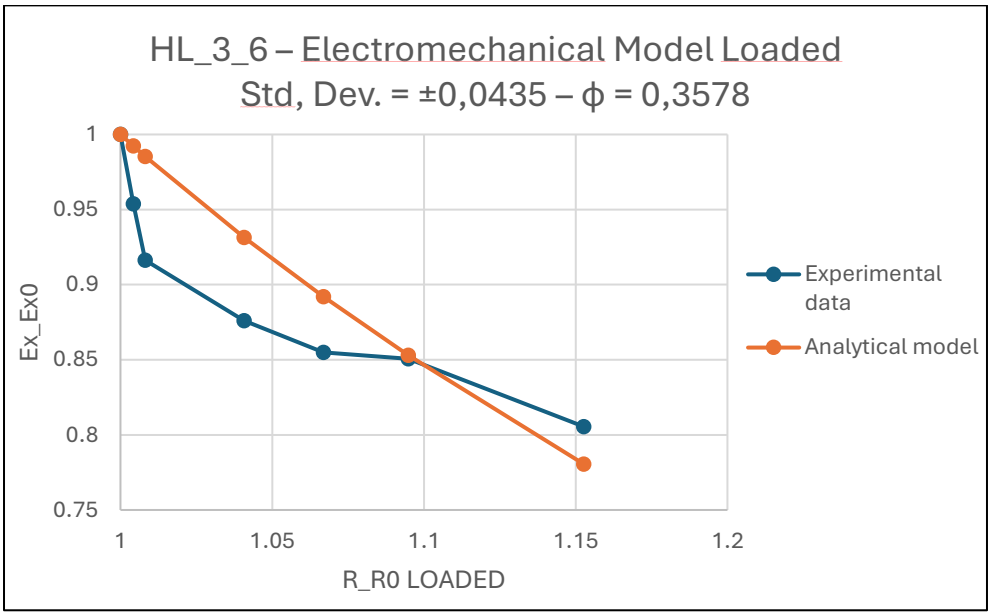

Figure 4.42 - Example of the electromechanical model graph calculated for each specimen. HL_3_6, static test, loaded case.

The r^2 values for the individual specimens are not very high, but they still indicate that the model predictions closely follow the experimental data behavior. Below are the graphs for the verification of the electrical and electromechanical models for the entire HL_3 laminate.

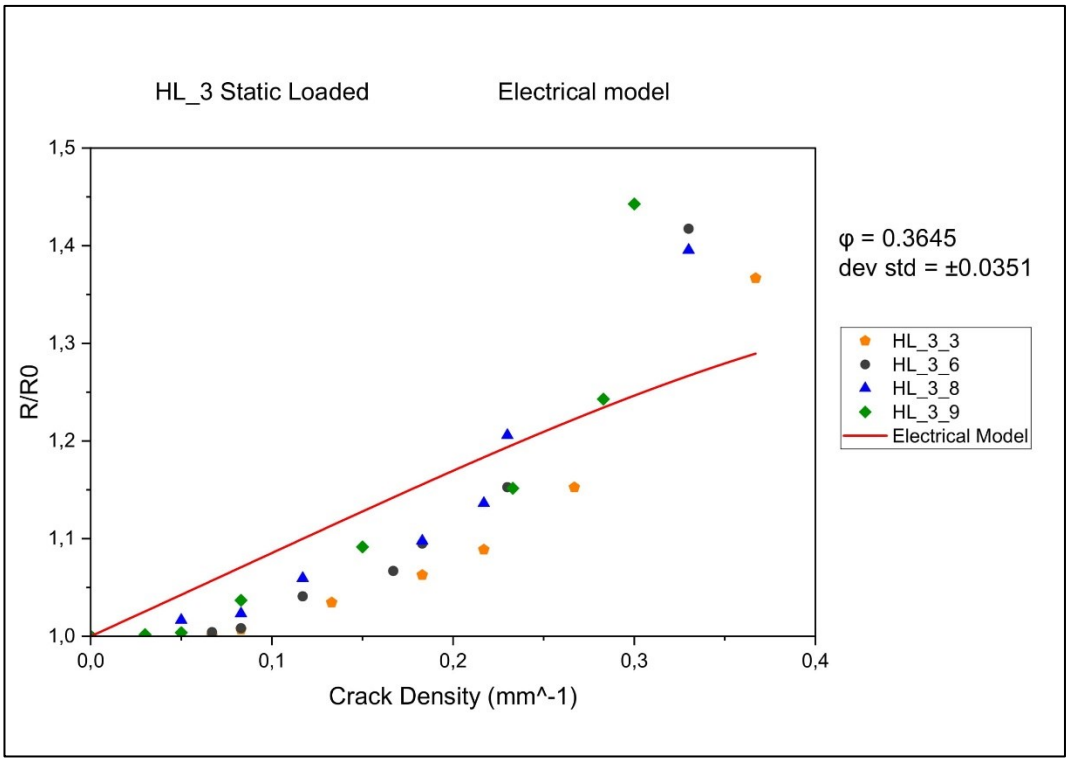

Figure 4.43 - Validation of the electrical model for laminate HL_3, static tested, loaded case.

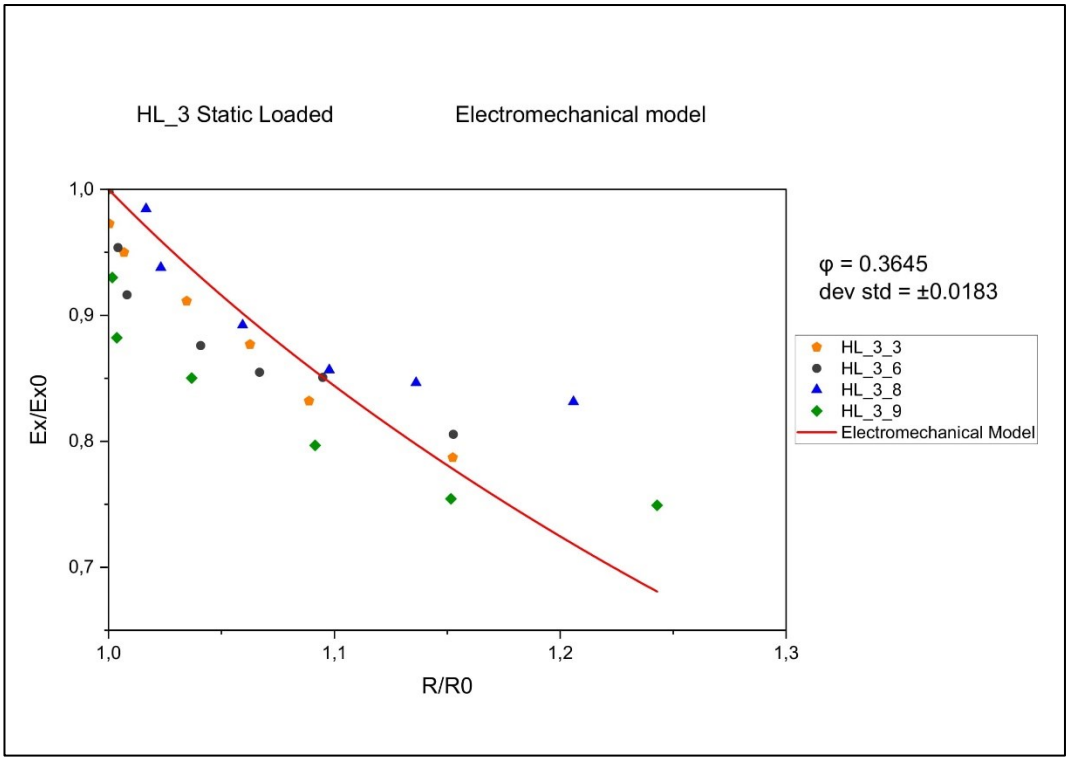

Figure 4.44 - Validation of the electromechanical model for laminate HL_3, static tested, loaded case.

The standard deviations for the individual specimens and for the entire laminate are higher compared to those obtained in the corresponding fatigue tests. As seen from the images above, there is greater dispersion of the experimental data compared to the model's predictions; this dispersion is also reflected in the r^2 value. Despite this, the model can still be considered valid.

For the Unloaded case, the following results were obtained:

HL_3 - Static Unloaded				
Specimen	**φ**	**Std Dev Electrical Model**	**Std Dev Electromechanical Model**	**r^2**
HL_3_3	0.9394	±0.0071	±0.0881	0.6458
HL_3_6	0.8693	±0.0083	±0.0495	0.8696
HL_3_8	0.8045	±0.0082	±0.0493	0.9328
HL_3_9	0.7675	±0.0131	±0.0183	0.8737
HL_3	0.8351	±0.0043	±0.0160	0.6397

Table 4.18 - Values of φ, standard deviation, and r2 for HL_3 laminate, static tested. Unloaded case.

The value of ΔR% obtained for the unloaded case (reported in *Table 4.18*) is significantly lower than that obtained for the loaded case, reflecting a lower sensitivity of the specimen to damage when it is not under load. This observation is confirmed by the calculated results; indeed, the value of φ obtained for the unloaded case is much higher than for the loaded case. Of particular note is the fact that, similarly to what was observed for the RM_2 laminate in the unloaded fatigue tests, there is an increase in the standard deviation when moving from the electric model verification to the electromechanical model verification. Below are the graphs for the verification of the electric and electromechanical models for specimen HL_3_6 in the unloaded case.

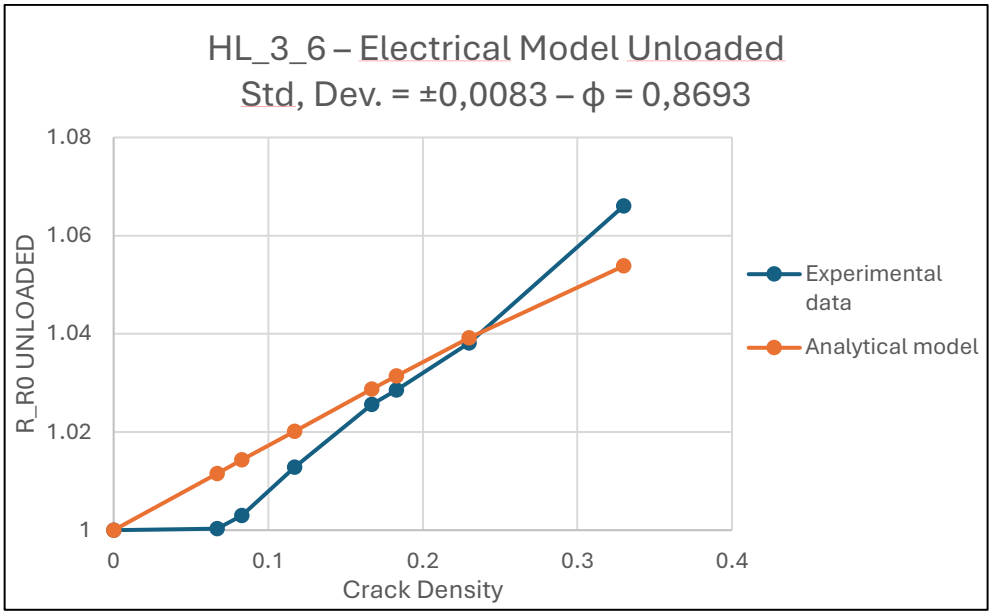

Figure 4.45 - Example of the electrical model graph calculated for each specimen. HL_3_6, static test, unloaded case.

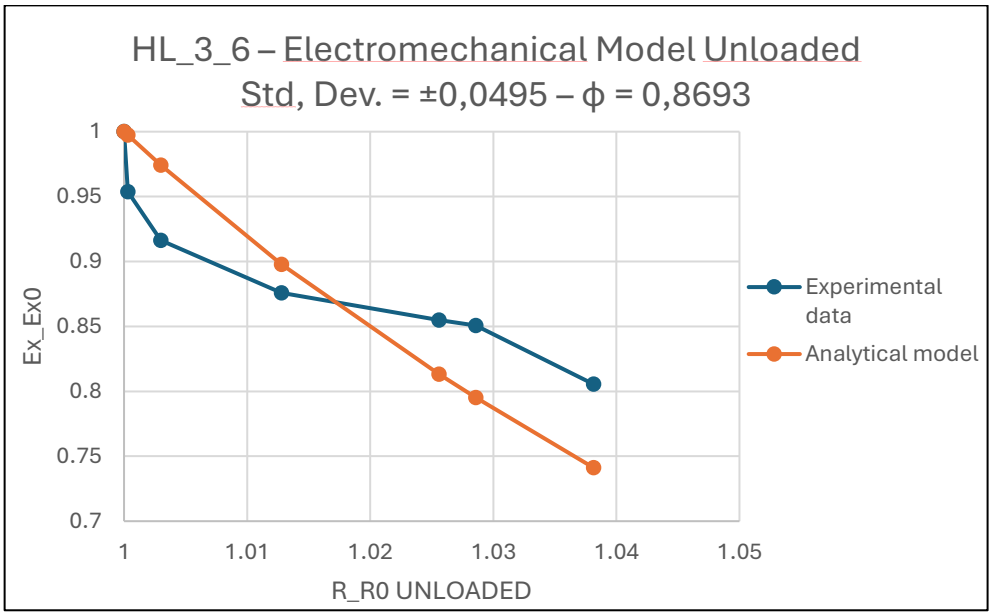

Figure 4.46 - Example of the electromechanical model graph calculated for each specimen. HL_3_6, static test, unloaded case.

The value of r^2 is quite good when considering the individual specimens, but it slightly decreases when evaluating the overall laminate, indicating a relatively significant dispersion in the experimental data, as evidenced by the following images.

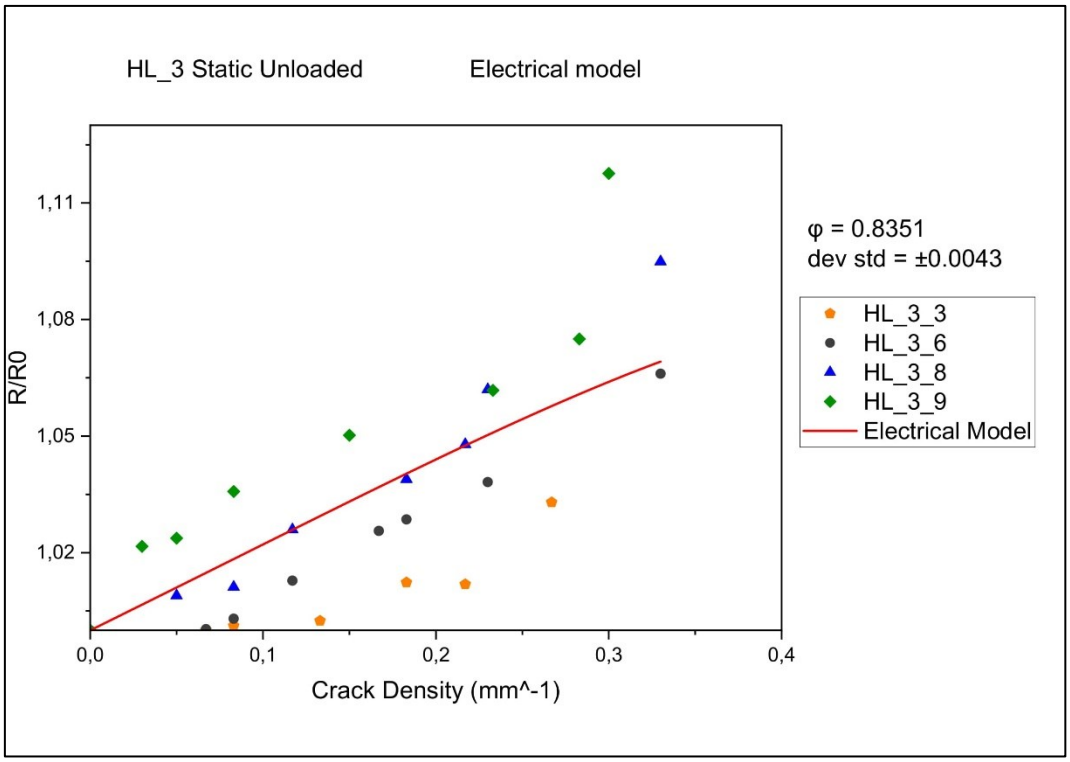

Figure 4.47 - Validation of the electrical model for laminate HL_3, static tested, unloaded case.

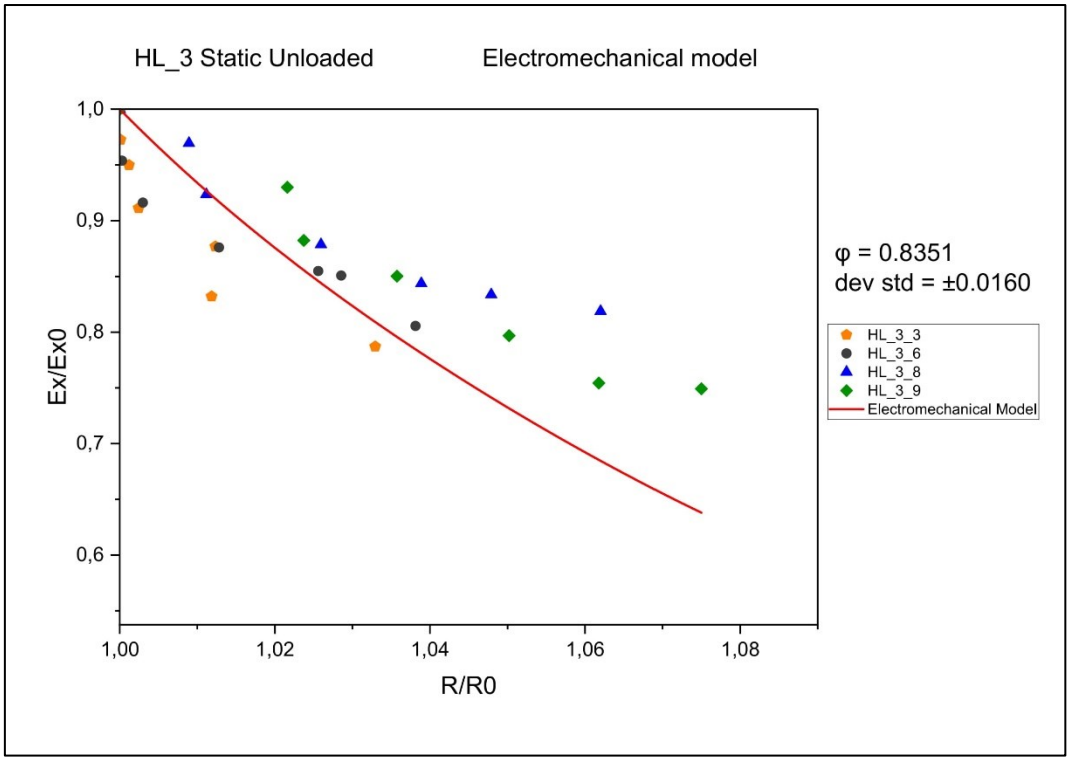

Figure 4.48 - Validation of the electromechanical model for laminate HL_3, static tested, unloaded case.

From the graph of the electromechanical model, it is apparent why the standard deviation is higher compared to the electrical model: there is a much more significant deviation of the experimental data, especially for the higher values of R/R_0.

4.4.2 Hand Laminated: HL_4

For the HL_4 plate, two specimens were tested: HL_4_1 and HL_4_9. The following table summarizes the results obtained.

HL_4 – Static Loaded				
Specimen	**φ**	**Std Dev Electrical Model**	**Std Dev Electromechanical Model**	**r^2**
HL_4_1	0.4135	± 0.0316	± 0.0548	0.8615
HL_4_9	0.2762	± 0.0762	± 0.0565	0.6935
HL_4	0.3323	± 0.0292	± 0.0393	0.7318

Table 4.19 - Values of φ, standard deviation, and r2 for HL_4 laminate, static tested. Loaded case.

The low value of φ indicates a high sensitivity to damage, which is consistent with expectations. In this case, there is no clear trend in the standard deviation suggesting either an increase or decrease when moving from the electrical model to the electromechanical model. The absolute values of the standard deviation are higher than those obtained from fatigue tests but still in line with those obtained statically for the HL_3 plate. Below are the graphs for the verification of the electrical and electromechanical models for the HL_4_1 specimen in the loaded case.

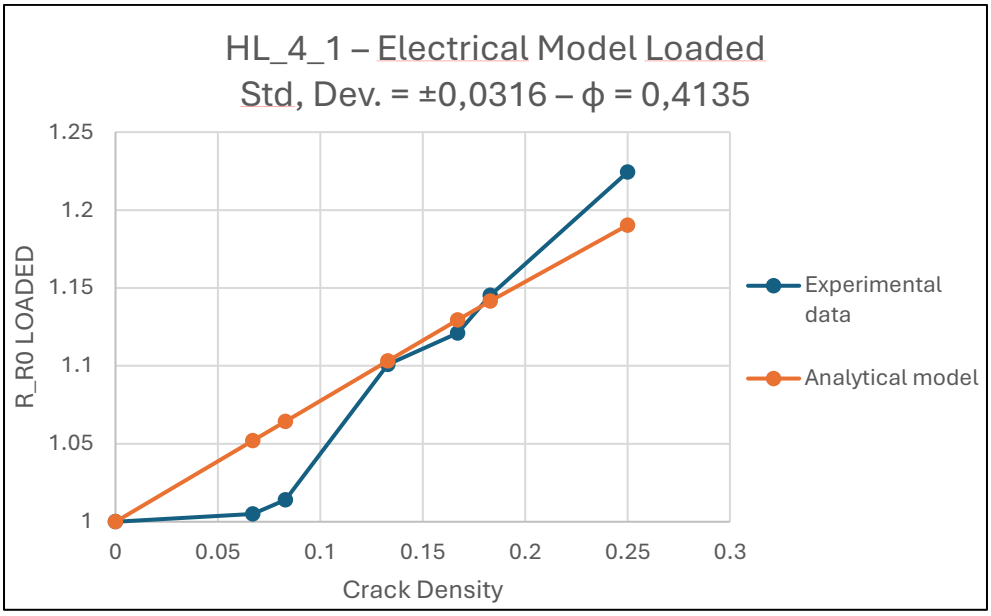

Figure 4.49 - Example of the electrical model graph calculated for each specimen. HL_4_1, static test, loaded case.

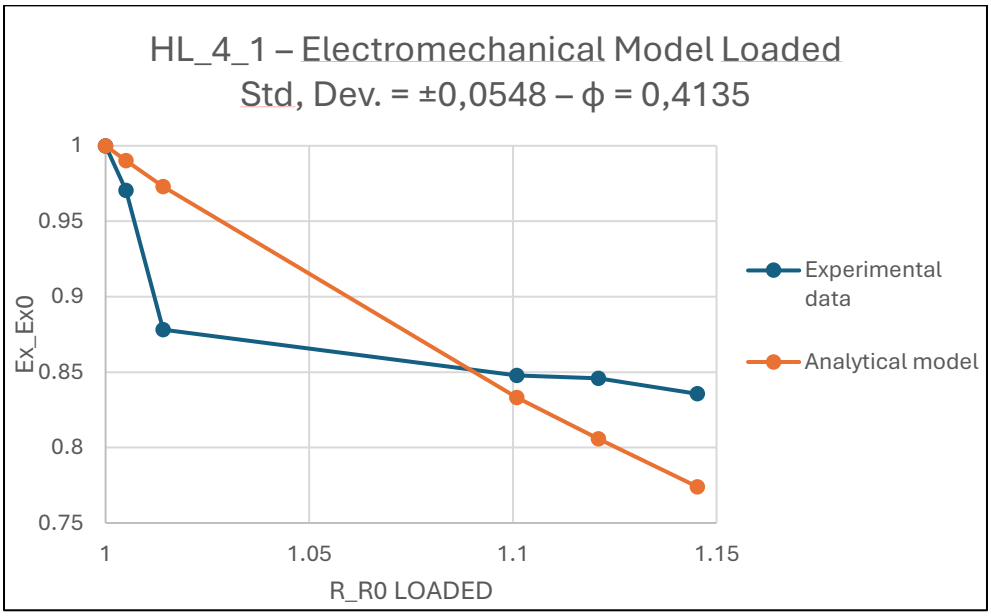

Figure 4.50 - Example of the electromechanical model graph calculated for each specimen. HL_4_1, static test, loaded case.

The r^2 values are generally quite good, even for the overall plate. For more accurate estimates that account for greater variability, it would have been advisable to test a larger number of specimens. Unfortunately, this was not possible due to a lack of material.

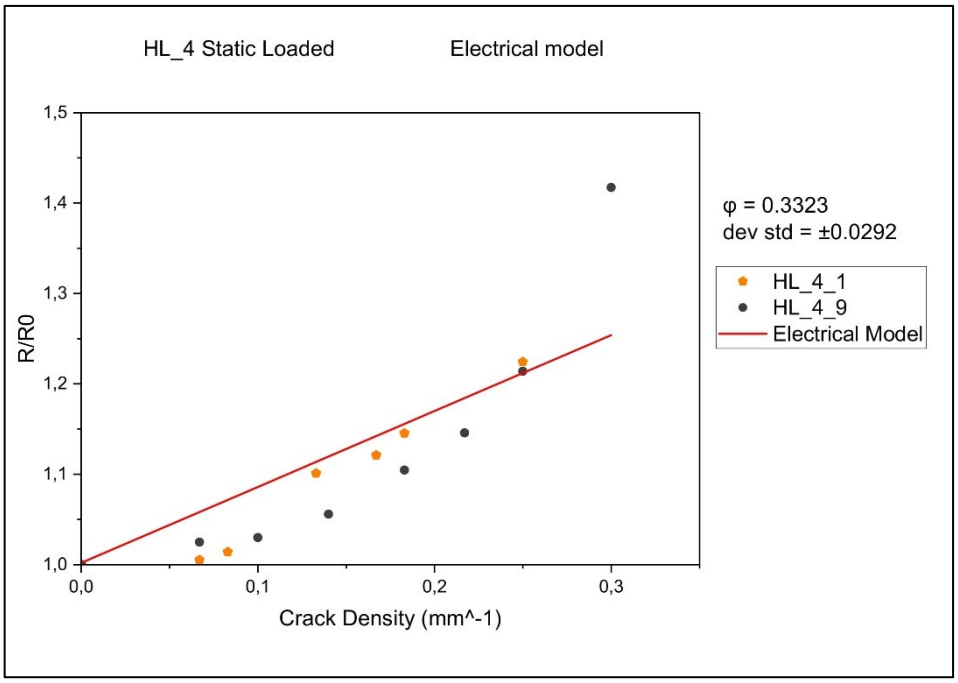

Figure 4.51 - Validation of the electrical model for laminate HL_4, static tested, loaded case.

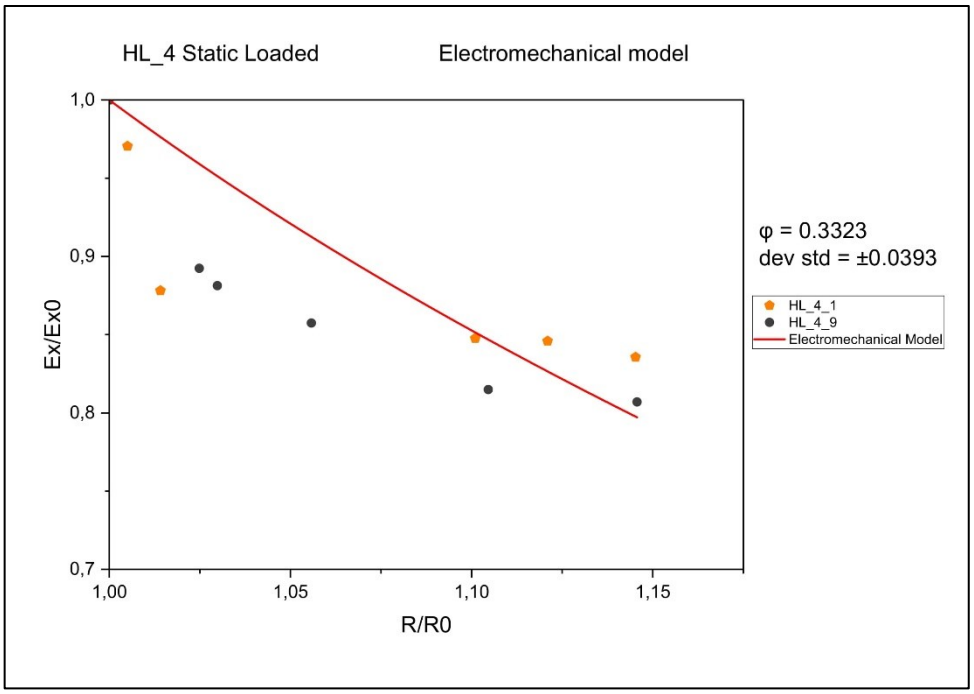

Figure 4.52 - Validation of the electromechanical model for laminate HL_4, static tested, loaded case.

It can be observed that the model works in this case, although the accuracy is not as high as in the loaded case for specimens tested under fatigue conditions.

For the unloaded case of the HL_4 laminate, the following values were obtained:

HL_4 – Static Unloaded				
Specimen	**φ**	**Std Dev Electrical Model**	**Std Dev Electromechanical Model**	**r^2**
HL_4_1	0.8332	±0.0082	±0.0647	0.8683
HL_4_9	0.7667	±0.0072	±0.0368	0.9502
HL_4	0.7932	±0.0054	±0.0320	0.8885

Table 4.20 - Values of φ, standard deviation, and r2 for HL_4 laminate, static tested. Unloaded case.

The values of φ maintain the trend of remaining higher in the unloaded case, highlighting a lower sensitivity to damage. The standard deviation values increase when moving from the validation of the electrical model to the electromechanical model, a factor that has been observed several times in the unloaded case. Below are the graphs for the validation of the electrical and electromechanical models for the specimen HL_4_1 in the unloaded case.

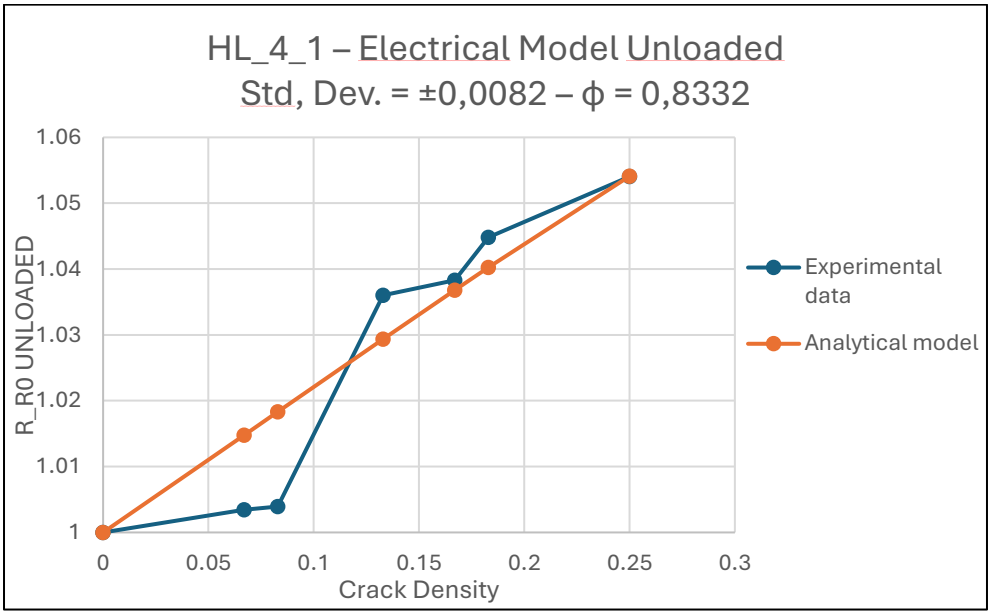

Figure 4.53 - Example of the electrical model graph calculated for each specimen. HL_4_1, static test, unloaded case.

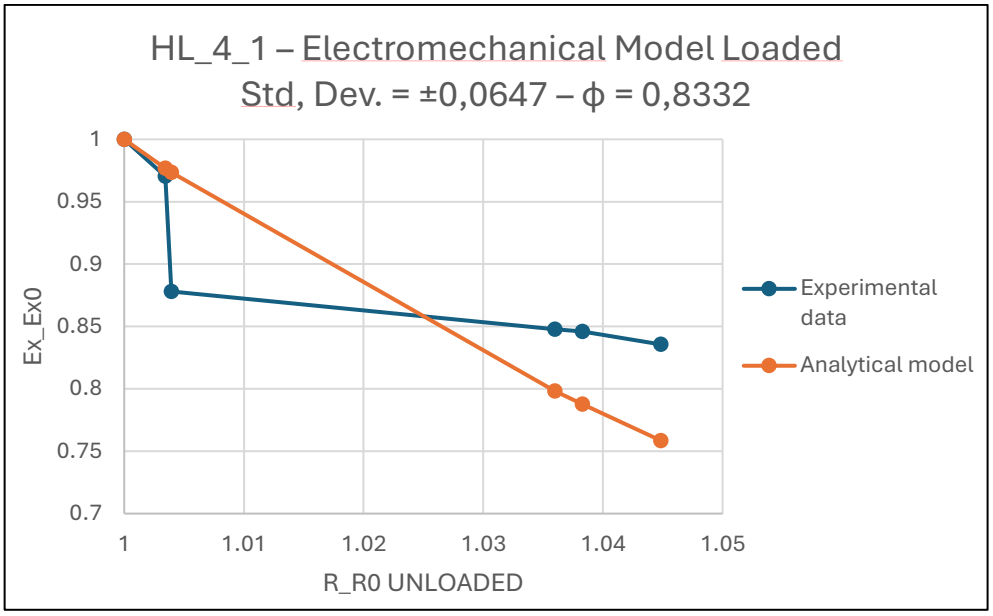

Figure 4.54 - Example of the electromechanical model graph calculated for each specimen. HL_4_1, static test, unloaded case.

The very high values of r2 indicate that the model predictions closely match the experimental data, demonstrating a high level of accuracy.

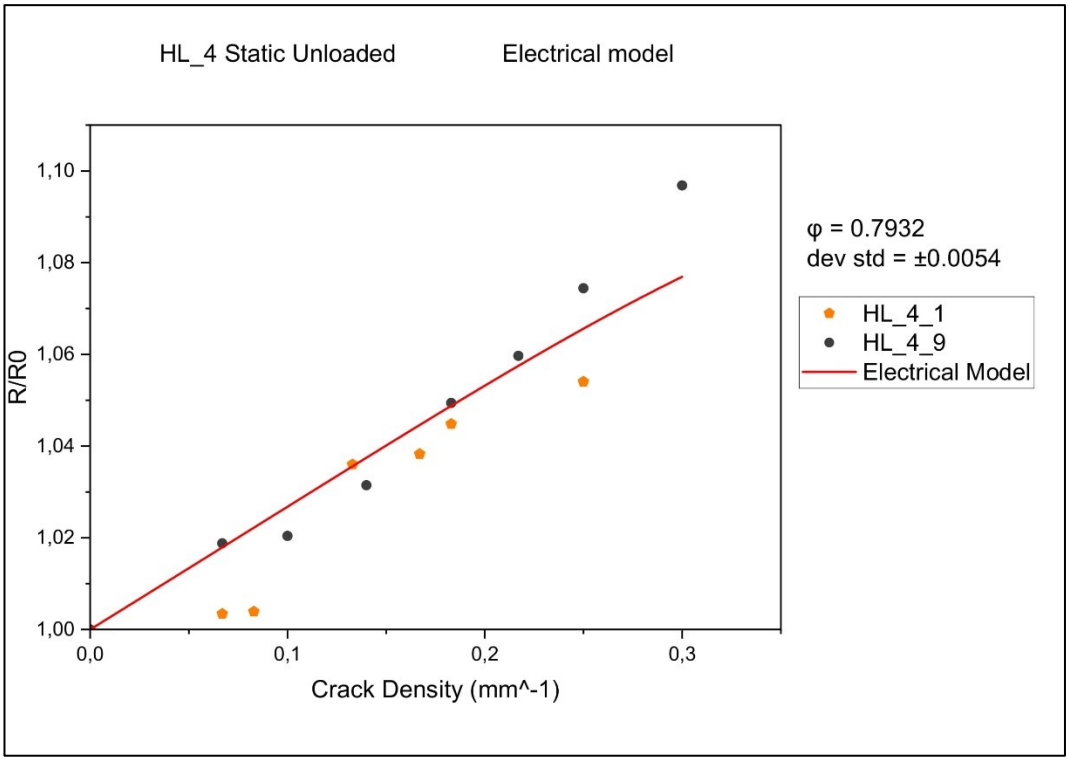

Figure 4.55 - Validation of the electrical model for laminate HL_4, static tested, unloaded case.

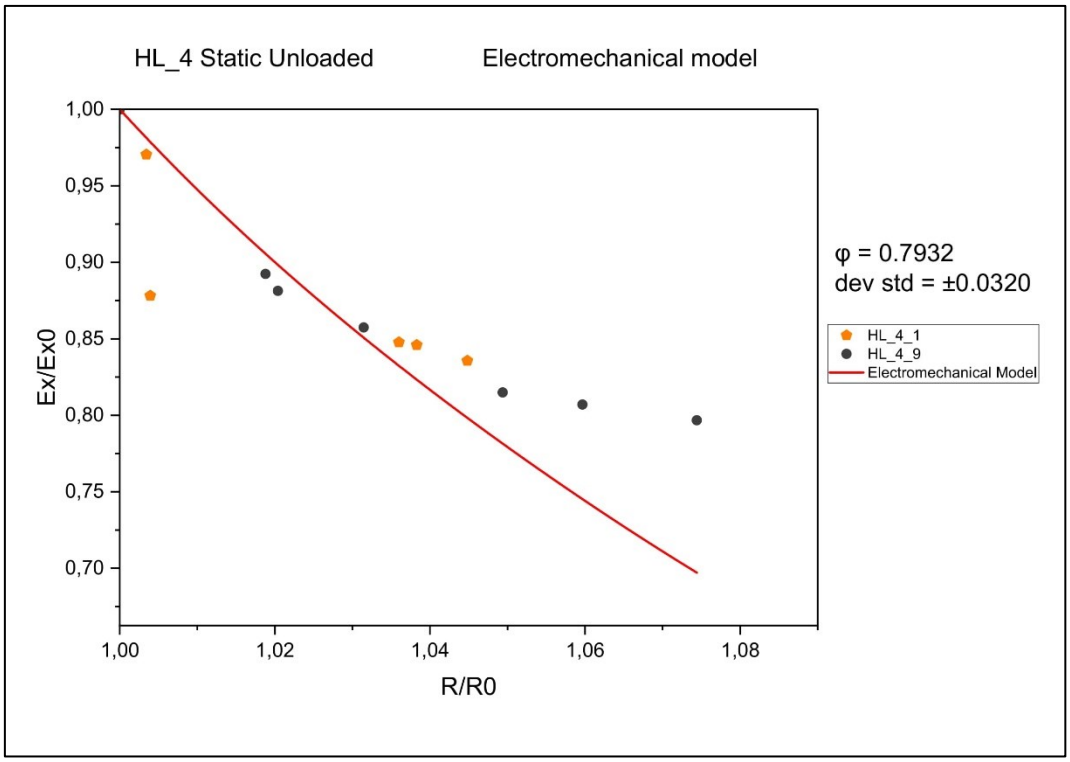

Figure 4.56 - Validation of the electromechanical model for laminate HL_4, static tested, unloaded case.

4.4.3 Roll Mill: RM_2

For the roll mill laminate type, only one specimen was tested due to a lack of material; therefore, the results may not be as accurate as those from the previous cases. However, the obtained results are still presented.

RM_2 – Static Loaded				
Specimen	**φ**	**Std Dev Electrical Model**	**Std Dev Electromechanical Model**	**r^2**
RM_2_2	0.7254	±0.0157	±0.0385	0.9158

Table 4.21 - Value of φ, standard deviation, and r2 for RM_2 laminate, static tested. Loaded case.

Similarly to the results obtained from the fatigue tests for roll mill laminates, in this case, the standard deviation increases when moving from the analytical model verification to the electromechanical model verification. The value of r^2 is very high, indicating that the model accurately predicts the behavior of the experimental data. However, further considerations cannot be made due to the lack of data. Below

are the verification graphs for the models of specimen RM_2_2 tested in the loaded case.

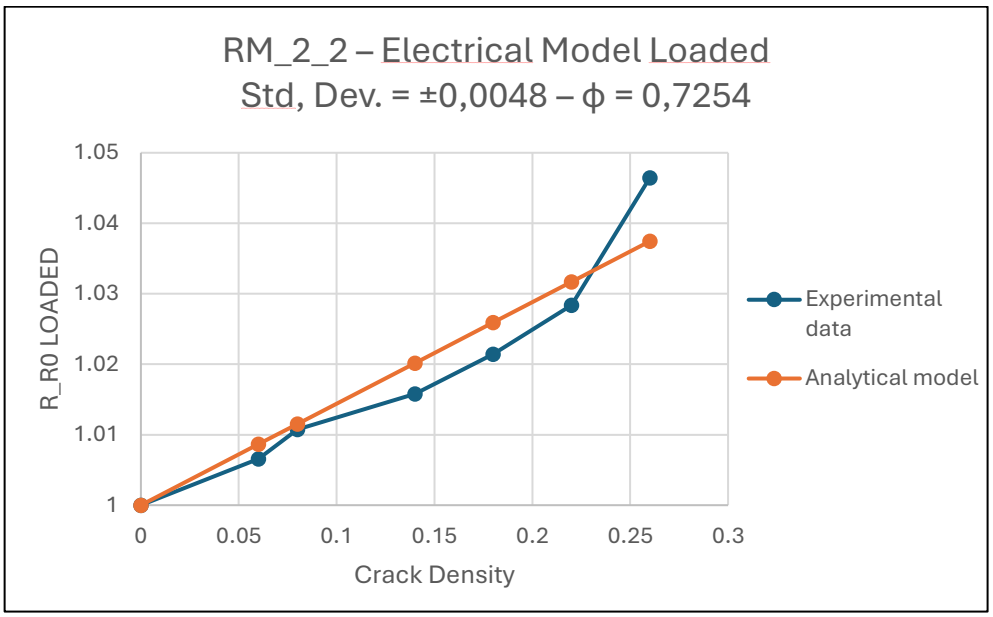

Figure 4.57 - Electrical model graph calculated for RM_2_2, static test, loaded case.

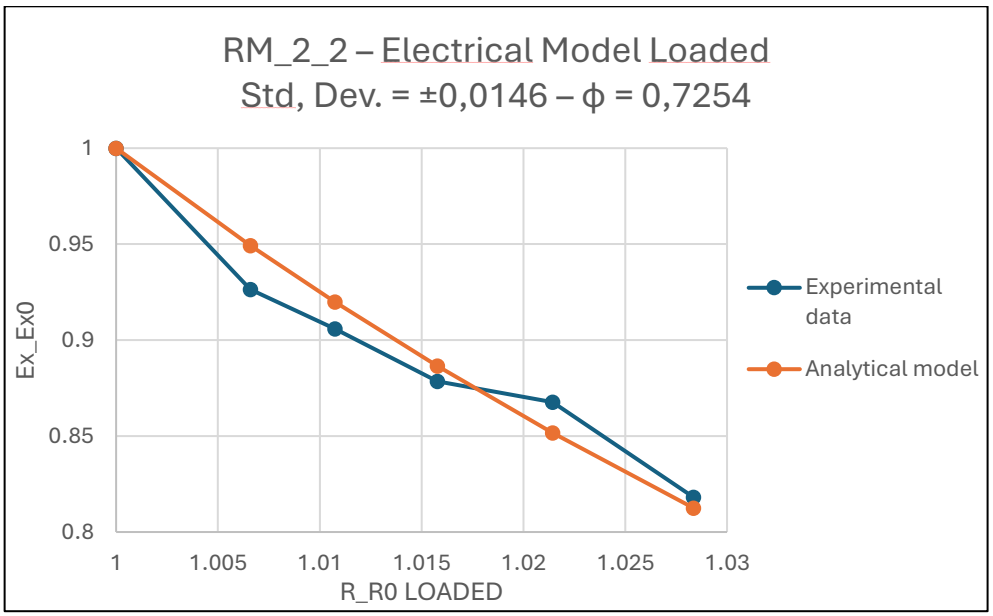

Figure 4.58 - Electromechanical model graph calculated for RM_2_2, static test, loaded case.

For the Unloaded case, the following results were obtained:

RM_2 – Static Unloaded				
Specimen	**φ**	**Std Dev Electrical Model**	**Std Dev Electromechanical Model**	**r^2**
RM_2_2	0.9314	±0.0009	±0.0145	0.9433

Table 4.22 - Values of φ, standard deviation, and r2 for RM_2 laminate, static tested. Unloaded case.

As expected, a higher value of φ is obtained in the Unloaded case, indicating that the specimen is less sensitive to damage. Similarly to before, the standard deviation increases when moving from the electrical model to the electromechanical model. Finally, the value of r2 is very high, meaning that the model accurately predicts the behavior of the experimental data. Below are the verification graphs for the models of the specimen RM_2_2 tested in the Unloaded case.

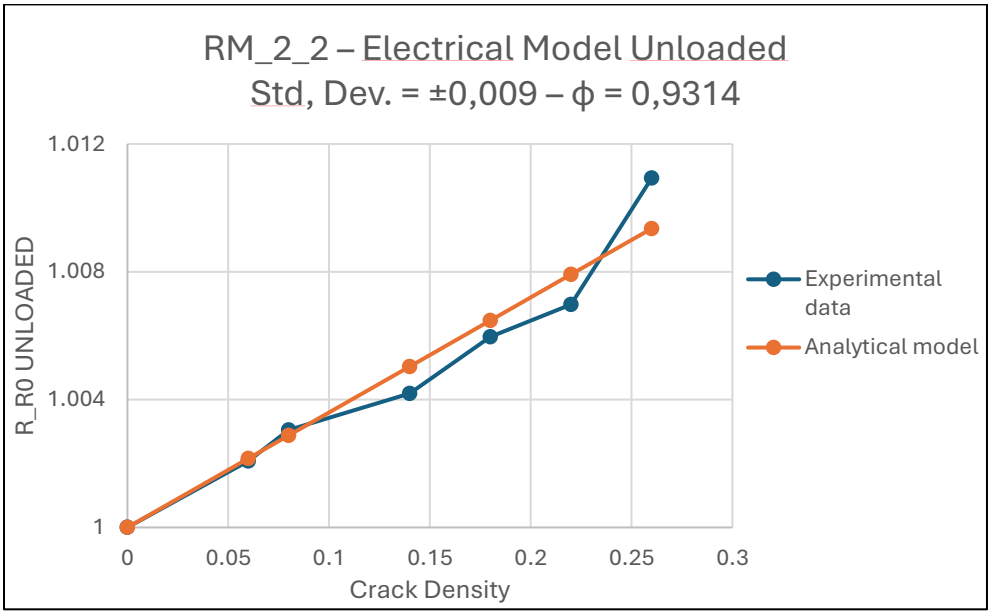

Figure 4.59 - Electrical model graph calculated for RM_2_2, static test, unloaded case.

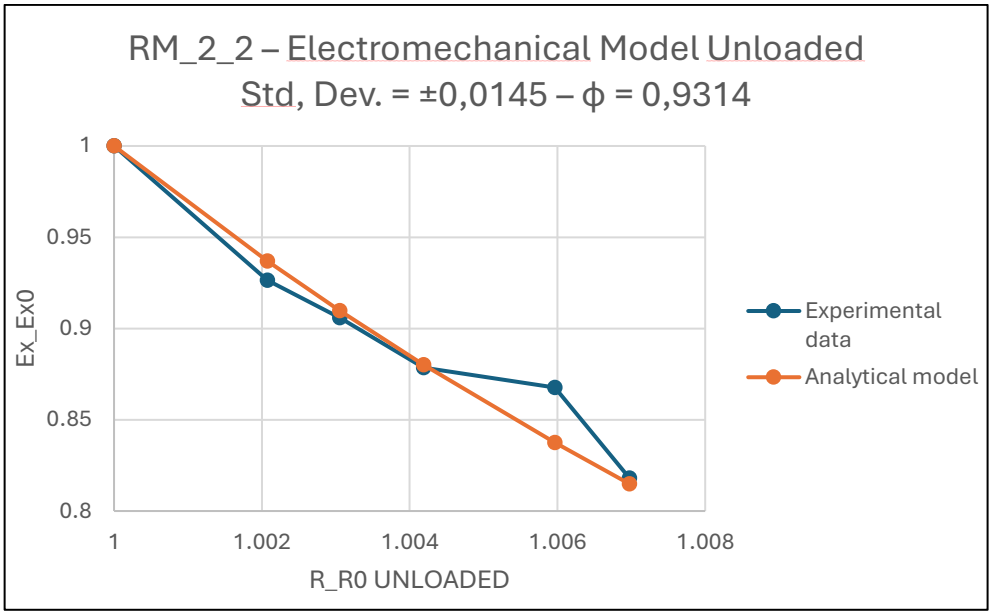

Figure 4.60 - Electromechanical model graph calculated for RM_2_2, static test, unloaded case.

4.5 Quasi-Isotropic Laminates Test Results

For the Quasi-Isotropic laminates, the same fatigue and static tests were performed as for the Cross-Ply laminates. Unfortunately, as previously mentioned, the analytical model suitable for this type of laminate [9] is not applicable in this case due to the evident delaminations present from the very first loading cycles. However, in this section, the results obtained from the tests are still reported. Similarly to what was observed for the Cross-Ply laminates, an increase in electrical resistance and a decrease in the elastic modulus were recorded for this type of specimens, both in the static and fatigue tests.

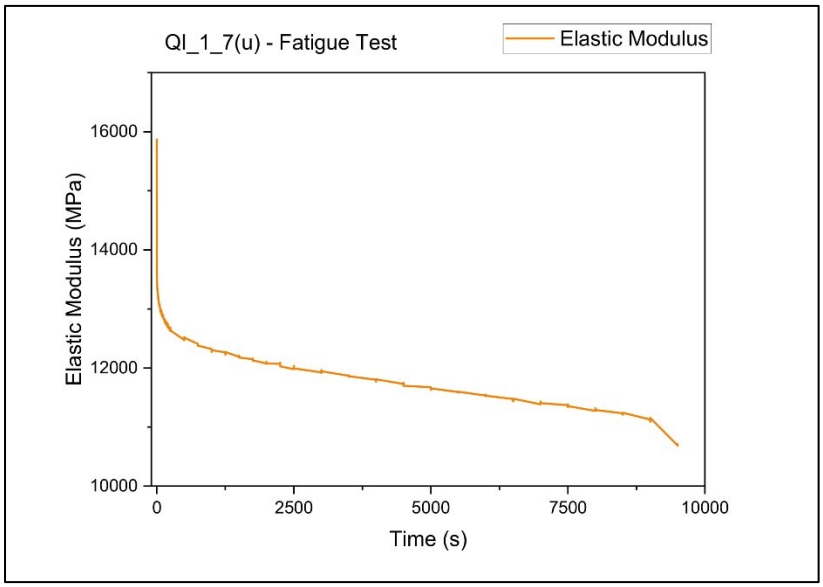

Figure 4.61 - Fatigue graph of QI_1_7(u), which is an unmodified specimen.

The graph of an unmodified specimen shows the trend of the elastic modulus recorded during the fatigue test conducted from 14 to 140 MPa, corresponding to 40% of the laminate's rupture stress, calculated to be 350 MPa. It is observed that there is a significant drop in the first few loading cycles, after which it stabilizes at a level of about 75% of the maximum elastic modulus for almost the entire life of the specimen. There is a further sudden decrease in the elastic modulus immediately before rupture. A similar behavior was observed in specimens characterized by resin modified with nanotubes.

By simultaneously observing the trend of the electrical resistance, the following graphs are obtained:

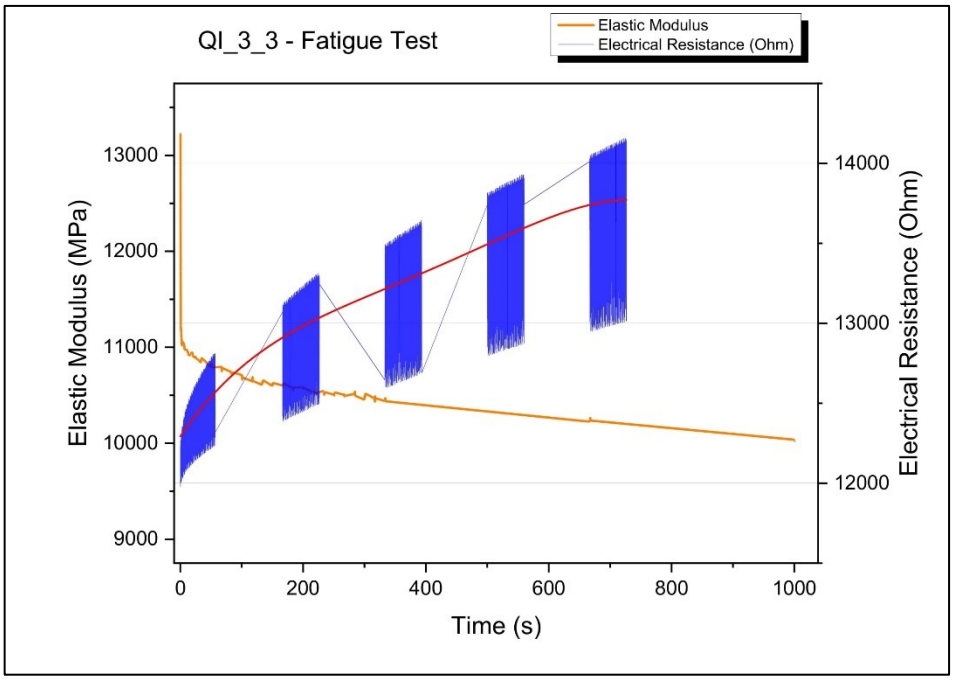

Figure 4.62 - QI_3_3, fatigue tested at 14-140 Mpa, with electrical resistance measurement.

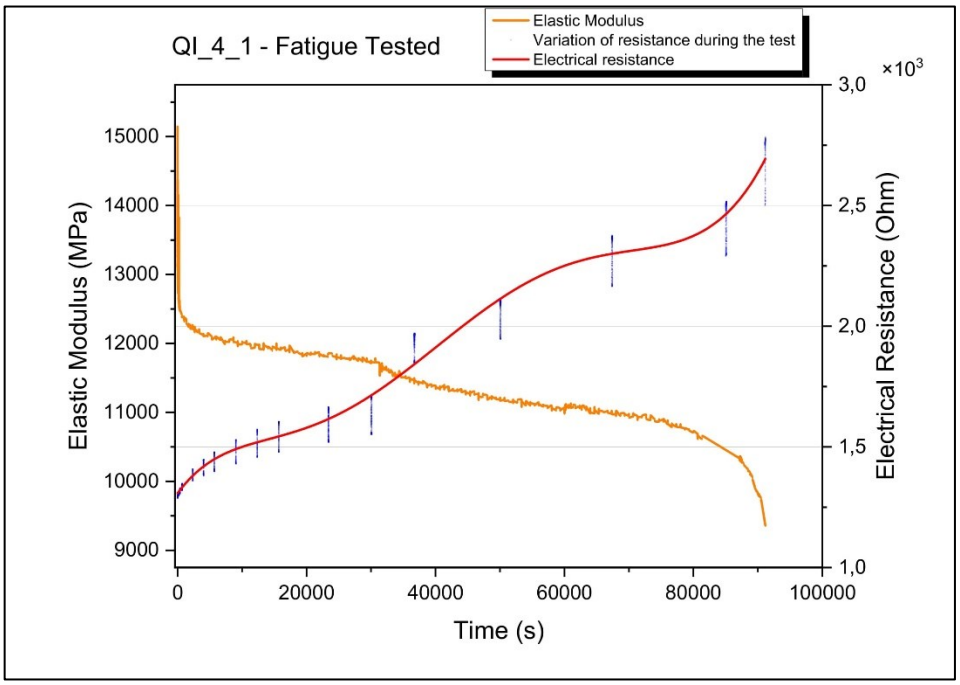

Figure 4.63 - QI_4_1 fatigue tested at 7-70 Mpa, with electrical resistance measurement.

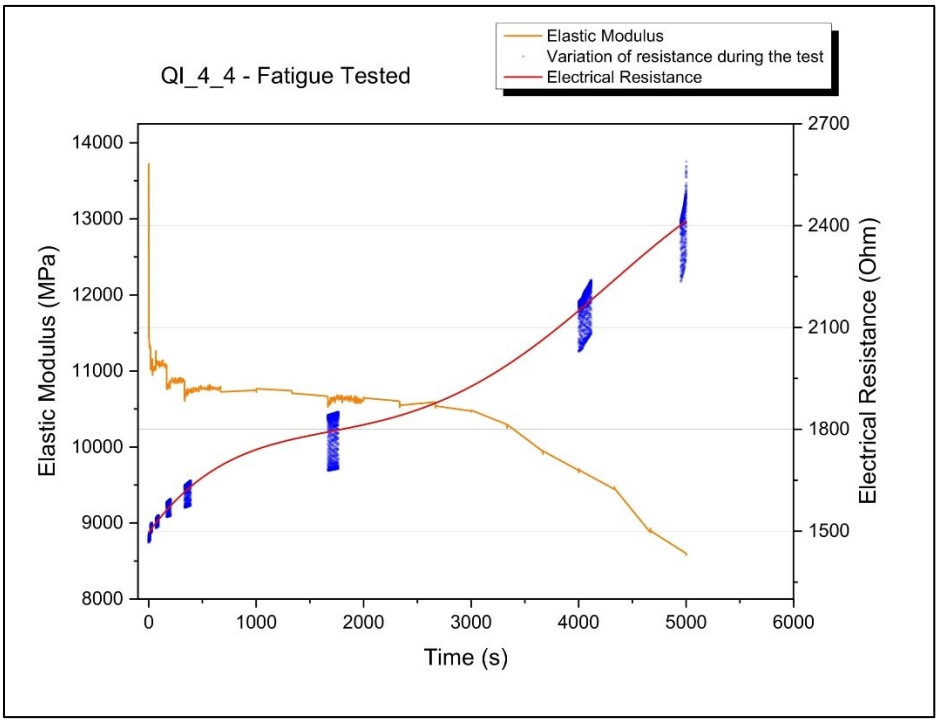

Figure 4.64 - QI_4_4 fatigue tested at 11-110 Mpa, with electrical resistance measurement.

In all the graphs, a rapid increase in electrical resistance is observed during the first few loading cycles, corresponding to the rapid decrease in elastic modulus. Later, especially in *Figure 4.64*, after the sharp rise in resistance, a plateau is reached, which lasts for most of the specimen's fatigue life. Finally, just before rupture, a further rapid increase in electrical resistance is observed, along with a sudden drop in elastic modulus. In *Figure 4.63*, at the point of a sudden drop in elastic modulus, roughly halfway through the specimen's life, there is an increase in electrical resistance. This suggests that the specimen, at that point, has undergone significant damage, such as extensive delamination or the detachment of a layer, leading to an increase in electrical resistance. A similar observation was made during the static tests, where a renewed increase in electrical resistance was recorded during the test.

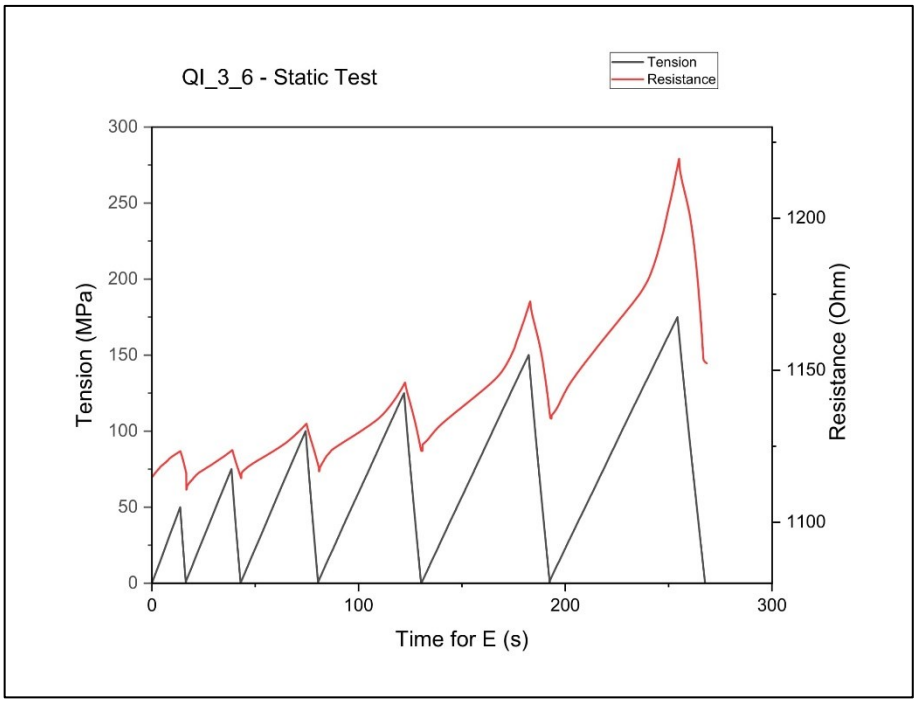

Figure 4.65 - QI_3_6 static test up to 175 Mpa, with electrical resistance measurement.

It can be observed from the graph that both the maximum electrical resistance under load (peak resistance) and the resistance when the specimen is unloaded increase.

Plates	ΔR_{LOADED}	$\Delta R_{UNLOADED}$
Quasi-Isotropic	8,55%	3,73%

Table 4.23 - Maximum increase of electrical resistance through the test.

Similarly to the Cross-Ply laminates, a more significant increase in resistance is observed under load compared to the unloaded case, indicating that the specimen shows some sensitivity to damage depending on the degree of crack opening. The values obtained are for explanatory and qualitative purposes only and should not be directly compared to those from other laminates. Indeed, during the quasi-isotropic laminate tests, numerous delaminations occurred right from the start, which likely distorted the electrical resistance values. Additionally, the test was concluded at a lower maximum voltage to avoid unanticipated failures. This phenomenon did not occur with the Cross-Ply laminates, and it is likely due to the layup of the QI laminates.

Continuing with qualitative considerations, the evolution of the number of transverse cracks that formed during the tests was also observed. In the following graphs, the values of stiffness loss and electrical resistance increase are compared with the crack density. Only transverse cracks were considered in the crack count, excluding longitudinal delaminations.

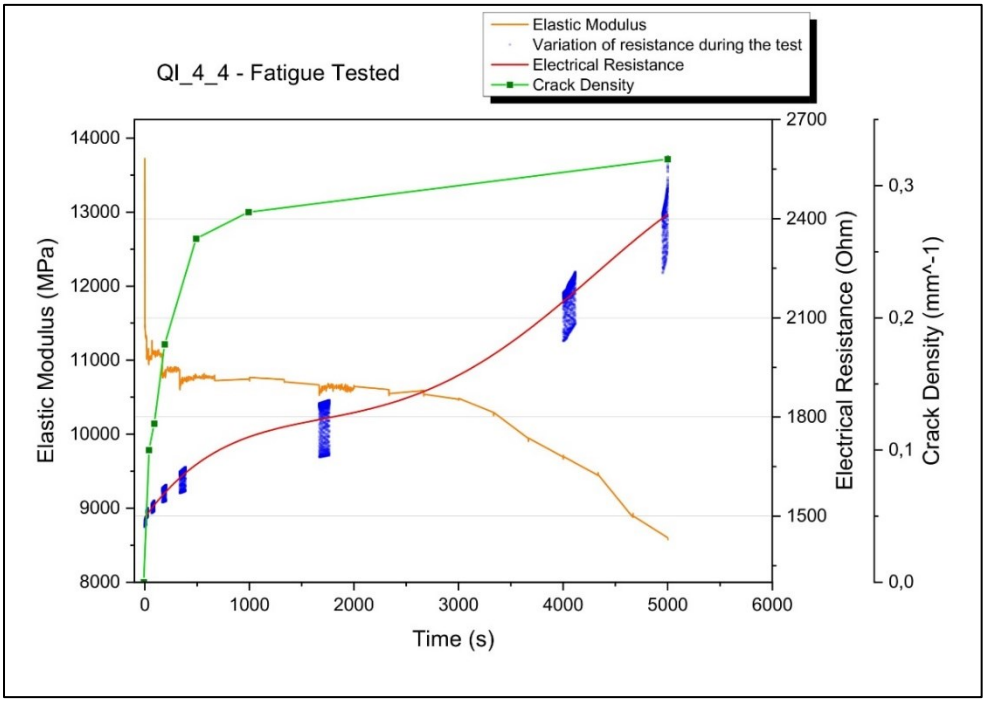

Figure 4.66 - QI_4_4 fatigue tested at 11-110 Mpa, with electrical resistance and crack density measurement.

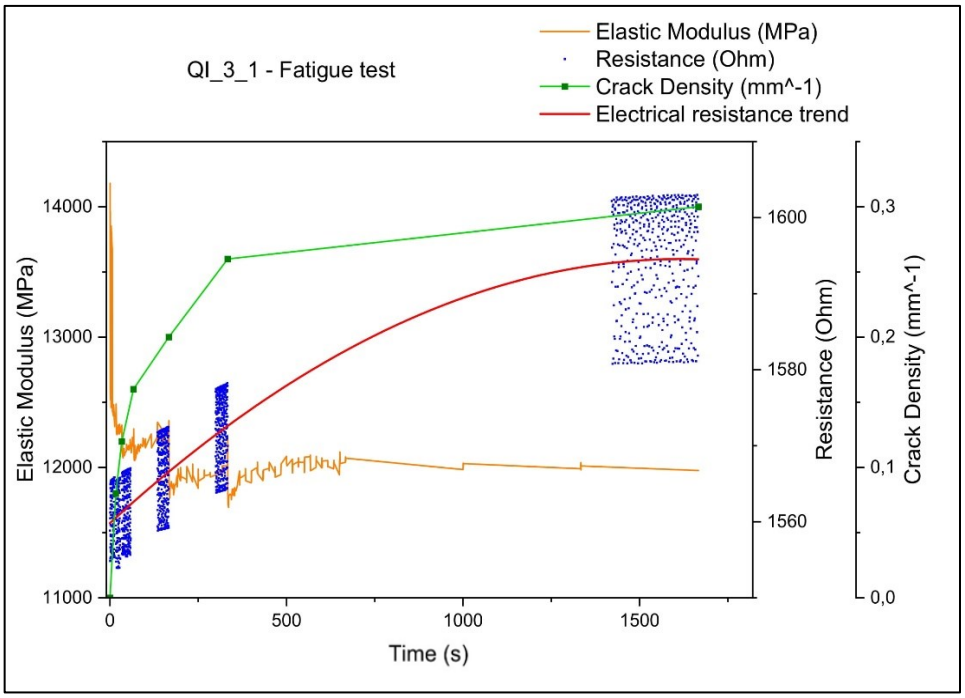

Figure 4.67 - QI_3_1 fatigue tested at 7-70 Mpa, with electrical resistance and crack density measurement.

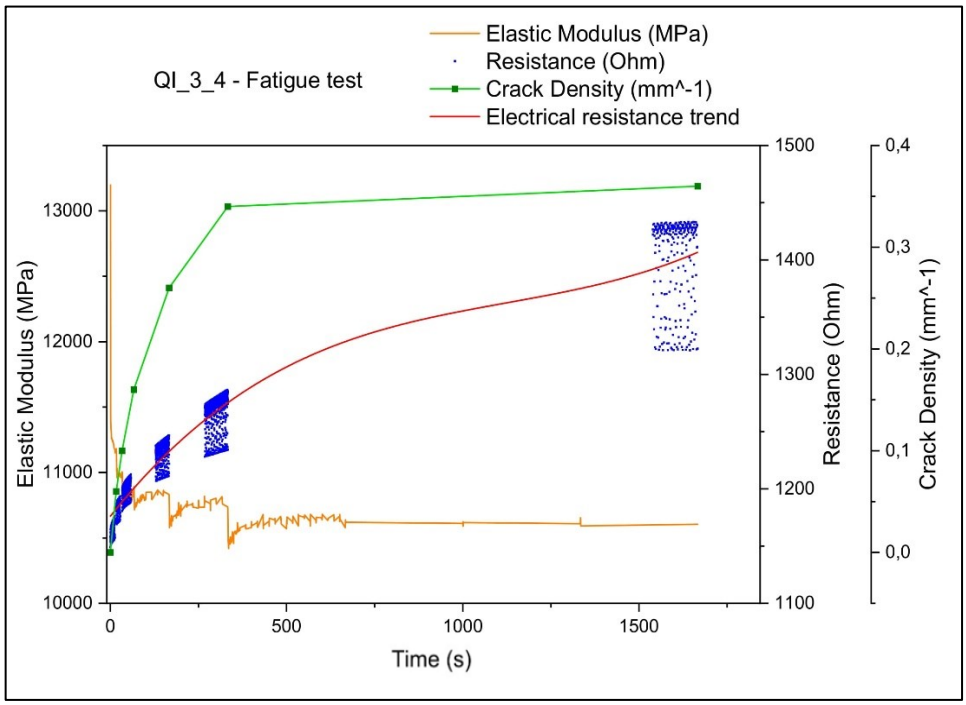

Figure 4.68 - QI_3_4 fatigue tested at 11-110 Mpa, with electrical resistance and crack density measurement.

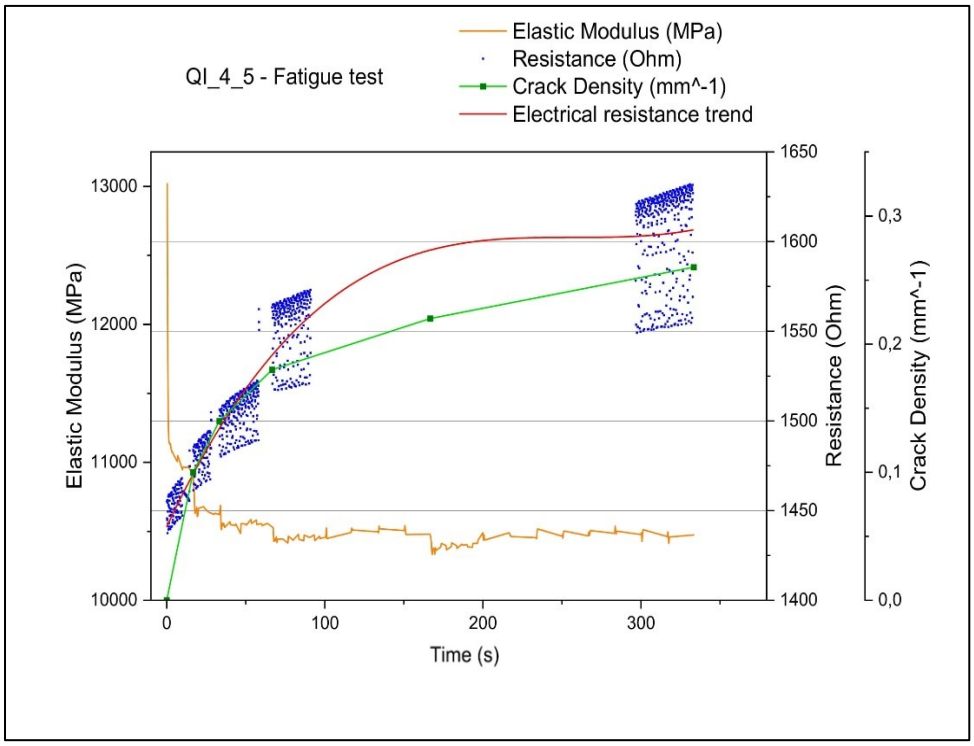

Figure 4.69 - QI_4_5 fatigue tested at 11-110 Mpa, with electrical resistance and crack density measurement.

The evolution of crack density in the quasi-isotropic laminates is very similar to that observed in the cross-ply specimens. Damage progression shows a rapid increase in the first few loading cycles, followed by a stabilization around a constant value of approximately 0,30 mm^{-1} or slightly higher. The electrical resistance follows a trend very similar to that of the crack density. The QI_4_5 specimen was tested only up to 1000 cycles, and it is observed that the crack density value is very similar to those calculated for the other specimens, where cracks were monitored up to 5000 cycles.

Similarly to the cross-ply laminates, quasi-isotropic specimens also reach crack saturation within a range comparable to that obtained for the cross-ply laminates, despite the use of different nanotubes. The only noticeable difference is that in the quasi-isotropic laminates, delaminations occur, sometimes significantly, from the early loading cycles.

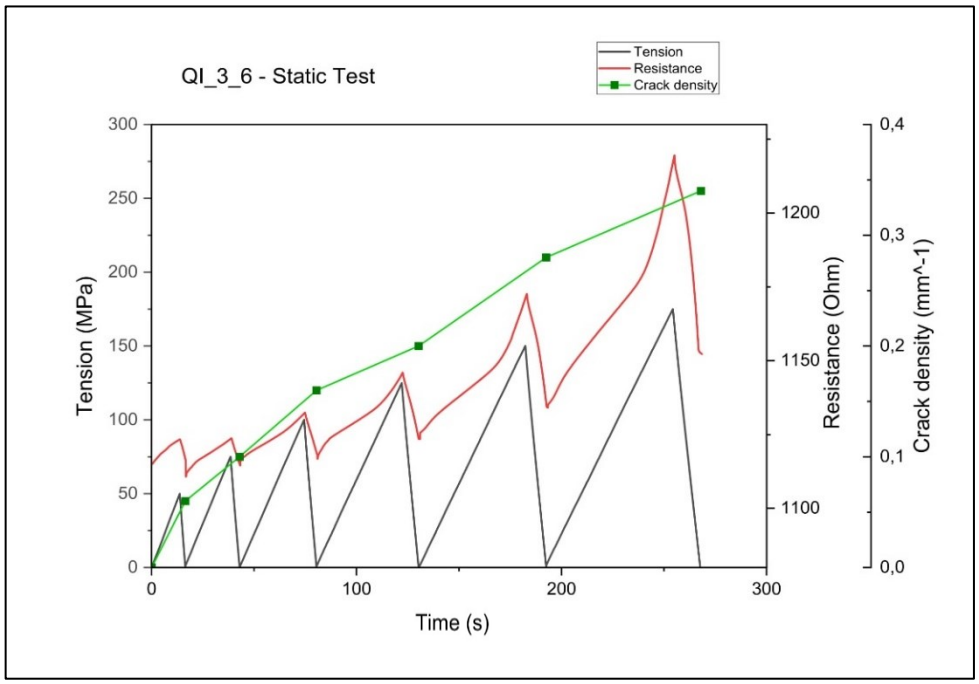

Figure 4.70 - QI_3_6 static test up to 175 Mpa, with electrical resistance and crack density measurement.

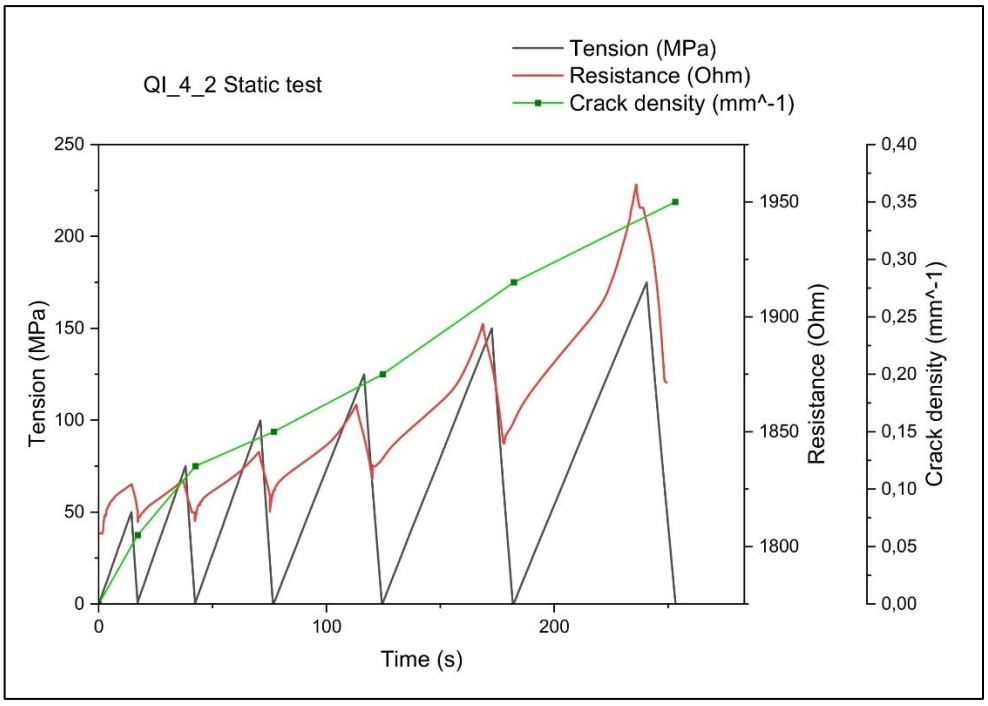

Figure 4.71 - QI_4_2 static test up to 175 Mpa, with electrical resistance and crack density measurement.

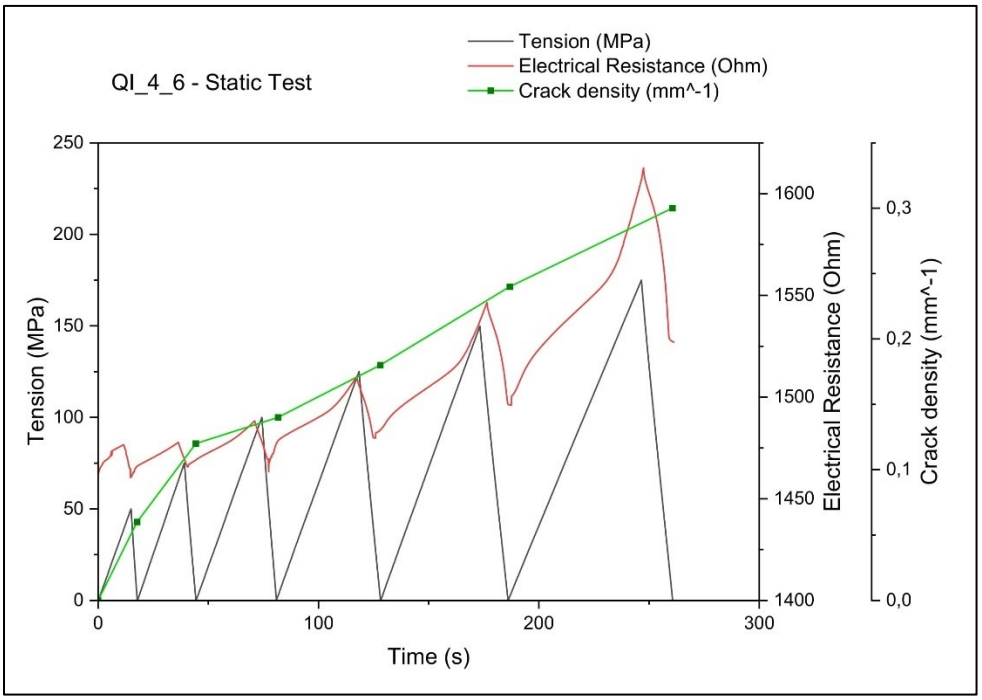

Figure 4.72 - QI_4_6 static test up to 175 Mpa, with electrical resistance and crack density measurement.

In the static tests performed, similarities between the quasi-isotropic laminates and cross-ply laminates were also observed. The tests showed that the crack density increases very rapidly from the first loading ramps and stabilizes at a saturation value slightly above 0,30 mm^{-1}. Compared to the cross-ply laminates, crack saturation is reached with lower loading ramps. In fact, the maximum load reached was 175 MPa to avoid unexpected breakages due to the rapid spread of delaminations, which were present in large quantities from the early loading cycles.

5 Conclusion

The results from the fatigue tests conducted are as follows for the laminates HL_3, HL_4, and RM_2, with the values of φ, standard deviation, and r^2:

Fatigue tests - Loaded				
Plate	**φ**	**Std Dev Electrical Model**	**Std Dev Electromechanical Model**	**r^2**
HL_3	0.5993	±0.0088	±0.0026	0.8827
HL_4	0.5431	±0.0112	±0.0050	0.7088
RM_2	0.6380	±0.0069	±0.0044	0.7803

Table 5.1 - Values of φ, standard deviation and r2 for each laminate, fatigue test, loaded case.

Fatigue tests - Unloaded				
Plate	**φ**	**Std Dev Electrical Model**	**Std Dev Electromechanical Model**	**r^2**
HL_3	0.7277	±0.0050	±0.0023	0.6464
HL_4	0.7442	±0.0054	±0.0023	0.2904
RM_2	0.9161	±0.0011	±0.0053	0.5405

Table 5.2 - Values of φ, standard deviation and r2 for each laminate, fatigue test, unloaded case.

It can be observed that for the Loaded case, the values of φ are lower than for the unloaded case. This indicates that under load, the material is more sensitive to damage, as the nanotube bridging phenomenon is reduced. Different laminates present different φ values, as they have slightly different characteristics, even though they have the same layup and were produced in the same way. The specimens from the same laminate can be considered to have the same φ; they also show slight differences from one another, but these are much smaller compared to the differences between two different laminates. The standard deviation tends to decrease significantly when moving from the electrical model to the electromechanical model. This trend is observed for all laminates, except for the RM_2 Unloaded laminate. Finally, the value of r^2 suggests that the model predicts the laminate behavior quite accurately in the loaded case. However, in the unloaded case, the predictions are much less accurate, with r^2 even reaching as low as 0.2904 for the HL_4 laminate, which indicates that the model does not predict the laminate

behavior at all. The r^2 value remains significantly lower in the unloaded case for the other specimens as well, suggesting that the analytical model used does not adequately describe the data for the unloaded condition. This observation is consistent with the findings reported in the referenced paper. [1].

From the static tests performed, the following results for φ, standard deviation, and r^2 were obtained for the laminates HL_3, HL_4, and RM_2:

Static tests - Loaded				
Plate	**φ**	**Std Dev Electrical Model**	**Std Dev Electromechanical Model**	**r^2**
HL_3	0.3645	±0.0351	±0.0183	0.7080
HL_4	0.3323	± 0.0292	± 0.0393	0.7318
RM_2	0.7254	±0.0157	±0.0385	0.9158

Table 5.3 - Values of φ, standard deviation and r2 for each laminate, static test, loaded case.

Static tests - Unloaded				
Plate	**φ**	**Std Dev Electrical Model**	**Std Dev Electromechanical Model**	**r^2**
HL_3	0.8351	±0.0043	±0.0160	0.6397
HL_4	0.7932	±0.0054	±0.0320	0.8885
RM_2	0.9314	±0.0009	±0.0145	0.9433

Table 5.4 - Values of φ, standard deviation and r2 for each laminate, static test, unloaded case.

The value of φ obtained for the loaded case indicates a greater sensitivity to damage for the specimens compared to the unloaded case, although, in general, the specimen manufactured via roll mill exhibits a significantly lower sensitivity compared to its hand-laid counterpart. The trend of the standard deviation is not very clear, as in some cases it increases when moving from the electrical model to the electromechanical model, while in other cases it decreases. Overall, the r^2 value indicates that the model predicts the behavior of the experimental data with good accuracy. However, it should be noted that only in the case of HL_3 was a sufficient number of specimens tested, with only two tested for HL_4 and only one for RM_2 due to a lack of additional material.

In conclusion, it has been demonstrated that there is a correlation between the internal damage of the material and the increase in electrical resistance. Furthermore, it has been verified that the material shows different sensitivity to damage depending on the loading conditions it is subjected to. Each laminate, under the same conditions, exhibits different sensitivity to damage, represented by the parameter φ, while specimens of the same laminate exhibit the same φ. It is also stated that the analytical model for health monitoring of cross-ply laminates [1] works and is able to predict the experimental data behavior with sufficient accuracy in the loaded case, where the material shows a greater sensitivity to damage. The model, however, in according to [1] does not describe the material behavior in the unloaded condition, where r^2 values are consistently lower across all cases in which a sufficient number of specimens were tested.

For quasi-isotropic laminates, the considerations made were mostly qualitative, due to the absence of a valid model to study the collected data. However, a correlation between the increase in internal damage and the increase in electrical resistance was also observed for these types of laminates. Similar to what was observed for cross-ply laminates, quasi-isotropic laminates also exhibit varying sensitivity to damage depending on the loading conditions. Furthermore, different laminates show different variations in electrical current during the test, suggesting that, similarly, different laminates will have different sensitivities to damage under the same loading conditions.

References

[1] P. A. Carraro, M. Zappalorto and M. Quaresimin, "Health monitoring of cross-ply laminates: Modelling the correlation," *Elsevier,* vol. Composites: Part A, no. 82, pp. 151-158, 2016.

[2] J. Knoll, B. Riecken, N. Kosmann, S. Chandrasekaran, K. Schulte and B. Fiedler, "The effect of carbon nanoparticles on the fatigue performance," *Elsevier,* vol. Composites: Part A, no. 67, pp. 233-240, 2014.

[3] D. Fritsch, C. Viets, E. Mannov, K. Schulte and B. Fiedler, "Nanocomposite Based Structural Health Monitoring Approaches for Fibre Reinforced Polymers," *HAL archives-ouvertes.fr,* Vols. HAL Id: hal-01022027, no. https://hal.inria.fr/hal-01022027, 2014.

[4] F. H. Gojny, M. H. Wichmann, B. Fiedler and K. Schulte, "Influence of different carbon nanotubes on the mechanical properties of epoxy matrix composites – A comparative study," *Elsevier,* vol. Composites Science and Technology, no. 65, pp. 2300-2313, 2005.

[5] Leopold, Augustin and e. al., "Influence of carbon nanoparticle modification on the mechanical and electrical properties of epoxy in small volumes," *Journal of Colloid and Interface Science,* pp. 620-632, 2017.

[6] L. Boger, "Load and health monitoring in glass fiber reinforced composites with an electrical conductive nanocomposite epoxy matrix," *Composite Science and Technology 68,* pp. 1886-1894, 2008.

[7] B. Fiedler and e. a. Augustin, "Health monitoring of CFRP using printed circuits," *Jet Composites Magazine,* pp. 61-63, 2017.

[8] C. Buggish, D. Gibhardt, N. Felmet, Y. Tetzner and B. Fiedler, "Strain sensing in GFRPvia fully integrated carbon nanotube epoxy film sensor," *Compositer Part C: Open Acces 6,* pp. 1-12, 2021.

[9] M. Zappalorto, P. Carraro, R. Pietrogrande and M. Quaresimin, "Modelling the electrical resistance of multidirectional laminates with off-axis cracks. https://doi.org/10.1016/j.compstruct.2020.111928," *Composite Structures,* vol. 111928, p. 237, 2020.

[10] H. Meeuw, J. Körbelin, D. V. Bernstorf, T. Augustin, W. Liebig and B. Fiedler, "Smart dispersion: Validation of OCT and impedance spectroscopy as solutions for in-situ dispersion analysis of CNP/EP-composites," *Elsevier.*

Appendix

Graphs for the validation of the analytical model – Fatigue test

HL_3_1

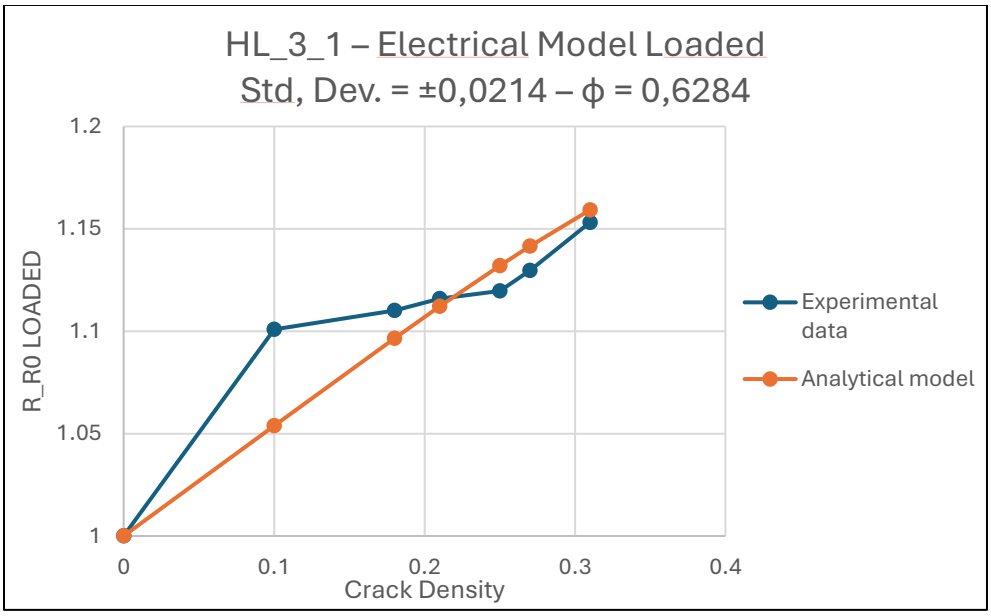

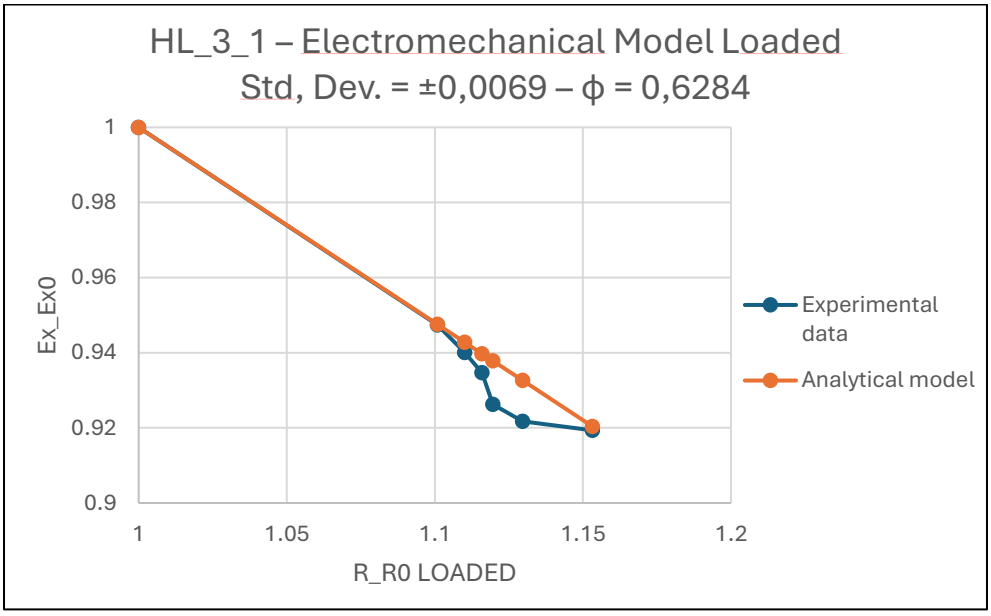

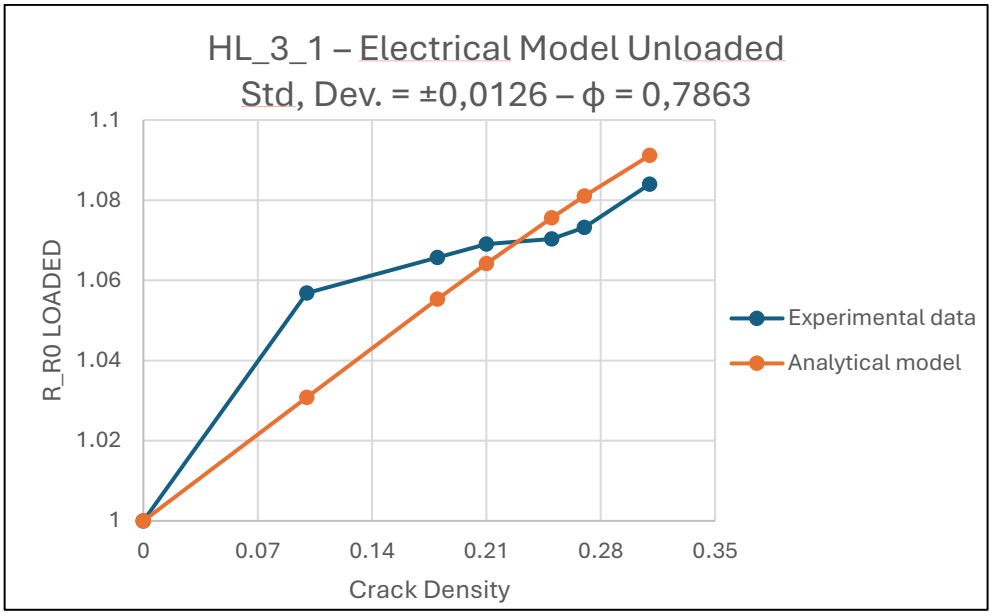
HL_3_1 – Electrical Model Unloaded
Std, Dev. = ±0,0126 – ϕ = 0,7863
R_R0 LOADED
1.1
1.08
1.06
1.04
1.02
1
0
0.07
0.14
0.21
0.28
0.35
Crack Density
Experimental data
Analytical model

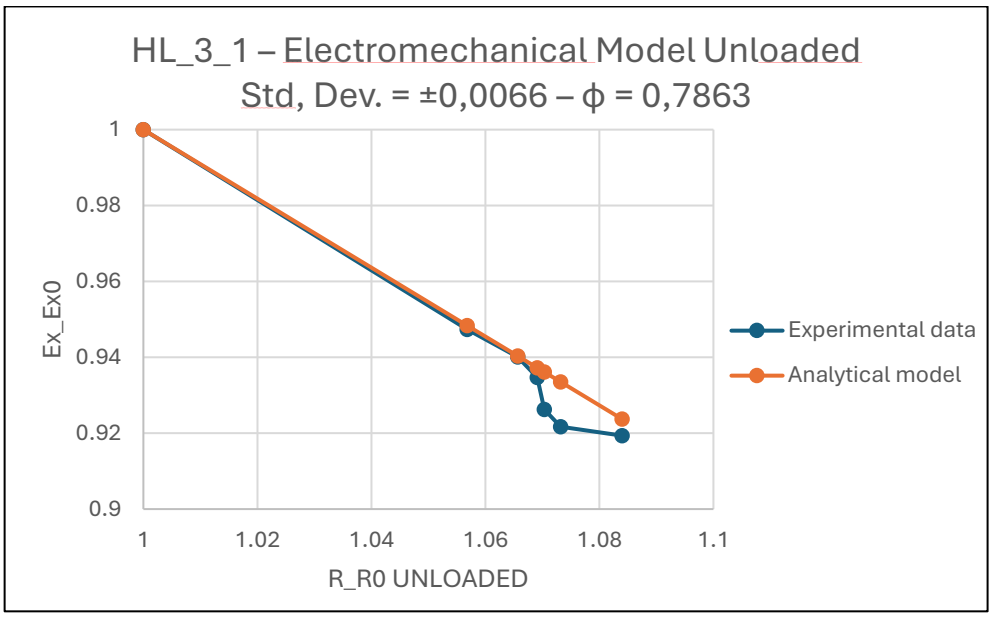
HL_3_1 – Electromechanical Model Unloaded
Std, Dev. = ±0,0066 – ϕ = 0,7863
Ex_Ex0
1
0.98
0.96
0.94
0.92
0.9
1
1.02
1.04
1.06
1.08
1.1
R_R0 UNLOADED
Experimental data
Analytical model

HL_3_4

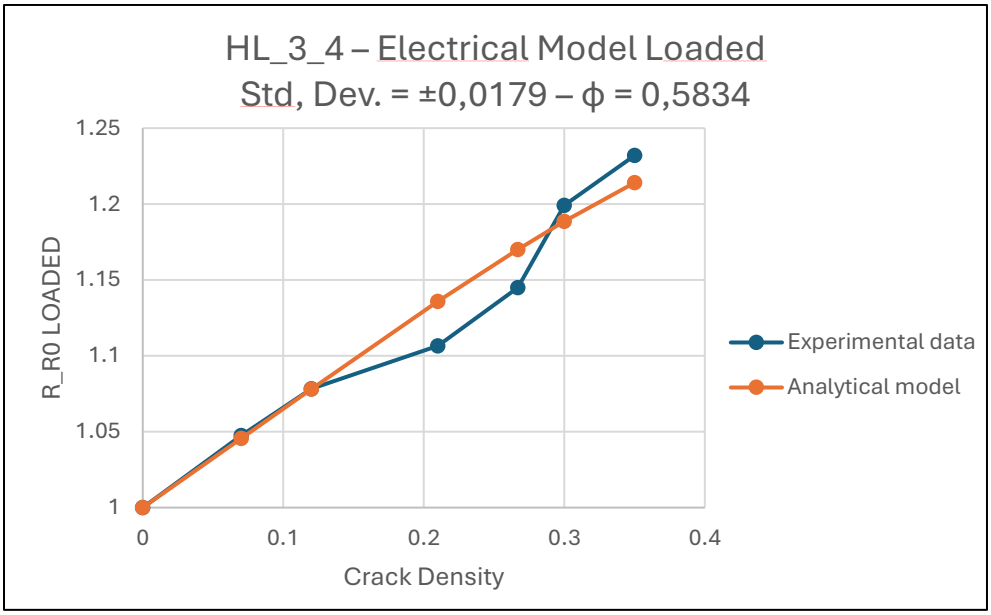
HL_3_4 – Electrical Model Loaded
Std, Dev. = ±0,0179 – ϕ = 0,5834
R_R0 LOADED
1.25
1.2
1.15
1.1
1.05
1
0
0.1
0.2
0.3
0.4
Crack Density
Experimental data
Analytical model

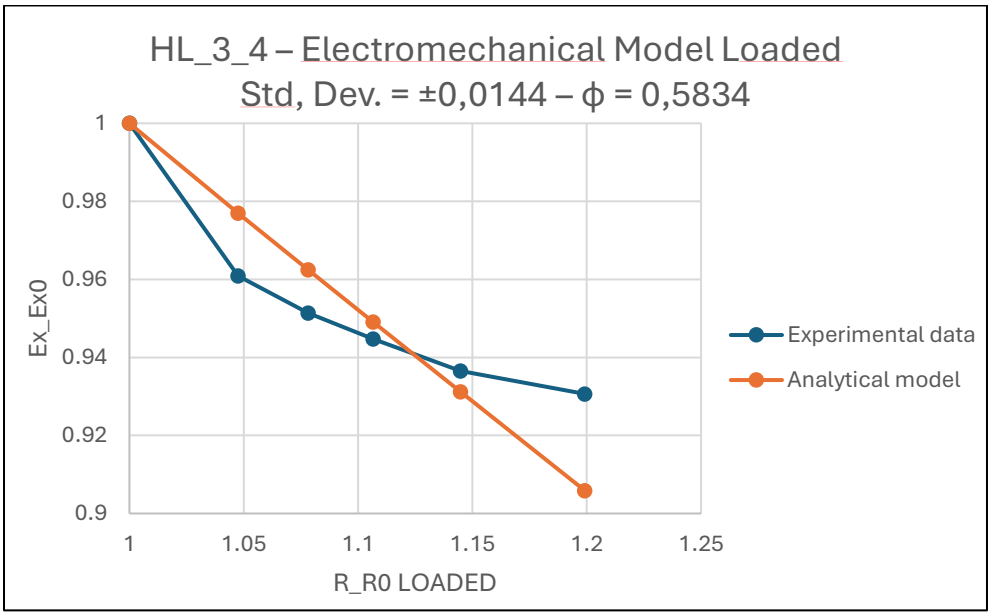
HL_3_4 – Electromechanical Model Loaded
Std, Dev. = ±0,0144 – ϕ = 0,5834
Ex_Ex0
1
0.98
0.96
0.94
0.92
0.9
1
1.05
1.1
1.15
1.2
1.25
R_R0 LOADED
Experimental data
Analytical model

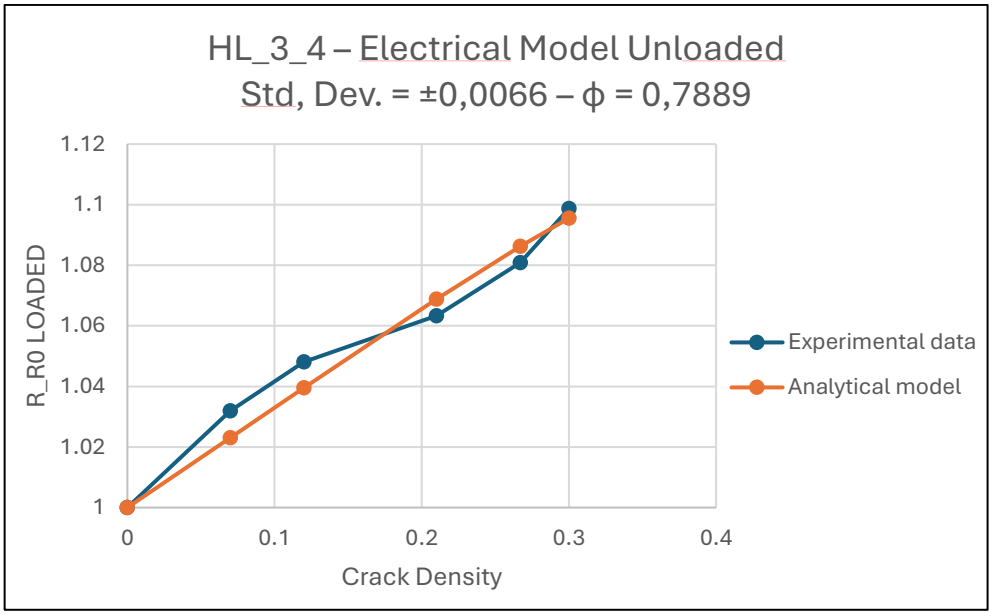
HL_3_4 – Electrical Model Unloaded
Std, Dev. = ±0,0066 – ϕ = 0,7889
R_R0 LOADED
1.12
1.1
1.08
1.06
1.04
1.02
1
0
0.1
0.2
0.3
0.4
Crack Density
Experimental data
Analytical model

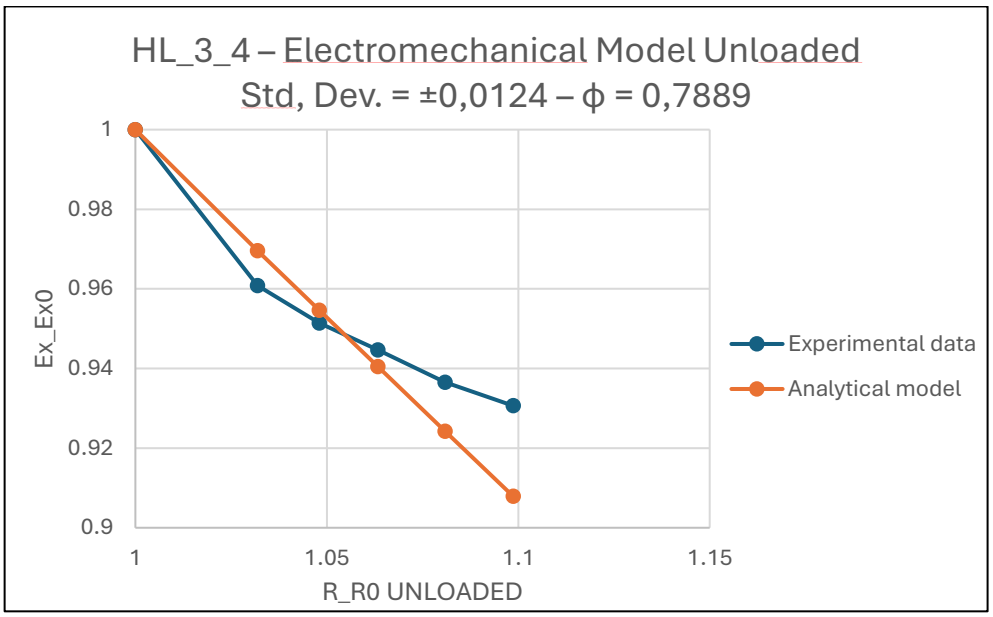
HL_3_4 – Electromechanical Model Unloaded
Std, Dev. = ±0,0124 – ϕ = 0,7889
Ex_Ex0
1
0.98
0.96
0.94
0.92
0.9
1
1.05
1.1
1.15
R_R0 UNLOADED
Experimental data
Analytical model

HL_3_5

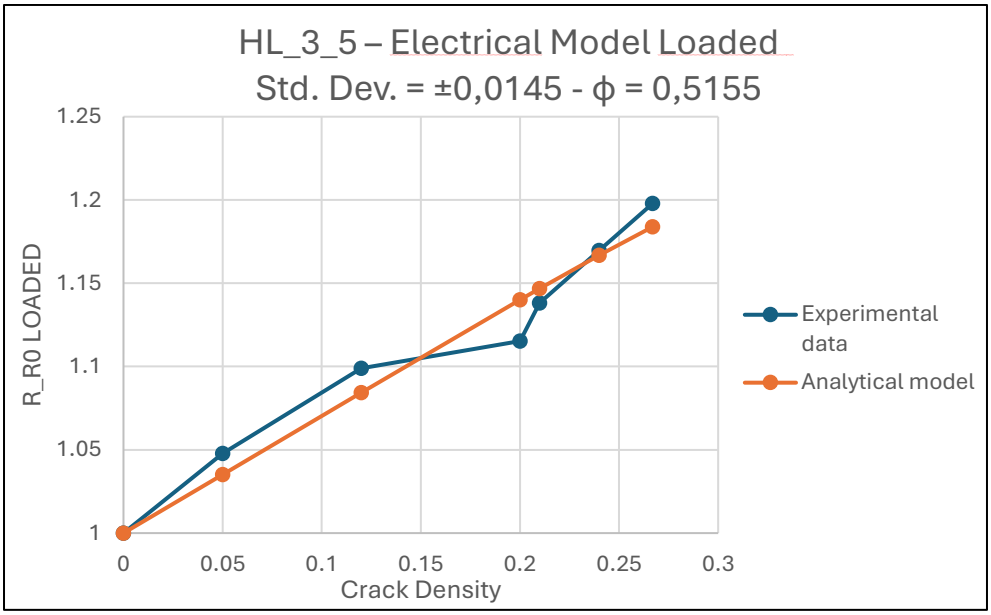
HL_3_5 – Electrical Model Loaded
Std. Dev. = ±0,0145 - ϕ = 0,5155
R_R0 LOADED
1.25
1.2
1.15
1.1
1.05
1
0
0.05
0.1
0.15
0.2
0.25
0.3
Crack Density
Experimental data
Analytical model

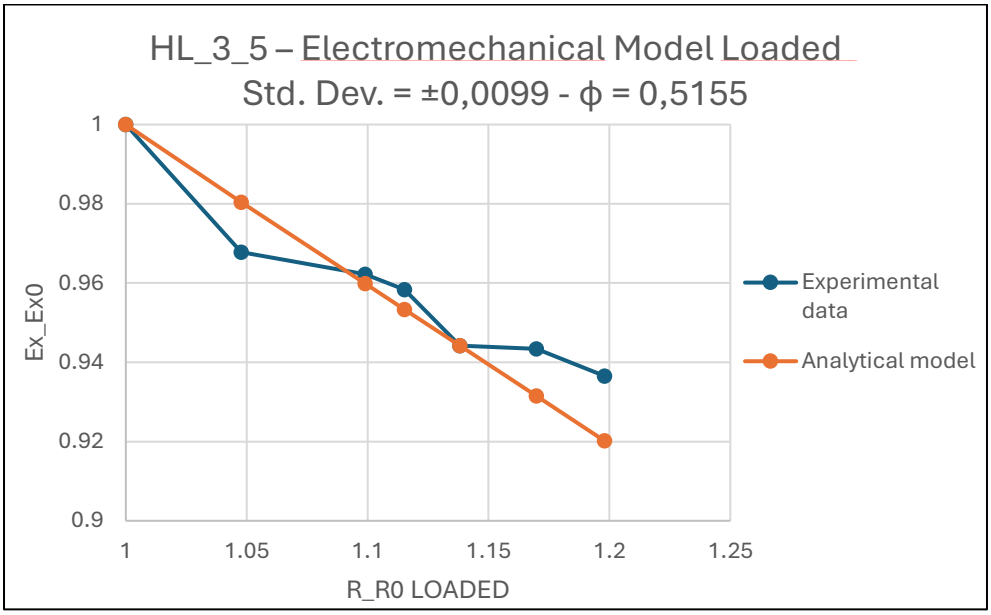
HL_3_5 – Electromechanical Model Loaded
Std. Dev. = ±0,0099 - ϕ = 0,5155
Ex_Ex0
1
0.98
0.96
0.94
0.92
0.9
1
1.05
1.1
1.15
1.2
1.25
R_R0 LOADED
Experimental data
Analytical model

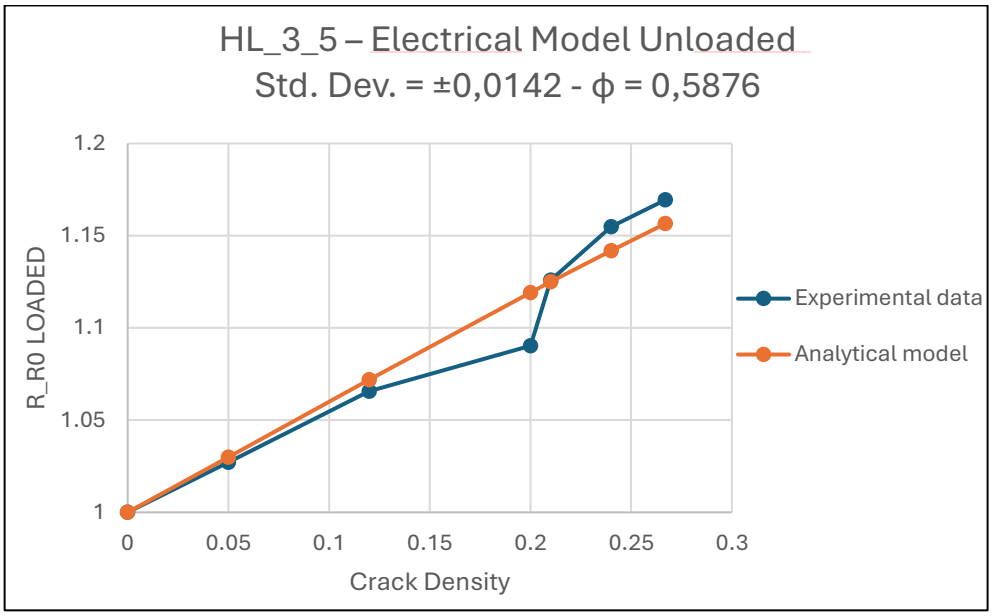
HL_3_5 – Electrical Model Unloaded
Std. Dev. = ±0,0142 - ϕ = 0,5876
R_R0 LOADED
1.2
1.15
1.1
1.05
1
0
0.05
0.1
0.15
0.2
0.25
0.3
Crack Density
Experimental data
Analytical model

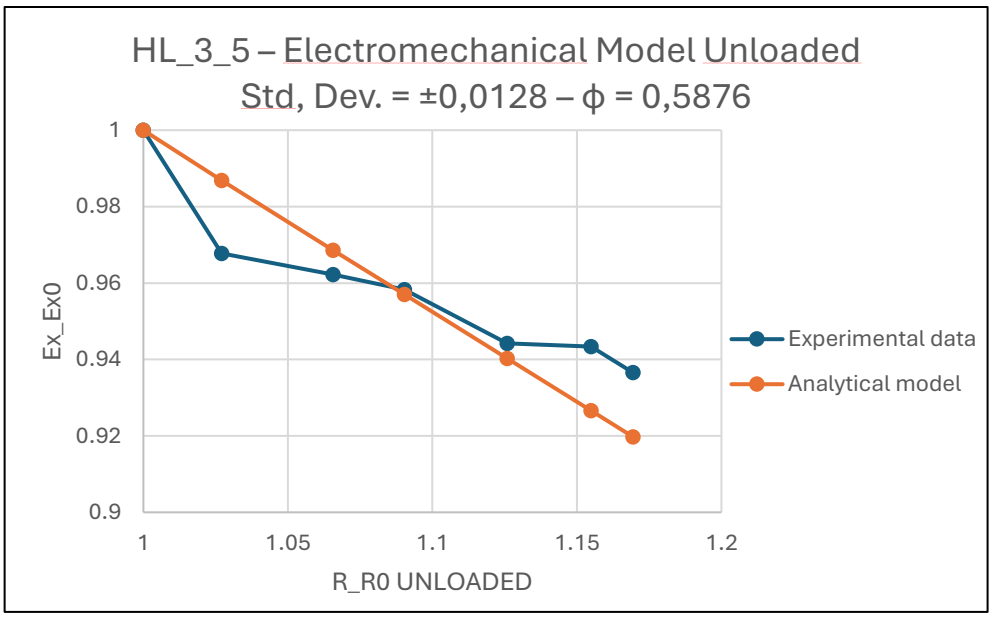
HL_3_5 – Electromechanical Model Unloaded
Std, Dev. = ±0,0128 – ϕ = 0,5876
Ex_Ex0
1
0.98
0.96
0.94
0.92
0.9
1
1.05
1.1
1.15
1.2
R_R0 UNLOADED
Experimental data
Analytical model

HL_3_7

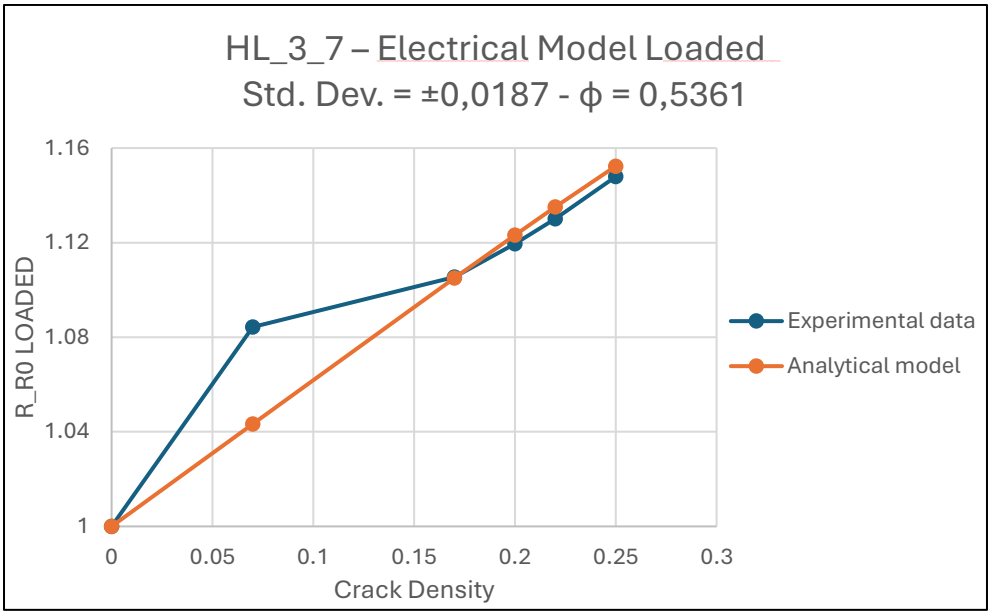
HL_3_7 – Electrical Model Loaded
Std. Dev. = ±0,0187 - ϕ = 0,5361
R_R0 LOADED
1.16
1.12
1.08
1.04
1
0
0.05
0.1
0.15
0.2
0.25
0.3
Crack Density
Experimental data
Analytical model

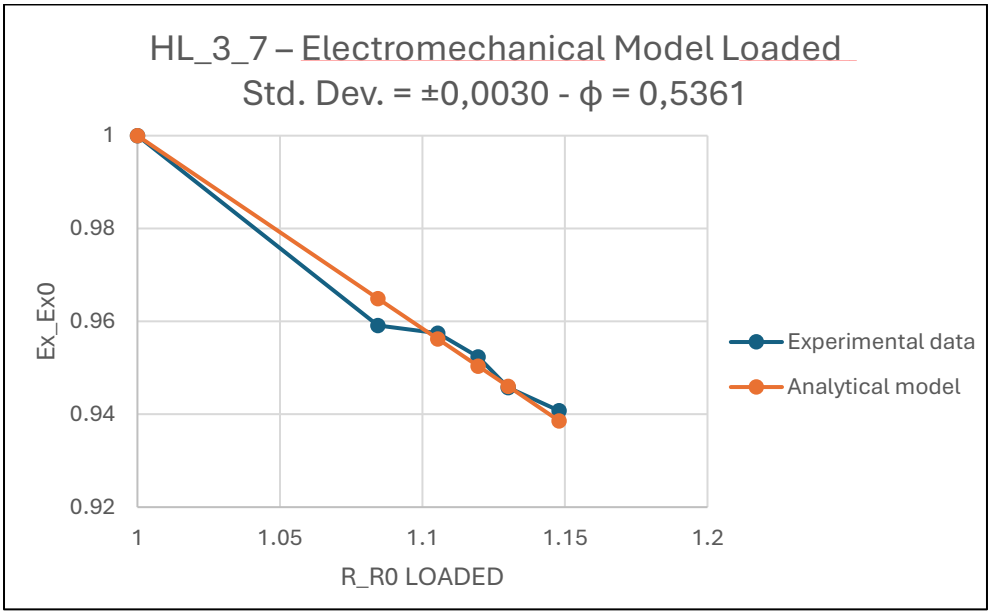
HL_3_7 – Electromechanical Model Loaded
Std. Dev. = ±0,0030 - ϕ = 0,5361
Ex_Ex0
1
0.98
0.96
0.94
0.92
1
1.05
1.1
1.15
1.2
R_R0 LOADED
Experimental data
Analytical model

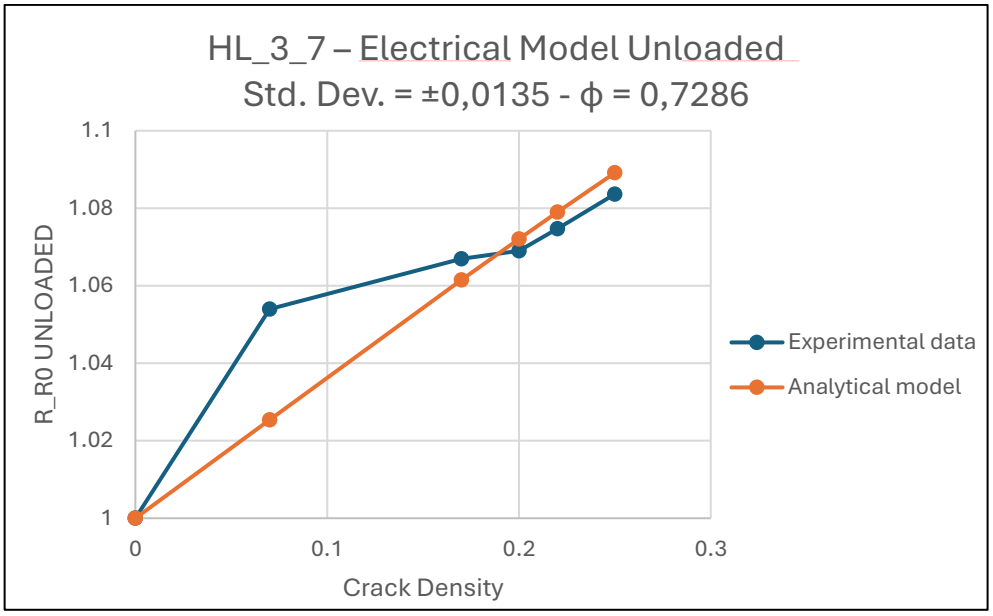
HL_3_7 – Electrical Model Unloaded
Std. Dev. = ±0,0135 - ϕ = 0,7286
R_R0 UNLOADED
1.1
1.08
1.06
1.04
1.02
1
0
0.1
0.2
0.3
Crack Density
Experimental data
Analytical model

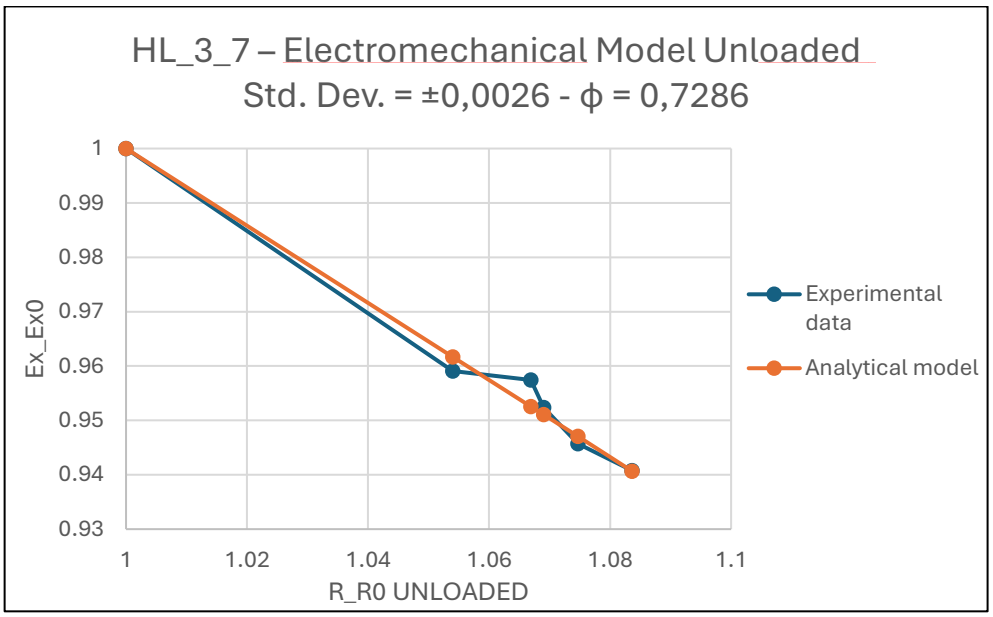
HL_3_7 – Electromechanical Model Unloaded
Std. Dev. = ±0,0026 - ϕ = 0,7286
Ex_Ex0
1
0.99
0.98
0.97
0.96
0.95
0.94
0.93
1
1.02
1.04
1.06
1.08
1.1
R_R0 UNLOADED
Experimental data
Analytical model

HL_4_4

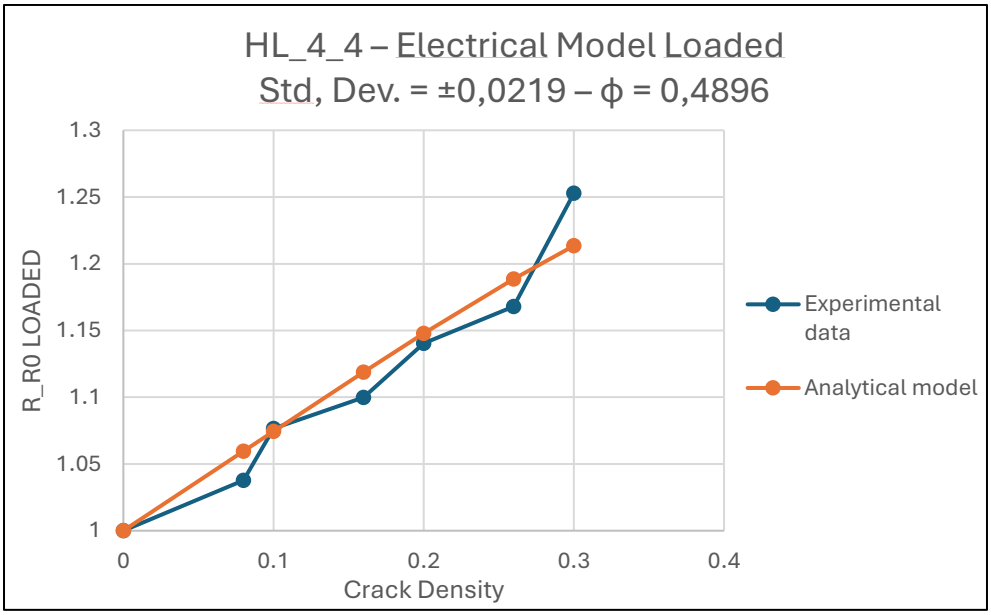
HL_4_4 – Electrical Model Loaded
Std, Dev. = ±0,0219 – ϕ = 0,4896
R_R0 LOADED
1.3
1.25
1.2
1.15
1.1
1.05
1
0
0.1
0.2
0.3
0.4
Crack Density
Experimental data
Analytical model

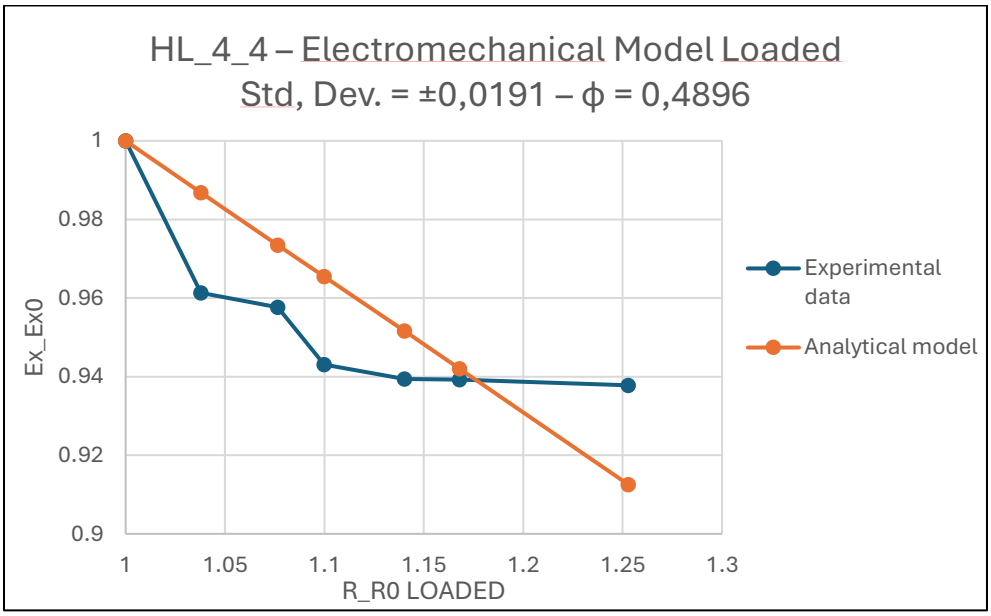
HL_4_4 – Electromechanical Model Loaded
Std, Dev. = ±0,0191 – ϕ = 0,4896
Ex_Ex0
1
0.98
0.96
0.94
0.92
0.9
1
1.05
1.1
1.15
1.2
1.25
1.3
R_R0 LOADED
Experimental data
Analytical model

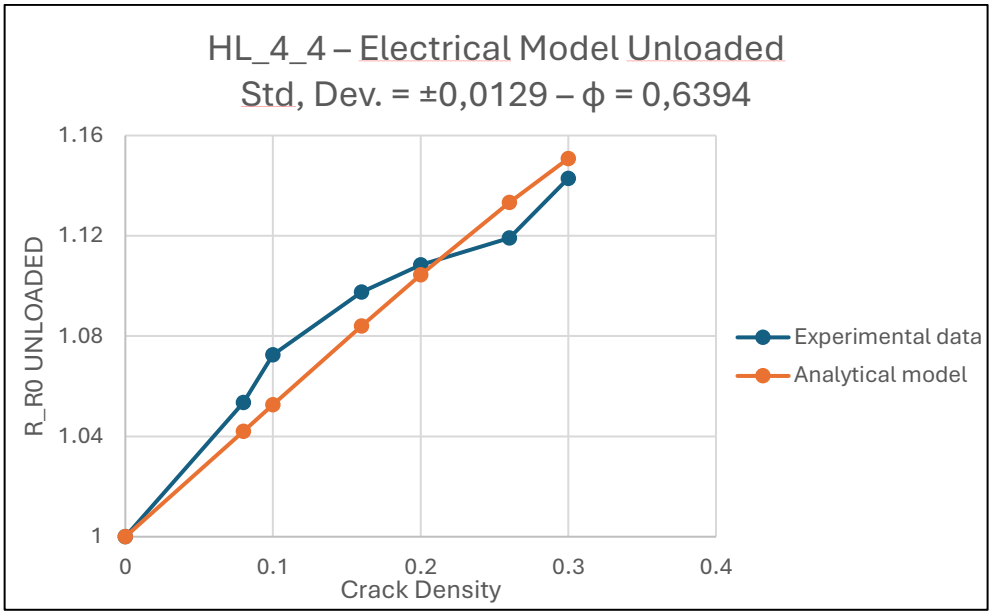
HL_4_4 – Electrical Model Unloaded
Std, Dev. = ±0,0129 – ϕ = 0,6394
R_R0 UNLOADED
1.16
1.12
1.08
1.04
1
0
0.1
0.2
0.3
0.4
Crack Density
Experimental data
Analytical model

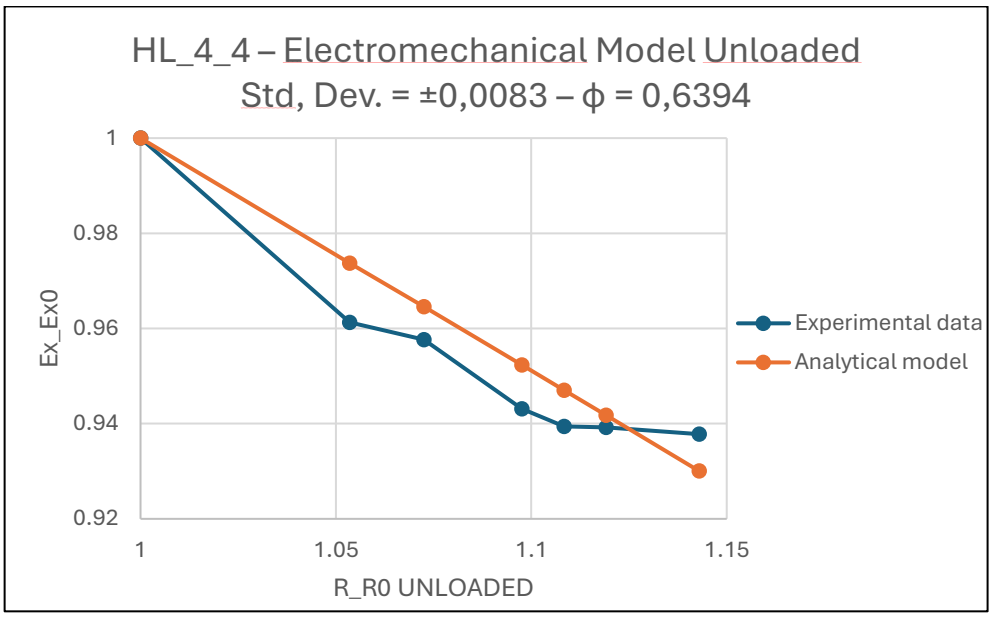
HL_4_4 – Electromechanical Model Unloaded
Std, Dev. = ±0,0083 – ϕ = 0,6394
Ex_Ex0
1
0.98
0.96
0.94
0.92
1
1.05
1.1
1.15
R_R0 UNLOADED
Experimental data
Analytical model

HL_4_5

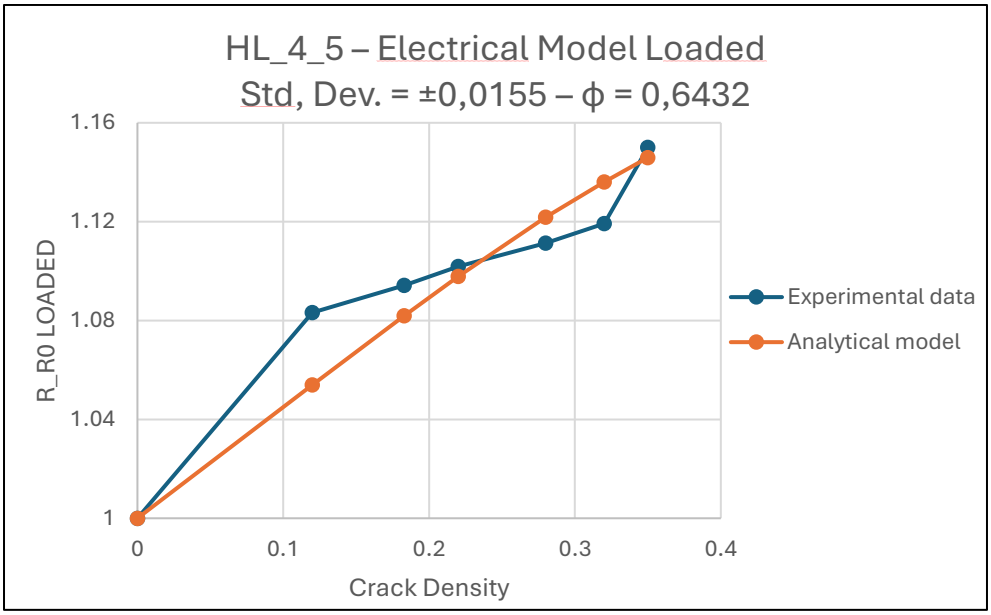
HL_4_5 – Electrical Model Loaded
Std, Dev. = ±0,0155 – ϕ = 0,6432
R_R0 LOADED
1.16
1.12
1.08
1.04
1
0
0.1
0.2
0.3
0.4
Crack Density
Experimental data
Analytical model

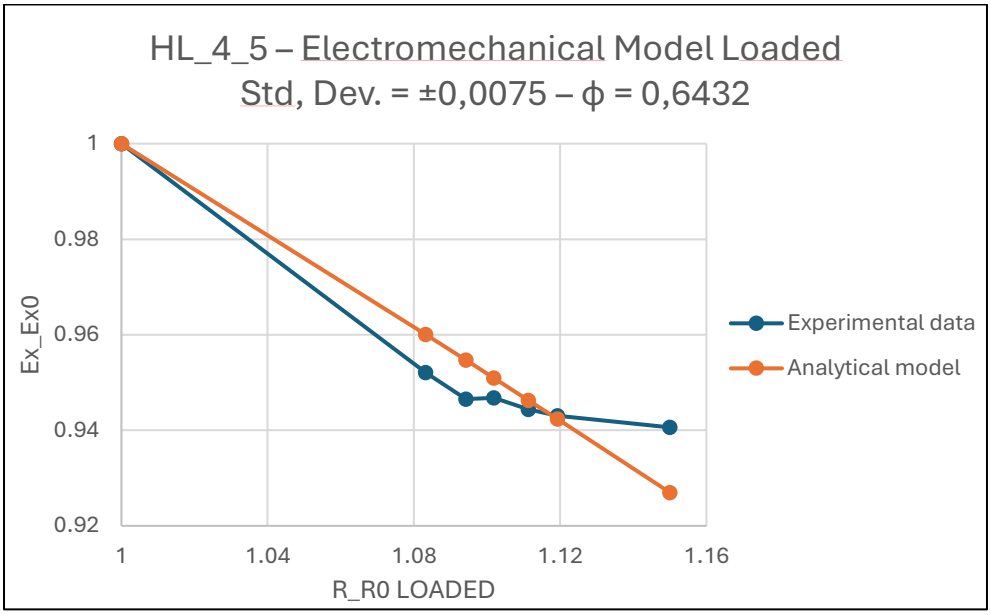
HL_4_5 – Electromechanical Model Loaded
Std, Dev. = ±0,0075 – ϕ = 0,6432
Ex_Ex0
1
0.98
0.96
0.94
0.92
1
1.04
1.08
1.12
1.16
R_R0 LOADED
Experimental data
Analytical model

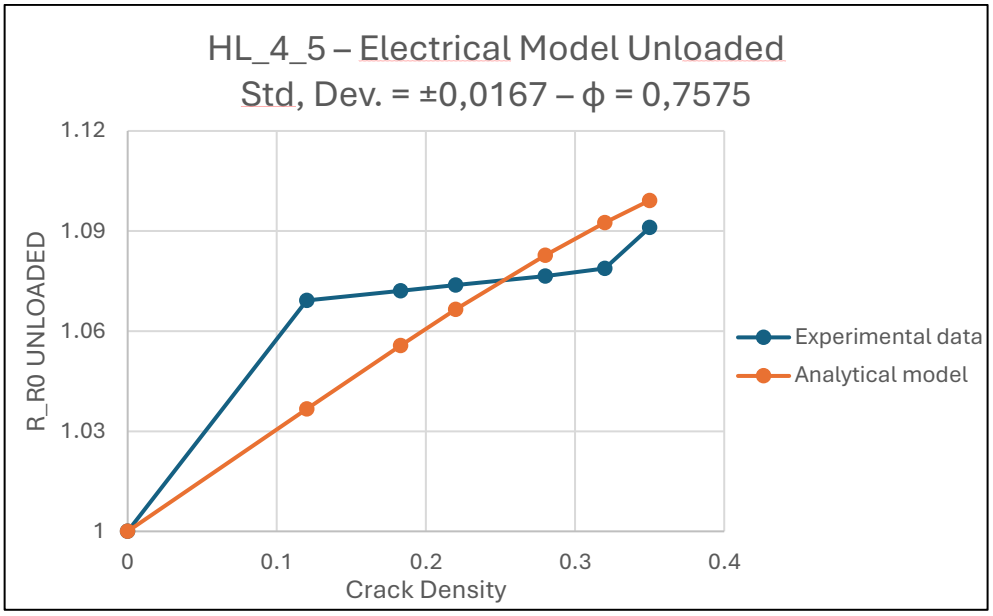
HL_4_5 – Electrical Model Unloaded
Std, Dev. = ±0,0167 – ϕ = 0,7575
R_R0 UNLOADED
1.12
1.09
1.06
1.03
1
0
0.1
0.2
0.3
0.4
Crack Density
Experimental data
Analytical model

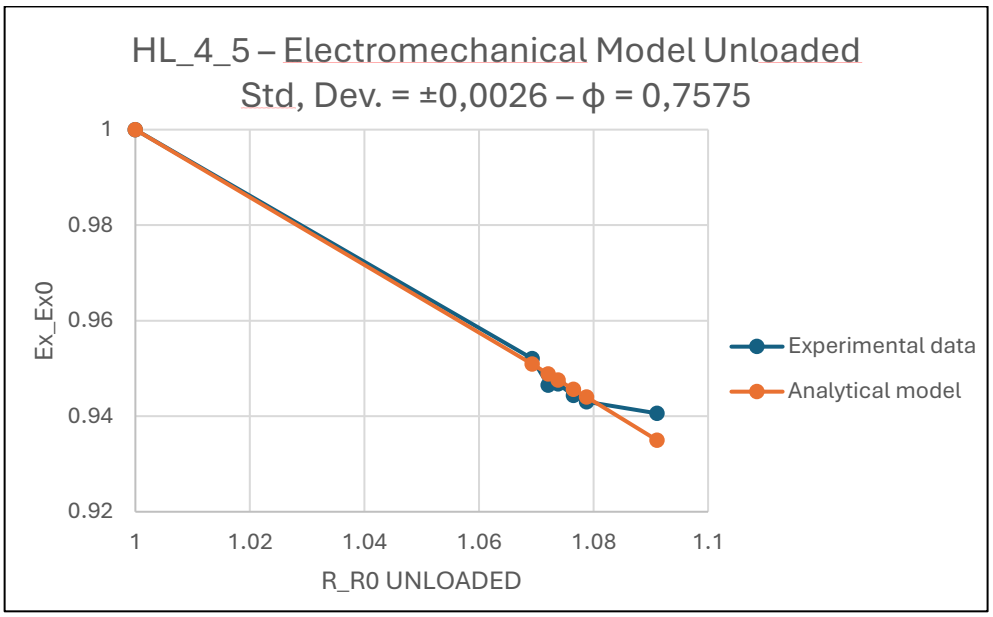
HL_4_5 – Electromechanical Model Unloaded
Std, Dev. = ±0,0026 – ϕ = 0,7575
Ex_Ex0
1
0.98
0.96
0.94
0.92
1
1.02
1.04
1.06
1.08
1.1
R_R0 UNLOADED
Experimental data
Analytical model

HL_4_7

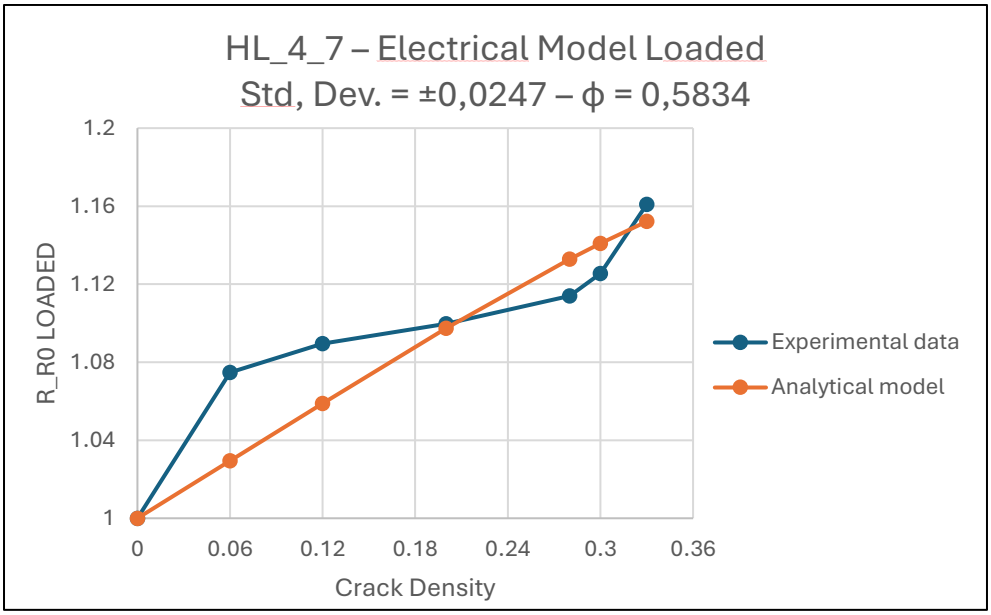
HL_4_7 – Electrical Model Loaded
Std, Dev. = ±0,0247 – ϕ = 0,5834
R_R0 LOADED
1.2
1.16
1.12
1.08
1.04
1
0
0.06
0.12
0.18
0.24
0.3
0.36
Crack Density
Experimental data
Analytical model

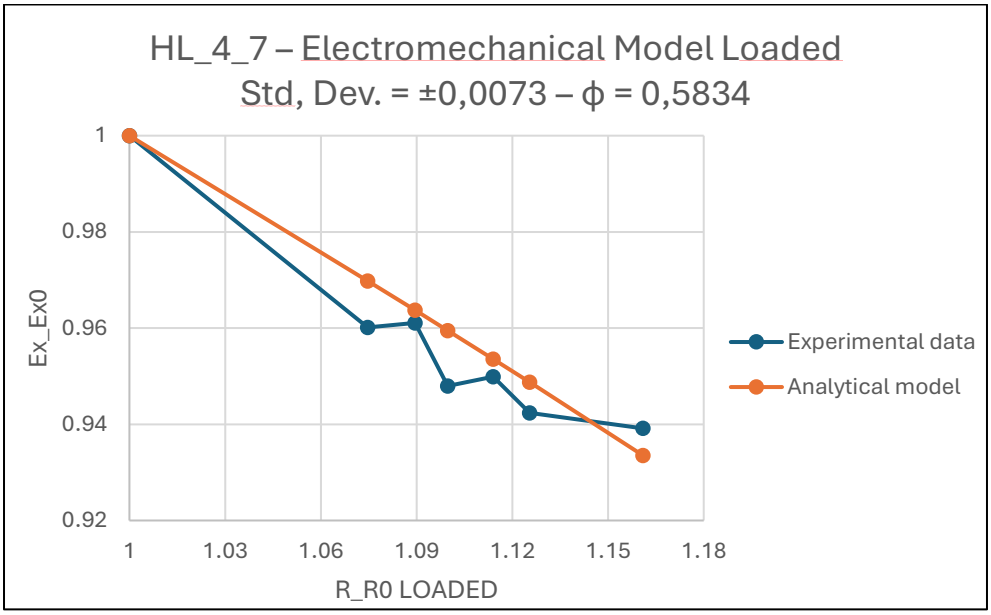
HL_4_7 – Electromechanical Model Loaded
Std, Dev. = ±0,0073 – ϕ = 0,5834
Ex_Ex0
1
0.98
0.96
0.94
0.92
1
1.03
1.06
1.09
1.12
1.15
1.18
R_R0 LOADED
Experimental data
Analytical model

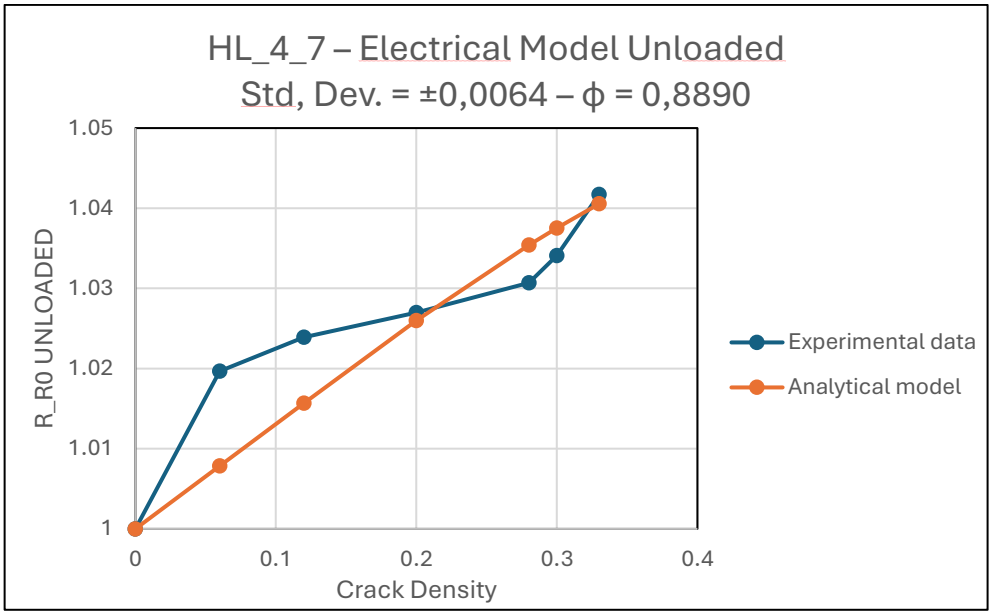
HL_4_7 – Electrical Model Unloaded
Std, Dev. = ±0,0064 – ϕ = 0,8890
R_R0 UNLOADED
1.05
1.04
1.03
1.02
1.01
1
0
0.1
0.2
0.3
0.4
Crack Density
Experimental data
Analytical model

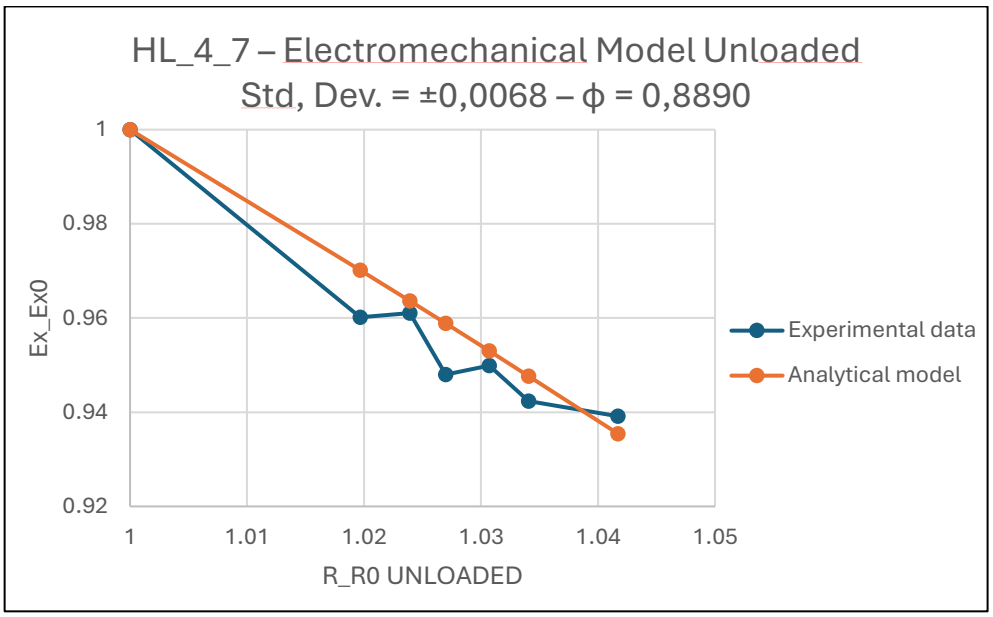
HL_4_7 – Electromechanical Model Unloaded
Std, Dev. = ±0,0068 – ϕ = 0,8890
Ex_Ex0
1
0.98
0.96
0.94
0.92
1
1.01
1.02
1.03
1.04
1.05
R_R0 UNLOADED
Experimental data
Analytical model

RM_2

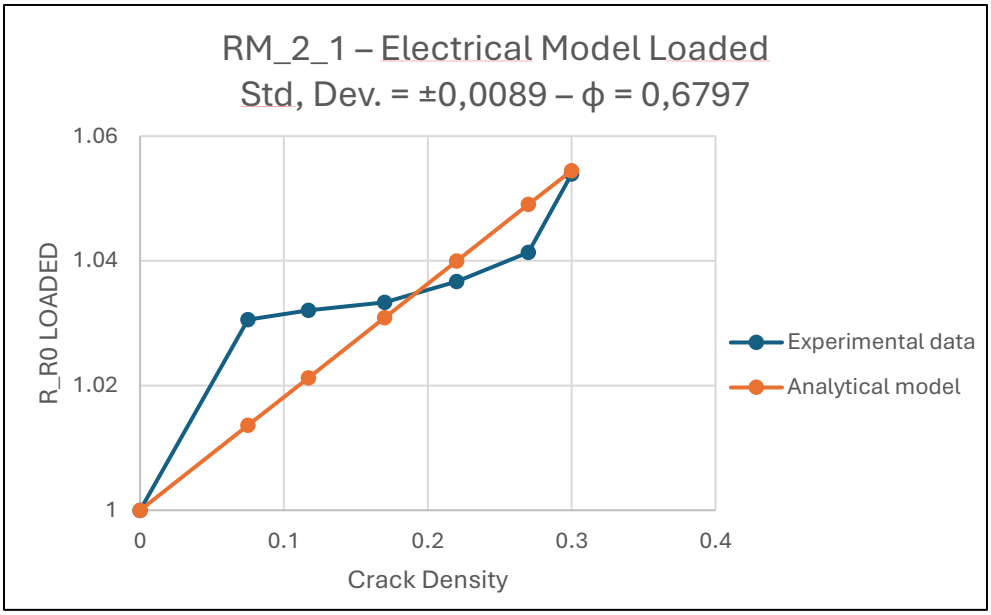
RM_2_1 – Electrical Model Loaded
Std, Dev. = ±0,0089 – ϕ = 0,6797
R_R0 LOADED
1.06
1.04
1.02
1
0
0.1
0.2
0.3
0.4
Crack Density
Experimental data
Analytical model

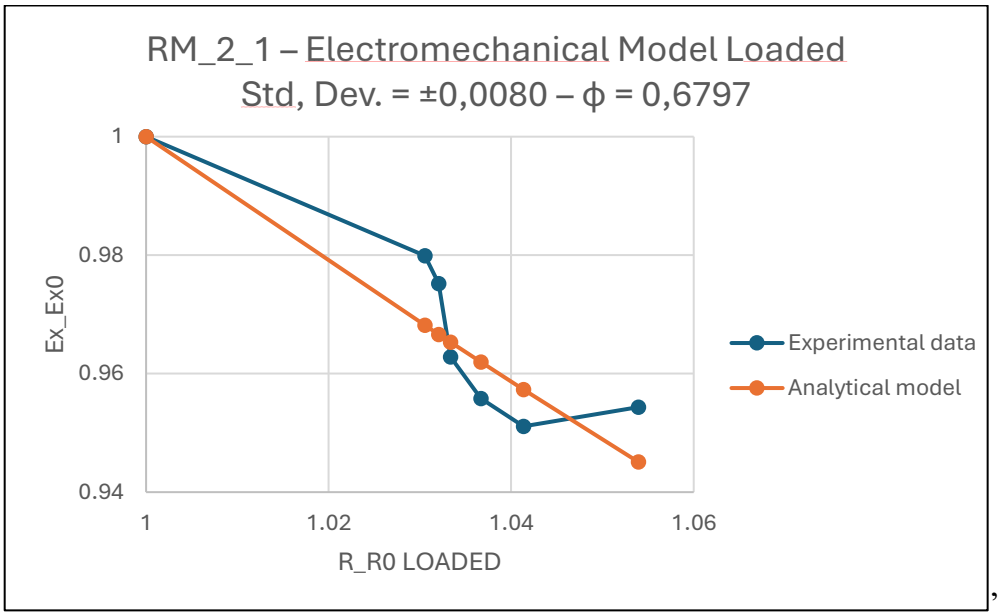
RM_2_1 – Electromechanical Model Loaded
Std, Dev. = ±0,0080 – ϕ = 0,6797
Ex_Ex0
1
0.98
0.96
0.94
1
1.02
1.04
1.06
R_R0 LOADED
Experimental data
Analytical model

,

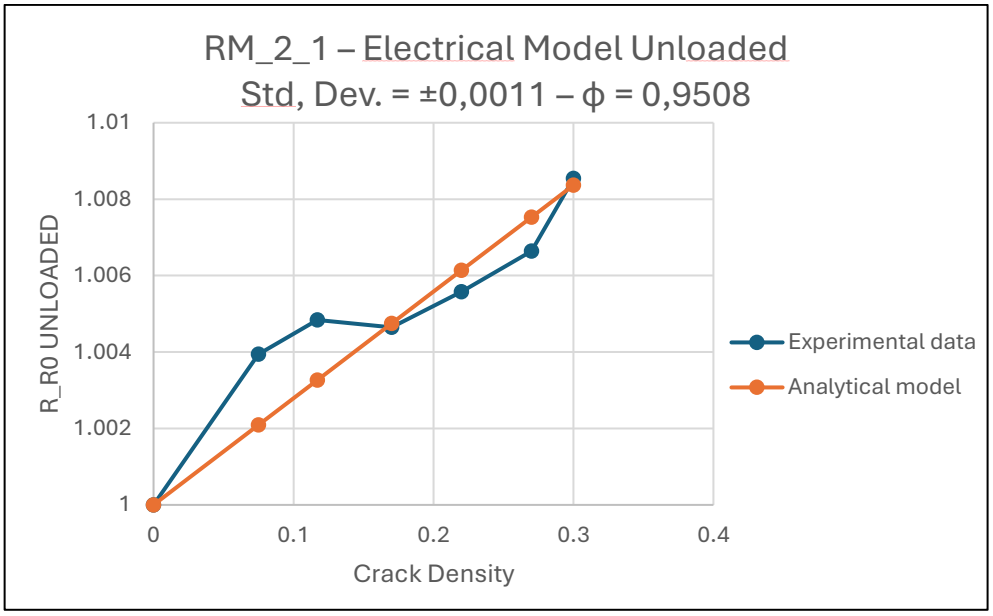
RM_2_1 – Electrical Model Unloaded
Std, Dev. = ±0,0011 – ϕ = 0,9508
R_R0 UNLOADED
1.01
1.008
1.006
1.004
1.002
1
0
0.1
0.2
0.3
0.4
Crack Density
Experimental data
Analytical model

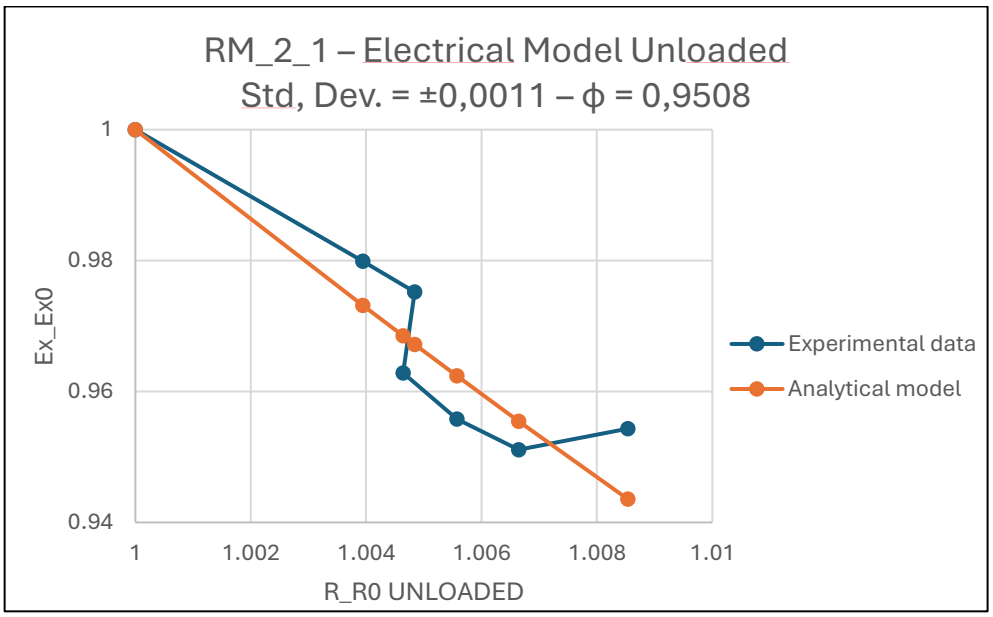
RM_2_1 – Electrical Model Unloaded
Std, Dev. = ±0,0011 – ϕ = 0,9508
Ex_Ex0
1
0.98
0.96
0.94
1
1.002
1.004
1.006
1.008
1.01
R_R0 UNLOADED
Experimental data
Analytical model

RM_2_9

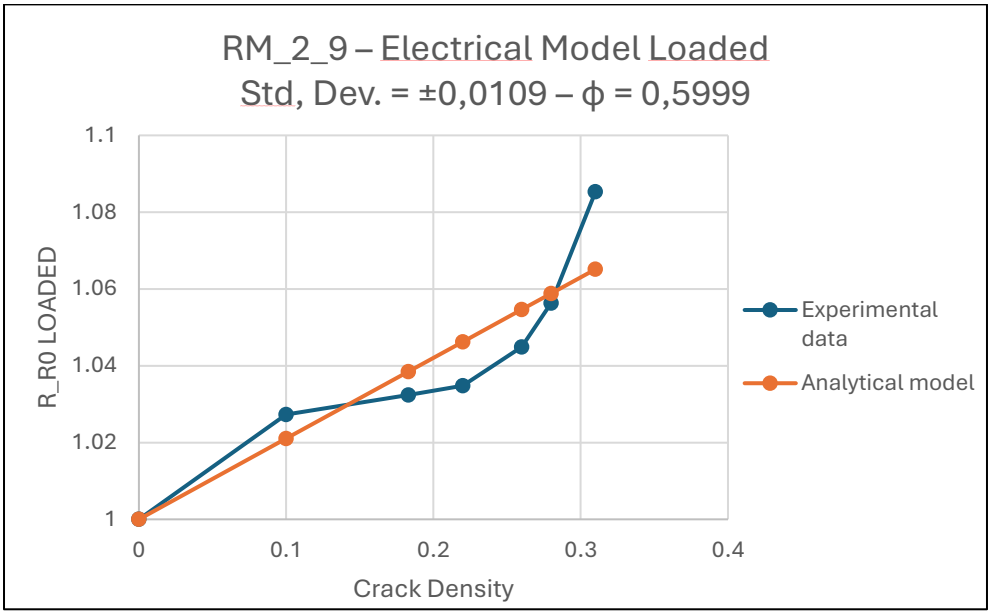
RM_2_9 – Electrical Model Loaded
Std, Dev. = ±0,0109 – ϕ = 0,5999
R_R0 LOADED
1.1
1.08
1.06
1.04
1.02
1
0
0.1
0.2
0.3
0.4
Crack Density
Experimental data
Analytical model

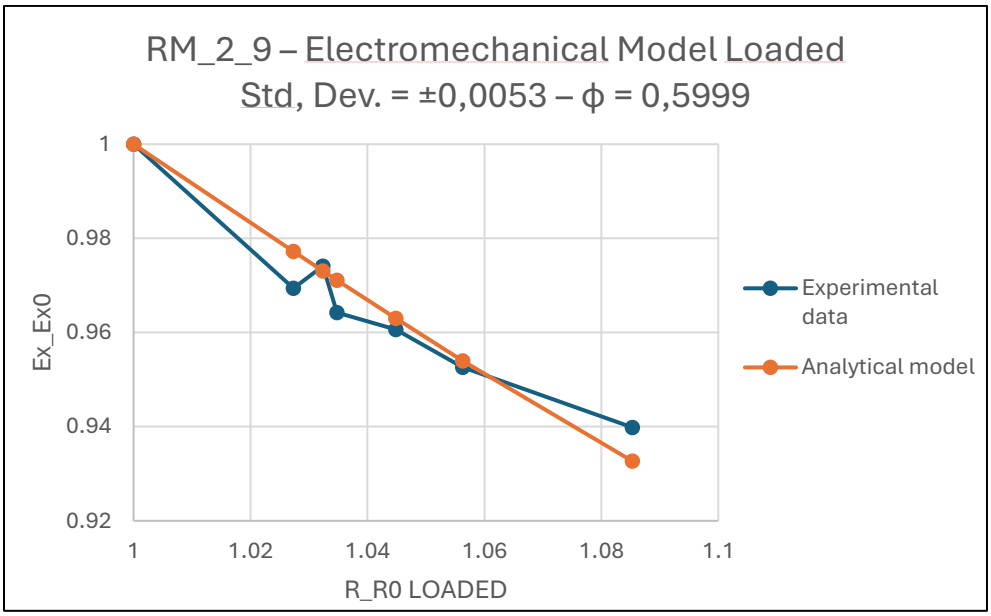
RM_2_9 – Electromechanical Model Loaded
Std, Dev. = ±0,0053 – ϕ = 0,5999
Ex_Ex0
1
0.98
0.96
0.94
0.92
1
1.02
1.04
1.06
1.08
1.1
R_R0 LOADED
Experimental data
Analytical model

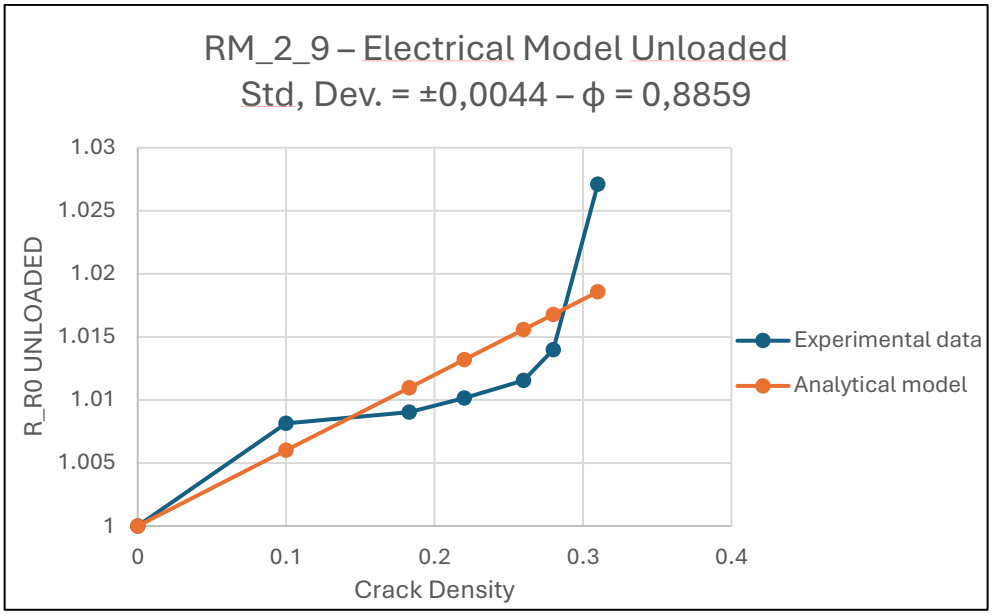
RM_2_9 – Electrical Model Unloaded
Std, Dev. = ±0,0044 – ϕ = 0,8859
R_R0 UNLOADED
1.03
1.025
1.02
1.015
1.01
1.005
1
0
0.1
0.2
0.3
0.4
Crack Density
Experimental data
Analytical model

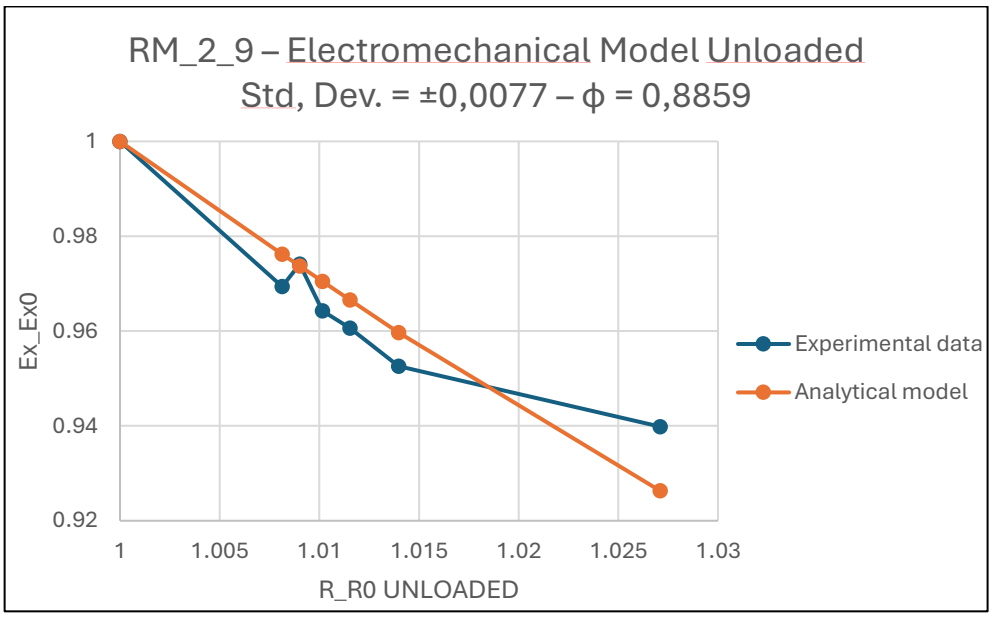
RM_2_9 – Electromechanical Model Unloaded
Std, Dev. = ±0,0077 – ϕ = 0,8859
Ex_Ex0
1
0.98
0.96
0.94
0.92
1
1.005
1.01
1.015
1.02
1.025
1.03
R_R0 UNLOADED
Experimental data
Analytical model

Graphs for the validation of the analytical model – Static test

HL_3_3

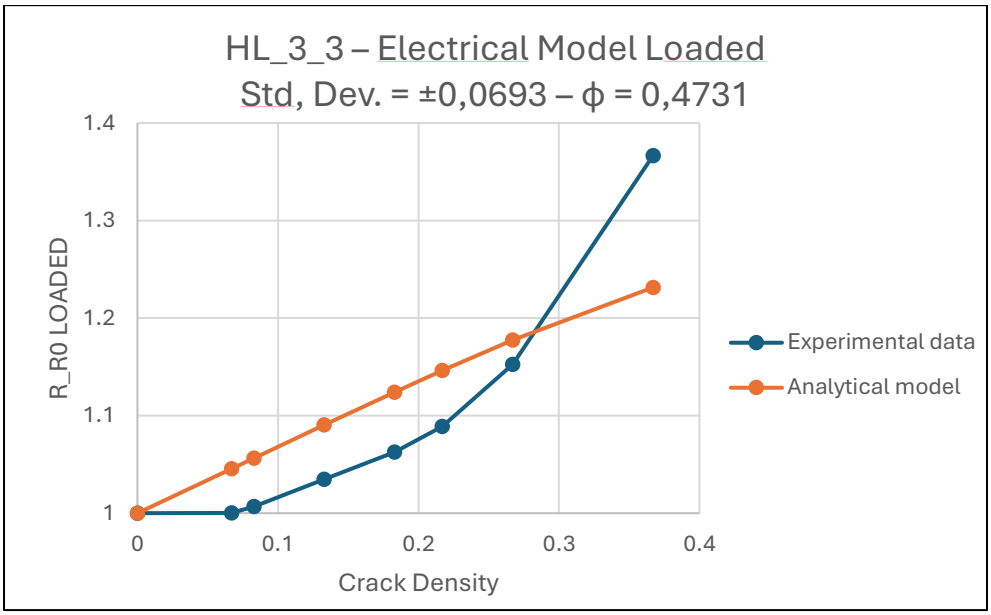

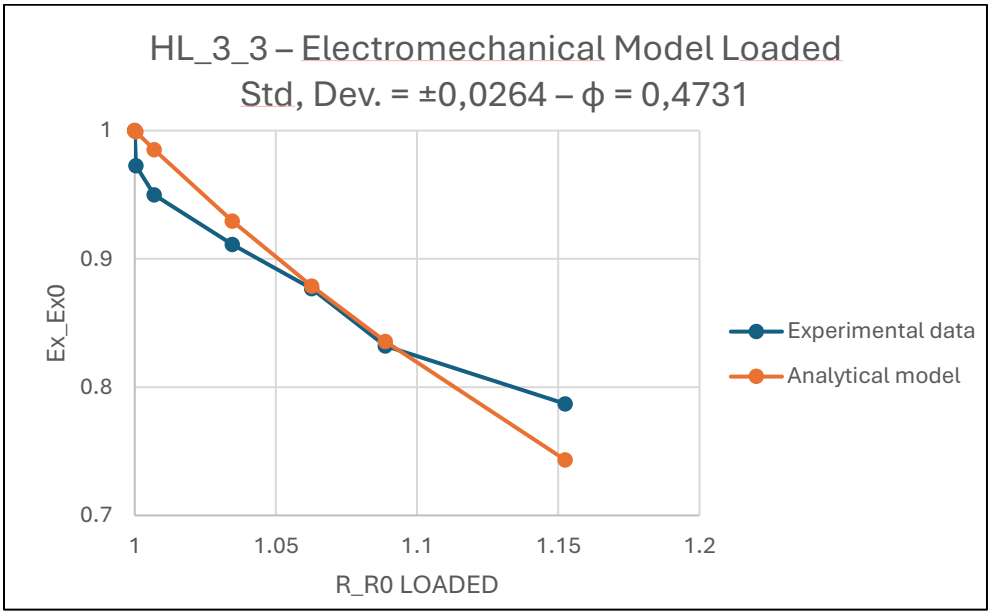

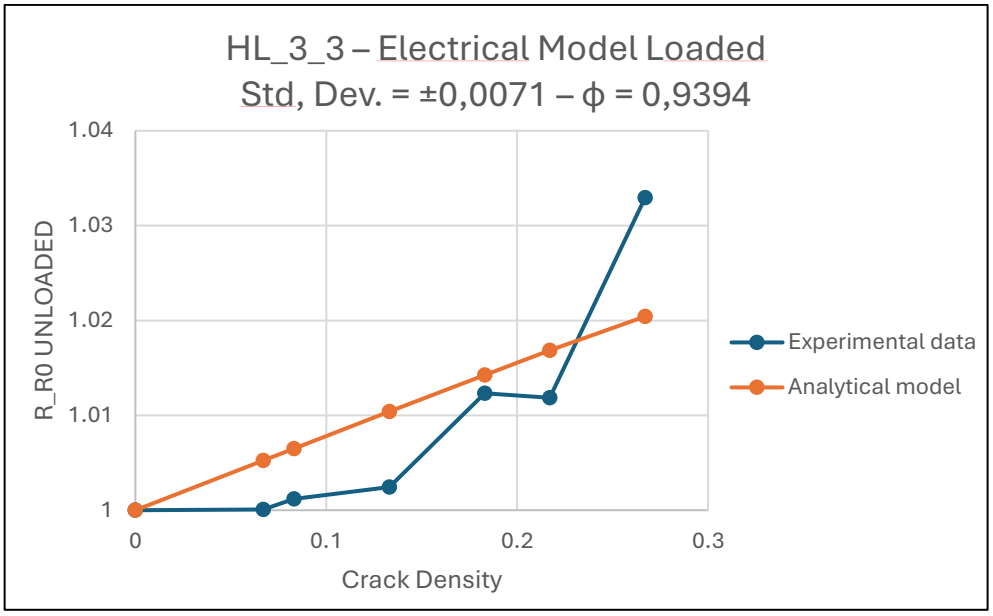
HL_3_3 – Electrical Model Loaded
Std, Dev. = ±0,0071 – ϕ = 0,9394
1.04
1.03
1.02
1.01
1
R_R0 UNLOADED
0
0.1
0.2
0.3
Crack Density
Experimental data
Analytical model

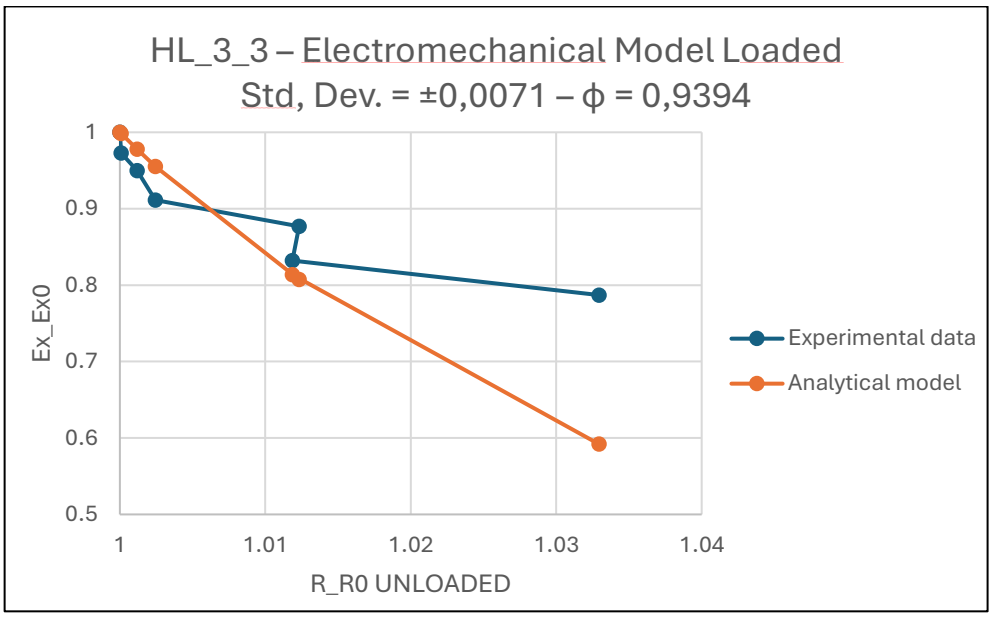
HL_3_3 – Electromechanical Model Loaded
Std, Dev. = ±0,0071 – ϕ = 0,9394
1
0.9
0.8
0.7
0.6
0.5
Ex_Ex0
1
1.01
1.02
1.03
1.04
R_R0 UNLOADED
Experimental data
Analytical model

HL_3_6

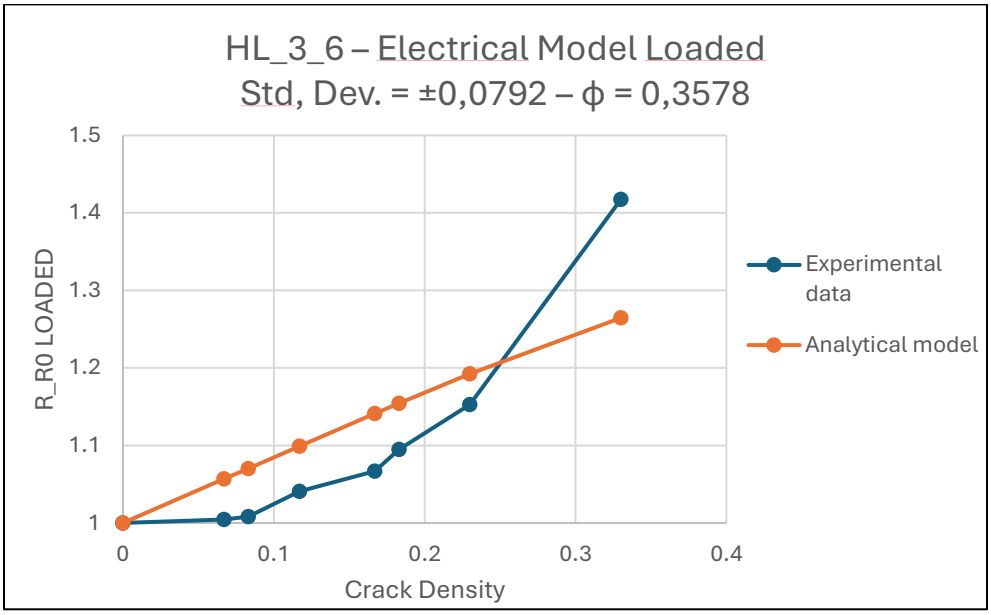
HL_3_6 – Electrical Model Loaded
Std, Dev. = ±0,0792 – ϕ = 0,3578
R_R0 LOADED
1.5
1.4
1.3
1.2
1.1
1
0
0.1
0.2
0.3
0.4
Crack Density
Experimental data
Analytical model

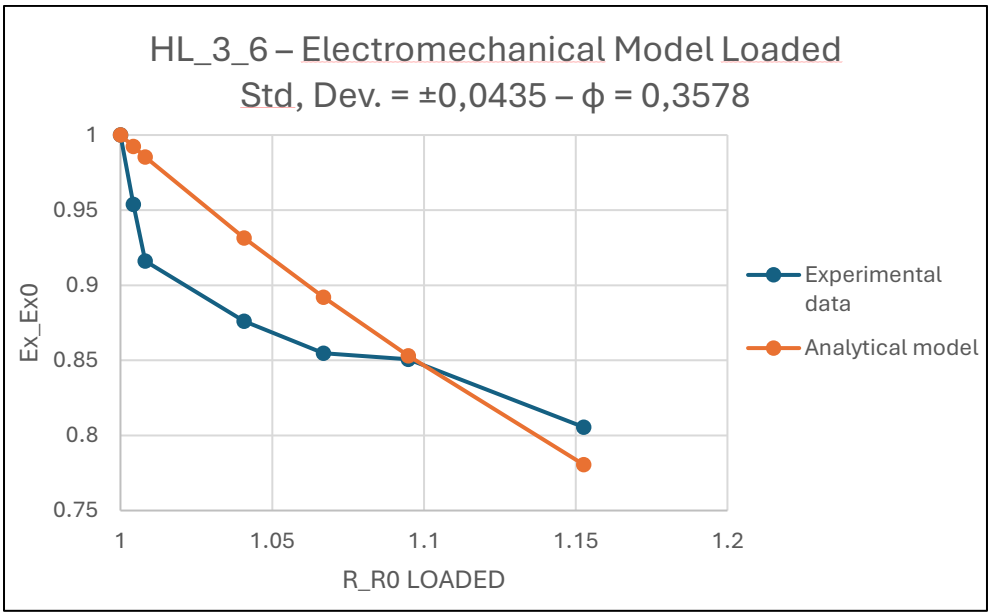
HL_3_6 – Electromechanical Model Loaded
Std, Dev. = ±0,0435 – ϕ = 0,3578
Ex_Ex0
1
0.95
0.9
0.85
0.8
0.75
1
1.05
1.1
1.15
1.2
R_R0 LOADED
Experimental data
Analytical model

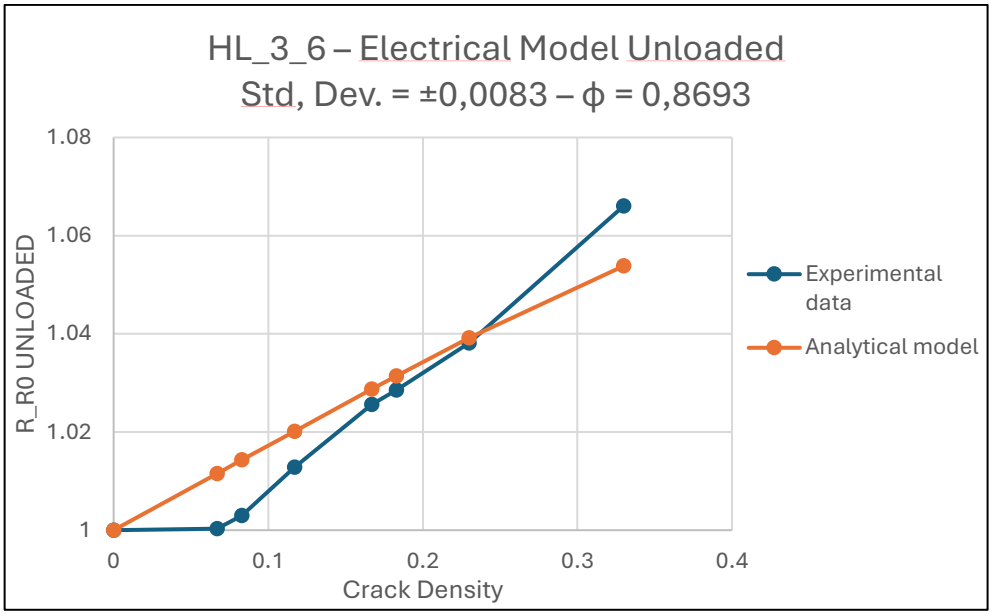
HL_3_6 – Electrical Model Unloaded
Std, Dev. = ±0,0083 – ϕ = 0,8693
R_R0 UNLOADED
1.08
1.06
1.04
1.02
1
0
0.1
0.2
0.3
0.4
Crack Density
Experimental data
Analytical model

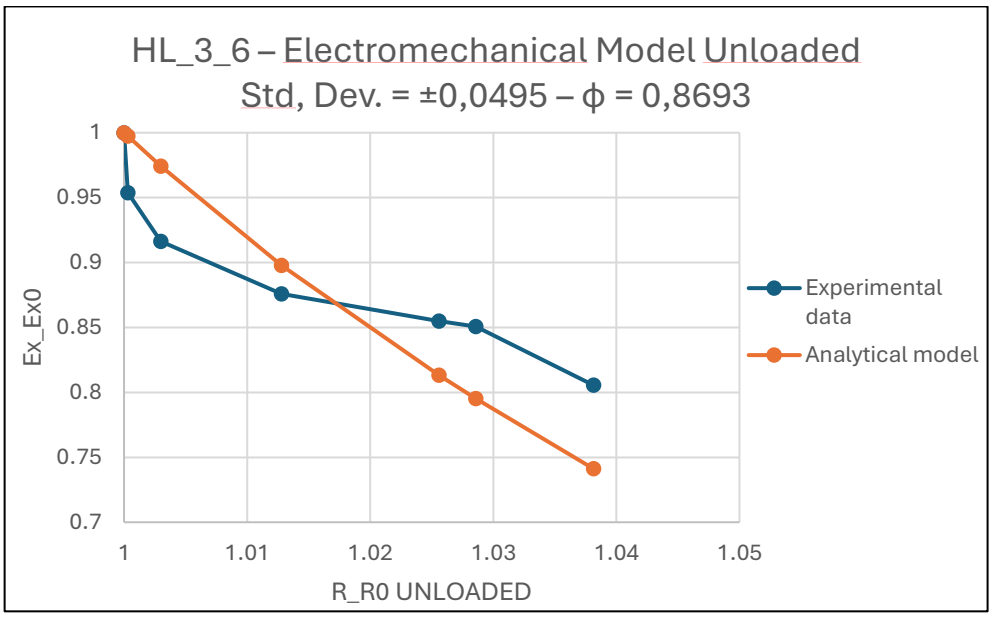
HL_3_6 – Electromechanical Model Unloaded
Std, Dev. = ±0,0495 – ϕ = 0,8693
Ex_Ex0
1
0.95
0.9
0.85
0.8
0.75
0.7
1
1.01
1.02
1.03
1.04
1.05
R_R0 UNLOADED
Experimental data
Analytical model

HL_3_8

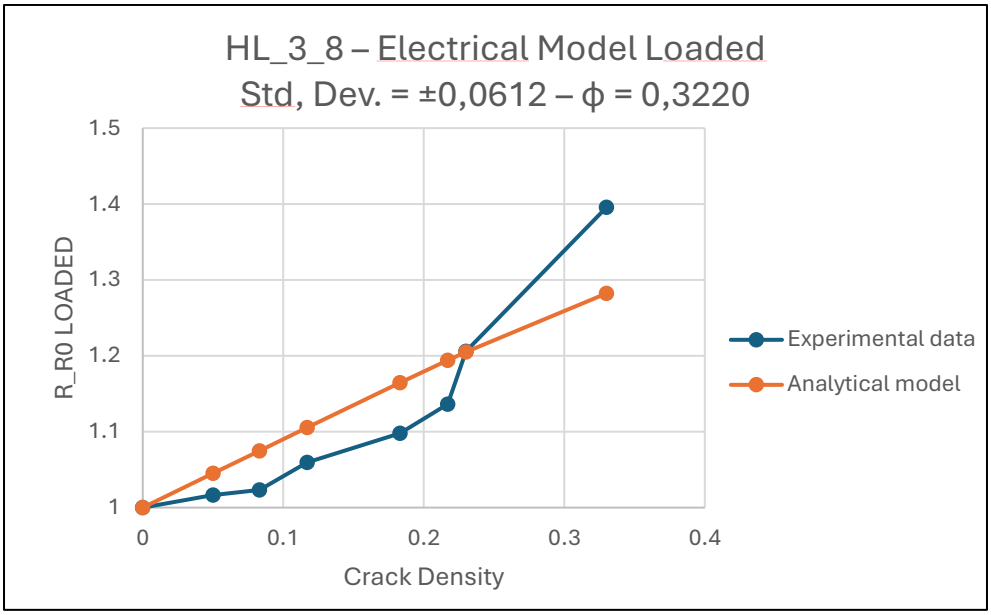
HL_3_8 – Electrical Model Loaded
Std, Dev. = ±0,0612 – ϕ = 0,3220
R_R0 LOADED
1.5
1.4
1.3
1.2
1.1
1
0
0.1
0.2
0.3
0.4
Crack Density
Experimental data
Analytical model

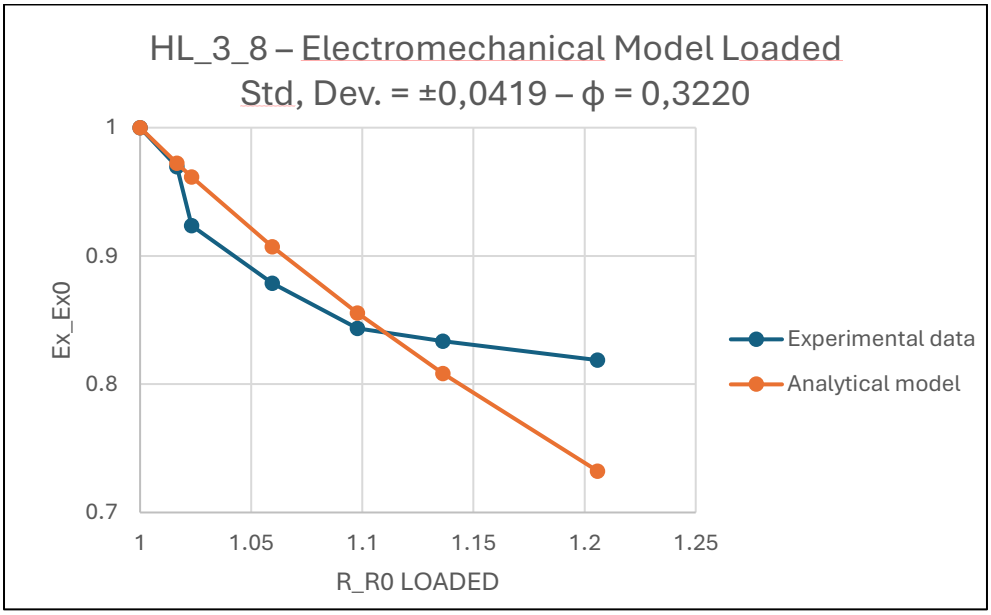
HL_3_8 – Electromechanical Model Loaded
Std, Dev. = ±0,0419 – ϕ = 0,3220
Ex_Ex0
1
0.9
0.8
0.7
1
1.05
1.1
1.15
1.2
1.25
R_R0 LOADED
Experimental data
Analytical model

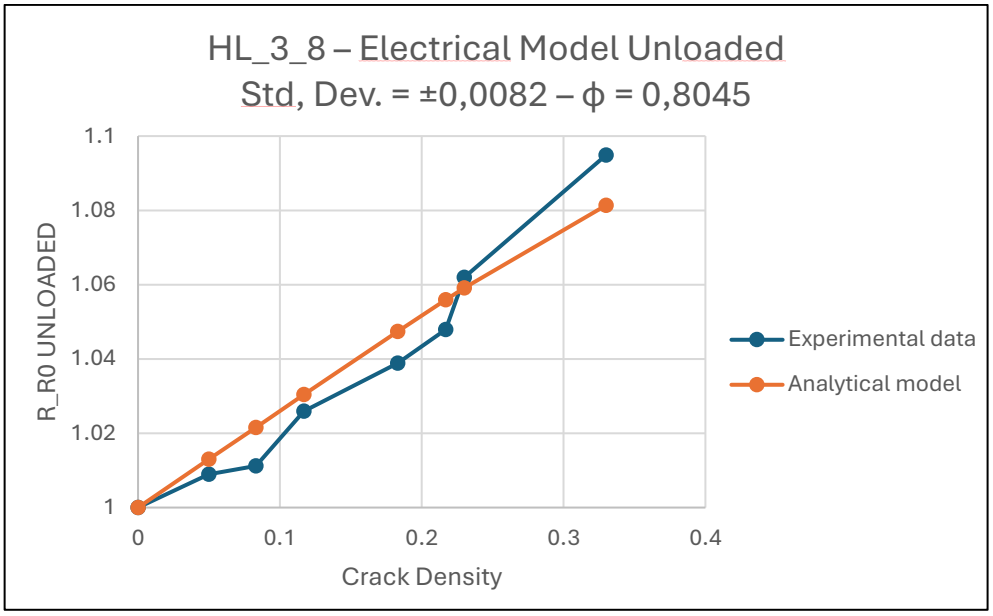
HL_3_8 – Electrical Model Unloaded
Std, Dev. = ±0,0082 – ϕ = 0,8045
R_R0 UNLOADED
1.1
1.08
1.06
1.04
1.02
1
0
0.1
0.2
0.3
0.4
Crack Density
Experimental data
Analytical model

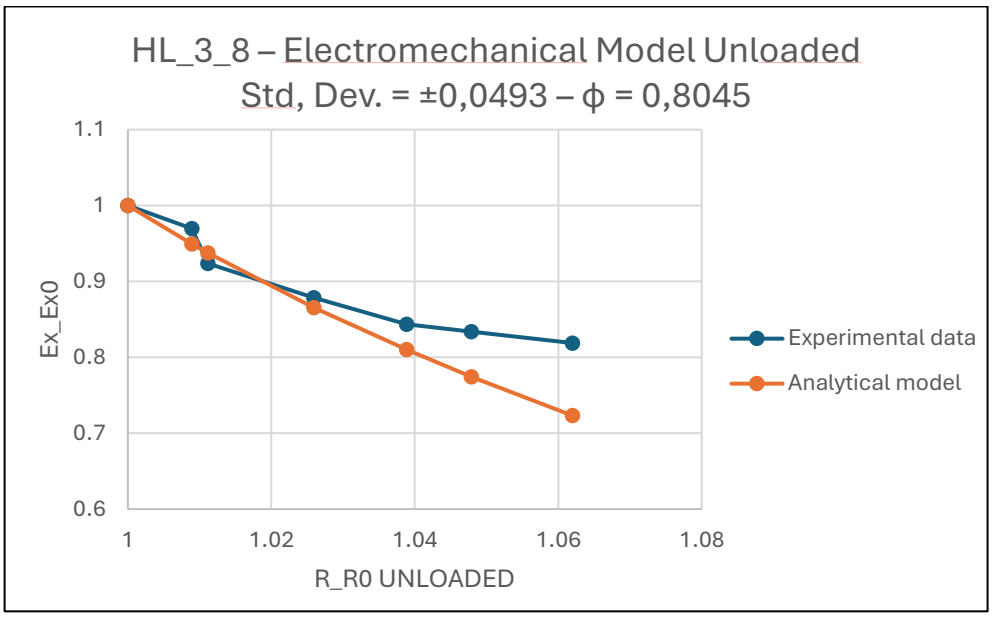
HL_3_8 – Electromechanical Model Unloaded
Std, Dev. = ±0,0493 – ϕ = 0,8045
Ex_Ex0
1.1
1
0.9
0.8
0.7
0.6
1
1.02
1.04
1.06
1.08
R_R0 UNLOADED
Experimental data
Analytical model

HL_3_9

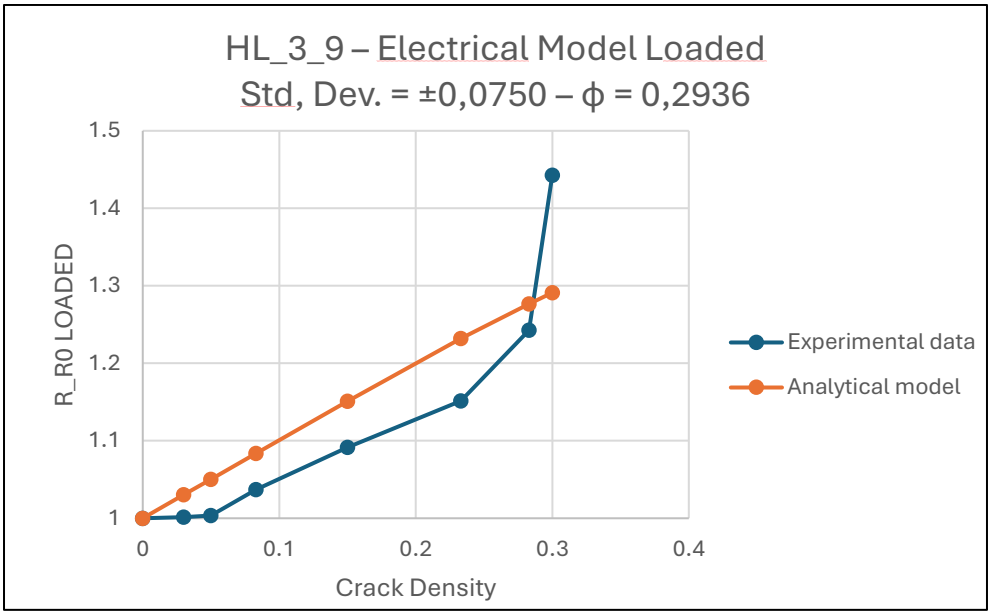
HL_3_9 – Electrical Model Loaded
Std, Dev. = ±0,0750 – ϕ = 0,2936
R_R0 LOADED
1.5
1.4
1.3
1.2
1.1
1
0
0.1
0.2
0.3
0.4
Crack Density
Experimental data
Analytical model

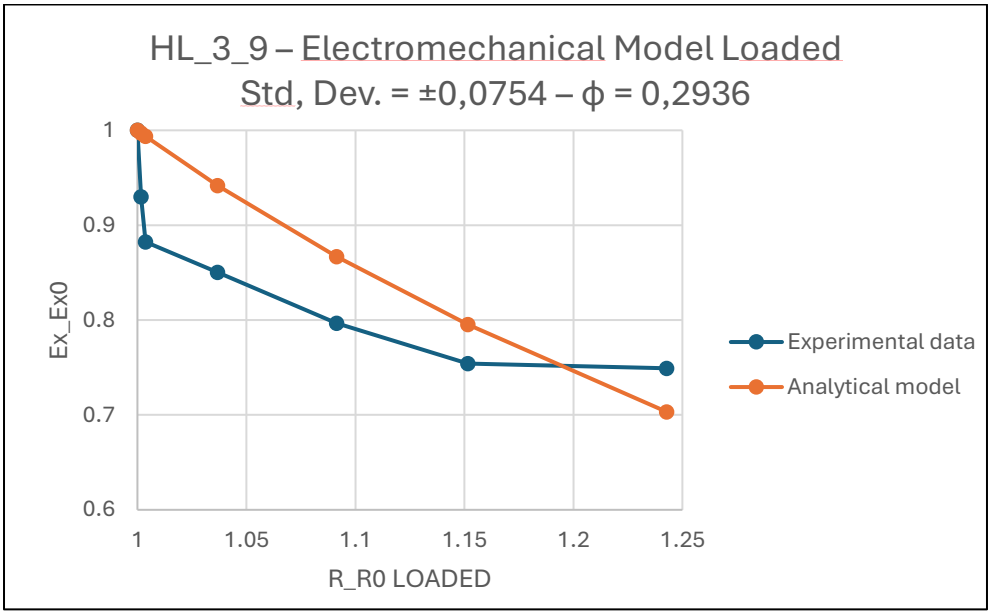
HL_3_9 – Electromechanical Model Loaded
Std, Dev. = ±0,0754 – ϕ = 0,2936
Ex_Ex0
1
0.9
0.8
0.7
0.6
1
1.05
1.1
1.15
1.2
1.25
R_R0 LOADED
Experimental data
Analytical model

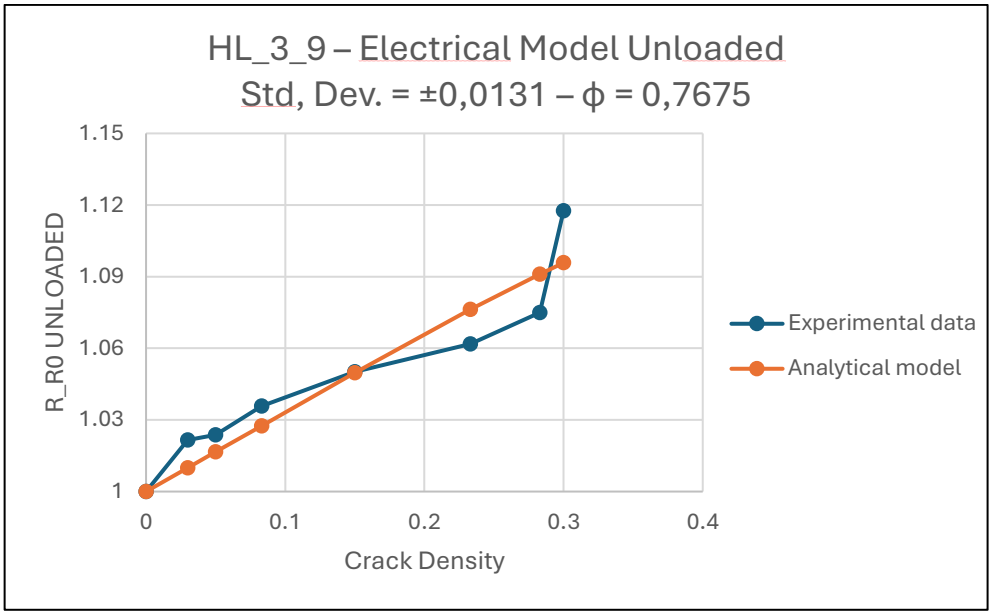
HL_3_9 – Electrical Model Unloaded
Std, Dev. = ±0,0131 – ϕ = 0,7675
R_R0 UNLOADED
1.15
1.12
1.09
1.06
1.03
1
0
0.1
0.2
0.3
0.4
Crack Density
Experimental data
Analytical model

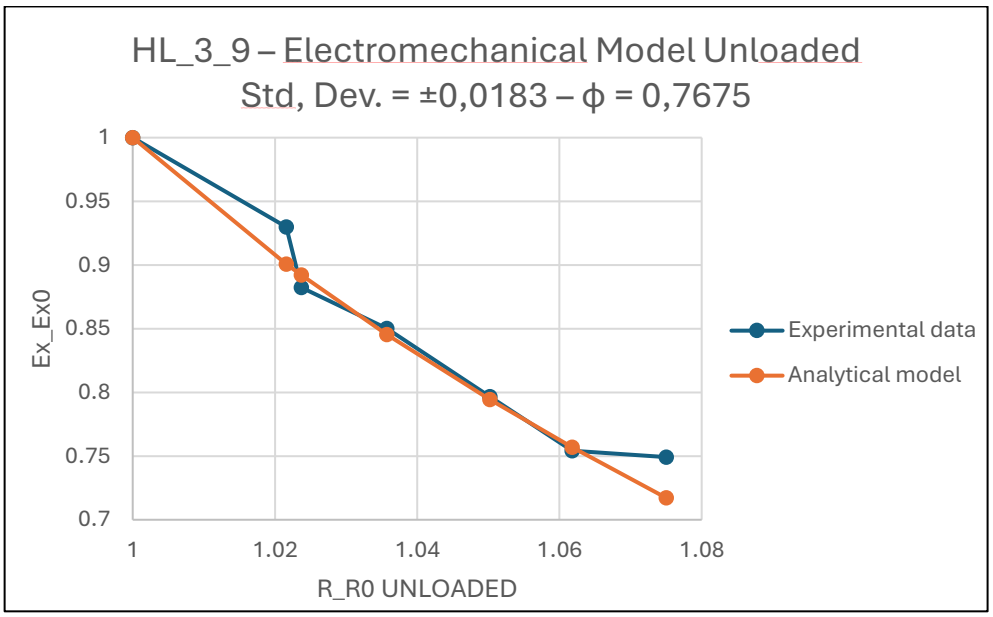
HL_3_9 – Electromechanical Model Unloaded
Std, Dev. = ±0,0183 – ϕ = 0,7675
Ex_Ex0
1
0.95
0.9
0.85
0.8
0.75
0.7
1
1.02
1.04
1.06
1.08
R_R0 UNLOADED
Experimental data
Analytical model

HL_4_1

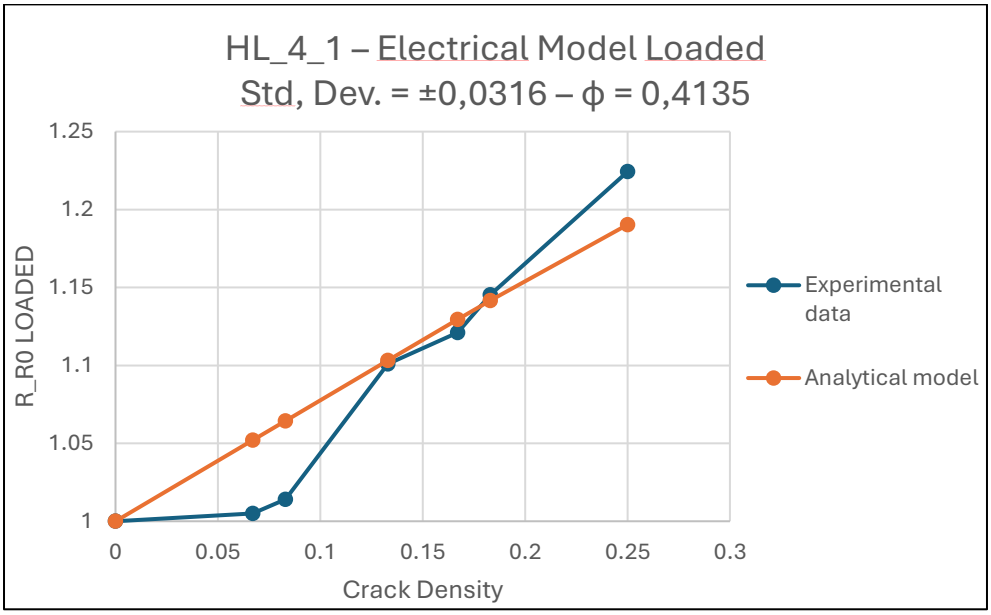
HL_4_1 – Electrical Model Loaded
Std, Dev. = ±0,0316 – ϕ = 0,4135
R_R0 LOADED
1.25
1.2
1.15
1.1
1.05
1
0
0.05
0.1
0.15
0.2
0.25
0.3
Crack Density
Experimental data
Analytical model

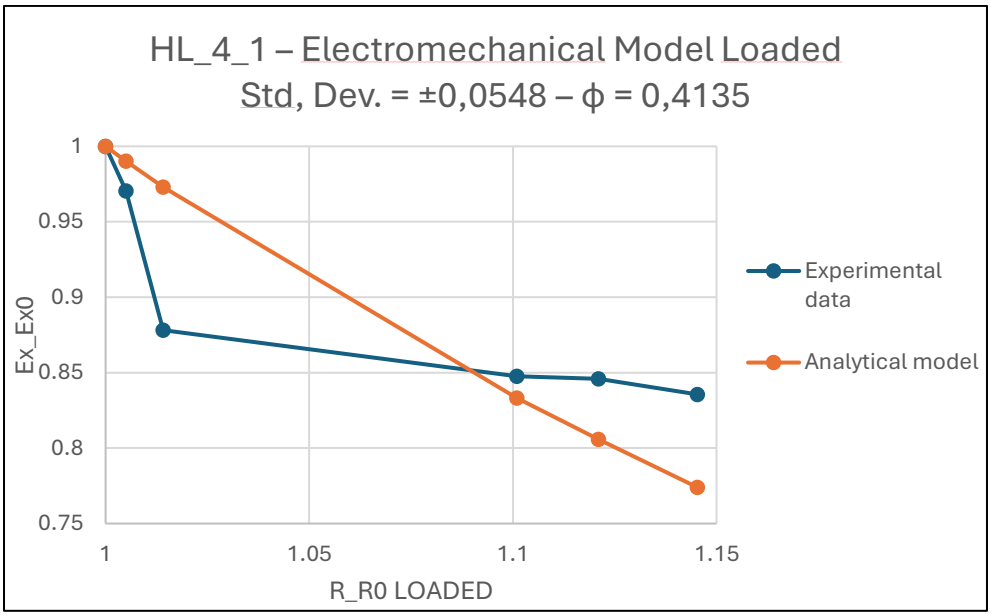
HL_4_1 – Electromechanical Model Loaded
Std, Dev. = ±0,0548 – ϕ = 0,4135
Ex_Ex0
1
0.95
0.9
0.85
0.8
0.75
1
1.05
1.1
1.15
R_R0 LOADED
Experimental data
Analytical model

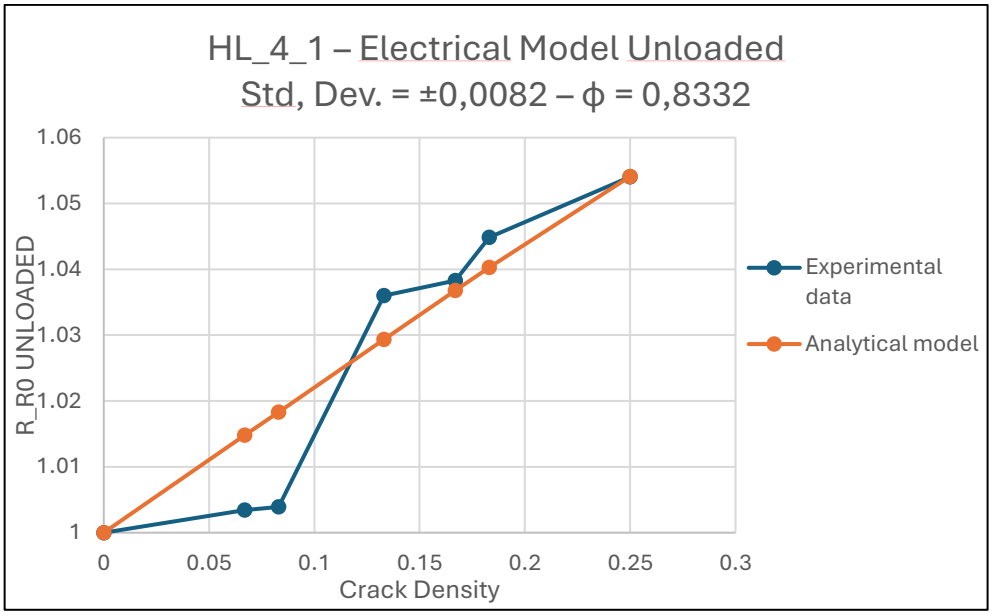
HL_4_1 – Electrical Model Unloaded
Std, Dev. = ±0,0082 – ϕ = 0,8332
R_R0 UNLOADED
1.06
1.05
1.04
1.03
1.02
1.01
1
0
0.05
0.1
0.15
0.2
0.25
0.3
Crack Density
Experimental data
Analytical model

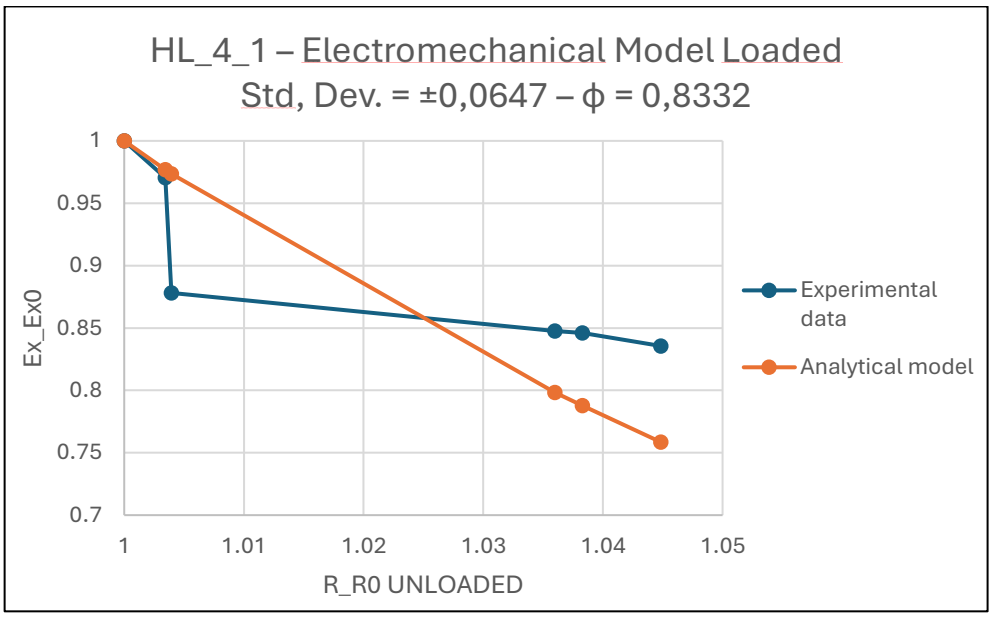
HL_4_1 – Electromechanical Model Loaded
Std, Dev. = ±0,0647 – ϕ = 0,8332
Ex_Ex0
1
0.95
0.9
0.85
0.8
0.75
0.7
1
1.01
1.02
1.03
1.04
1.05
R_R0 UNLOADED
Experimental data
Analytical model

HL_4_9

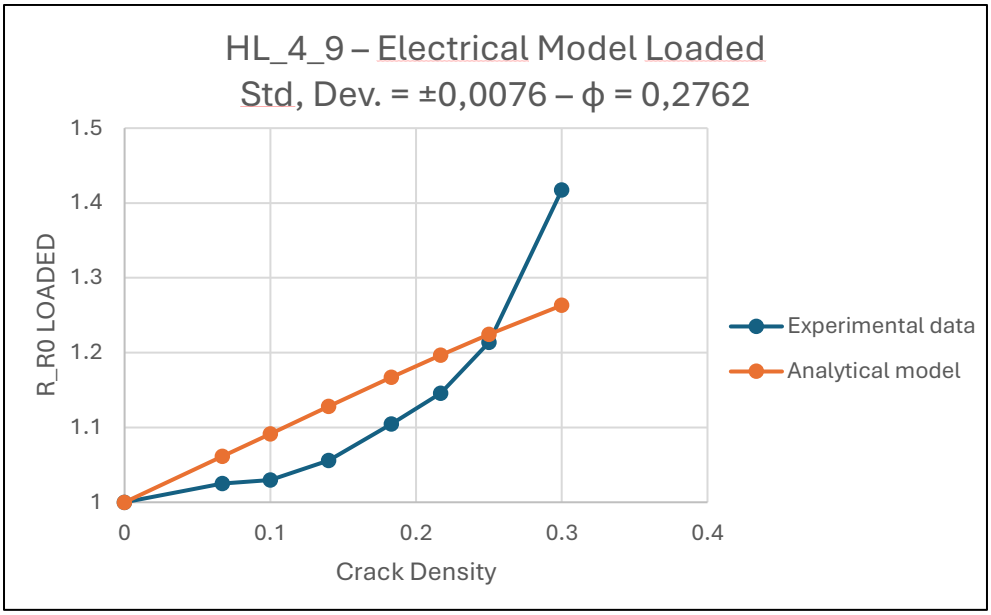
HL_4_9 – Electrical Model Loaded
Std, Dev. = ±0,0076 – ϕ = 0,2762
R_R0 LOADED
1.5
1.4
1.3
1.2
1.1
1
0
0.1
0.2
0.3
0.4
Crack Density
Experimental data
Analytical model

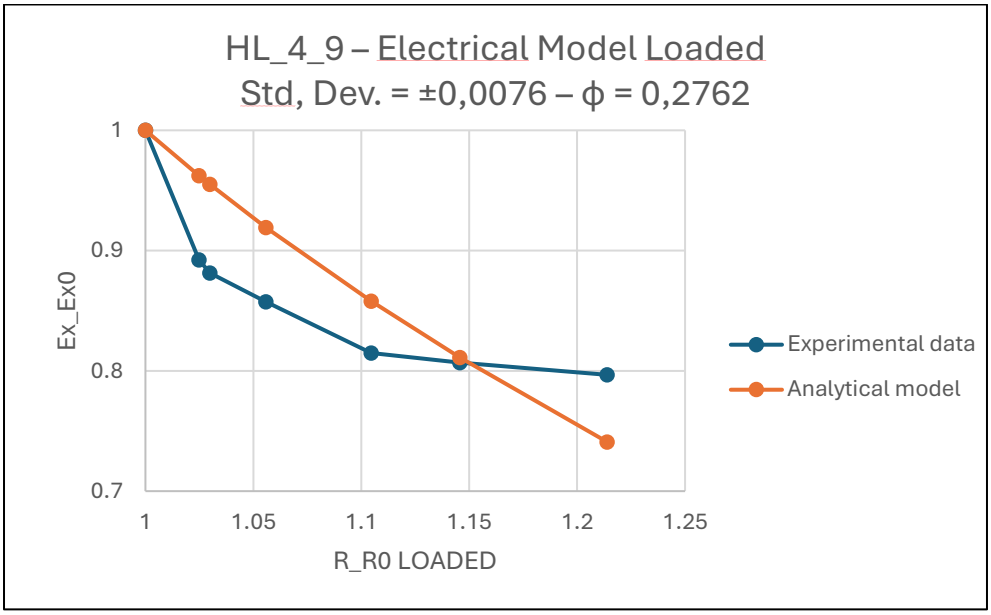
HL_4_9 – Electrical Model Loaded
Std, Dev. = ±0,0076 – ϕ = 0,2762
Ex_Ex0
1
0.9
0.8
0.7
1
1.05
1.1
1.15
1.2
1.25
R_R0 LOADED
Experimental data
Analytical model

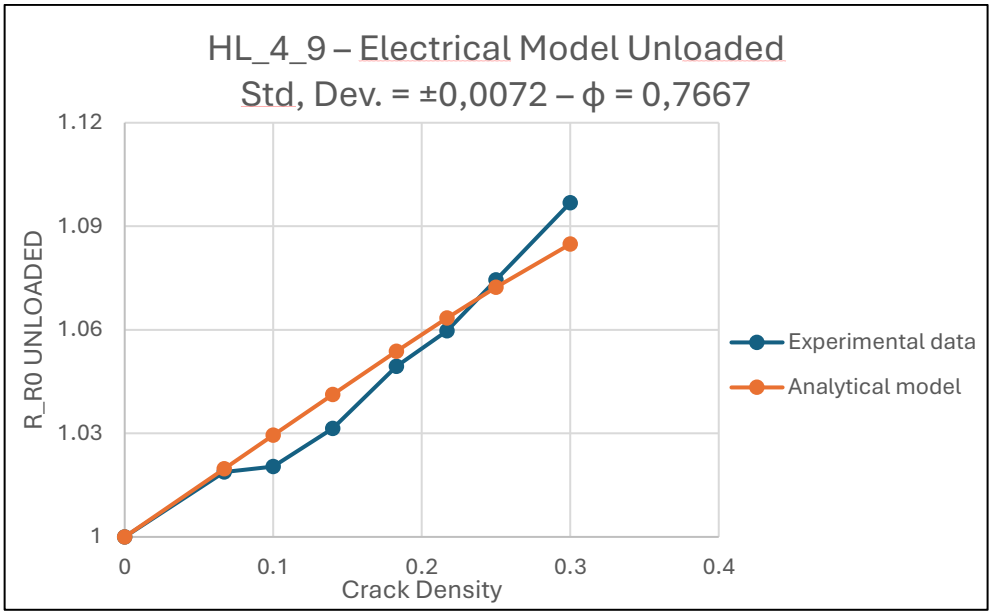
HL_4_9 – Electrical Model Unloaded
Std, Dev. = ±0,0072 – ϕ = 0,7667
R_R0 UNLOADED
1.12
1.09
1.06
1.03
1
0
0.1
0.2
0.3
0.4
Crack Density
Experimental data
Analytical model

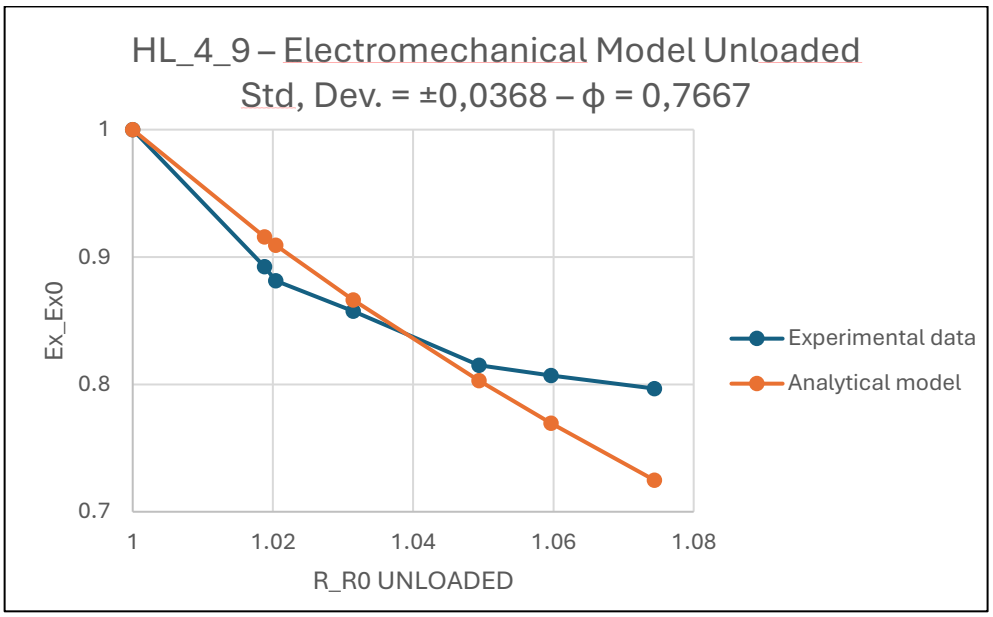
HL_4_9 – Electromechanical Model Unloaded
Std, Dev. = ±0,0368 – ϕ = 0,7667
Ex_Ex0
1
0.9
0.8
0.7
1
1.02
1.04
1.06
1.08
R_R0 UNLOADED
Experimental data
Analytical model

RM_2_2

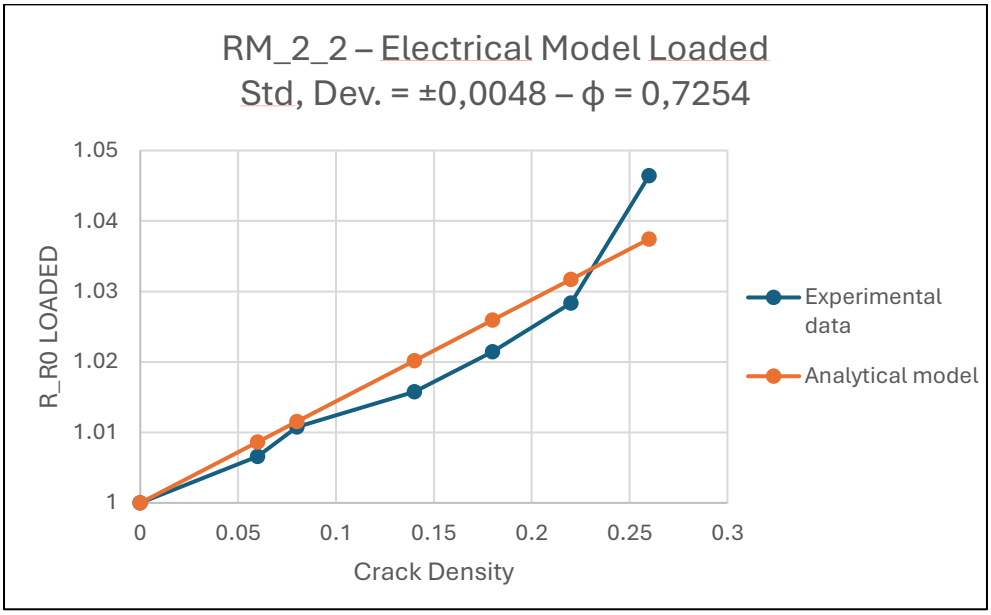
RM_2_2 – Electrical Model Loaded
Std, Dev. = ±0,0048 – ϕ = 0,7254
R_R0 LOADED
1.05
1.04
1.03
1.02
1.01
1
0
0.05
0.1
0.15
0.2
0.25
0.3
Crack Density
Experimental data
Analytical model

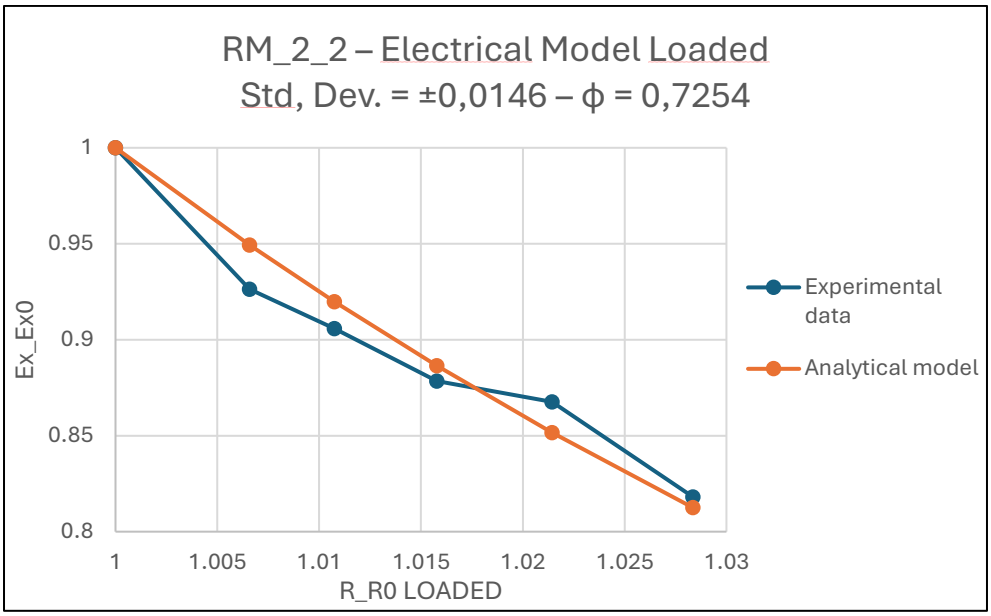
RM_2_2 – Electrical Model Loaded
Std, Dev. = ±0,0146 – ϕ = 0,7254
Ex_Ex0
1
0.95
0.9
0.85
0.8
1
1.005
1.01
1.015
1.02
1.025
1.03
R_R0 LOADED
Experimental data
Analytical model

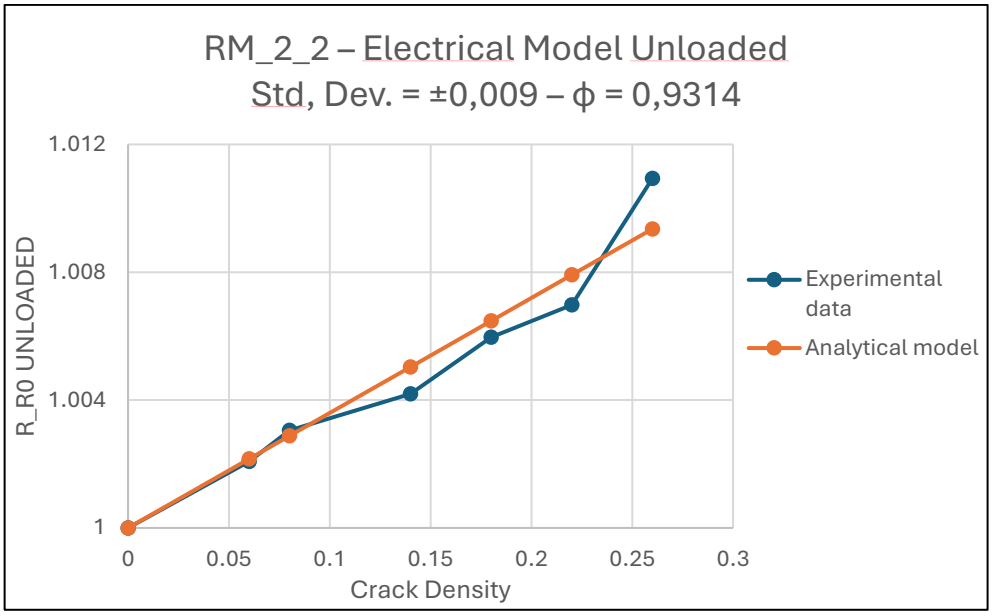
RM_2_2 – Electrical Model Unloaded
Std, Dev. = ±0,009 – ϕ = 0,9314
1.012
1.008
1.004
1
R_R0 UNLOADED
0
0.05
0.1
0.15
0.2
0.25
0.3
Crack Density
Experimental data
Analytical model

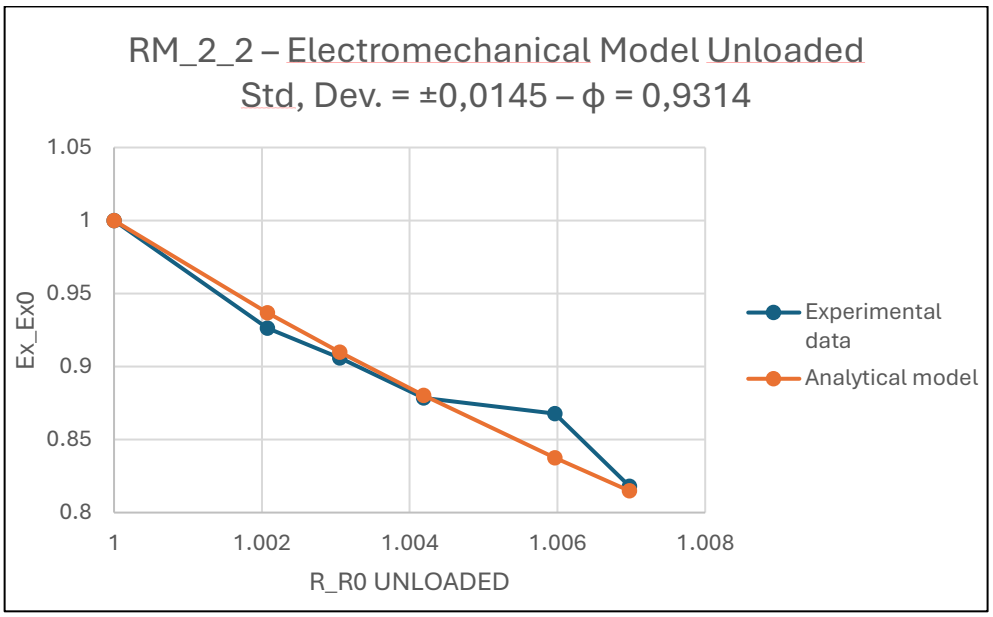
RM_2_2 – Electromechanical Model Unloaded
Std, Dev. = ±0,0145 – ϕ = 0,9314
1.05
1
0.95
0.9
0.85
0.8
Ex_Ex0
1
1.002
1.004
1.006
1.008
R_R0 UNLOADED
Experimental data
Analytical model